

國立臺灣大學理學院化學研究所



碩士論文

Department of Chemistry

College of Science

National Taiwan University

Master Thesis

以抑制核蛋白三聚體之生成設計及合成抗流感藥物

Design and Synthesis of Anti-influenza Drugs by  
Inhibiting the Formation of Nucleoprotein Trimer

黃乙洲

Yi-Chou Huang

指導教授：方俊民 博士

Advisor: Jim-Min Fang, Ph.D.

中華民國 106 年 7 月

July, 2017

## 誌謝

時光飛逝，轉眼間兩年過去了，至今也取得碩士學位。依稀記得兩年前得知錄取化學所時的興奮及雀躍，但或者更多的是伴隨在其後的妄自菲薄。

因此，最先要感謝的是我的指導老師，方俊民老師，在推甄放榜後的眾多競爭者中，願意讓我加入實驗室這個大家庭。在這兩年中，老師對我的耐心、教導、以及建議都讓我銘記於心，同時也使我能察覺到自己的缺點，儘管經過兩年後這些問題並沒有完全解決，但也得到了改善。老師在生活上也很關心我。在最後這段時間，老師也不厭其煩地幫我批改論文，讓我能順利完成這本碩士論文。謝謝羅禮強老師、王宗興老師以及鄭婷仁老師願意擔任我的口試委員，並在口試時給予我指導與建議。另外，謝謝蔡蘊明老師在實驗室 meeting 上分享合成及實驗上的建議。也謝謝在中研院的呂紹宏學長提供協助。

對於 JMF 實驗室的大家，我一直認為，不論熟識程度高低、喜歡與否，能相遇即是緣分，所以很感謝大家能出現在我的碩士生涯中。其中首先謝謝許哲生及張仁堯學長讓我在一開始能迅速習慣陌生的環境。謝謝林隆誌學長帶我進入系上的壘球隊，認識許多其他實驗室的學長。謝謝洪偉晟學長跟我討論實驗上的各種問題。謝謝彭啟鈞學長常常分享人生的經驗，既是同事也像長輩，很令人安心。謝謝陳思涵和黃夢若等學長姊舉辦節日活動讓我留下深刻的回憶。也要特別謝謝徐欣傳及李薇立在我實驗卡關時給予鼓勵和建議，待我如同屆好友一般，並且抽空來參加我的口試。還有專題生周久淳在我忙碌時幫忙，教學相長。除此之外，要特別謝謝我同屆的同學瑋心及鼎棋，一起度過實驗的難關和修課，互相打氣。

謝謝我的父母一路上的支持，雖然在錄取台大時只是對我說一聲簡短的恭喜，不過我知道在這兩個字中，包含著我自己心中還要多好幾倍的喜悅。

托那麼多人的幫助，所以我要畢業了！song 啦！

## 摘要

流行性感冒病毒造成每年的流行病，有時甚至造成更嚴重的全球性流行病。全球每年因流行性感冒而死亡的人數高達 250,000 至 500,000 人。

甲型流感病毒會根據神經胺酸酶 (NA) 和血液凝集素 (HA) 以不同亞型進行表現。抗流感藥物，如克流感及瑞樂沙是作為神經胺酸酶 (NA) 的抑制劑。在宿主細胞核中形成核糖核蛋白複合物 (RNPs) 是造成甲型流感病毒致病的主要原因之一。核糖核蛋白複合物由 RNA 聚合酶、RNA 片段及核蛋白 (NP) 所構成。由於核蛋白在不同亞型的流感病毒中較為恆定，故我們將 NP-NP 作用力作為發展新型流感藥物的目標。

E339A...R416A 鹽橋作用力是核蛋白單體間不可或缺的作用力。先前，由一個中央研究院的研究團隊利用高通量藥物篩選系統從資料庫中篩選出一些小分子化合物作為前導化合物。以化合物 A 的結構為基礎，我們設計並合成一些小分子去破壞鹽橋以及其他作用力，包含氫鍵、疏水和  $\pi$ - $\pi$  堆疊等作用力，進而提升對於流感病毒的抑制效果。此外，為了確認核蛋白單體間實際的鍵結位置，我們合成了一些芳基疊氮衍生物用於進行光親合標記實驗。

在本篇研究中，我們首先在化合物 A 的嗎啉基團置換成 1,1-二苯甲胺基團，合成出化合物 **13a** 以及 **13b**。另外，我們也合成出苄胺衍生物 **22a** 和 **22b**。我們也進一步合成出 4-疊氮苄胺基衍生物 **30**、1-苄-1-(4-疊氮苄)甲胺基衍生物 **36** 以及 1,1-雙(4-疊氮苄)甲胺基衍生物 **42** 用於光親合標記實驗。在生物活性檢測結果中指出，化合物 **13a** 具有和化合物 A 相近的抗流感活性。疊氮化合物 **36** 以及 **42** 也具有好的抗流感活性，並作為有潛力的光親合標記探針。然而，化合物 **22a** 和 **30** 顯示出較低的抗流感活性，並且化合物 **13b** 及 **22b** 也因疏水性過高而無法進行生物活性檢測。

## Abstract



Influenza viruses cause yearly epidemics and occasionally more severe pandemics, which lead to high fatality. The worldwide death toll of influenza epidemics is in the range of 250,000 to 500,000 each year.

Influenza A virus is characterized as different subtypes according to neuraminidase (NA) and hemagglutinin (HA). The anti-influenza drugs Tamiflu and Relenza act as NA inhibitors. Formation of ribonucleoprotein complexes (RNPs) in the nucleus of the host cell is one of the main causes of influenza A virus pathogenesis. RNPs are composed of RNA polymerase, RNA fragment and nucleoprotein (NP). Because NP is substantially more conserved, we chose to develop the anti-influenza drugs by disrupting the NP–NP interaction.

E339A...R416A salt bridge interaction between NP monomers is essential. A research team in Academia Sinica has previously conducted a high-throughput screening of the chemical library to identify some small molecules as anti-influenza agents by disrupting the NP–NP interaction. Based on the structure of compound **A**, we thus designed and synthesized small molecules that may disrupt the salt bridge interaction, and further impose on other interactions, including hydrogen bonding, hydrophobic interaction and  $\pi$ – $\pi$  stacking interaction, to increase their inhibitory

activities against influenza viruses. To verify the binding sites between NP monomers, we further synthesized the aryl azide derivatives for photoaffinity labeling experiments.


In this study, we first synthesized (1,1-diphenylmethyl)amino derivatives **13a** and **13b** replacing the morpholine group in the compound **A**. The benzylamino derivatives **22a** and **22b** were also synthesized. We further synthesized the 4-azidobenzylamino derivative **30**, 1-phenyl-1-(4-azidophenyl)methylamino derivative **36** and 1,1-bis(4-azidophenyl)methylamino derivative **42** for photoaffinity labeling experiments. The MTS bioassay indicated that compound **13a** had anti-influenza activity similar to compound **A**. The azido compounds **36** and **42** had good anti-influenza activity to serve as potential photoaffinity labeling probes. Nevertheless, the compounds **22a** and **30** showed lower anti-influenza activity, and compound **13b** and **22b** were too hydrophobic to do bioassay.

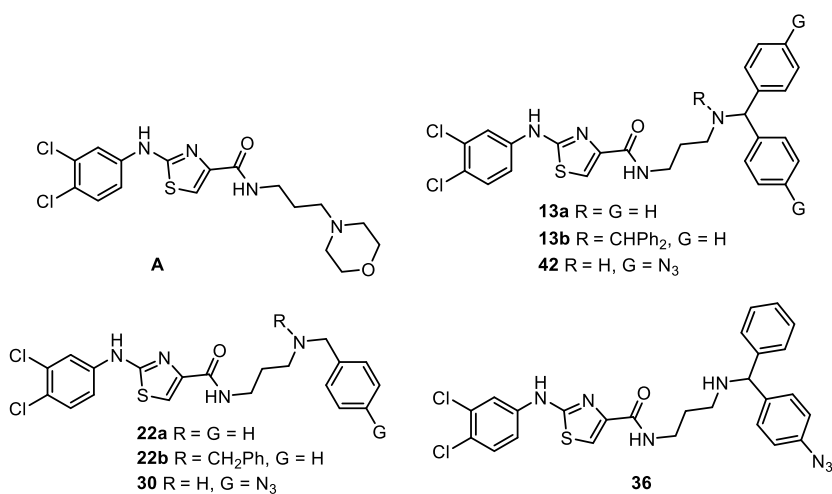



# Table of Contents



<b>Acknowledgement</b> .....	<b>I</b>
<b>Abstract in Chinese</b> .....	<b>II</b>
<b>Abstract in English</b> .....	<b>III</b>
<b>Table of Contents</b> .....	<b>V</b>
<b>Index of Schemes</b> .....	<b>VII</b>
<b>Index of Figures</b> .....	<b>VIII</b>
<b>Index of Tables</b> .....	<b>XI</b>
<b>Abbreviations</b> .....	<b>XIII</b>
<b>Chapter 1. Introduction</b> .....	<b>1</b>
<b>1.1 Influenza A virus</b> .....	<b>1</b>
<b>1.2 Ribonucleoprotein (RNP) and its structure</b> .....	<b>4</b>
<b>1.3 Virus life cycle</b> .....	<b>9</b>
<b>1.3.1 RNP transcription and replication</b> .....	<b>10</b>
<b>1.3.2 RNP assembly</b> .....	<b>14</b>
<b>1.3.3 Transportation of RNP into host cell</b> .....	<b>16</b>
<b>1.3.4 Transportation of RNP out of host cell</b> .....	<b>18</b>



<b>1.4 Anti-influenza drugs targeting the RNP.....</b>	<b>20</b>
<b>1.4.1 Interactions between RNA and RNA polymerase in RNP.....</b>	<b>21</b>
<b>1.4.2 Interactions between NP and RNA polymerase in RNP.....</b>	<b>22</b>
<b>1.4.3 Interactions between NP and viral RNA segment in RNP.....</b>	<b>23</b>
<b>1.4.4 Interactions between NP monomers in RNP.....</b>	<b>24</b>
<b>1.5 Photoaffinity labeling.....</b>	<b>27</b>
<b>1.6 Previous research on anti-influenza agents targeting NP trimerization....</b>	<b>30</b>
<b>Chapter 2. Results and Discussion.....</b>	<b>34</b>
<b>2.1 Research motivation.....</b>	<b>34</b>
<b>2.2 Strategy for designing effective anti-influenza drugs.....</b>	<b>34</b>
<b>2.3 Modifications at terminal amine group.....</b>	<b>39</b>
<b>2.4 Synthesis of (1,1-diphenylmethyl)amino derivatives 13a and 13b.....</b>	<b>40</b>
<b>2.5 Synthesis of benzylamino derivatives 22a and 22b.....</b>	<b>44</b>
<b>2.6 Synthesis of derivatives bearing azidophenyl group for photoaffinity</b>	
<b>labeling.....</b>	<b>45</b>
<b>2.7 Bioassay.....</b>	<b>50</b>
<b>2.8 Conclusion.....</b>	<b>52</b>
<b>2.9 Prospect.....</b>	<b>54</b>



<b>Chapter 3. Experimental Section</b> .....	59
<b>3.1 General part</b> .....	59
<b>3.2 Procedure of bioassay</b> .....	60
<b>3.2.1 Material and methods</b> .....	60
<b>3.2.2 Determination of influenza virus TCID<sub>50</sub></b> .....	60
<b>3.2.3 Determination of EC<sub>50</sub> of NP inhibitors</b> .....	61
<b>3.3 Synthetic procedure and characterization of compounds</b> .....	62
<b>References</b> .....	95
<b>Appendix</b> .....	110

### Index of Schemes

<b>Scheme 1.</b> Photolysis of aryl azide.....	29
<b>Scheme 2.</b> Photolysis of diazirine.....	29
<b>Scheme 3.</b> First synthetic strategy for (1,1-diphenylmethyl)amino derivative <b>13a</b> ....	41
<b>Scheme 4.</b> Unsuccessful synthesis of compound <b>13a</b> through S <sub>N</sub> 2 reaction from another direction.....	43
<b>Scheme 5.</b> Successful synthesis of compounds <b>13a</b> (JMF4172) and <b>13b</b> (JMF4195).....	44



<b>Scheme 6.</b> Synthesis of benzylamino derivatives <b>22a</b> (JMF4286) and <b>22b</b> (JMF4196) .....	45
<b>Scheme 7.</b> Synthesis of 4-azidobenzyl derivative <b>30</b> (JMF4287).....	46
<b>Scheme 8.</b> Synthesis of 1-phenyl-1-(4-azidophenyl)methylamino derivative <b>36</b> (JMF4288).....	47
<b>Scheme 9.</b> Synthesis of 1,1-bis(4-azidophenyl)methylamino derivative <b>42</b> (JMF4289).....	50

## Index of Figures

<b>Figure 1.</b> Structure of influenza A virus.....	2
<b>Figure 2.</b> Diagram of RNP structure.....	5
<b>Figure 3.</b> Cryo-EM reconstruction of RNP.....	5
<b>Figure 4.</b> Diagram of intersubunit interactions in the RNA polymerase complex.....	6
<b>Figure 5.</b> Crystal structure of influenza A virus NP trimer.....	8
<b>Figure 6.</b> The influenza A virus life cycle.....	10
<b>Figure 7.</b> A model of RNP transcription and replication: (A) steps in the RNP transcription process, and (B) steps in the RNP replication process.....	13
<b>Figure 8.</b> Directionality of NP assembly onto RNP complexes.....	15

<b>Figure 9.</b> Transportation of the RNPs from virion to nucleus.....	17
<b>Figure 10.</b> Transportation of the progeny RNPs out of host cell from nucleus.....	19
<b>Figure 11.</b> Docking the atomic structure of (A) NPs and (B) RNA polymerase into the RNP model.....	20
<b>Figure 12.</b> Effect of point mutations and insertions on the RNA polymerase binding of the conserved sequences at (A) the 3' end and (B) the 5' end.....	21
<b>Figure 13A.</b> The crystal structure of NP.....	22
<b>Figure 13B.</b> The activities of the NP mutants in the minigenome dual-luciferase assay.....	22
<b>Figure 13C.</b> The activities of the NP mutants in the vRNA template minigenome assay.....	22
<b>Figure 13D.</b> Relative amounts of vRNA and mRNA produced by the NP mutants in the cRNA template minigenome assay.....	22
<b>Figure 14.</b> Electrostatic potential distribution of NP.....	23
<b>Figure 15.</b> Inter-subunit interactions mediated by the tail loop.....	24
<b>Figure 16.</b> Viral RNA synthesis activities of NP mutants by the minigenome assay.....	25
<b>Figure 17A.</b> Oligomerization behavior of NP tail loop mutants as shown by gel	

filtration chromatography.....	26
<b>Figure 17B.</b> Oligomerization behavior of NP D491 mutants as shown by gel filtration chromatography.....	26
<b>Figure 17C.</b> RNA synthesis activities of NP mutants determined in the vRNA- and cRNA-templated minigenome assays.....	26
<b>Figure 18.</b> A cartoon representation for the process of photoaffinity labeling.....	28
<b>Figure 19A.</b> Interactions including the tail-loop (green) and its binding pocket (gold).....	31
<b>Figure 19B.</b> Structure and inhibitory effect of compound <b>A</b> .....	31
<b>Figure 19C.</b> The modeled structure of the NP– <b>A</b> complex.....	31
<b>Figure 20.</b> Small molecules that inhibit viral replication via binding to NP.....	32
<b>Figure 21.</b> NP surface map of residues affecting aryl piperazine amide efficacy.....	33
<b>Figure 22.</b> X-ray structure of <b>C</b> –NP complex.....	33
<b>Figure 23.</b> The strategy for designing anti-influenza drugs based on the structure of compound <b>A</b> .....	35
<b>Figure 24.</b> Bioassay of compound <b>A</b> and its derivatives with different heterocycle core structures.....	37

**Figure 25.** Bioassay of compound **A** analogs with various aliphatic chain lengths.....38

**Figure 26.** Bioassay of derivatives with various terminal functional groups.....38

**Figure 27.** <sup>1</sup>H NMR spectra of the presumed bromination compound (**A**) and crude compound **33** (**B**) in CDCl<sub>3</sub> solution.....49

**Figure 28.** Mechanism of MTS assay and anti-influenza activity (EC<sub>50</sub>) of compounds **13a** (JMF4172), **22a** (JMF4286), **30** (JMF4287), **36** (JMF4288) and **42** (JMF4289).....52

**Figure 29.** General structural features of compound **A** analogs possessing anti-influenza activity..... 54

**Figure 30.** Anti-influenza activity (EC<sub>50</sub>) of compounds **43**, **44**, **45** and **46**.....57

**Figure 31.** Proposed drug candidates in the future work.....58

## Index of Tables

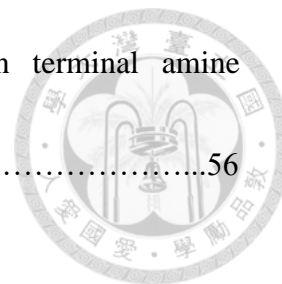
**Table 1.** Anti-influenza EC<sub>50</sub> values (μM) of compound **A** analogs.....36

**Table 2.** Unsuccessful S<sub>N</sub>2 reactions of compound **11**.....42

**Table 3.** Attempts to prepare compound **34** by alkylation reaction of amine **24** with the presumed bromination compound.....48

**Table 4.** Calculated partition coefficient (clogP) of the above-synthesized compound **A**

analogs with various  $R^1$  and  $R^2$  substituents on terminal amine  
group.....56

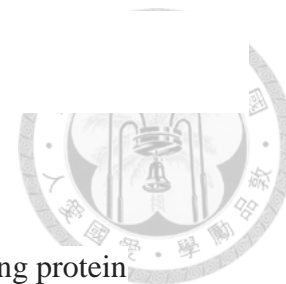


## Abbreviations



<b>AIBN</b>	azobis(isobutyronitrile)
<b>AUC</b>	analytical ultracentrifugation
<b>Boc</b>	<i>tert</i> -butoxycarbonyl
<b>BPO</b>	benzoyl peroxide
<b>clogP</b>	calculated partition coefficient
<b>CPE</b>	cytopathic effect
<b>cRNA</b>	complementary RNA
<b>DIEA</b>	<i>N,N</i> -diisopropylethylamine
<b>DLS</b>	dynamic light-scattering
<b>DMF</b>	<i>N,N</i> -dimethylformamide
<b>DMSO</b>	dimethylsulfoxide
<b>EC<sub>50</sub></b>	half maximal effective concentration
<b>EDCI</b>	1-ethyl-3-(3-dimethylaminopropyl)carbodiimide
<b>EtOAc</b>	ethyl acetate
<b>GDP</b>	guanosine diphosphate
<b>GTP</b>	guanosine triphosphate
<b>HA</b>	hemagglutinin

<b>HOBt</b>	1-hydroxybenzotriazole hydrate
<b>HPLC</b>	high performance liquid chromatography
<b>HRB</b>	human immunodeficiency virus Rev binding protein
<b>IR</b>	infrared
<b>ISC</b>	intersystem crossing
<b>Log D</b>	logarithm distribution of coefficient D
<b>Log P</b>	logarithm partition coefficient P
<b>MDCK</b>	Madin-Darby canine kidney
<b>Me</b>	methyl
<b>mRNA</b>	messenger RNA
<b>MS</b>	mass spectrometry
<b>MTOC</b>	microtubule organizing center
<b>NA</b>	neuraminidase
<b>NBS</b>	<i>N</i> -bromosuccinimide
<b>NEP</b>	nuclear export protein
<b>NMM</b>	<i>N</i> -methylnmorpholine
<b>NMR</b>	nuclear magnetic resonance
<b>NP</b>	nucleoprotein



<b>nt</b>	nucleotide
<b>PAGE</b>	polyacrylamide gel electrophoresis
<b>Pd/C</b>	palladium on activated charcoal
<b>RE</b>	recycling endosome
<b>RNP</b>	ribonucleoprotein
<b>TFA</b>	trifluoroacetic acid
<b>THF</b>	tetrahydrofuran
<b>TLC</b>	thin layer chromatography





## Chapter 1. Introduction



### 1.1 Influenza A virus

Influenza is a highly infectious respiratory disease causing yearly epidemics and occasionally more severe pandemics. Influenza features symptoms such as high fever, coryza, cough, headache, prostration, and inflammation.<sup>1</sup> In the majority of cases, acute symptoms like high fever are sustainable for 7 to 10 days, and chronic symptoms like weakness and fatigue may extend for 2 to 3 weeks.<sup>1</sup> Influenza frequently occurs in winter outbreaks, and people within all age brackets are suffering.<sup>1</sup>

Patients with pulmonary or cardiac disease, or diabetes mellitus are extremely possible for developing a few complications from influenza A virus including hemorrhagic bronchitis, pneumonia and cardiorespiratory failure.<sup>1</sup> These complications lead to high fatality with the worldwide death toll in the range of 250,000 to 500,000 each year.<sup>2</sup> There have been several severe influenza A virus outbreaks or pandemics in the recorded history including 1918 (H1N1 Spanish flu), 1957 (H2N2 Asia flu), 1968 (H3N2 Hong Kong flu), 1977 (H1N1 Russia flu), 2003 (H5N1 bird flu), 2009 (H1N1 swine flu), and the most recent one in 2013 (H7N9 bird flu).<sup>3</sup> In 1957, the outbreak caused more than 66,000 deaths in the United States.<sup>4</sup> In 1918, the most devastating pandemics claimed about 50 million lives in the world.<sup>5</sup>

Influenza A virus is a member of Orthomyxoviridae family. The global-shaped influenza A virus is composed of two parts, lipid bilayer envelope and core (Figure 1).<sup>6</sup>


Lipid bilayer envelope is tightly joined with matrix proteins, M1 and M2. The glycoproteins neuraminidase (NA) and hemagglutinin (HA) are located on the surface of lipid bilayer envelope. Eight segments of negative-sense single-stranded RNAs, RNA polymerases and nucleoprotein (NP) are inside the core.

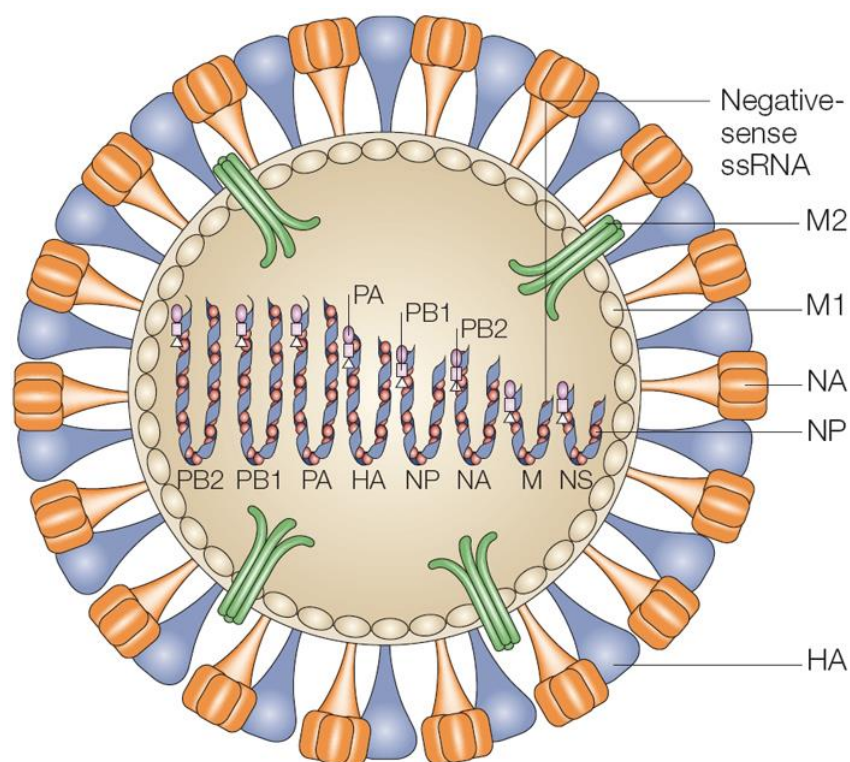


**Figure 1.** Structure of influenza A virus.<sup>6</sup>

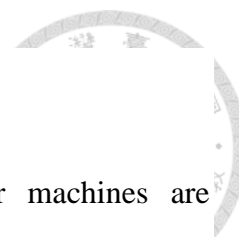
The envelope is a lipid bilayer structure which is derived from cell membrane of the host cell. The mature influenza A virus is coated with cell membrane of the host cell, and separates itself from the host cell by budding.

Matrix proteins, M1 and M2 construct the shell skeleton of influenza A virus,



functionalizing as maintenance of spatial structure and the transportation into and out of the host cell. M1 is located on the cytoplasmic side of the lipid envelope in a layered manner, and M2 penetrates through the lipid envelope. M1 is assembled with other viral proteins in the nucleus of the host cell after the transcription and replication of the viral RNA segments. However, the association of M2 occurs in the late infection, when M2 is distributed on the inner wall of the cell membrane of the host cell (Section 1.3.4).

The glycoproteins HA and NA are divided into eighteen and eleven classes, respectively, which lead to different subtypes of influenza A virus.<sup>7, 8</sup> HA is presented in cylindrical shape. HA binds to the receptor on the erythrocyte surface of animals, such as human, bird, swine and mouse, thus causing cell coagulation.<sup>9</sup> HA is indispensable for transporting influenza A virus into host cell. HA is hydrolyzed into two parts, heavy chain and light chain. The former one is able to bind to the sialic acid receptor on the cell membrane of the host cell. The latter one is able to assist fusion of virus envelope and host cell membrane.<sup>10</sup> NA is a mushroom-shaped tetrameric glycoprotein. When the mature influenza A virus leaves host cell by budding, the HAs of influenza A virus keep contact with the host cell. NA is capable of catalyzing the hydrolysis of the glycosidic bond of sialic acid on the surface glycoprotein of host cell, thus cleaving the connection with virus.<sup>11</sup>



## 1.2 Ribonucleoprotein (RNP) and its structure

Ribonucleoprotein particles (RNPs) as independent molecular machines are responsible for replication, transcription and packaging of viral RNA. RNPs are composed of negative-sense single-stranded RNAs, heterotrimeric RNA polymerase and multiple copies of NP monomers (Figure 2).<sup>12</sup> RNPs have been isolated from the WSN (H1N1) strain of influenza A virus by means of chemical treatments, extractions, and gradient centrifugation.<sup>13</sup> The electron microscopy diagrams indicate that RNPs feature a distinct and interesting double-helical hairpin conformation. The structure of RNPs can be divided into three parts: RNA polymerase end, central filament region and looped end (Figure 3).<sup>14</sup> Two opposite polarity strands of NP oligomers combine with each other along the central filament region, and both of two strands are connected by terminal looped structure.<sup>14,15</sup> RNPs are uniform in thickness but variable in length. Their double-helical structures are approximately 150 Å in diameter and range from 500 Å to 1300 Å in length. The diameter of terminal loops is approximately 75 Å.<sup>13</sup> Besides, distance between two neighboring binding sites in a NP oligomer is approximately 70 Å, in agreement with the fact that one NP is associated with 24 nucleotides of viral RNAs.<sup>16, 17, 18</sup>

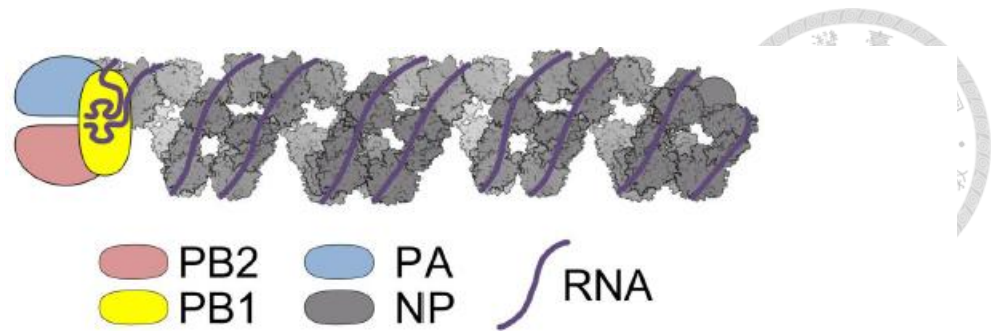


**Figure 2.** Diagram of RNP structure.<sup>12</sup>

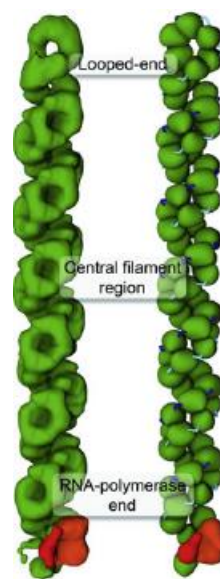


**Figure 3.** Cryo-EM reconstruction of a RNP.<sup>14</sup>

RNA polymerase is a heterotrimeric protein complex, which contains three domains, PB1, PB2 and PA (Figure 4).<sup>19</sup> PB1 is the largest domain and the core among RNA polymerase. Until now, it is only known that the N-terminal fragment (amino acids 1–15) of PB1 domain interacts with PA domain and the C-terminal fragment, which forms a three-helical bundle (amino acids 678–757) to interact with the N-terminus of PB2 domain. In the RNP structure, PB1 and PB2 domains but not PA

domain attach to two terminal NP monomers at two opposite polarity NP oligomer strands.<sup>20</sup> PB1 domain binds to 3' and 5' termini of viral RNA.<sup>14</sup> It is worth noting that each domain of RNA polymerase has its own functions.<sup>19</sup> PB1 domain possesses catalytic active site of RNA polymerase. PB2 domain contains binding site of the 5' pre-mRNA cap for viral RNA transcription. PA domain expresses the endonuclease activity, which is essential for cap-snatching.

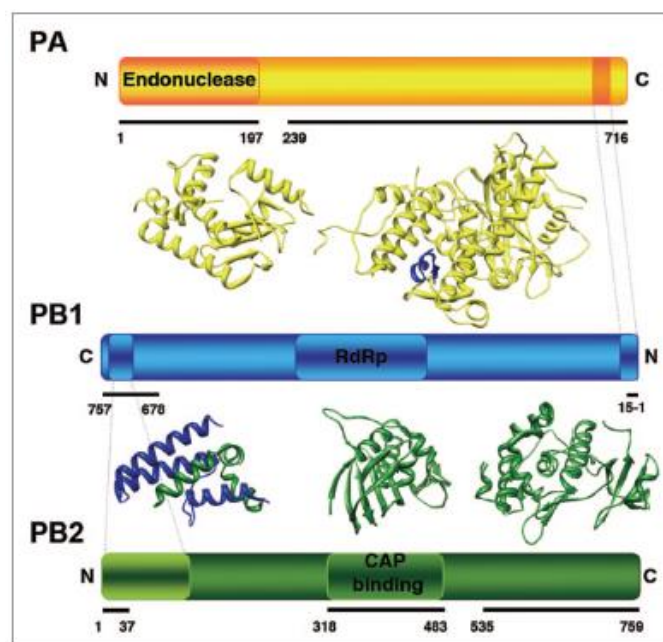
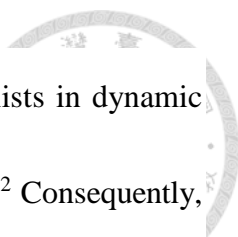


**Figure 4.** Diagram of intersubunit interactions in the RNA polymerase complex.<sup>19</sup>

NP is a multifunctional protein as the building blocks of RNPs. Primary functions of NP are to encapsidate viral RNA to promote and maintain its assembling into double-helical hairpin RNP structure and to assist replication, transcription and



packaging of viral RNA. NP features a meniscus shape and usually exists in dynamic equilibrium between monomeric and oligomeric forms (Figure 5).<sup>14, 21, 22</sup> Consequently, despite trimeric form is most widespread, oligomeric forms with various sizes and monomeric form are also found. NP monomer is generally divided into three domains: head, body, and tail loop. The region at the top of the head domain intimately interacts with PB1 and PB1 domains of RNA polymerase.<sup>23</sup> The RNA binding groove between the head domain and body domain contains a large amount of basic amino acids, thus creating a positive electrostatic environment to bind to viral RNA by the interactions with the negative electrostatic phosphodiester backbones.<sup>2, 21, 24</sup> The oligomerization of NPs is derived from the interactions, such as salt bridge, hydrophobic and  $\pi$ - $\pi$  interactions, between the tail loop structure and the binding pocket site on the neighboring NP.<sup>21, 25</sup> Another interaction between NPs has also been found by NP dimer formation of the NP deletion mutant.<sup>26</sup> This new interaction is hypothesized to be responsible for transforming linear, single-stranded RNPs into double-helical structures. However, in cytoplasm, oligomerization of NPs is restricted because NP self-assemblies are extremely weak in the absence of viral RNA. Surprisingly, once NP has oligomerized, NPs dissociate only at a very slow rate in the absence of bound viral RNA.<sup>26</sup> In addition, NP is also related to replication, transcription and packaging of viral RNA, but they are depended on the lengths of viral RNAs on RNPs, consistent

with the fact that NP is completely dispensable for replication and transcription of short viral RNAs less than 76 nucleotides, in previous researches.<sup>27-32</sup>

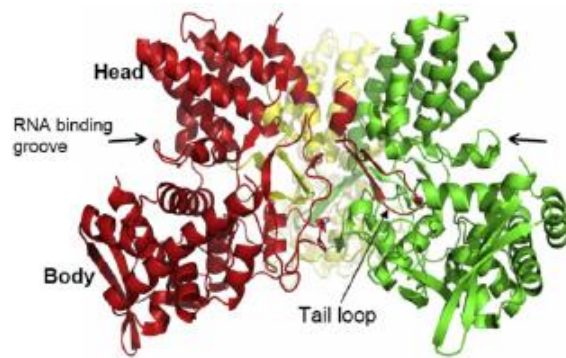
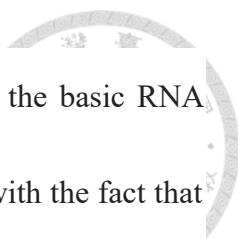


**Figure 5.** Crystal structure of influenza A virus NP trimer.<sup>21</sup>

The entire Influenza A virus genome is 13,588 base long and is contained in eight single-stranded RNA segments that code for several proteins, including RNA, HA, NP, NA, polymerase subunits (PB2, PB2 and PA), two matrix proteins (M1 and M2) and two distinct non-structural proteins (NS1 and NEP). The eight single-stranded RNA segments are associated with RNA polymerase and NPs to form eight RNPs for replication and transcription. The 3' and 5' termini of all eight RNA segments of influenza A virus contain conserved sequences of 12 and 13 nucleotides, respectively. These two sequences, which attach to PB1 domain of RNA polymerase, are partially complementary to form a panhandle structure.<sup>33</sup> The panhandle is proved to be a cis-acting signal polyadenylation<sup>34</sup> and may be necessary for the endonuclease activity





of the RNA polymerase.<sup>35</sup> Viral RNAs are encapsidated by binding to the basic RNA binding grooves of NPs at the outer surface of the RNPs, in agreement with the fact that viral RNAs in the RNPs are readily disrupted under RNase treatment.<sup>36</sup>

### **1.3 Virus life cycle**

The RNPs of the influenza A virus play a critical role throughout the virus life cycle (Figure 6).<sup>14</sup> In the period of infection, HA, which is on the surface of the influenza A virus, binds to the sialic acid receptor on the cell membrane of the host cell.<sup>37</sup> The influenza A virus enters the host cell by means of receptor-mediated endocytosis, and then fuses with the early endosome. Next, viral RNPs (vRNPs) are released from the endosome into the cytoplasm followed by nuclear import of the vRNPs. In the nucleus, vRNPs serve as active template for not only the synthesis of viral mRNA by transcription but also positive-sense, anti-genomic, complementary RNAs (cRNAs).<sup>38</sup> Viral mRNA is translated to produce a variety of essential building blocks for the influenza A virus, such as M1, M2, NS1, nuclear export protein (NEP), HA, NA, PB1, PB2, PA and NP. PB1, PB2, PA and NP are exported back to the nucleus, and associated with nascent vRNAs and cRNAs to construct vRNPs and cRNPs. The cRNPs can act as replication templates for the synthesis of nascent vRNAs.

Finally, nascent vRNPs are exported out of the nucleus into cytoplasm, then leave the host cell by budding through two other proteins, M1 and NEP.

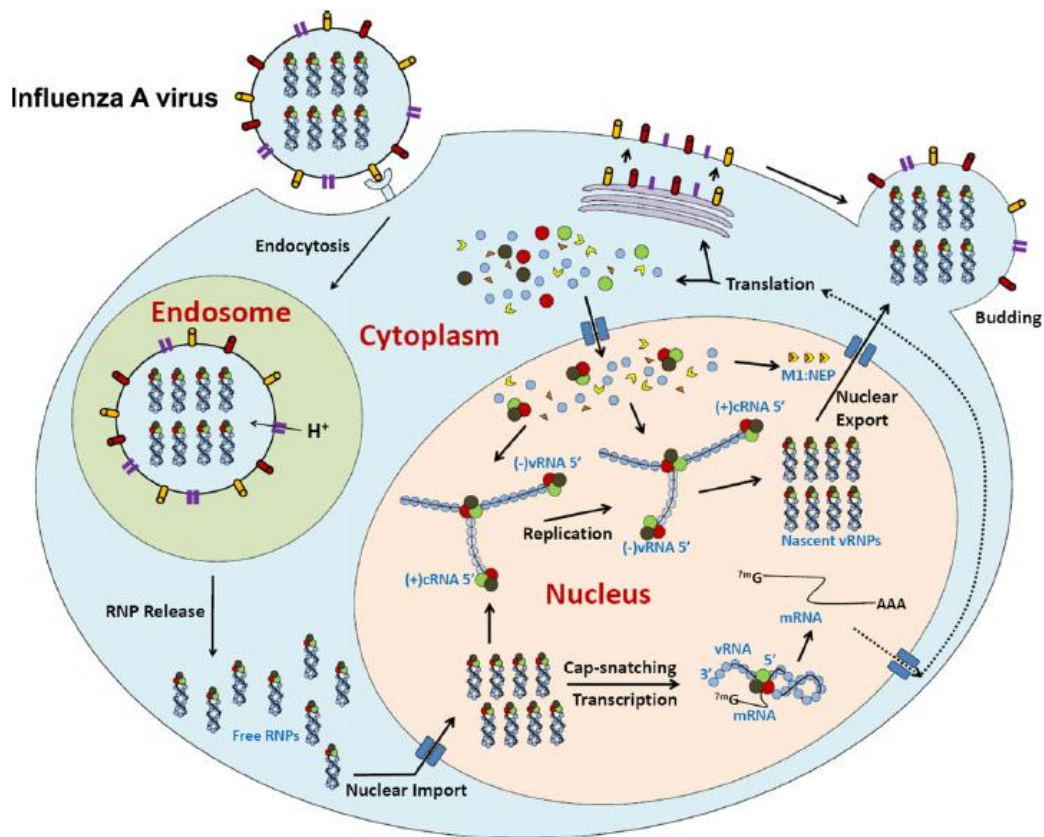
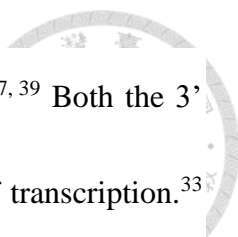


**Figure 6.** The influenza A virus life cycle.<sup>14</sup>

### 1.3.1 RNP transcription and replication

Most interestingly, in the RNP transcription and replication, it is RNP structure instead of naked viral RNA that serves as the template. RNA polymerase complexes and viral RNAs as building blocks are indispensable for transcription and replication.

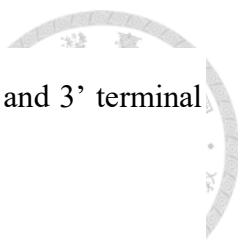
Some studies have revealed that having RNA polymerase mutants in PB1, PB2 and PA



domains or lacking RNA polymerase all hamper the activity of RNP.<sup>27, 39</sup> Both the 3' and 5' terminal sequences of viral RNA play a key role in initiation of transcription.<sup>33</sup>

However, NP is totally dispensable for transcription and replication of short viral RNA-dependent RNPs (less than 76 nucleotides) *in vivo*. This fact demonstrates that NP is characterized as an elongation factor for the RNA polymerase but is not involved in the initiation and termination of transcription.<sup>27</sup> Furthermore, the newly synthesized RNA polymerase and NP also stabilize replicative intermediates, i.e. nascent cRNA and vRNA, which are disrupted by host cell nucleases in the absence of these two stabilizing proteins.<sup>39, 40</sup>

Viral transcription process is initiated by cap-snatching. The 5'-capped primers 10 to 13-nucleotide long are cleaved from pre-mRNAs of the host cell by RNA endonuclease (Figure 7A).<sup>41</sup> The capped primers are recognized by RNA polymerase and continue to elongate the transcription of the template (step 2). The 5' end of the template is seized to form a running knot structure with a shrinking loop length (step 3). Viral transcription process is prematurely terminated by polyadenylation at an oligo-U sequence about 25 nucleotides away from 5' end of the template through RNA polymerase stuttering mechanism, which is the process to transcribe a nucleotide several times without progressing further on the mRNA chain, owing to steric hindrance of the



shrinking loop (step 4).<sup>34, 42, 43</sup> Finally, the mRNA with 5' terminal cap and 3' terminal poly-A sequence is generated.

The progeny mRNA is then translated to produce essential proteins for constructing vRNP and cRNP for viral replication. Viral replication is a primer independent process and starts *de novo* to generate full-length replica of cRNA template (Figure 7B).<sup>41</sup> Viral replication is initiated by a second RNA polymerase binding to the RNA polymerase of cRNP to form a linear structure (steps 2 and 3). The second RNA polymerase is responsible for replicative activity and elongates along the NP-cRNA template from 3' to 5' end. The 3' end of parental cRNA continues carrying out further replication rounds, resulting in numerous progeny vRNAs produced from a single cRNA template (steps 4 and 5). During replication, the progeny vRNA is stabilized and protected by associating with NPs and a third RNA polymerase at 5' end of the progeny vRNA once it is newly synthesized.<sup>14, 39, 44, 45, 46</sup> However, the termination mechanism of viral replication has not been confirmed. To permit the complete replica of cRNA template, the RNA polymerase at the 5' end of the parental cRNA template will dislocate, forced by replicative RNA polymerase to avoid polyadenylation. One mechanism is temporary dislocation, causing the replacement of the parental RNA polymerase by consecutive replicative RNA polymerase. The other mechanism is permanent dislocation, causing the formation of the linear NP-cRNA complex (step n).

Finally, vRNPs are generated and serve as templates for secondary transcription or transport out of the nucleus of the host cell.

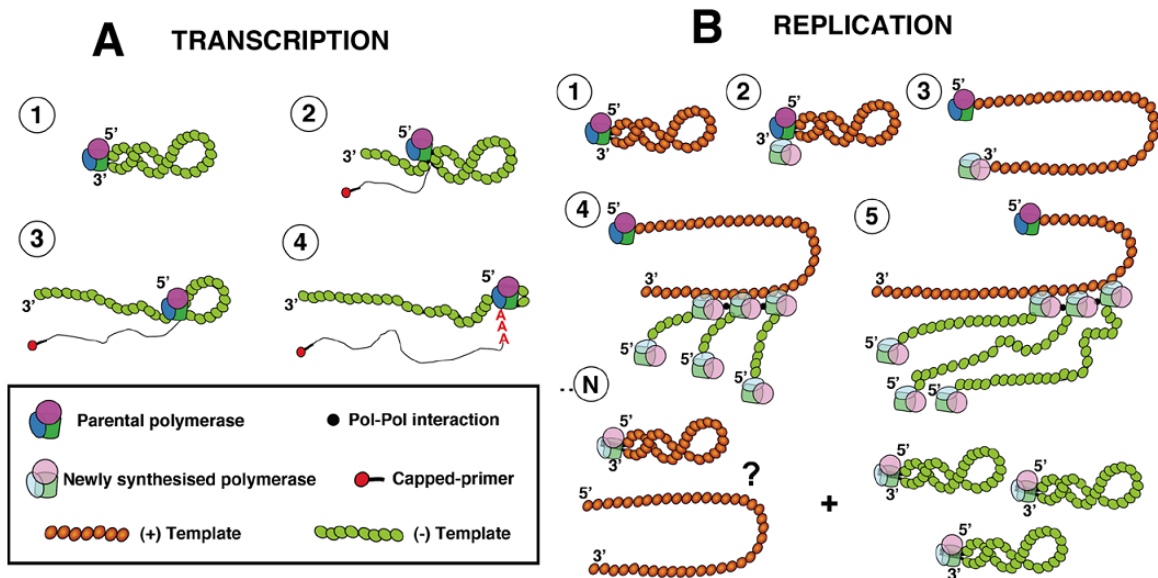
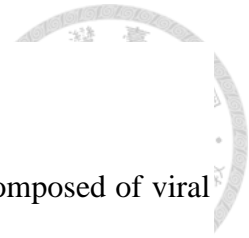


**Figure 7.** A model of RNP transcription and replication: (A) steps in the RNP transcription process, and (B) steps in the RNP replication process.<sup>41</sup>

It is commonly thought that there is a switch from transcription to replication mode.<sup>19, 47</sup> This kind of switch means that the newly synthesized virus proteins from parental vRNPs transcription are necessary for the following replication process and both RNA polymerase and NP are probable to be the crucial switching factors. Nevertheless, in some recent studies, the active stabilization model demonstrates that the synthesis of cRNA or mRNA from vRNPs is stochastic in the presence of preexisting RNA polymerase and NP in the early infection.<sup>27, 39</sup>



### 1.3.2 RNP assembly

It is well known that the RNP complex of influenza A virus is composed of viral RNA polymerase, NPs and viral RNA segment. Despite the fact that the process of RNP assembly is poorly understood, some special rules and the interactions among these three building blocks have been discussed.<sup>14, 20, 21, 26</sup> The newly synthesized NPs from transcription in cytoplasm mostly exist as monomers until they are imported into nucleus to come across vRNAs and cRNAs. NP oligomerization in vitro is a slow process whose rate depends on the length of the viral RNA segment, i.e. the rate increases as the length increases.<sup>48</sup> This fact reveals that there is a cooperative effect for NP oligomerization during viral RNA encapsidation.<sup>49, 50</sup> Additionally, an interesting question whether NP is assembled either tail loop or binding pocket first has also been investigated by mutational analysis of nascent RNPs coexpression with wild-type NP and NP mutants (Figure 8).<sup>27</sup> The results show that only the experiments in presence of NP E339A mutant in the binding pocket fail to assemble the RNPs. The RNP assembly is independent of NP R416A mutant in the tail loop and NP G1(4) mutant in the RNA binding groove. Accordingly, it is the tail loop rather than the binding pocket of NP that is first assembled onto the RNP.

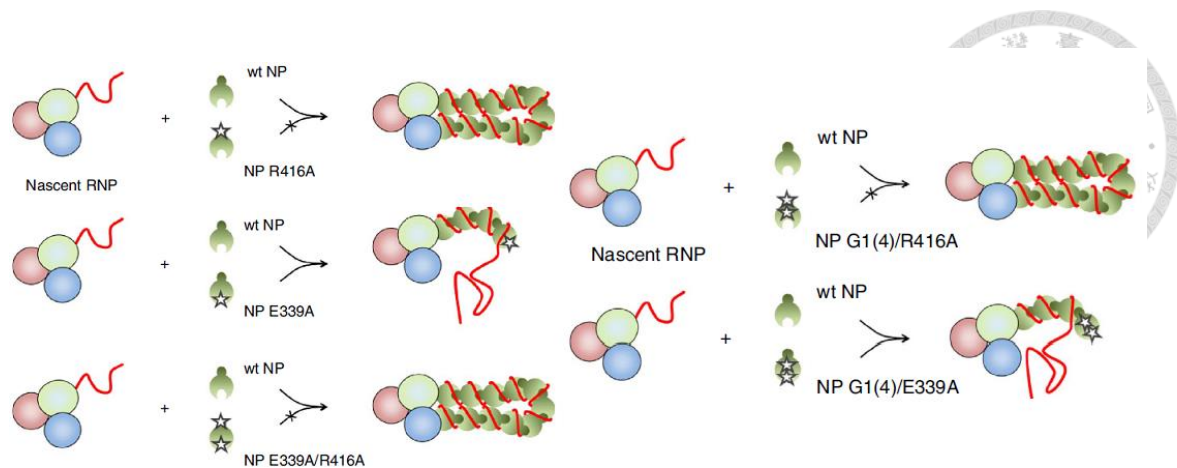
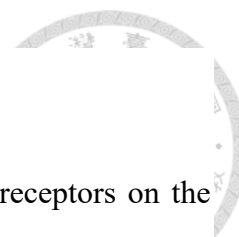


**Figure 8.** Directionality of NP assembly onto RNP complexes.<sup>27</sup>

In the association of NPs with viral RNA segment, some evidences show that the interactions between NP and RNA polymerase would promote the binding of NPs to the viral RNA segment.<sup>20, 31, 51</sup>

It has been hypothesized that phosphorylation may play a crucial role in adjusting the NP polymerization and the RNA binding activity of NP.<sup>50, 52, 53</sup> Furthermore, several host factors are involved in the RNP replication and assembly.<sup>54–58</sup> For instance, RAF-2p48/UAP56 and Tat-SF1, which likely perform as chaperones to restrain the unwanted aggregation of NP, facilitate the association of NPs with the viral RNA segment.<sup>55, 58</sup>



### 1.3.3 Transportation of RNP into host cell

In early infection, HAs of influenza A virus bind to sialic acid receptors on the cell membrane of host cell, and the influenza A virus enters the host cell through clathrin-dependent receptor-mediated endocytosis or micropinocytosis (Figure 9).<sup>12</sup> Clathrin and the adaptor epsin 1 adhere to the receptor at the inner side of the cell membrane. After that, the cell membrane progressively caves inward into a clathrin-coated pit and enters the host cell by endocytosis forming a clathrin-coated vesicle. The adaptor epsin 1 and clathrin are dissociated from the vesicle through opsonization followed by transportation into an early endosome. But filament-shaped viruses are too large to fit into a clathrin-coated pit, they enter the host cell through micropinocytosis.

When the early endosome becomes mature, the acidity in the endosome raises to about pH 5.2.<sup>59</sup> The enhanced acidity leads to the conformational changes of M2 and then changes the curvature of viral membrane. Alteration in pH also change the conformation of HA, causing the insertion into endosomal membrane and the subsequent membrane fusion. Finally, uncoated RNPs are released into cytoplasm of the host cell.

The RNPs are transported onto the nucleus membrane of the host cell by diffusion without the assistance of microtubules, intermediate filaments or actin filaments.<sup>61, 62</sup>



Before nuclear import, the RNPs interact with nuclear pore complexes (NPCs) and go through numerous times of association and dissociation.<sup>60</sup> Afterward, the RNPs are imported into nucleus by means of NP binding to importin  $\alpha$ , which subsequently attaches to importin  $\beta$  to promote nuclear import.<sup>61, 62</sup> The interactions of the RNPs with importins are also different from host to host, leading to a more complicated mode.

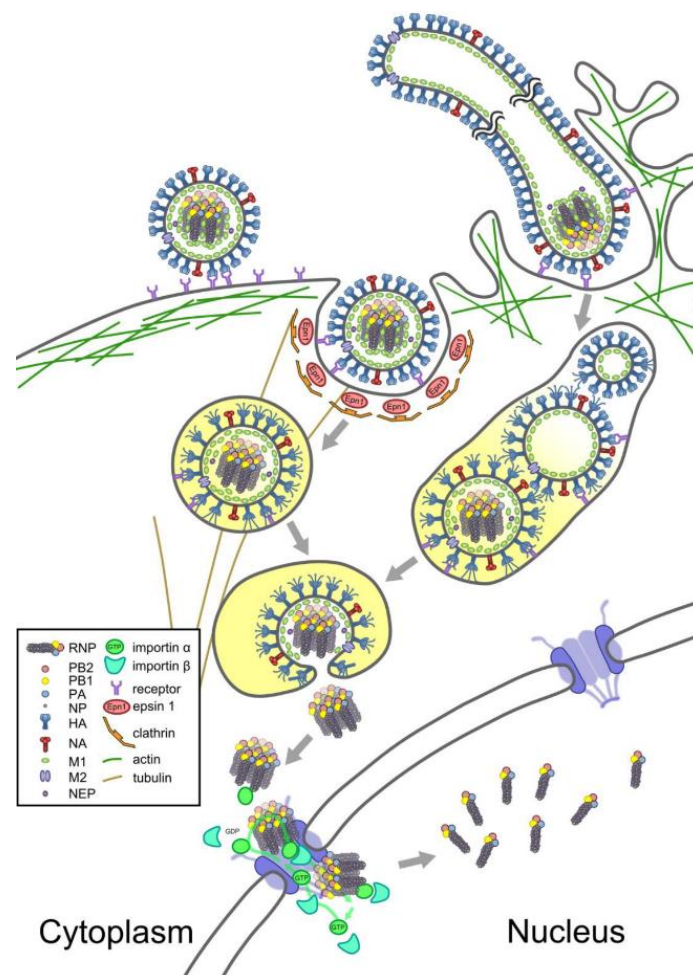
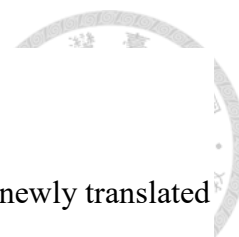


**Figure 9.** Transportation of the RNPs from virion to nucleus.<sup>12</sup>



### 1.3.4 Transportation of RNP out of host cell

After synthesis of progeny vRNPs in the nucleus of host cell, the newly translated NEPs are transported from cytoplasm to nucleus through the nuclear pore, without the assistance of importins, and bound to the M1 located on the RNPs (Figure 10).<sup>12</sup> The M1–NEP complex, which is capable of recognizing the exportin Crm1, connects the RNPs to Crm1.<sup>63–66</sup> Next, Crm1 is activated to promote nuclear export by binding to Ran-GTP, which is generated by the chromatin-bound Ran guanine exchange factor Rcc1.

As the RNPs are exported from nucleus to cytoplasm, the human immunodeficiency virus Rev binding protein (HRB) dissociates Crm1–Ran-GTP from the RNPs.<sup>67</sup> RNPs bind to recycling endosomes (RE) at the surrounding region of the nucleus by mediation of active (GTP-bound) Rab11, a GTPase that attaches to RE and PB2 subunit of the RNA polymerase.<sup>68–72</sup> The interaction of Rab11 with RE promotes not only the vesicular transportation of the RNPs from cytoplasm to cell membrane along the microtubule network extended from the microtubule organizing center (MTOC) but also aggregation of the RNPs.<sup>69–71</sup> Finally, the aggregated RNP complexes are released from RE through hydrolysis of GTP, transferring Rab11 to its inactive (GDP-bound) form.

Eight RNPs containing specific viral RNA segments are packaged and assembled with other viral proteins to form a sphere- or filament-shaped virion, which leaves the host cell by budding. The NAs and HAs densely load on the cell membrane and extrude outwards from the host cell, leading to the budding formation and termination through membrane disconnection.<sup>73</sup>

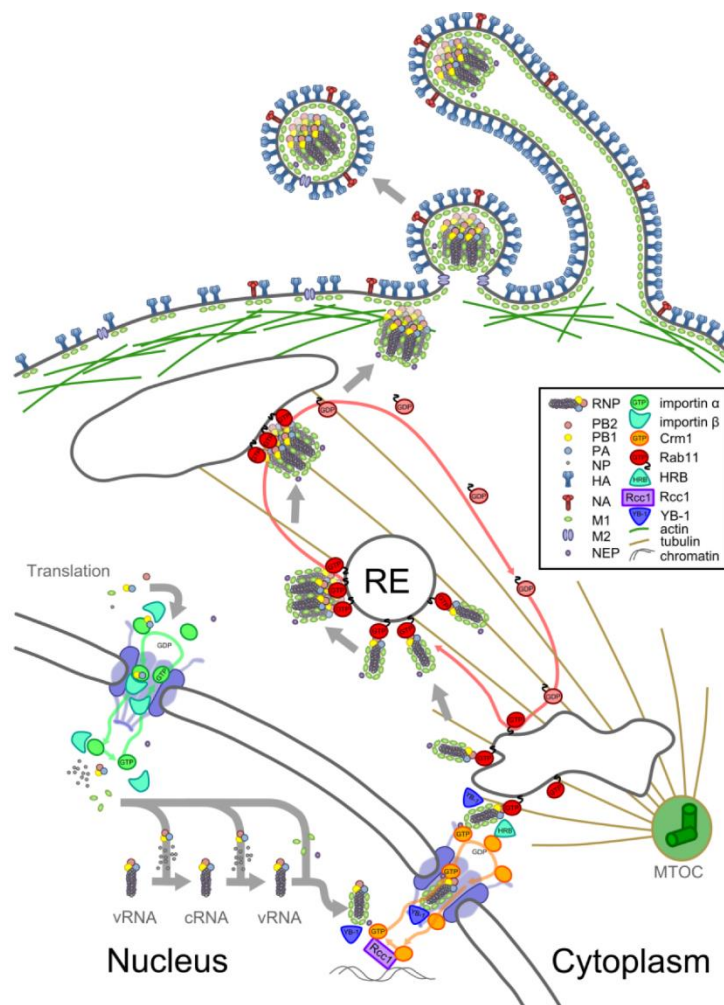


**Figure 10.** Transportation of the progeny RNPs out of host cell from nucleus.<sup>12</sup>

## 1.4 Anti-influenza drugs targeting the RNP

As the RNP is indispensable in the virus life cycle, interference of the interactions among the RNA polymerase, NP and the viral RNA segment is regarded as a feasible approach to design anti-influenza drugs. These interactions have also been investigated. Ortin et al. have constructed the three-dimensional structure of a biologically active recombinant mini-RNP, which contains only 248 nucleotides.<sup>16</sup> From the cryo-electron microscope image, the model recombinant RNP features a ring structure comprising nine NPs, and two of them attach to the RNA polymerase. The specific interactions among the model recombinant RNP are also determined by mutational analyses and by docking the atomic structures of NPs and the RNA polymerase into its cryo-electron microscope structure (Figure 11).<sup>16</sup>

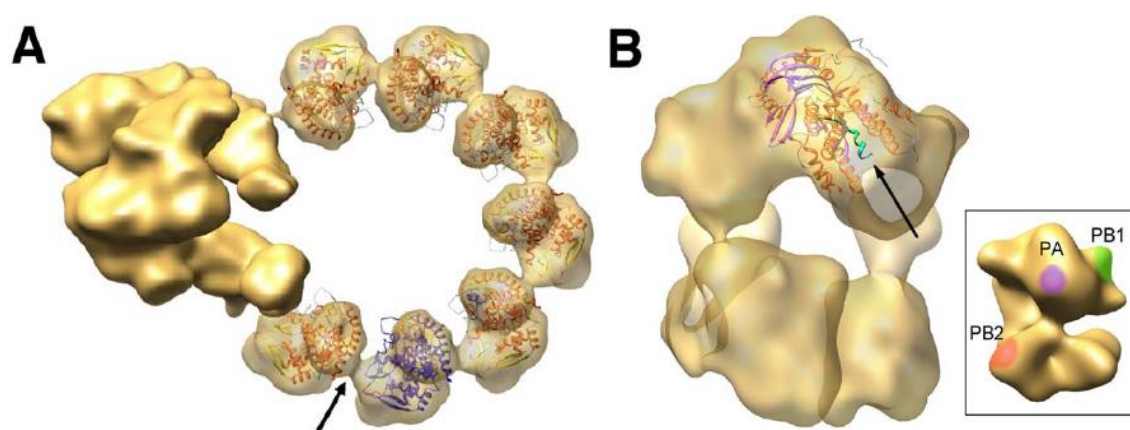


**Figure 11.** Docking the atomic structure of (A) NPs and (B) RNA polymerase into the RNP model.<sup>16</sup>

### 1.4.1 Interactions between RNA and RNA polymerase in RNP

The 3' and 5' ends of viral RNA segment, which contain the partially complementary and conserved sequences, are associated with the RNA polymerase to form a panhandle structure.<sup>33</sup> Brownlee et al. have investigated the binding sites on the viral RNA segment. They prepare individual transversions or insertions mutants at each nucleotide of the 3' and 5' ends of the conserved sequences to examine their bindings with RNA polymerase. The cross-linking is analyzed by immunoprecipitation. According to obvious decreased binding, the binding sites are determined to locate on the positions 9–12 of the 3' end and the positions 1'–3' and 8'–11' of the 5' end (Figure 12).<sup>33, 74</sup>

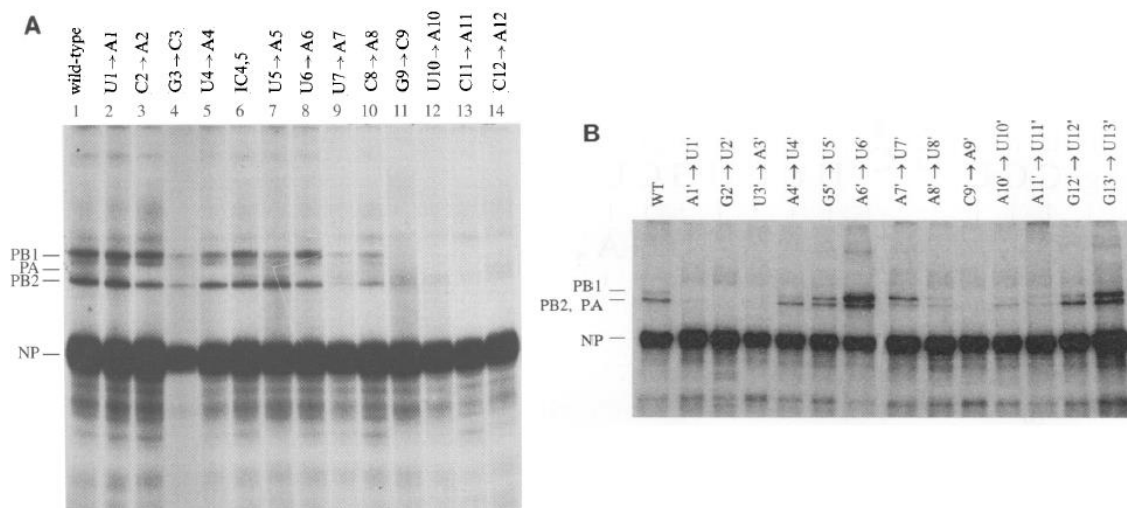


**Figure 12.** Effect of point mutations and insertions on the RNA polymerase binding of the conserved sequences at (A) the 3' end and (B) the 5' end.<sup>33, 74</sup>

## 1.4.2 Interactions between NP and RNA polymerase in RNP

It has been reported that NP binds to the PB1 and PB2 subunits but not PA subunit of the RNA polymerase.<sup>20</sup> Furthermore, Marklund et al. have investigated the binding sites on NP. They prepare the double-alanine mutants in the A to E regions to show that the NP mutant in the B region suppresses the activity of viral RNA synthesis (Figure 13A and 13B).<sup>23</sup> They further use a series of NPs having single mutation in the B region to test the activity of NP. The results demonstrate that amino acids R204, W207, and R208 in the head domain of NP are essential for binding with RNA polymerase (Figure 13C and 13D).<sup>23</sup>

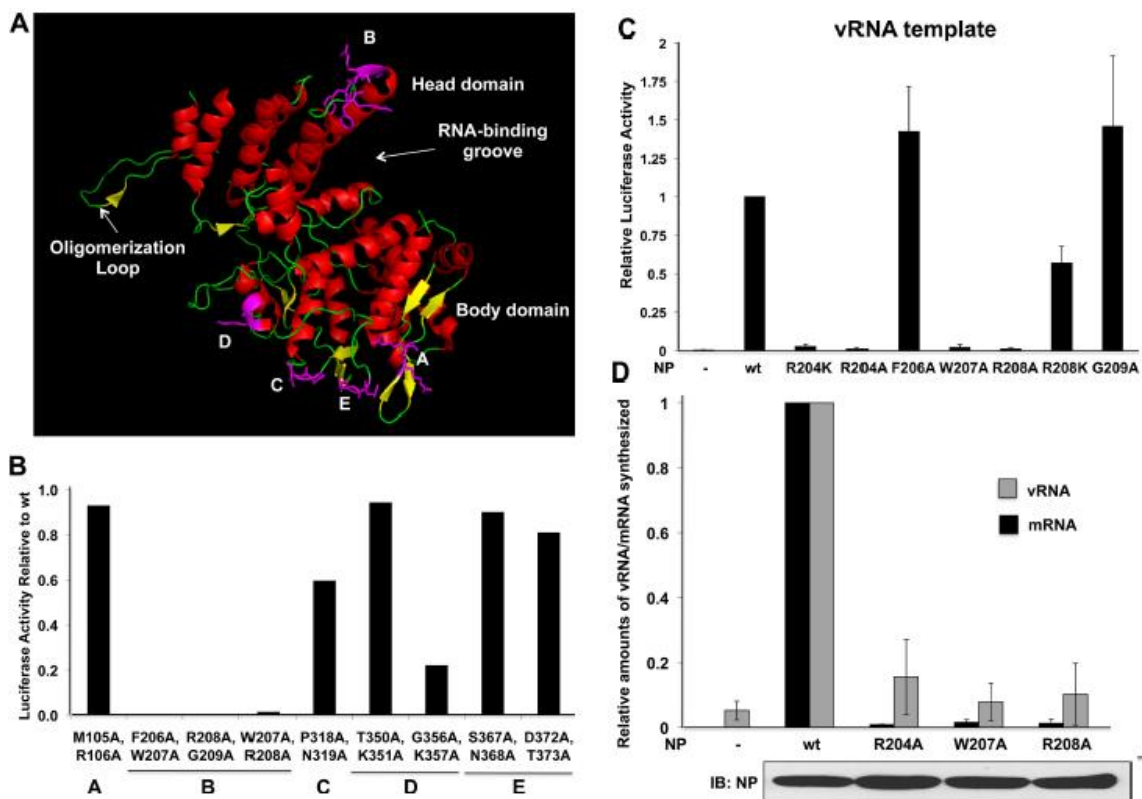


**Figure 13.** (A) The crystal structure of NP. (B) The activities of the NP mutants in the



minigenome dual-luciferase assay. (C) The activities of the NP mutants in the vRNA template minigenome assay. (D) Relative amounts of vRNA and mRNA produced by the NP mutants in the cRNA template minigenome assay.<sup>23</sup>

### 1.4.3 Interactions between NP and viral RNA segment in RNP

The binding sites of viral NP to RNA segment are located on a positive electrostatic groove between the head and body domains (Figure 14).<sup>21</sup> By mutational analysis, many basic amino acids including R65, R150, R152, R156, R174, R175, R195, R199, R213, R214, R221, R236, R355, K357, R361 and R391 on the surface of the groove are required for binding with viral RNA.<sup>75</sup> These basic amino acids bind to the viral RNA segment by the electrostatic interactions with the negatively charged phosphodiester backbone.

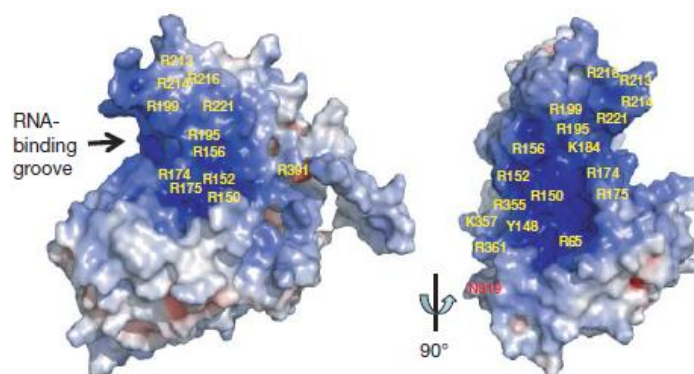


**Figure 14.** Electrostatic potential distribution of NP. Positive and negative electrostatic potentials are shown in blue and red, respectively.<sup>21</sup>



#### 1.4.4 Interactions between NP monomers in RNP

NPs most commonly exist as trimers. It is thought that the NP oligomerization is majorly derived by the interactions between the tail loop of NP with the binding pocket of another NP (Figure 15).<sup>21</sup> There are two more factors to regulate the NP oligomerization, including maintenance of the tail loop conformation and stabilization of the NP oligomer.<sup>76</sup>

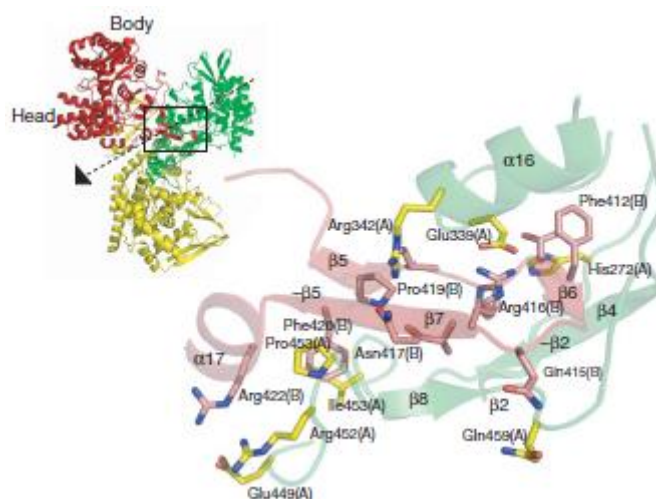


**Figure 15.** Inter-subunit interactions mediated by the tail loop.<sup>21</sup>

Several interactions for the NP oligomerization have been investigated by mutational analysis and docking experiments.<sup>16, 25, 26, 27, 76</sup> One of the most important interactions is the E339...R416 salt bridge interaction. Ye et al. prepare the E339A mutant in the binding pocket, R416A mutant in the tail loop and the  $\Delta$ 402–428 tail loop deletion mutant for the minigenome assay. According to the obvious decreased



activities in viral RNA synthesis, the results confirm that the E339...R416 salt bridge interaction is essential for the NP oligomerization (Figure 16).<sup>26</sup>

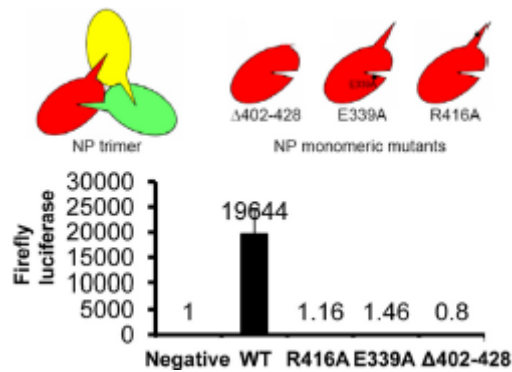


**Figure 16.** Viral RNA synthesis activities of NP mutants by the minigenome assay.<sup>26</sup>

Ye and coworkers have also found a new interaction other than the tail loop-binding pocket interaction by gel filtration chromatography (Figure 17A).<sup>26</sup> The diagram shows that the tail loop deletion NP mutant mostly exists as monomer; but surprisingly, NP dimer is observed. They thus investigate the interactions of the Y487R, Y487D, and D491A mutants by minigenome assay. According to the obvious decreased activities in viral RNA synthesis, all the three amino acids are required for the interaction to form the NP dimer (Figure 17C).<sup>26</sup> Consistent with this result, gel filtration chromatography indicates that NP dimer is not formed in the presence of the NP mutants containing D491A mutation (Figure 17B).<sup>26</sup>

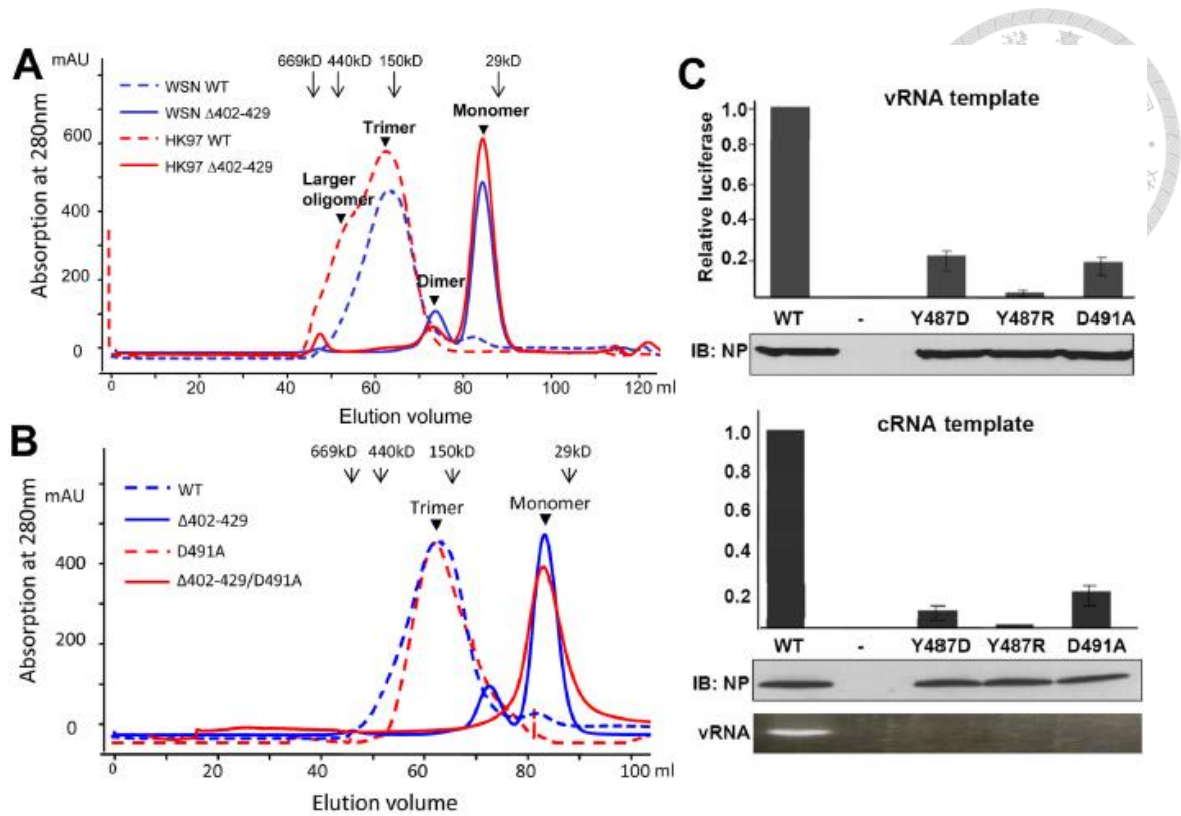


**Figure 17.** (A) Oligomerization behavior of NP tail loop mutants as shown by gel filtration chromatography. (B) Oligomerization behavior of NP D491 mutants as shown by gel filtration chromatography. (C) RNA synthesis activities of NP mutants determined in the vRNA- and cRNA-templated minigenome assays.<sup>26</sup>

## 1.5 Photoaffinity labeling

The concept of photoaffinity labeling was initially described in 1969.

Photoaffinity labeling is a technique generally applied in investigating the structural characteristics of a compound in the function of biological systems, such as identification of the pharmacophore binding sites and isolation of unknown receptors or enzymes. Photoaffinity labeling uses a photoreactive group to capture the target molecule, particularly proteins, through a photo-triggered cross coupling reaction. The ideal photoaffinity labeling contains following properties: (1) high stability under various pH conditions in the dark; (2) similar activity to original pharmacophore; (3) activation by specific wavelength without damage to biological sample; (4) generation of highly reactive species upon irradiation; (5) no preference to couple with any kind of amino acids; and (6) a stable coupling product for subsequent analyses. Nevertheless, to date, there is no photoaffinity labeling that fulfills all the above-mentioned properties.

A representative photoaffinity labeling probe includes three parts: a photoreactive group, a pharmacophore in the core structure and a reporter unit. Aryl azide and diazirine derivatives are widely utilized as photoreactive groups. Biotin, fluorophores and radioactive isotopes are widely used as reporter units. In the process of photoaffinity labeling, a photoaffinity agent is first incubated with the biological target.

Upon irradiation, the photoreactive group generates highly reactive species to react with

the target protein by covalent bond formation. Afterward, the reporter unit is detected to identify the biological targets<sup>77</sup> (Figure 18).

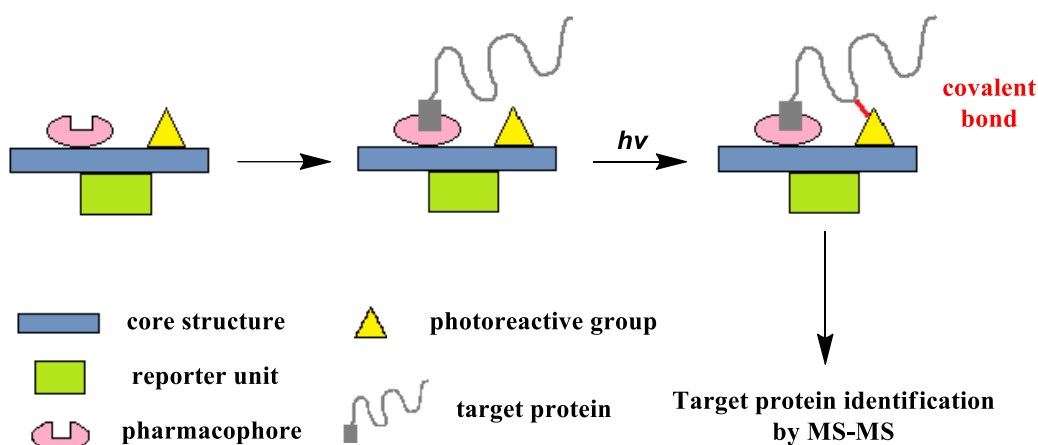
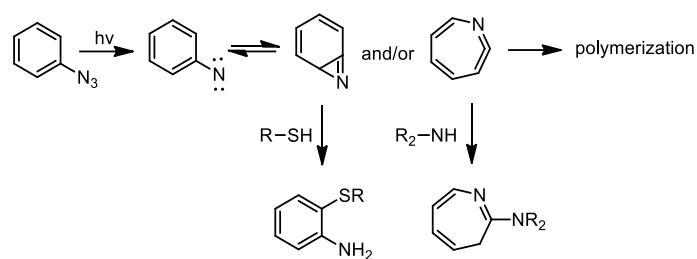


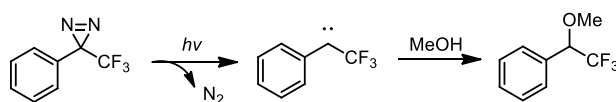
**Figure 18.** A cartoon representation for the process of photoaffinity labeling.

Aryl azide derivatives, which are commonly prepared from their commercially available synthons, are stable in the dark, but highly reactive upon irradiation. Upon irradiation, aryl azide is photolyzed to produce a reactive singlet phenylnitrene for cross coupling reaction with the target protein (Scheme 1). Nevertheless, the singlet phenylnitrene may proceed with side reactions through a ring expansion and form 1,2-didehydroazepine derivatives by nucleophilic attack. The singlet phenylnitrene may also form dimeric product by intersystem crossing (ISC) to the triplet state (<sup>3</sup>N). The maximum absorption wavelength of aryl azide is under 280 nm; irradiation at 280 nm will impair the biological systems.<sup>78</sup>



**Scheme 1.** Photolysis of aryl azide.

Diazirine group is another suitable photoreactive group less frequently used than aryl azide group, because the synthesis of diazirine derivatives is much more complicated.<sup>79</sup> Upon irradiation, diazirine is photolyzed to produce a highly reactive singlet carbene for forming a covalent bond with the target protein through C–C, C–H, O–H or X–H (X = heteroatom) insertion (Scheme 2). Nevertheless, the produced singlet carbene may also be quenched by water, causing a low labeling yield. The maximum absorption wavelength of diazirine is around 350–380 nm with lower energy than that of aryl azide, thus causing less damage to the biological systems.



**Scheme 2.** Photolysis of diazirine.

## 1.6 Previous research on anti-influenza agents targeting NP trimerization

To search for a feasible target for designing new anti-influenza drugs, a research team in Academia Sinica focuses on interference with the E339...R416 salt bridge interaction between the tail loop and the binding pocket of NP (Figure 19A).<sup>25</sup> This salt bridge interaction is essential for formation of NP trimers and oligomers by mutational analysis, which shows that the E339A, R416A and tail loop mutants possess appreciable decreased activities in RNA transcription and replication.

They have also conducted a high-throughput screening to identify some small molecules as anti-influenza agents by disrupting the NP–NP interaction. As a result, compound **A** performs the best inhibitory effect (Figure 19B).<sup>25</sup> Furthermore, the computer modeling of the NP–**A** complex (Figure 19C)<sup>25</sup> shows that the benzene ring of compound **A** interacts with Phe304, Trp330, Ala336 and Ala387 in a hydrophobic site originally occupied by Phe412 of the tail loop through  $\pi$ – $\pi$  stacking or hydrophobic interactions, and the (anilinothiazole)carboxamide group of compound **A** can mimic Arg416 of the tail loop to interact with Glu339 through salt bridge interaction. Additionally, the (morpholino)propyl group of compound **A** can be docked into the pocket site that is originally occupied by Ile408 and Pro419 of the tail loop.

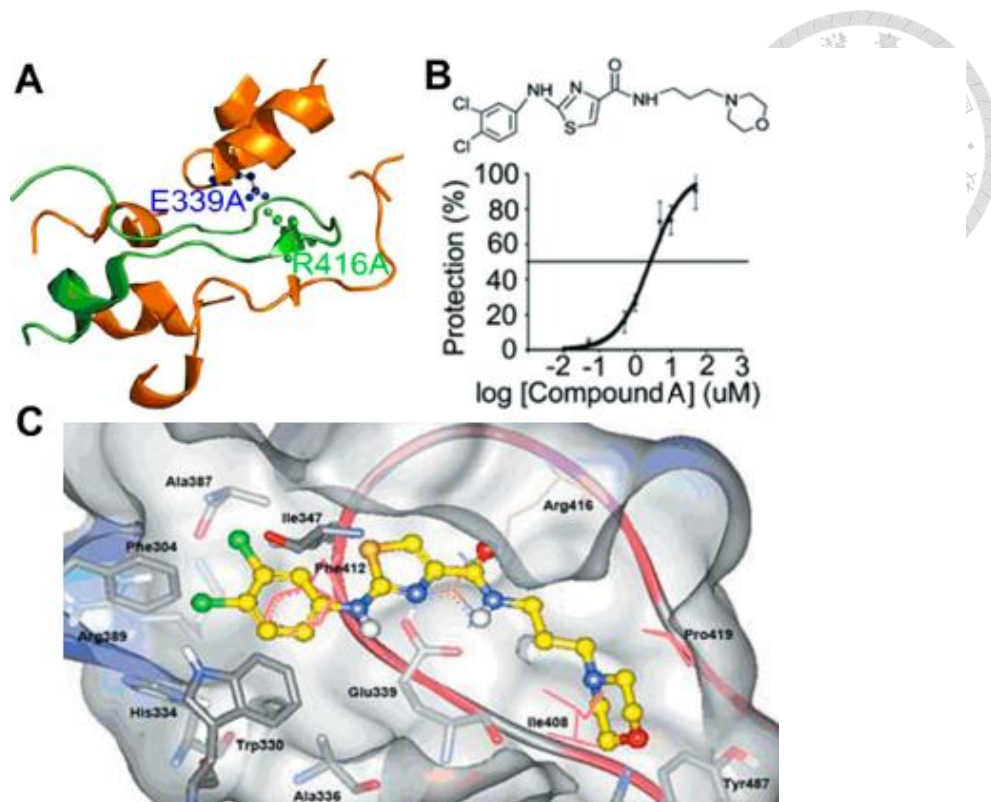
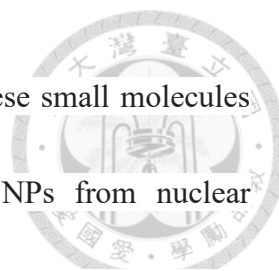


**Figure 19.** (A) Interactions including the tail-loop (green) and its binding pocket (gold). (B) Structure and inhibitory effect of compound A. (C) The modeled structure of the NP–A complex.<sup>25</sup>

Additionally, there are other studies on NP small molecule inhibitors. Some research groups recently reported that the small molecules bearing aryl piperazine amide structures were leading agents through high-throughput screening of a chemical library.<sup>80–86</sup> From bioassay, nucleozin, compounds **B** and **C** containing the moiety of isoxazole phenyl ring, showed efficient anti-influenza activity against A/WSN/33 H1N1 influenza virus. The isoxazole ring structure could be replaced by a triazole ring to produce compounds **D** and **E**, which also displayed similar



anti-influenza effect (Figure 20).<sup>80</sup> The inhibitory mechanism of these small molecules has been revealed. The NP inhibitors restrain the RNPs and NPs from nuclear accumulation because the formation of higher-order NP oligomers would prevent their migration from cytoplasm into nucleus.<sup>81–84</sup> The excessive NP aggregation was confirmed by native polyacrylamide gel electrophoresis (PAGE),<sup>82</sup> dynamic light-scattering (DLS)<sup>84</sup> and analytical ultracentrifugation (AUC).<sup>83</sup>

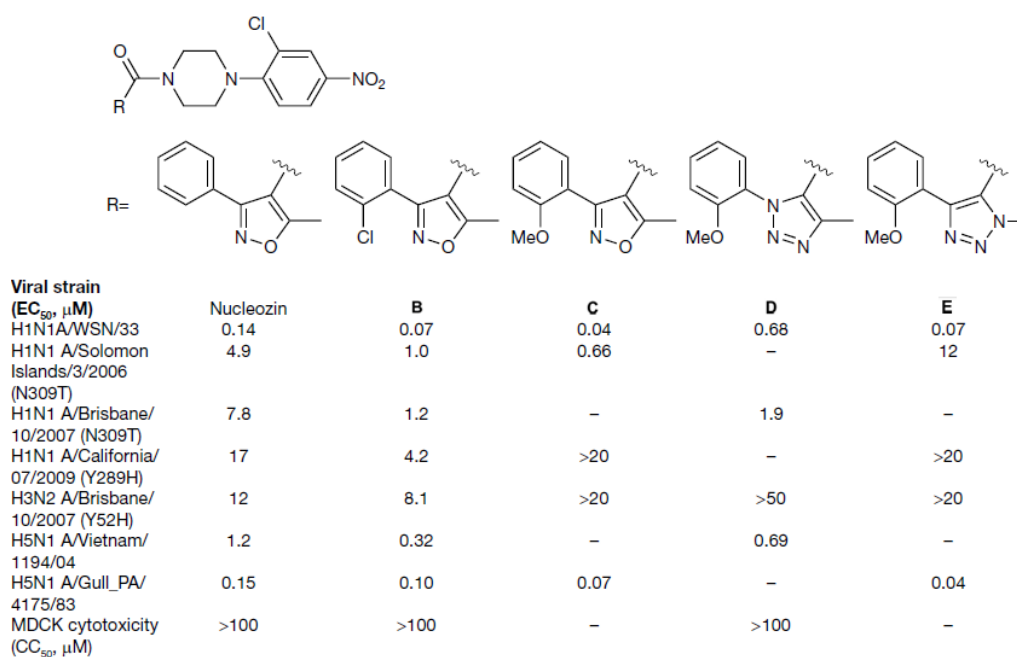
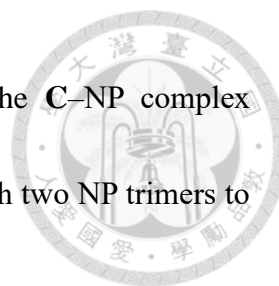


**Figure 20.** Small molecules that inhibit viral replication via binding to NP.<sup>80</sup>

The binding sites between NP and these small molecules have also been investigated through docking model and mutational analysis.<sup>82–84</sup> Several studies demonstrated that two binding pockets Y52 and Y289/N309 play important roles in the





binding mode (Figure 21).<sup>80</sup> The co-crystal X-ray structure of the C–NP complex further showed that six molecules of compound C are associated with two NP trimers to form (NP A)–(NP B) dimeric trimers (i.e. hexamer) (Figure 22).<sup>84</sup>

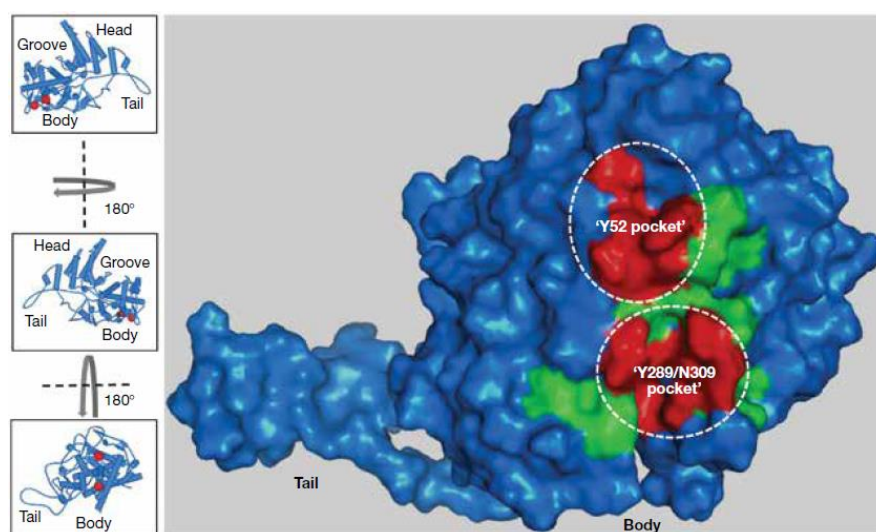


**Figure 21.** NP surface map of residues affecting aryl piperazine amide efficacy.<sup>80</sup>

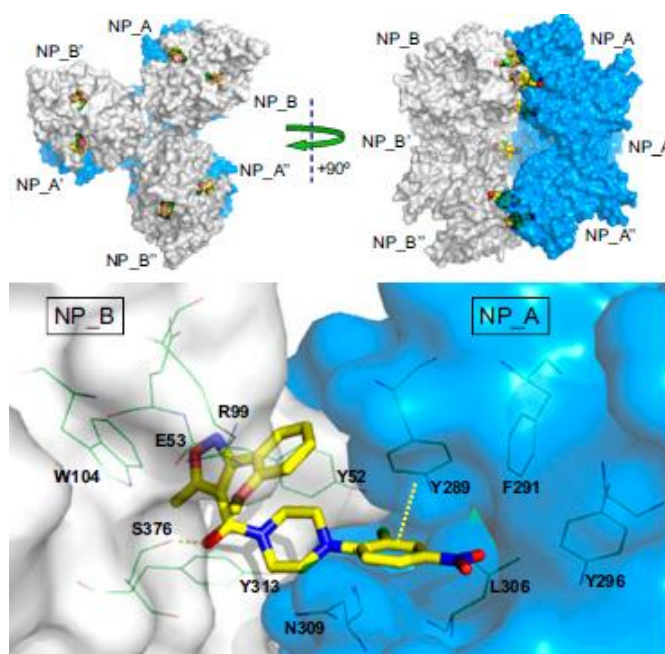


**Figure 22.** X-ray structure of C–NP complex.<sup>84</sup>

## Chapter 2. Results and Discussion



### 2.1 Research motivation

In the recorded history, several devastating influenza outbreaks have stimulated the development of new anti-influenza drugs. The virus RNP plays a crucial role in virus life cycle, and destroying the bindings of NP–NP, NP–RNA or NP–RNA polymerase, which have been reported to effectively suppress the propagation of influenza viruses, can serve as feasible targets for design of anti-influenza drugs.

Because NP is substantially more conserved than other targets, such as viral RNA, RNA polymerase and NA, in various influenza virus subtypes, we aim to develop new anti-influenza drugs by disrupting the NP–NP interaction that inhibits the formation of NP trimer and oligomer.

We expect to synthesize small molecules, which can competitively displace the tail loop of NP from the binding pocket and enhance the inhibitory effects on influenza A virus.

### 2.2 Strategy for designing effective anti-influenza drugs

According to the result of previous research (Section 1.6), we design the anti-influenza drug targeting NP trimerization based on the structure of compound **A**. From the model structure of the NP–**A** complex (Figure 19C), the design can be divided

into three parts: (1) the benzene ring on the left hand side, (2) the heterocycle in the middle, and (3) the aliphatic group on the right hand side (Figure 23). The benzene ring structure would interact with the amino acid residues in the binding pocket through  $\pi$ - $\pi$  stacking or hydrophobic interactions. The heterocycle structure would mimic R416 of the tail loop to interact with E339 through salt bridge interaction. In addition, the aliphatic groups probably interact with the amino acid residues in the binding pocket through hydrogen bonding or hydrophobic interactions.

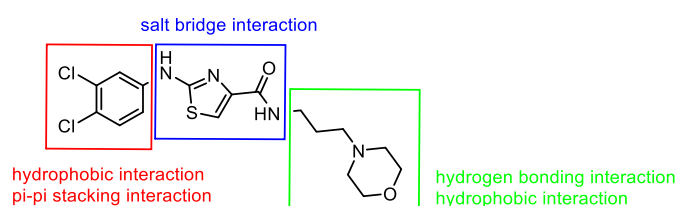


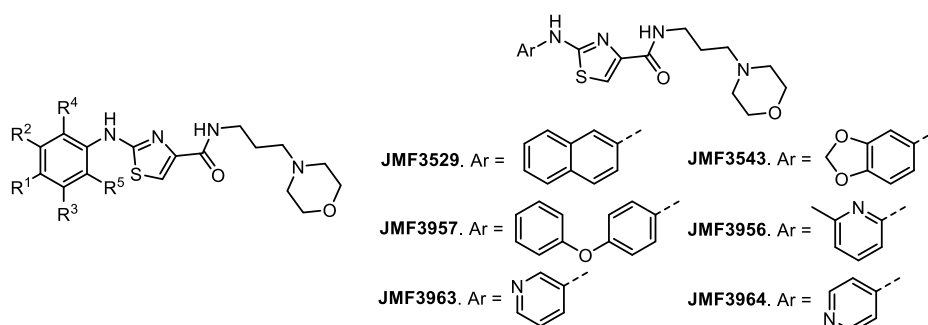
**Figure 23.** The strategy for designing anti-influenza drugs based on the structure of compound **A**.

In the previous work of our group, the analogs of compound **A** containing various substituents on the benzene ring have been examined (Table 1). As a result, compound **A** with 3,4-dichlorobenzene moiety still displays the best inhibitory effect against H1N1 influenza virus with  $EC_{50} = 1.6 \mu\text{M}$ . The compound having a chlorine atom at *para*-position ( $R^1$ ), such as JMF3367 and JMF3544, also shows similar activity. When the benzene ring is replaced with other aromatic rings, only the naphthalene derivative

(JMF3529) displays the inhibitory effect compatible with compound **A**.



**Table 1.** Anti-influenza EC<sub>50</sub> values (μM) of compound **A** analogs.



Compound	R <sup>1</sup>	R <sup>2</sup>	R <sup>3</sup>	R <sup>4</sup>	R <sup>5</sup>	EC <sub>50</sub> (μM)
<b>A</b>	Cl	Cl	H	H	H	1.6
<b>JMF3366</b>	H	H	H	H	H	> 10 <sup>2</sup>
<b>JMF3367</b>	Cl	H	H	H	H	2.4
<b>JMF3368</b>	H	Cl	H	H	H	> 10 <sup>2</sup>
<b>JMF3515</b>	CH <sub>3</sub>	CH <sub>3</sub>	H	H	H	9.6
<b>JMF3528</b>	F	F	H	H	H	> 10 <sup>2</sup>
<b>JMF3544</b>	Cl	Cl	Cl	H	H	2.3
<b>JMF3545</b>	NO <sub>2</sub>	H	H	H	H	> 10 <sup>2</sup>
<b>JMF3590</b>	CN	H	H	H	H	> 10 <sup>2</sup>
<b>JMF3664</b>	CH <sub>3</sub>	H	H	H	H	> 10 <sup>2</sup>
<b>JMF3665</b>	F	H	H	H	H	> 10 <sup>2</sup>
<b>JMF3715</b>	Cl	H	H	Cl	H	> 10 <sup>2</sup>
<b>JMF3716</b>	Cl	H	H	Cl	Cl	> 10 <sup>2</sup>
<b>JMF3773</b>	OMe	H	H	H	H	> 10 <sup>2</sup>
<b>JMF3774</b>	OH	H	H	H	H	> 10 <sup>2</sup>
<b>JMF3775</b>	Br	H	H	H	H	10.0
<b>JMF3785</b>	CF <sub>3</sub>	H	H	H	H	> 10 <sup>2</sup>
<b>JMF3906</b>	SMe	H	H	H	H	> 10 <sup>2</sup>

Compound	EC <sub>50</sub> (μM)	Compound	EC <sub>50</sub> (μM)	Compound	EC <sub>50</sub> (μM)
<b>JMF3529</b>	6.1	<b>JMF3957</b>	> 10 <sup>2</sup>	<b>JMF3963</b>	> 10 <sup>2</sup>
<b>JMF3543</b>	> 10 <sup>2</sup>	<b>JMF3956</b>	> 10 <sup>2</sup>	<b>JMF3964</b>	> 10 <sup>2</sup>

Besides the thiazole ring in the middle of compound **A**, imidazole, pyridine and pyrimidine have been used as the alternative heterocycles. From the bioassay results, we found that the thiazole and pyrimidine derivatives (compound **A** and JMF3706) display high inhibitory effects. Consequently, the compounds containing thiazole and pyrimidine cores are promising choices for designing anti-influenza drugs (Figure 24).

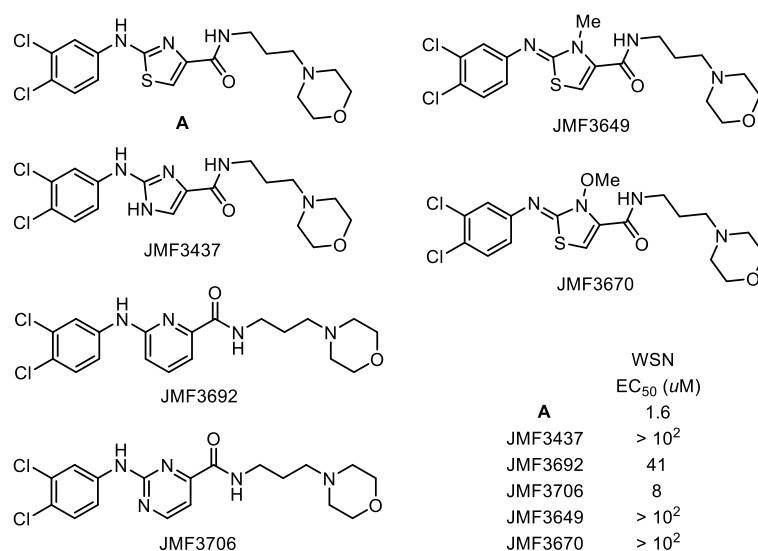
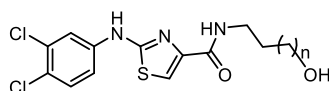


**Figure 24.** Bioassay of compound **A** and its derivatives with different heterocycle core structures.

The compound **A** analogs with aliphatic chain of different lengths, including ethyl, propyl, butyl, pentyl and hexyl groups, on the right hand side have been synthesized for bioassay. The propyl derivative (JMF4022) displays the highest inhibitory effect, indicating the chain length of propyl group is the most suitable distance for designing

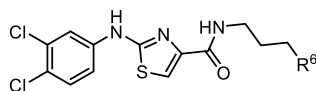
drug (Figure 25).



	WSN
	EC <sub>50</sub> (μM)
JMF4068, n = 0	> 10 <sup>2</sup>
JMF4022, n = 1	2.6
JMF4089, n = 2	> 10 <sup>2</sup>
JMF4090, n = 3	> 10 <sup>2</sup>
JMF4091, n = 4	> 10 <sup>2</sup>

**Figure 25.** Bioassay of compound **A** analogs with various aliphatic chain lengths.

Furthermore, a number of functional groups located at the terminal of aliphatic chain have also been investigated. From the bioassay result, the derivatives JMF3804, JMF3805, JMF3922 and JMF4022 with the functional groups capable of forming hydrogen bonds display high inhibitory effects, while the alkyl derivative JMF3960 is inactive (Figure 26).



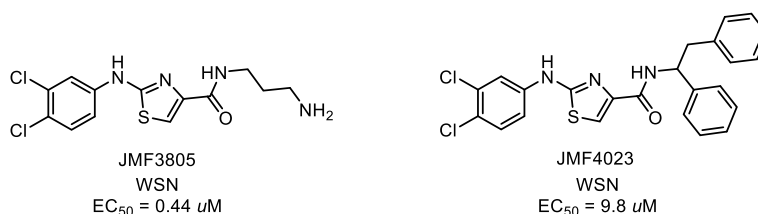
	WSN
	EC <sub>50</sub> (μM)
JMF3803, R <sup>6</sup> = Cl,	2.7
JMF3804, R <sup>6</sup> = N <sub>3</sub> ,	1.4
JMF3805, R <sup>6</sup> = NH <sub>2</sub> ,	0.44
JMF3960, R <sup>6</sup> = CH <sub>3</sub> ,	>10 <sup>2</sup>
JMF3922, R <sup>6</sup> = OMe,	1.1
JMF4022, R <sup>6</sup> = OH,	2.6

**Figure 26.** Bioassay of derivatives with various terminal functional groups.

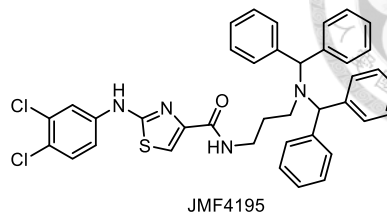
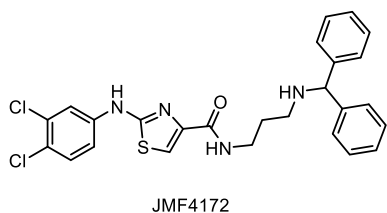
In summary, the 3,4-dichloro anilino-thiazole-carboxamide structure of compound **A** serves as one of the best choices for designing effective anti-influenza drugs, and introduction of proper functional groups at the terminal of propyl chain is favorable by providing hydrogen bondings.

### 2.3 Modifications at terminal amine group

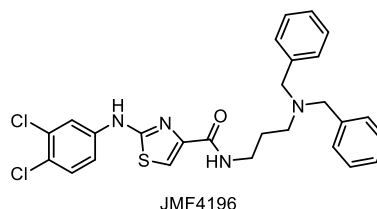
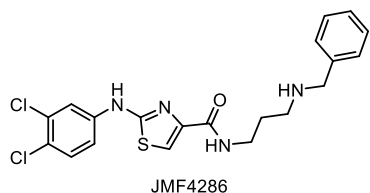
Because of the high inhibitory effects of the compounds with free amino (JMF3805) or 1,2 diphenylethyl group (JMF4023), the terminal group probably interacts with the amino acid residues in the binding pocket through not only hydrogen bondings but also  $\pi$ - $\pi$  stacking or hydrophobic interactions. Therefore, we designed and synthesized a few (1,1-diphenylmethyl)amino and benzylamino derivatives as drug candidates that might enhance the hydrogen bonding,  $\pi$ - $\pi$  stacking or hydrophobic interactions with influenza nucleoprotein. The designed drug candidates including **13a** (JMF4172), **13b** (JMF4195), **22a** (JMF4286) and **22b** (JMF4196) still have the 3,4-dichloroanilino-thiazole-carboxamide structure and preserve the propyl chain.



(1,1-Diphenylmethyl)amino derivative targets:



Benzylamino derivative targets:

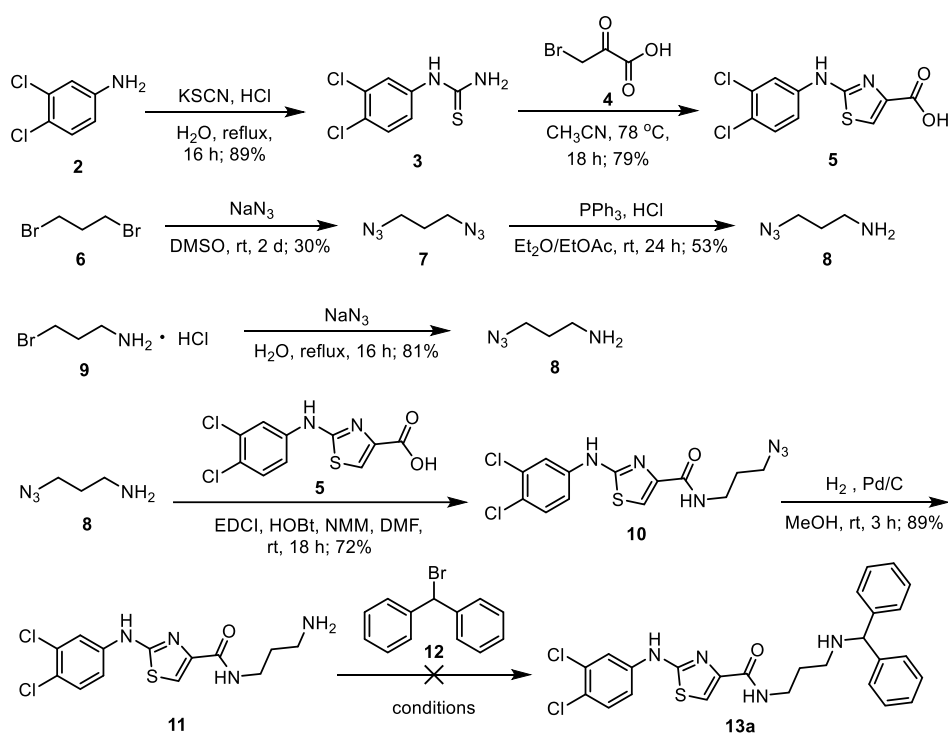


## 2.4 Synthesis of (1,1-diphenylmethyl)amino derivatives **13a** and **13b**

In our first synthesis of (1,1-diphenylmethyl)amino derivative **13a** (Scheme 3), 3,4-dichloroaniline (**2**) was firstly reacted with potassium isocyanate in the presence of HCl at 100 °C for 16 h to give the thiourea compound **3**, which then proceeded to a cyclization reaction with 3-bromopyruvic acid (**4**) at 78 °C for 18 h to give (anilinothiazole)carboxylic acid **5** for the subsequent amide coupling reaction. On the other hand, the amine counterpart for the amide coupling reaction was prepared. The S<sub>N</sub>2 reaction of 1,3-dibromopropane (**6**) with sodium azide was performed at room temperature for two days to provide 1,3-diazidopropane (**7**). Without further purification, compound **7** was immediately subjected to Staudinger reaction with one equivalent of



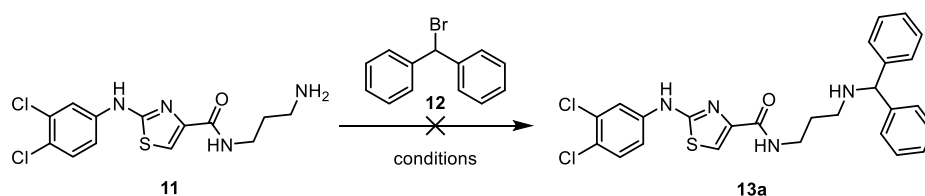
triphenylphosphine at room temperature for 24 h to afford 3-azidopropan-1-amine (**8**) through the reduction of one of the azido substituents.<sup>87, 88</sup> However, the triphenylphosphine oxide side product was quite difficult to be removed from the reaction mixture. Alternatively, 3-bromopropylamine (as the hydrochloride salt **9**) was reacted with sodium azide at 100 °C for 16 h to give 3-azidopropan-1-amine (**8**),<sup>89</sup> which underwent the amide coupling reaction with carboxylic acid **5** at room temperature for 18 h to give amide **10**. The azide reduction was performed in MeOH at room temperature for 3 h under an atmosphere of hydrogen using palladium on activated charcoal as the catalyst to give the amino compound **11**.



**Scheme 3.** First synthetic strategy for (1,1-diphenylmethyl)amino derivative **13a**.

Nevertheless, compound **13a** could not be obtained through the S<sub>N</sub>2 reaction of amino compound **11** with bromodiphenylmethane (**12**) in various conditions using different bases, solvents, temperatures and additives (Table 2). Using K<sub>2</sub>CO<sub>3</sub> as base, MeCN or DMF as solvent, no reaction occurred at room temperature (entries 1 and 3). Recovery of compound **11** was confirmed by mass, <sup>1</sup>H and <sup>13</sup>C NMR spectra. A complicated mixture resulted at elevated temperature (entries 2 and 4). No desired product was shown by thin-layer chromatography (TLC). The alkylation reaction also failed by using *N,N*-diisopropylethylamine (DIEA) or Et<sub>3</sub>N as the base.

**Table 2.** Unsuccessful S<sub>N</sub>2 reactions of compound **11**.

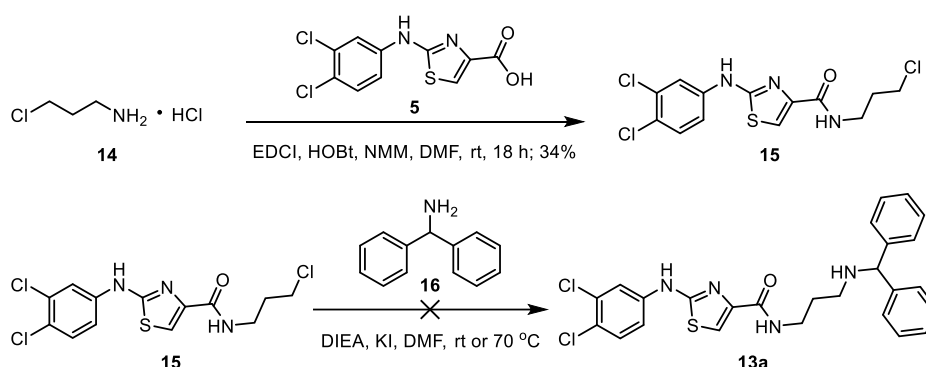


Entry	Solvent	Base	Additive	Temp. (°C)	Time (h)	Result
1	MeCN (anhydrous)	K <sub>2</sub> CO <sub>3</sub>	None	25	24	NR <sup>a</sup>
2	MeCN (anhydrous)	K <sub>2</sub> CO <sub>3</sub>	None	40	18	Messy, no product <sup>b</sup>
3	DMF	K <sub>2</sub> CO <sub>3</sub>	KI	25	18	NR <sup>a</sup>
4	DMF	K <sub>2</sub> CO <sub>3</sub>	KI	70	17	Messy, no product <sup>b</sup>
5	DMF	DIEA	KI	70	24	Messy, no product <sup>b</sup>
6	DMF	Et <sub>3</sub> N	KI	70	26	Messy, no product <sup>b</sup>

<sup>a</sup> NR represents no reaction. <sup>b</sup> Separation by column chromatography.

Compound **15** bearing a chlorine atom was synthesized by the coupling reaction

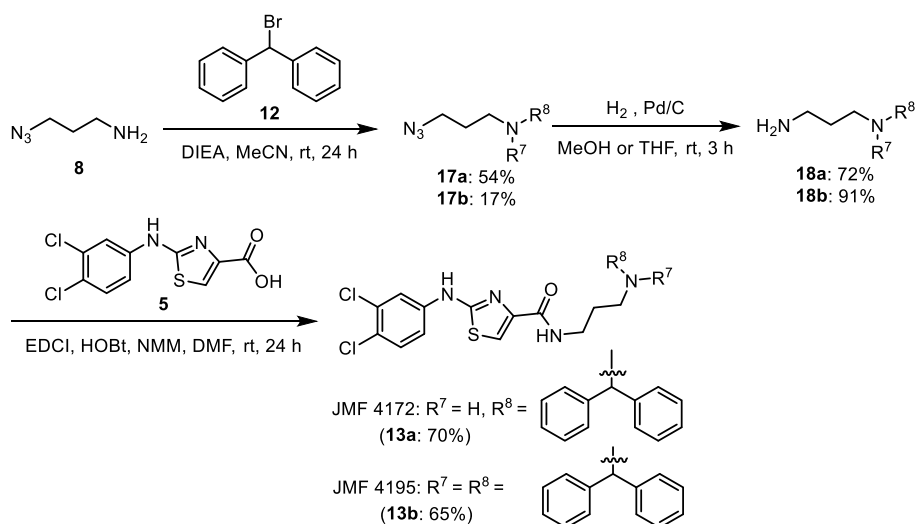
of 3-chloropropylamine (as the hydrochloride salt **14**) with (anilinothiazole)carboxylic acid **5** (Scheme 4). was also prepared for the synthesis of biphenyl derivative **13a** through  $S_N2$  type substitution reaction from the other direction. However, the substitution reaction of **15** with diphenylmethanamine (**16**) still failed to afford (1,1-diphenylmethyl)amino derivative **13a** in the presence of DIEA and KI. No reaction occurred at room temperature, but an incomplete reaction and complicated mixture results at 70 °C without the desired product.



**Scheme 4.** Unsuccessful synthesis of compound **13a** through  $S_N2$  reaction from another direction.

Consequently, a modified synthetic route to compound **13a** was adapted (Scheme 5). Unlike the first synthetic strategy, this synthetic route started with preparation of (diphenylamino)propylamine (**18a**) for the subsequent amide formation with the carboxylic acid **5**. The reaction of 3-azidopropan-1-amine (**8**) with

bromodiphenylmethane (**12**) gave the mono- and dialkylation products **17a** and **17b** in 54% and 17% yields, respectively. The subsequent azide reduction of **17a** and **17b** were performed under an atmosphere of hydrogen using palladium on activated charcoal as catalyst in MeOH or THF solutions to provide diamine compounds **18a** and **18b**, respectively. Finally, compounds **13a** (JMF4172) and **13b** (JMF4195) were successfully synthesized through amide formation between acid **5** and amine **18a** (or **18b**).

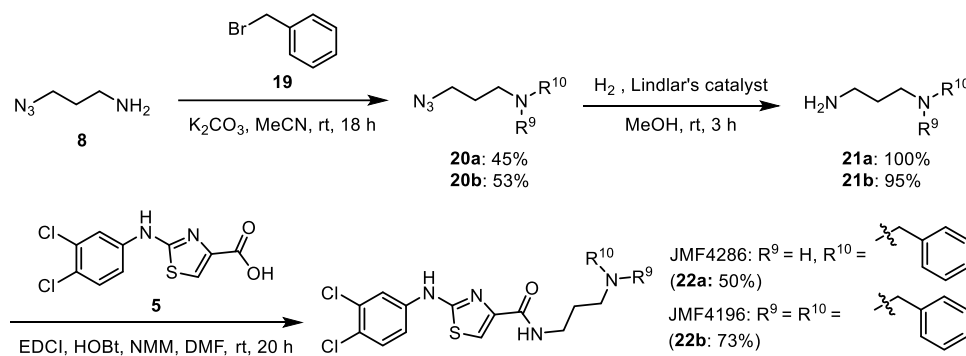


**Scheme 5.** Successful synthesis of compounds **13a** (JMF4172) and **13b** (JMF4195).

## 2.5 Synthesis of benzylamino derivatives **22a** and **22b**

By the procedure similar to that for compounds **13a** and **13b** (Scheme 5), 3-azidopropan-1-amine (**8**) was first reacted with benzyl bromide **19** to give mono- and dialkylation products **20a** and **20b** (Scheme 6). When palladium on activated charcoal was used as catalyst in the azide reduction, no reduction of compound **20b** was

observed in THF solution, and compound **20b** underwent debenzoylation in EtOAc/MeOH (1:3) solution. Therefore, less reactive Lindlar's catalyst was employed for azide reduction of compounds **20a** and **20b** to afford compounds **21a** and **21b**. The coupling reactions of **21a** and **21b** with acid **5** were successfully carried out to afford compounds **22a** (JMF4286) and **22b** (JMF4196).



**Scheme 6.** Synthesis of benzylamino derivatives **22a** (JMF4286) and **22b** (JMF4196).

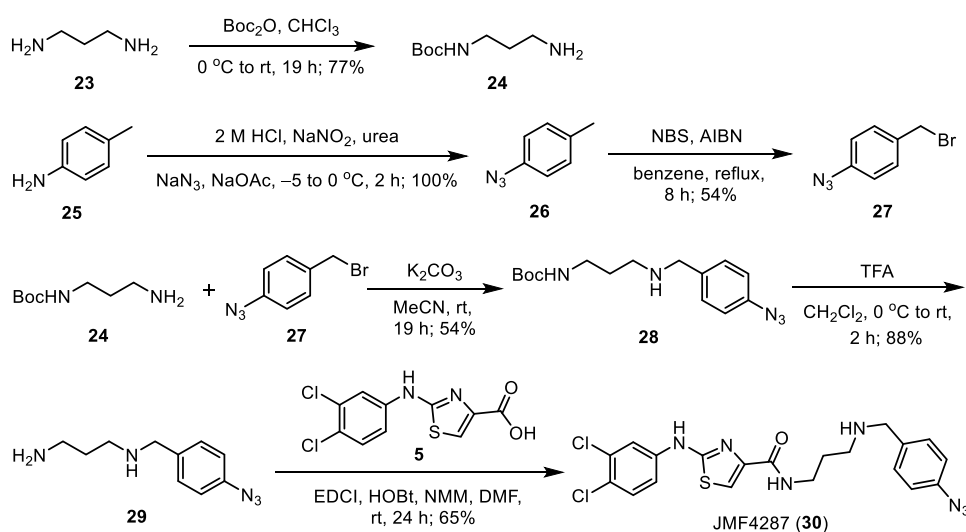
## 2.6 Synthesis of derivatives bearing azidophenyl group for photoaffinity labeling

With the aim to confirm the real binding sites between NP and the above-prepared inhibitors (**13a**, **13b**, **22a**, and **22b**), the derivatives bearing azidophenyl groups were designed and synthesized for photoaffinity labeling experiments.

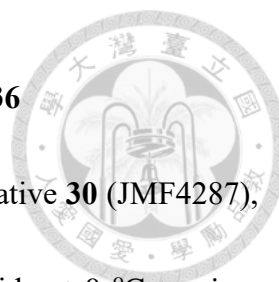
### Synthesis of 4-azidobenzylamino derivative **30**

At first, excess 1,3-diaminopropane **23** (10 equiv) was reacted with di-*tert*-butyl

dicarbonate (Boc<sub>2</sub>O) to provide the mono-Boc protected diamine **24**<sup>90, 91</sup> (Scheme 7). A known method<sup>92</sup> was applied to synthesize 1-azido-4-(bromomethyl)benzene (**27**). Thus, *p*-toluidine (**25**) was reacted with sodium nitrite and sodium azide at 0 °C to give 1-azido-4-methylbenzene (**26**) via the diazonium intermediate. The bromination was carried out using *N*-bromosuccinimide (NBS) as the bromine radical source and azobisisobutyronitrile (AIBN) as the radical initiator to give 1-azido-4-(bromomethyl)benzene (**27**). Afterward, an S<sub>N</sub>2 reaction of amine **24** with the bromo compound **27** was performed in the presence of K<sub>2</sub>CO<sub>3</sub> base to afford the monoalkylation product **28**. The Boc protecting group in compound **28** was removed by treatment with trifluoroacetic acid (TFA) in CH<sub>2</sub>Cl<sub>2</sub> solution, giving amine compound **29**, which underwent a coupling reaction with acid **5** to afford compound **30** (JMF4287) carrying an azidophenyl moiety.

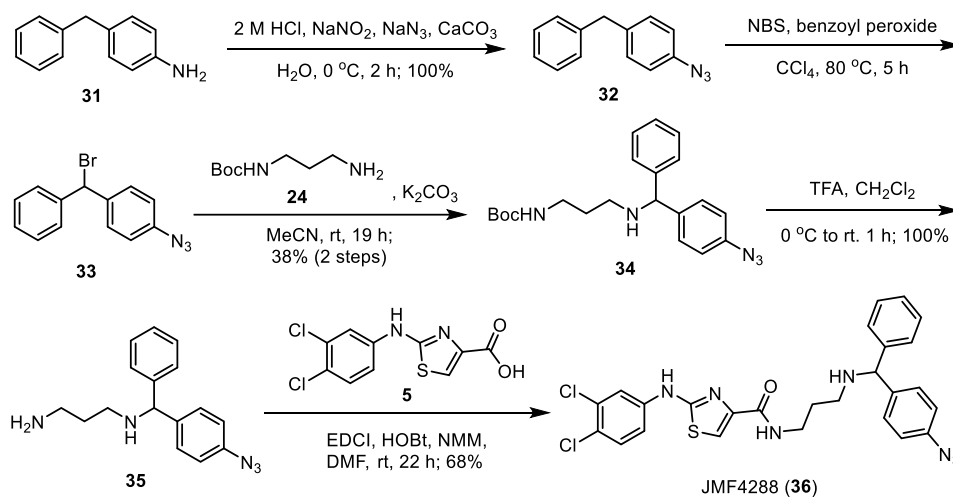


**Scheme 7.** Synthesis of 4-azidobenzyl derivative **30** (JMF4287).



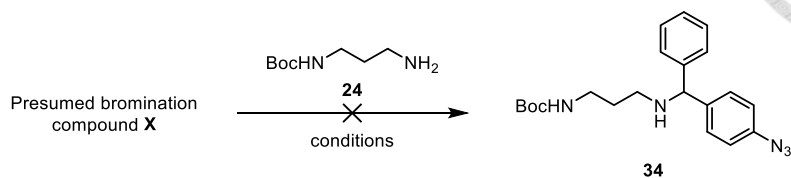
## Synthesis of 1-phenyl-1-(4-azidophenyl)methylamino derivative **36**

By the procedure similar to that for 4-azidobenzylamino derivative **30** (JMF4287), 4-benzylaniline **31** was reacted with sodium nitrite and sodium azide at 0 °C to give 1-azido-4-benzylbenzene **32**<sup>93</sup> (Scheme 8). The subsequent bromination of compound **32** using NBS and AIBN under the conditions similar to that depicted in Scheme 7 turned out to be complicated with presumed formation of the bromination product as shown by TLC analysis. The presumed bromination compound **X** was separated by column chromatography and subjected to reaction with amine **24** (Table 3). However, the desired alkylation product **34** was not obtained in the presence of various bases and KI additive.



**Scheme 8.** Synthesis of 1-phenyl-1-(4-azidophenyl)methylamino derivative **36** (JMF4288).

**Table 3.** Attempts to prepare compound **34** by alkylation reaction of amine **24** with the presumed bromination compound.



Entry	Solvent	Base	Additive	Temp. (°C)	Time	Result
1	MeCN	K <sub>2</sub> CO <sub>3</sub>	None	25	5 d	NR <sup>a</sup>
2	MeCN	DIEA	None	25	24 h	NR <sup>a</sup>
3	MeCN	1 M NaOH <sub>(aq)</sub>	None	25	70 h	NR <sup>a</sup>
4	MeCN	1 M NaOH <sub>(aq)</sub>	KI	25	72 h	NR <sup>a</sup>

<sup>a</sup> NR represents that no compound **34** was obtained.

Alternatively, bromination of compound **32** was realized by using NBS in the presence of benzoyl peroxide (BPO) as radical initiator to provide monobromination compound **33** without further purification.<sup>94</sup> The benzylic proton of **33** appeared at  $\delta$  6.32, whereas the presumed bromination compound **X** showed a proton signal at a different position ( $\delta$  5.43) in the <sup>1</sup>H NMR spectra (Figure 27). In consequence, the bromination compound might be hydrolyzed to compound **X** during column chromatographic separation. Without further purification, compound **33** was reacted with amine compound **24** to give a monoalkylation product **34**. After deprotection of the Boc group by TFA in CH<sub>2</sub>Cl<sub>2</sub> solution, the intermediate amine product **35** was reacted with acid **5** to give compound **36** (JMF4288).



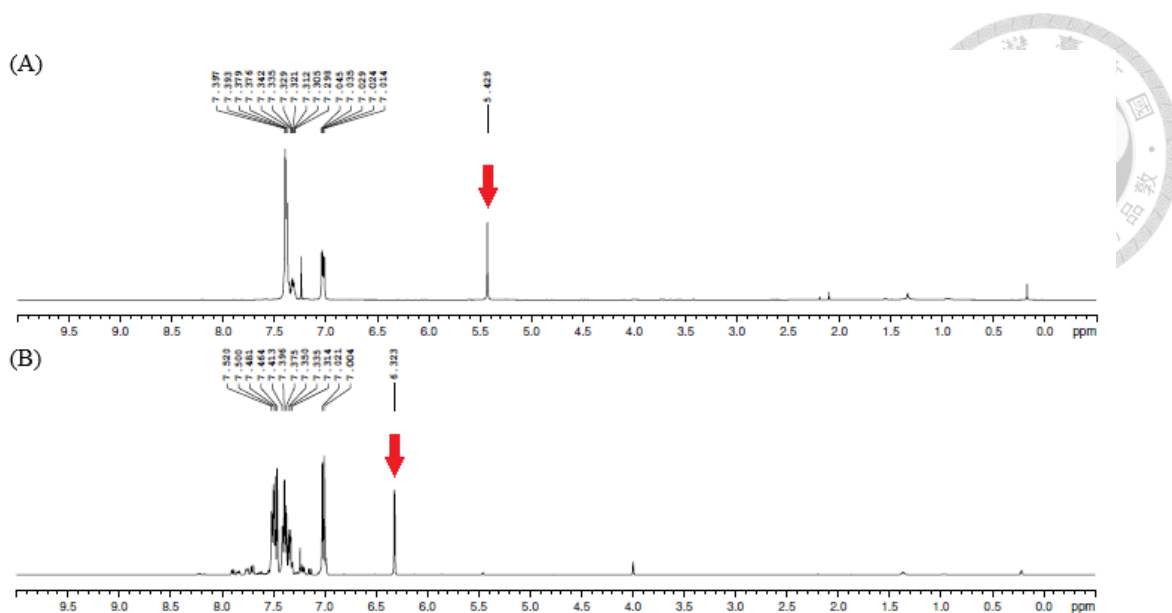
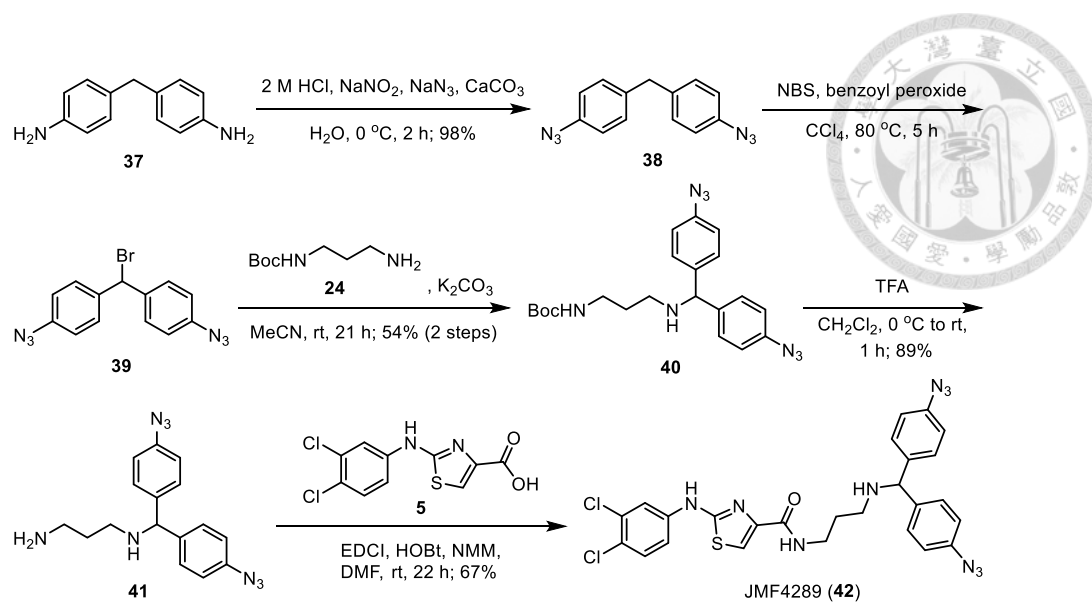


**Figure 27.**  $^1\text{H}$  NMR spectra of the presumed bromination compound **X** (A) and crude compound **33** (B) in  $\text{CDCl}_3$  solution.

### Synthesis of 1,1-bis(4-azidophenyl)methylamino derivative **42**

By a procedure similar to that for compound **32**, 4,4'-methylenedianiline (**37**) was reacted with sodium nitrite and sodium azide at  $^\circ\text{C}$  to give bis(4-azidophenyl)methane (**38**). Bromination of compound **38** with NBS in the presence of benzoyl peroxide provided compound **39** (Scheme 9). Without further purification, the crude bromo compound **39** was reacted with amine **24** to produce the monoalkylation product **40**, which was subsequently treated with TFA in  $\text{CH}_2\text{Cl}_2$  solution to remove the Boc protecting group, giving compound **41**. Finally, the 1,1-bis(4-azidophenyl)methylamino derivative **42** (JMF4289) was successfully synthesized by coupling reaction of amine **41** with (anilinothiazole)carboxylic acid **5**.

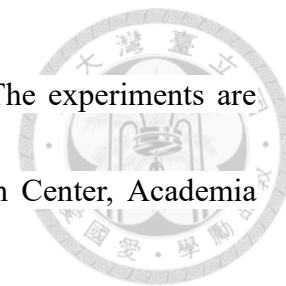


**Scheme 9.** Synthesis of 1,1-bis(4-azidophenyl)methylamino derivative **42** (JMF4289).

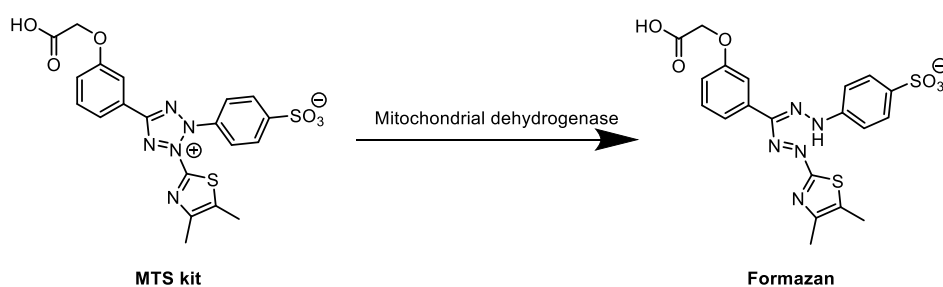
## 2.7 Bioassay

Anti-influenza activities of the above-prepared drug candidates are evaluated against the wild-type WSN H1N1 virus and expressed as half maximal effective concentration ( $EC_{50}$ ), which refers to the concentration of test compound causing 50% survival rate of the Madin-Darby canine kidney (MDCK) epithelial cells after viral infection. This  $EC_{50}$  parameter is commonly quantified by MTS assay. MTS is prone to reduction in the existence of mitochondrial dehydrogenase of living cells, and the absorption wavelength of the reduced product (Formazan) is 490 nm (Figure 28). After MDCK cells are incubated with influenza virus and test compound, an MTS kit is applied to determine the survival cells by colorimetric analysis of the absorbance at 490 nm. Therefore, the  $EC_{50}$  value of a test compound can be determined by plotting the cell

survival rates with the test compound at various concentrations. The experiments are conducted in Dr. Ting-Jen Cheng's lab at the Genomics Research Center, Academia Sinica.



The preliminary bioassay indicated that compound **13a** (JMF4172) had anti-influenza activity similar to that of compound **A**. Photoaffinity labeling probe **42** (JMF4289) also displayed anti-influenza activity similar to that of compound **A**, whereas compound **36** (JMF4288) had lower anti-influenza activity ( $EC_{50} = 13.1 \mu\text{M}$ ). However, it is not consistent with our expectation that benzylamino derivative **22a** (JMF4286) show lower anti-influenza activity ( $EC_{50} = 42.7 \mu\text{M}$ ), and photoaffinity labeling probe **30** (JMF4287) had almost no anti-influenza activity ( $EC_{50} > 10^2 \mu\text{M}$ ). In addition, compounds **13b** (JMF4195) and **22b** (JMF4196) are not soluble in  $\text{H}_2\text{O}$  or DMSO for biological assay due to high hydrophobicity.



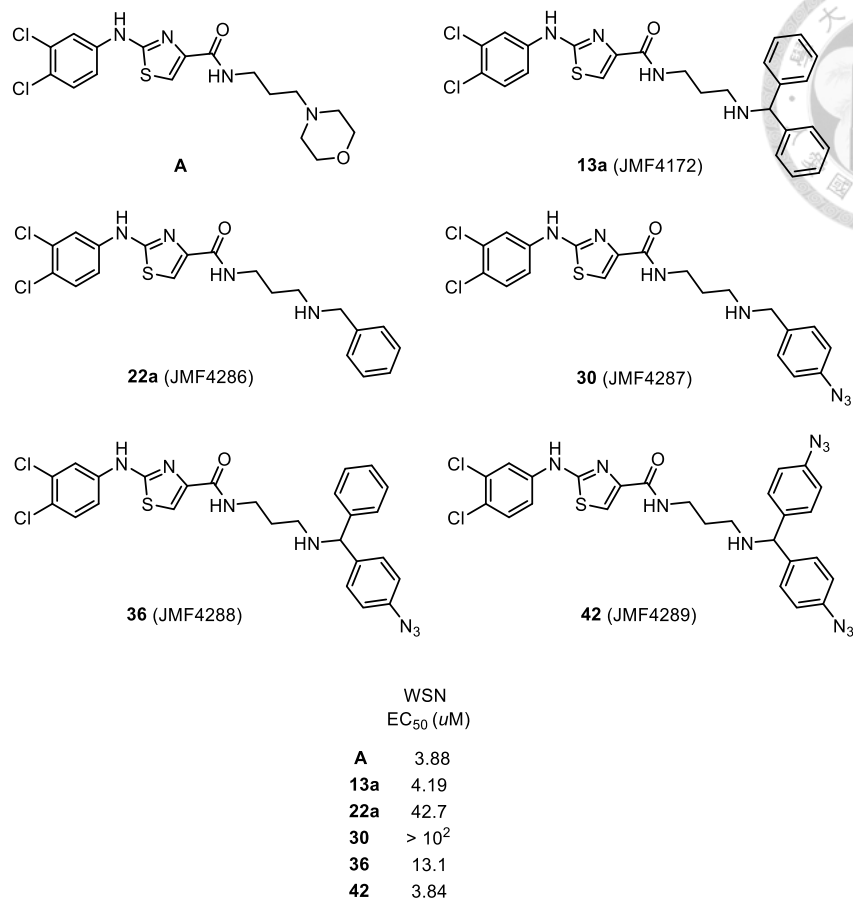



**Figure 28.** Mechanism of MTS assay and anti-influenza activity (EC<sub>50</sub>) of compounds **13a** (JMF4172), **22a** (JMF4286), **30** (JMF4287), **36** (JMF4288) and **42** (JMF4289).

## 2.8 Conclusion

NP is known as a more conserved target than other targets in various influenza subtypes. NP is also a building block of RNP, which plays an important role in virus life cycle. Compound **A**, which was previously found through high-throughput screening, was utilized as a lead compound for designing anti-influenza drugs to interfere with NP trimerization. In this study, we focused on modifications of the functional groups on the right hand side of compound **A**. Thus, we first synthesized (1,1-diphenylmethyl)amino



derivatives **13a** and **13b** bearing (1,1-diphenylmethyl)amino group on the right hand side as inspired by JMF3805 and JMF4023. The benzylamino derivatives **22a** and **22b** were also synthesized. In order to investigate the binding sites between NP monomers, we further synthesized the 4-azidobenzylamino derivative **30**, 1-phenyl-1-(4-azidophenyl)methylamino derivative **36** and 1,1-bis(4-azidophenyl)methylamino derivative **42** for photoaffinity labeling experiments. The MTS bioassay indicated that compound **13a** had anti-influenza activity similar to compound **A**, while compound **13b** was too hydrophobic to do bioassay. The azido compounds **36** and **42** had good anti-influenza activity to serve as potential photoaffinity labeling probes. Nevertheless, the compounds **22a** and **30** showed lower anti-influenza activity, and compound **22b** was too hydrophobic to do bioassay.

In summary, we have synthesized seven compound **A** analogs to investigate the structure–activity relationship against influenza A virus. Among these compounds, three analogs had anti-influenza activity similar to compound **A**, including two photoaffinity labeling probes. Based on the structure–activity relationship in this work and our previous work, we can establish a general structure for designing efficient anti-influenza drug candidates (Figure 29). The 3,4-dichlorobenzene moiety on the left hand side favors high inhibitory effect against H1N1 influenza virus. The compound **A** analogs containing heterocyclic thiazole core in the middle display good anti-influenza activity.

Only the compounds with three-carbon aliphatic chain bearing the functional groups, such as amine, alcohol and ether groups capable of forming hydrogen bonds display high inhibitory activity. In addition, introduction of aryl groups to the terminal of the aliphatic chain proves to maintain good anti-influenza activity.

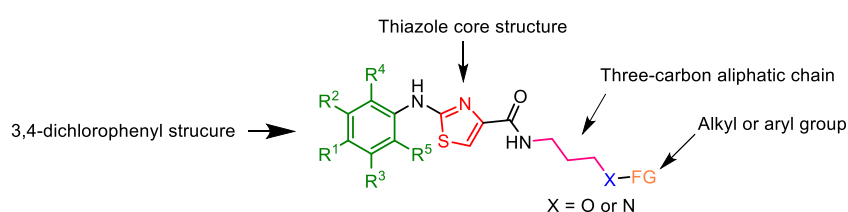



**Figure 29.** General structural features of compound **A** analogs possessing anti-influenza activity.

## 2.9 Prospect

In the future, we shall proceed with the photoaffinity labeling experiments by using aryl azide compounds **36** (JMF4288) and **42** (JMF4289), which have high anti-influenza activity. On the other hand, we shall prepare the salt forms of compounds **13b** (JMF4195) and **22b** (JMF4195) to improve the low solubility in buffer solvent for bioassay.

Lipophilicity refers to the ability of a compound for partition between polar and non-polar solvents (two immiscible solvents). Lipophilicity plays a crucial role in oral administration of drugs. The hydrophilic compounds are incapable of passing through



the lipid bilayers of intestinal epithelium in hydrophobic property. However, the compounds having too high lipophilicity will be trapped in lipid bilayers of intestinal epithelium, causing poor absorption. Thus, an ideal drug requires the lipophilicity in a moderate range for reasonable solubility in water medium and ability to pass cell membrane.

The logarithm partition coefficient P (log P) is a parameter widely used to calculate the lipophilicity of unionized compound. Log P is defined as a ratio of an unionized compound in two immiscible phases (usually utilizing octanol as the organic phase and water as the aqueous phase). The more hydrophobic compound has the higher log P value. The upper limit of log P value is 5 for bioavailability.

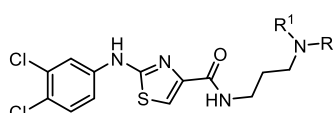
$$\log P_{oct/wat} = \log \left( \frac{[solute]_{octanol}^{unionized}}{[solute]_{water}^{unionized}} \right)$$

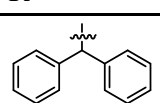
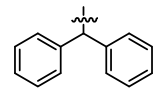
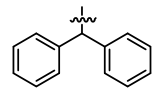
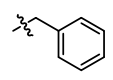
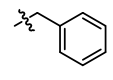
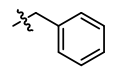
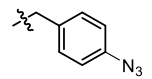
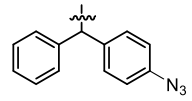
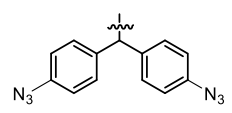
The logarithm distribution of coefficient D (log D) is the ratio of the concentration of both unionized and ionized compounds in two immiscible phases. Log P is pH independent, while log D varies with the function of pH values. High pH environment facilitates ionization of an acidic compound, leading to decrease of the log D value and vice versa.

$$\log D_{oct/wat} = \log \left( \frac{[solute]_{octanol}^{unionized} + [solute]_{octanol}^{ionized}}{[solute]_{water}^{unionized} + [solute]_{water}^{ionized}} \right)$$

The calculated *clogP* values of examined compounds are shown in Table 4. The (1,1-diphenylmethyl)amino derivatives **13a**, **13b**, **36** and **42** displayed the calculated *clogP* values higher than 5, despite compounds **13a** and **42** had anti-influenza activity similar to compound **A**. Benzylamino derivatives **22a**, **22b** and **30** also showed the calculated *clog P* values higher than 5, whereas compound **22a** and **30** had lower inhibitory activity.

**Table 4.** Calculated partition coefficient (*clogP*) of the above-synthesized compound **A** analogs with various R<sup>1</sup> and R<sup>2</sup> substituents on terminal amine group.



R <sup>1</sup>	R <sup>2</sup>	Product	<i>clogP</i>
H		<b>13a</b>	7.42
		<b>13b</b>	11.0
H		<b>22a</b>	6.07
		<b>22b</b>	8.32
H		<b>30</b>	6.51
H		<b>36</b>	7.86
H		<b>42</b>	8.30



Therefore, enhancing the hydrophilicity based on these (1,1-diphenylmethyl)amino compounds is necessary. The designing strategy is inspired by the recent researches (Figure 30). Compound **43** bearing a 4-chloro-3,5-difluorophenyl structure on the left hand side had anti-influenza activity better than compound **A**. Compound **44**, **45** and **46**, which contain methyl, ethyl and isopropyl ether group on the right hand side, all display high anti-influenza activity.

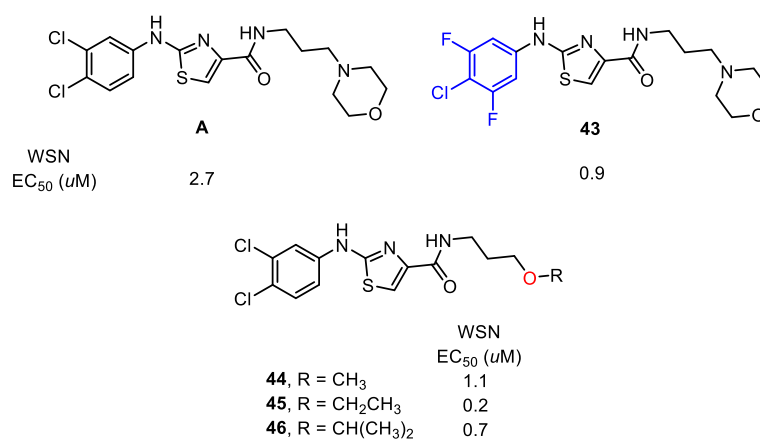


**Figure 30.** Anti-influenza activity (EC<sub>50</sub>) of compounds **43**, **44**, **45** and **46**.

In the future, we plan to synthesize several target compounds bearing 4-chloro-3,5-difluorophenyl moiety on the left hand side to achieve higher hydrophilicity and anti-influenza activity. In the meantime, we shall keep the structural motif of (1,1-diphenyl)methyl amine or ether on the right hand side, but with the azide being reduced to amine group to decrease the lipophilicity (Figure 31).

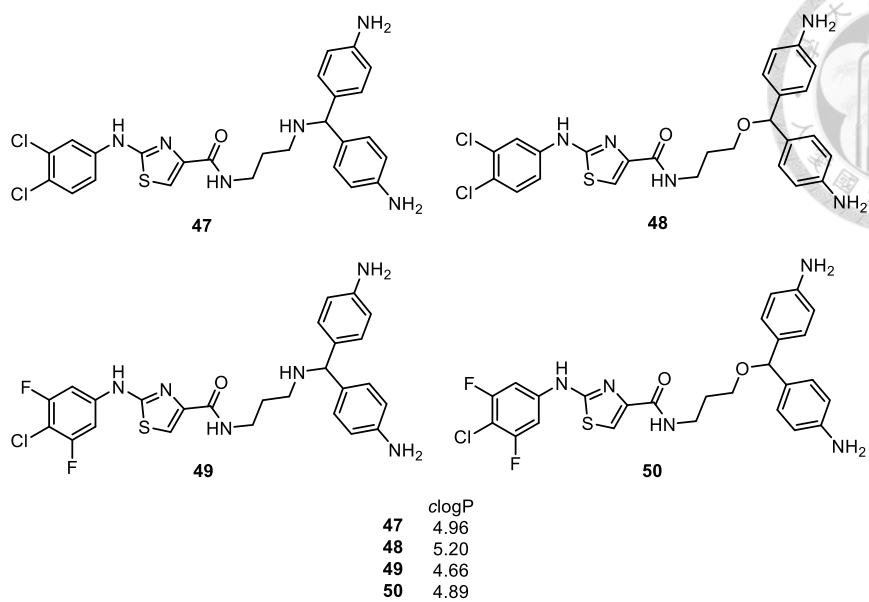


**Figure 31.** Proposed drug candidates in the future work.

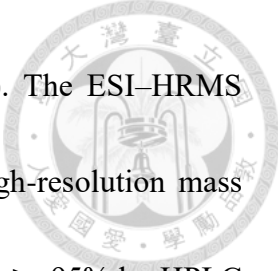
## Chapter 3. Experimental Section



### 3.1 General part

All reagents and solvents were reagent grade and were used without further purification unless otherwise specified. All solvents were anhydrous grade unless indicated otherwise.  $\text{CH}_2\text{Cl}_2$  was distilled from  $\text{CaH}_2$ . All non-aqueous reactions were performed in dried glassware with continuous stirring under argon or nitrogen atmosphere. Reactions were monitored by thin-layer chromatography on 0.25 mm E. Merck silica gel 60 F<sub>254</sub> glass plates using  $\text{KMnO}_4$ , *p*-anisaldehyde, ninhydrin and iodine vapor as visualizing agents. E. Merck silica gel 60 (0.040–0.063 mm particle sizes) and LiChroprep RP-18 (0.040–0.063 mm particle sizes) were used for flash column chromatography.

Infrared (IR) spectra were recorded on Thermo Nicolet iS-5 FT-IR spectrometer. Nuclear magnetic resonance (NMR) spectra were obtained on Bruker Avanced-400 (400 MHz) or Bruker A VIII (400 MHz) NMR. Chemical shifts ( $\delta$ ) are given in parts per million (ppm) relative to  $\delta_{\text{H}}$  7.24 for  $\text{CHCl}_3$ ,  $\delta_{\text{C}}$  77.00 (central line of triplet) for  $\text{CDCl}_3$ ,  $\delta_{\text{H}}$  3.31 for  $\text{CD}_2\text{HOD}$ ,  $\delta_{\text{C}}$  48.15 for  $\text{CD}_3\text{OD}$ ,  $\delta_{\text{H}}$  2.49 for  $\text{CD}_3(\text{CD}_2\text{H})\text{SO}$  and  $\delta_{\text{C}}$  39.50 for  $(\text{CD}_3)_2\text{SO}$ . Coupling constants ( $J$ ) are given in hertz (Hz) and the splitting patterns are reported as s (singlet), d (doublet), t (triplet), q (quartet), quint (quintet), m (multiplet), dd (double of doublets), ddd (double of doublets of doublets), ddt (doublet of doublet of



triplet), dt (double of triplet), td (triple of doublet) and br (broad). The ESI–HRMS experiments were conducted on a Bruker Daltonics BioTOF III high-resolution mass spectrometer. Purity of synthesized compounds was confirmed to be  $\geq 95\%$  by HPLC analysis (Agilent HP-1100) with detection at 254 nm wavelength.

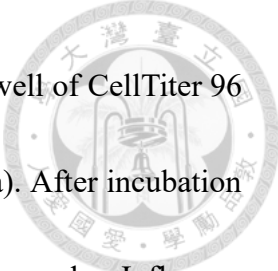
## **3.2 Procedure of bioassay**

### **3.2.1 Material and methods**

Influenza A/WSN/1933 (H1N1) virus was acquired from Dr. Shin-Ru at Chang Gung University in Taiwan. All viruses were cultured in the allantoic cavities of 10-day-old embryonated chicken eggs for 72 h, and were purified through sucrose gradient centrifugation. Madin–Darby canine kidney (MDCK) cells were acquired from American Type Culture Collection (Manassas, VA), and were cultured in DMEM (Dulbecco’s modified Eagle medium, GibcoBRL) containing 10% fetal bovine serum (GibcoBRL) and penicillin–streptomycin (GibcoBRL) under 5% CO<sub>2</sub> at 37 °C.

### **3.2.2 Determination of influenza virus TCID<sub>50</sub>**

The TCID<sub>50</sub>, which represents 50% tissue culture infectious dose was determined by sequential dilution of the influenza virus stock solution onto 100  $\mu$ L MDCK cells at  $1 \times 10^5$  cells/mL in 96-well microplates. The infected cells were incubated under 5%



CO<sub>2</sub> at 37 °C for 48 h, and were added to each well with 100 μL per well of CellTiter 96 Aqueous Non-Radioactive Cell Proliferation Assay reagent (Promega). After incubation at 37 °C for 15 min, absorbance at 490 nm was detected on a plate reader. Influenza virus TCID<sub>50</sub> was determined through Reed–Muench method.

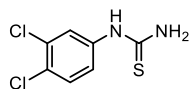
### 3.2.3 Determination of EC<sub>50</sub> of NP inhibitors

The anti-influenza activities of nucleoprotein inhibitors were evaluated by the EC<sub>50</sub> values that were the concentrations of NP inhibitor for 50% protection of the H1N1 cytopathic effect (CPE). Diluted H1N1 (50 μL) at 100 TCID<sub>50</sub> were mixed with equal volumes of NP inhibitors at a variety of concentrations. The mixtures were used to infect 100 μL of MDCK cells at  $1 \times 10^5$  cells/mL in 96 wells. After incubation under 5% CO<sub>2</sub> at 37 °C for 48 h, the CPE were confirmed through CellTiter 96 Aqueous Non-Radioactive Cell Proliferation Assay reagent as mentioned above. EC<sub>50</sub> values of NP inhibitors were determined by fitting the curve of percent CPE versus the concentrations of NP inhibitor utilizing Graph Pad Prism 4.



### 3.3 Synthetic procedure and characterization of compounds

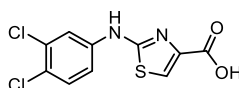
#### 1-(3,4-Dichlorophenyl)thiourea (**3**)<sup>95</sup>



3,4-Dichloro aniline **2** (810 mg, 5 mmol) and potassium isocyanate (2.14 g, 22 mmol) were dissolved in 1 M HCl aqueous solution (12.5 mL) in a round-bottomed flask. The mixture was stirred under reflux for 16 h and abundant precipitate formed. The suspension was filtered and rinsed with water to give thiourea compound **3** (974 mg, 89% yield) without further purification.

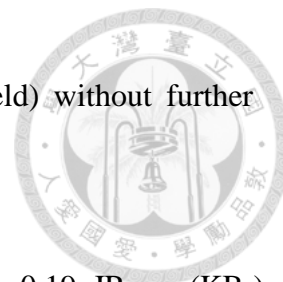
$C_7H_6Cl_2N_2S$ ; beige solid; TLC ( $CH_2Cl_2$ )  $R_f = 0.10$ ; IR  $\nu_{max}$  (KBr) 3467, 3421, 3289, 3162, 2971, 1901, 1625, 1589, 1568, 1518, 1467, 1384, 1342, 1290, 1249, 1194, 1126, 1065, 1031, 917, 879, 837, 809, 710, 671  $cm^{-1}$ ;  $^1H$  NMR (400 MHz,  $DMSO-d_6$ )  $\delta$  9.86 (1 H, s), 7.90 (1 H, d,  $J = 2.5$  Hz), 7.53 (1 H, d,  $J = 8.7$  Hz), 7.36 (1 H, dd,  $J = 2.5, 8.7$  Hz);  $^{13}C$  NMR (100 MHz,  $DMSO-d_6$ )  $\delta$  181.4, 139.6, 130.7, 130.4, 125.9, 124.1, 122.9.

#### 2-((3,4-Dichlorophenyl)amino)thiazole-4-carboxylic acid (**5**)



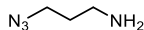
A solution of thiourea **3** (222 mg, 1 mmol) and 3-bromopyruvic acid **4** (167 mg, 1 mmol) in  $CH_3CN$  (3 mL) was stirred at 78 °C for 18 h. The suspension was filtered and

rinsed with cold CH<sub>3</sub>CN to give compound **5** (229 mg, 79% yield) without further purification.



C<sub>10</sub>H<sub>6</sub>Cl<sub>2</sub>N<sub>2</sub>O<sub>2</sub>S; beige solid; TLC (MeOH/CH<sub>2</sub>Cl<sub>2</sub> = 1:40) *R<sub>f</sub>* = 0.19; IR  $\nu_{\text{max}}$  (KBr) 3376, 1753, 1654, 1350, 1228, 1148, 1114, 1049, 988, 966, 935, 878, 859, 832, 787, 711, 665 cm<sup>-1</sup>; <sup>1</sup>H NMR (400 MHz, DMSO-*d*<sub>6</sub>)  $\delta$  8.12 (1 H, d, *J* = 1.4 Hz), 7.76 (1 H, s), 7.52 (1 H, d, *J* = 1.4 Hz), 7.52 (1 H, s); <sup>13</sup>C NMR (100 MHz, DMSO-*d*<sub>6</sub>)  $\delta$  162.3, 162.2, 143.4, 140.9, 131.3, 130.8, 122.6, 119.4, 118.0, 117.2; ESI-HRMS (negative mode) calcd for C<sub>10</sub>H<sub>5</sub>Cl<sub>2</sub>N<sub>2</sub>O<sub>2</sub>S: 286.9949, found: *m/z* 286.9942 [M – H]<sup>-</sup>.

### 3-Azidopropan-1-amine (**8**)<sup>89</sup>

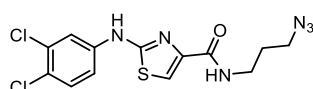


To a solution of 3-bromopropylamine hydrochloride salt (**9**) (500 mg, 2.28 mmol) in water (1.5 mL) was added a solution of sodium azide (500 mg, 7.75 mmol) in water (2.25 mL). The clear light brown mixture was stirred under reflux for 16 h. After the reaction was complete, CH<sub>2</sub>Cl<sub>2</sub> (8 mL) was added at 0 °C, followed by addition of KOH pellets (0.6 g) at < 10 °C. The organic layer was separated, and the aqueous layer was extracted with CH<sub>2</sub>Cl<sub>2</sub> (2 × 5 mL). The organic layers were combined and dried over K<sub>2</sub>CO<sub>3</sub>, filtered, and concentrated under reduced pressure to give 3-azidopropan-1-amine (**8**) (185 mg, 81% yield) without further purification. It is noted

that the product is volatile under reduced pressure or high vacuum system.

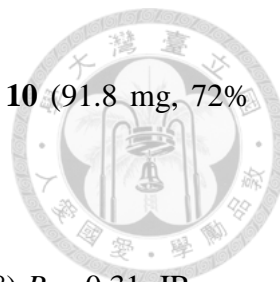
$C_3H_8N_4$ ; pale yellow oil; IR  $\nu_{max}$  (KBr) 3339, 2930, 2867, 2098, 2030, 1654, 1560, 1438, 1372, 1261, 1095, 1019, 799  $cm^{-1}$ ;  $^1H$  NMR (400 MHz,  $CDCl_3$ )  $\delta$  3.35 (2 H, t,  $J = 6.8$  Hz), 2.78 (2 H, t,  $J = 6.8$  Hz), 1.71 (2 H, quint,  $J = 6.8$  Hz), 1.26 (2 H, br, s);  $^{13}C$  NMR (100 MHz,  $CDCl_3$ )  $\delta$  49.1, 39.3, 32.4.

### ***N*-(3-Azidopropyl) 2-((3,4-dichlorophenyl)amino)thiazole-4-carboxamide (10)**



Carboxylic acid **5** (100 mg, 0.35 mmol) was first dissolved in anhydrous DMF (3 mL) in a two-necked flask, and *N*-methylmorpholine (NMM) (304 mg, 3.05 mmol) was added under argon. A solution of 1-ethyl-3-(3-dimethylaminopropyl)carbodiimide (EDCI) (236 mg, 1.54 mmol) and 1-hydroxybenzotriazole hydrate (HOBt) (233 mg, 1.54 mmol) in anhydrous DMF (3 mL) was added, followed by addition of a solution of 3-azidopropan-1-amine (**8**) (70 mg, 0.70 mmol) in anhydrous DMF (1 mL). The mixture was stirred at room temperature for 18 h. Upon completion of the reaction, DMF was removed under reduced pressure. The residue was acidified with 1 M  $HCl_{(aq)}$ , and then extracted with water and  $CH_2Cl_2$ . The organic layer was basified by 1 M  $NaOH_{(aq)}$ , and extracted with  $CH_2Cl_2$ . The organic layers were combined, dried over  $MgSO_4$ , filtered, and concentrated under reduced pressure. The residue was purified by flash column

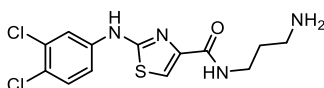




chromatography (silica gel, EtOAc/CH<sub>2</sub>Cl<sub>2</sub> = 1:8) to afford amide **10** (91.8 mg, 72% yield).

C<sub>13</sub>H<sub>12</sub>Cl<sub>2</sub>N<sub>6</sub>OS; pale yellow solid; TLC (EtOAc/CH<sub>2</sub>Cl<sub>2</sub> = 1:8) *R<sub>f</sub>* = 0.31; IR *v*<sub>max</sub> (KBr) 3396, 3270, 3175, 3105, 3055, 2928, 2869, 2099, 1667, 1609, 1537, 1474, 1391, 1309, 1234, 1181, 1134, 1028, 898, 864, 809, 769, 688, 665 cm<sup>-1</sup>; <sup>1</sup>H NMR (400 MHz, CDCl<sub>3</sub>) δ 8.50 (1 H, s), 7.70 (1 H, d, *J* = 1.3 Hz), 7.44 (1 H, s), 7.40 (1 H, t, *J* = 5.9 Hz), 7.36 (1 H, s), 7.35 (1 H, d, *J* = 1.3 Hz), 3.53 (2 H, q, *J* = 6.6 Hz), 3.42 (2 H, t, *J* = 6.6 Hz), 1.89 (2 H, quin, *J* = 6.6 Hz); <sup>13</sup>C NMR (100 MHz, CDCl<sub>3</sub>) δ 163.2, 161.6, 145.6, 139.6, 132.9, 130.8, 125.8, 119.5, 117.2, 113.8, 49.4, 37.2, 28.8; ESI-HRMS (negative mode) calcd for C<sub>13</sub>H<sub>11</sub>Cl<sub>2</sub>N<sub>6</sub>OS: 369.0092, found: *m/z* 369.0093 [M – H]<sup>-</sup>.

#### ***N*-(3-Aminopropyl) 2-((3,4-dichlorophenyl)amino)thiazole-4-carboxamide (11)**



To a solution of azido compound **10** (388 mg, 1.05 mmol) in MeOH (10.5 mL) was added 10% palladium on activated charcoal (Pd/C) (112 mg, 0.11 mmol). The suspension was stirred under an atmosphere of hydrogen at room temperature for 3 h, and the completion of reaction was confirmed by TLC using ninhydrin as visualizing agent. The mixture was filtered through a pad of Celite. The filtrate was concentrated under reduced pressure to provide amine **11** (320 mg, 89% yield) without further



purification.

$C_{13}H_{14}Cl_2N_4OS$ ; pale yellow oil; TLC (MeOH/CH<sub>2</sub>Cl<sub>2</sub>/Et<sub>3</sub>N = 1:9:0.5)  $R_f = 0.37$ ;

IR  $\nu_{max}$  (KBr) 3684, 3405, 3271, 3174, 3100, 2918, 2867, 2171, 1660, 1592, 1537, 1473,

1387, 1313, 1252, 1233, 1179, 1155, 1125, 1080, 1026, 945, 869, 826, 763, 700, 665

cm<sup>-1</sup>; <sup>1</sup>H NMR (400 MHz, CDCl<sub>3</sub>)  $\delta$  8.05 (1 H, t,  $J = 5.4$  Hz), 7.81 (1 H, d,  $J = 2.5$  Hz),

7.44 (1 H, s), 7.34 (1 H, d,  $J = 8.5$  Hz), 7.23 (1 H, dd,  $J = 8.5, 2.5$  Hz), 3.55 (2 H, q,  $J =$

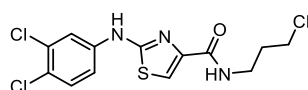
6.0 Hz), 2.88 (2 H, t,  $J = 6.3$  Hz), 1.73 (2 H, quin,  $J = 6.3$  Hz); <sup>13</sup>C NMR (100 MHz,

CDCl<sub>3</sub>)  $\delta$  162.9, 161.4, 146.3, 139.7, 132.9, 130.7, 125.6, 119.4, 117.2, 113.5, 40.4,

38.2, 32.0; ESI-HRMS calcd for  $C_{13}H_{15}Cl_2N_4OS$ : 345.0344, found:  $m/z$  345.0362 [M +

H]<sup>+</sup>.

#### ***N*-(3-Chloropropyl) 2-((3,4-dichlorophenyl)amino)thiazole-4-carboxamide (15)**



Carboxylic acid **5** (500 mg, 1.73 mmol) was first dissolved in anhydrous DMF (10 mL) in a two-necked flask, and NMM (2.1 g, 20.8 mmol) was added under argon. A solution of EDCI (1.18 g, 7.61 mmol) and HOBT (1.17 g, 7.61 mmol) in anhydrous DMF (15 mL) was added, followed by addition of a solution of 3-chloropropylamine hydrochloride (**14**) (450 mg, 3.46 mmol) in anhydrous DMF (10 mL). The mixture was stirred at room temperature for 18 h. Upon completion of the reaction, DMF was

removed under reduced pressure. The residue was acidified with 1 M HCl<sub>(aq)</sub>, and then extracted with water and CH<sub>2</sub>Cl<sub>2</sub>. The organic layer was basified by 1 M NaOH<sub>(aq)</sub>, and extracted with CH<sub>2</sub>Cl<sub>2</sub>. The organic layers were combined, dried over MgSO<sub>4</sub>, filtered, and concentrated under reduced pressure. The residue was purified by flash column chromatography (silica gel, EtOAc/CH<sub>2</sub>Cl<sub>2</sub> = 1:8) to afford amide **15** (216 mg, 34% yield).

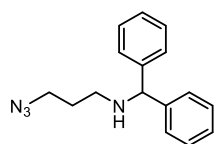
C<sub>13</sub>H<sub>12</sub>Cl<sub>3</sub>N<sub>3</sub>OS; pale yellow solid; TLC (EtOAc/CH<sub>2</sub>Cl<sub>2</sub> = 1:8) *R<sub>f</sub>* = 0.28; IR *v*<sub>max</sub> (KBr) 3401, 3280, 3181, 3116, 3063, 1663, 1612, 1545, 1475, 1434, 1391, 1311, 1234, 1178, 1132, 1114, 1027, 1000, 958, 900, 865, 808, 762, 714, 683, 661 cm<sup>-1</sup>; <sup>1</sup>H NMR (400 MHz, CD<sub>3</sub>OD) δ 7.77 (1 H, d, *J* = 2.5 Hz), 7.70 (1 H, dd, *J* = 8.9, 2.5 Hz), 7.52 (1 H, s), 7.42 (1 H, d, *J* = 8.9 Hz), 3.67 (2 H, t, *J* = 6.5 Hz), 3.55 (2 H, t, *J* = 6.7 Hz), 2.09 (2 H, quin, *J* = 6.7 Hz); <sup>13</sup>C NMR (100 MHz, CD<sub>3</sub>OD) δ 163.8, 163.0, 146.1, 141.1, 132.6, 130.9, 124.5, 118.9, 117.4, 114.2, 42.5, 37.3, 32.7; ESI-HRMS (negative mode) calcd for C<sub>13</sub>H<sub>11</sub>Cl<sub>3</sub>N<sub>3</sub>OS: 361.9688, found: *m/z* 361.9698 [M – H]<sup>-</sup>.

### 3-Azido-*N*-benzhydrylpropan-1-amine

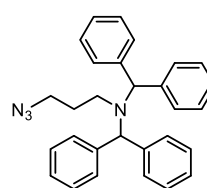
(17a)

and


### 3-azido-*N,N*-(dibenzhydryl)propan-1-amine (17b)



17a



17b

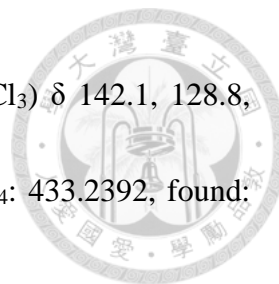


A solution of 3-azidopropan-1-amine (**8**) (100 mg, 1 mmol) in anhydrous MeCN (1 mL) was placed in a two-necked flask, and DIEA (194 mg, 1.5 mmol) was added under argon. Subsequently, a diluted solution of bromodiphenylmethane **12** (346 mg, 1.4 mmol) in anhydrous MeCN (4 mL) was added dropwise. The clear light yellow mixture was stirred at room temperature for 24 h. The mixture was concentrated under reduced pressure, and the residue was purified by flash column chromatography (silica gel, hexane/CH<sub>2</sub>Cl<sub>2</sub> = 4:1 to EtOAc/hexane = 1:14 gradients) to give mono- and dialkylation products **17a** (145 mg, 54% yield) and **17b** (72 mg, 17% yield).

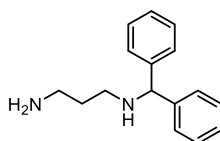
**17a**: C<sub>16</sub>H<sub>18</sub>N<sub>4</sub>; pale yellow oil; TLC (EtOAc/hexane = 1:14) *R<sub>f</sub>* = 0.29; IR *v*<sub>max</sub> (KBr) 3323, 3061, 3025, 2937, 2825, 2096, 1598, 1493, 1453, 1345, 1300, 1259, 1186, 1119, 1028, 746, 703 cm<sup>-1</sup>; <sup>1</sup>H NMR (400 MHz, CDCl<sub>3</sub>) δ 7.48 (4 H, d, *J* = 7.8 Hz), 7.37 (4 H, t, *J* = 7.5 Hz), 7.28 (2 H, t, *J* = 7.6 Hz), 4.88 (1 H, s), 3.41 (2 H, t, *J* = 6.9 Hz), 2.72 (2 H, t, *J* = 6.7 Hz), 1.81 (2 H, quin, *J* = 6.7 Hz), 1.59 (1 H, br, s); <sup>13</sup>C NMR (100 MHz, CDCl<sub>3</sub>) δ 143.9, 128.3, 127.1, 126.9, 67.4, 49.4, 45.0, 29.3; ESI-HRMS calcd for C<sub>16</sub>H<sub>19</sub>N<sub>4</sub>: 267.1610, found: *m/z* 267.1623 [M + H]<sup>+</sup>.

**17b**: C<sub>29</sub>H<sub>28</sub>N<sub>4</sub>; colorless oil; TLC (hexane/CH<sub>2</sub>Cl<sub>2</sub> = 4:1) *R<sub>f</sub>* = 0.44; IR *v*<sub>max</sub> (KBr) 3084, 3061, 3026, 2924, 2854, 2094, 1599, 1492, 1453, 1260, 1185, 1079, 1027, 743, 700 cm<sup>-1</sup>; <sup>1</sup>H NMR (400 MHz, CDCl<sub>3</sub>) δ 7.42 (8 H, d, *J* = 7.8 Hz), 7.33 (8 H, t, *J* = 7.5 Hz), 7.25 (4 H, t, *J* = 7.2 Hz), 5.14 (2 H, s), 2.82 (2 H, t, *J* = 7.4 Hz), 2.61 (2 H, t, *J* =

6.9 Hz), 0.95 (2 H, quin,  $J = 7.4$  Hz);  $^{13}\text{C}$  NMR (100 MHz,  $\text{CDCl}_3$ )  $\delta$  142.1, 128.8, 128.3, 127.0, 69.1, 49.7, 45.6, 28.0; ESI-HRMS calcd for  $\text{C}_{29}\text{H}_{29}\text{N}_4$ : 433.2392, found:  $m/z$  433.2404  $[\text{M} + \text{H}]^+$ .



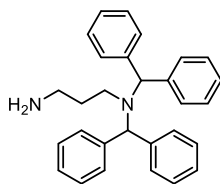
### ***N*-Benzhydrylpropane-1,3-diamine (18a)**



To a solution of azido compound **17a** (50 mg, 0.19 mmol) in MeOH (1.9 mL) was added 10% Pd/C (20 mg, 0.02 mmol). The suspension was stirred under an atmosphere of hydrogen at room temperature for 3 h, and the completion of reaction was confirmed by TLC using ninhydrin as visualizing agent. The mixture was filtered through a pad of Celite. The filtrate was concentrated under reduced pressure to provide amine **18a** (41 mg, 91% yield) without further purification.

$\text{C}_{16}\text{H}_{20}\text{N}_2$ ; colorless oil; TLC (MeOH/ $\text{CH}_2\text{Cl}_2 = 1:9$ )  $R_f = 0.24$ ; IR  $\nu_{\text{max}}$  (KBr) 3060, 3027, 2930, 2845, 1597, 1492, 1452, 1387, 1303, 1115, 1028, 745, 702  $\text{cm}^{-1}$ ;  $^1\text{H}$  NMR (400 MHz,  $\text{CD}_3\text{OD}$ )  $\delta$  7.39 (4 H, d,  $J = 7.3$  Hz), 7.29 (4 H, t,  $J = 7.7$  Hz), 7.19 (2 H, t,  $J = 7.4$  Hz), 4.82 (1 H, s), 2.89 (2 H, t,  $J = 7.0$  Hz), 2.63 (2 H, t,  $J = 6.9$  Hz), 1.79 (2 H, quin,  $J = 7.0$  Hz);  $^{13}\text{C}$  NMR (100 MHz,  $\text{CD}_3\text{OD}$ )  $\delta$  144.1, 128.7, 127.5, 127.2, 67.5, 45.7, 39.4, 28.9; ESI-HRMS calcd for  $\text{C}_{16}\text{H}_{21}\text{N}_2$ : 241.1705, found:  $m/z$  241.1707  $[\text{M} + \text{H}]^+$ .

***N,N*-(Dibenzhydrylpropane)-1,3-diamine (18b)**

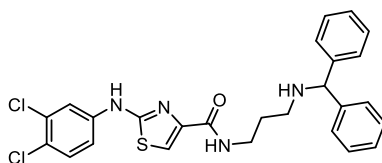


To a solution of azido compound **17b** (157 mg, 0.36 mmol) in THF (3.7 mL) was added 10% Pd/C (39 mg, 0.04 mmol). The suspension was stirred under an atmosphere of hydrogen at room temperature for 3 h, and the completion of reaction was confirmed by TLC using ninhydrin as visualizing agent. The mixture was filtered through a pad of Celite. The filtrate was concentrated under reduced pressure, and the residue was purified by column chromatography (silica gel, MeOH/CH<sub>2</sub>Cl<sub>2</sub> = 1:9) to provide amine **18b** (65 mg, 45% yield).

C<sub>29</sub>H<sub>30</sub>N<sub>2</sub>; colorless oil; TLC (MeOH/CH<sub>2</sub>Cl<sub>2</sub> = 1:9) *R<sub>f</sub>* = 0.51; IR  $\nu_{\text{max}}$  (KBr) 3083, 3059, 3025, 2960, 2927, 2868, 1598, 1491, 1452, 1185, 1127, 1074, 1028, 745, 701 cm<sup>-1</sup>; <sup>1</sup>H NMR (400 MHz, CDCl<sub>3</sub>)  $\delta$  7.41 (8 H, d, *J* = 7.3 Hz), 7.30 (8 H, t, *J* = 7.4 Hz), 7.22 (4 H, t, *J* = 7.2 Hz), 5.12 (2 H, s), 2.77 (2 H, t, *J* = 7.6 Hz), 2.09 (2 H, t, *J* = 7.0 Hz), 0.85 (2 H, quin, *J* = 7.3 Hz); <sup>13</sup>C NMR (100 MHz, CDCl<sub>3</sub>)  $\delta$  142.2, 128.8, 128.2, 126.9, 69.2, 45.5, 39.5, 31.3; ESI-HRMS calcd for C<sub>29</sub>H<sub>31</sub>N<sub>2</sub>: 407.2487, found: *m/z* 407.2484 [M + H]<sup>+</sup>.

***N***-**(3-(Benzhydrylamino)propyl)**

**2-((3,4-dichlorophenyl)amino)thiazole-4-carboxamide (13a)**



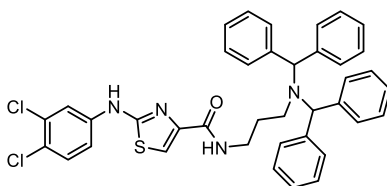
Carboxylic acid **5** (54 mg, 0.19 mmol) was first dissolved in anhydrous DMF (0.4 mL) in a two-necked flask, and NMM (164 mg, 1.62 mmol) was added under nitrogen. A solution of EDCI (127 mg, 0.82 mmol) and HOBT (126 mg, 0.82 mmol) in anhydrous DMF (1.5 mL) was added, followed by addition of a solution of amine **18a** (41 mg, 0.17 mmol) in anhydrous DMF (1.5 mL). The mixture was stirred at room temperature for 24 h. Upon completion of the reaction, DMF was removed under reduced pressure. The residue was acidified with 1 M HCl<sub>(aq)</sub>, and then extracted with water and CH<sub>2</sub>Cl<sub>2</sub>. The organic layer was basified by 1 M NaOH<sub>(aq)</sub>, and extracted with CH<sub>2</sub>Cl<sub>2</sub>. The organic layers were combined, dried over MgSO<sub>4</sub>, filtered, and concentrated under reduced pressure. The residue was purified by flash column chromatography (silica gel, EtOAc/CH<sub>2</sub>Cl<sub>2</sub> = 1:2) to afford amide **13a** (61 mg, 70% yield).

C<sub>26</sub>H<sub>24</sub>Cl<sub>2</sub>N<sub>4</sub>OS; yellow oil; TLC (EtOAc/CH<sub>2</sub>Cl<sub>2</sub> = 1:2) *R<sub>f</sub>* = 0.28; IR *v*<sub>max</sub> (KBr) 3405, 3269, 3173, 3098, 3045, 2926, 2851, 1652, 1594, 1537, 1493, 1474, 1450, 1390, 1305, 1233, 1179, 1130, 1027, 864, 810, 747, 702 cm<sup>-1</sup>; <sup>1</sup>H NMR (400 MHz, CDCl<sub>3</sub>) δ 8.34 (1 H, br, s), 7.87 (1 H, t, *J* = 5.7 Hz), 7.64 (1 H, d, *J* = 2.5 Hz), 7.44 (1 H, s), 7.38

(4 H, d,  $J = 7.3$  Hz), 7.31 (1 H, d,  $J = 8.8$  Hz), 7.23 (4 H, t,  $J = 7.6$  Hz), 7.15 (2 H, t,  $J = 7.2$  Hz), 4.80 (1 H, s), 3.56 (2 H, q,  $J = 6.3$  Hz), 2.71 (2 H, t,  $J = 6.3$  Hz), 1.89 (1 H, br, s), 1.80 (2 H, quin,  $J = 6.3$  Hz);  $^{13}\text{C}$  NMR (100 MHz,  $\text{CDCl}_3$ )  $\delta$  163.0, 161.5, 146.0, 143.8, 139.7, 132.9, 130.7, 128.4, 127.2, 127.0, 125.6, 119.5, 117.1, 113.4, 67.7, 46.2, 38.4, 29.5; ESI-HRMS calcd for  $\text{C}_{26}\text{H}_{25}\text{Cl}_2\text{N}_4\text{OS}$ : 511.1126, found:  $m/z$  511.1151 [ $\text{M} + \text{H}$ ] $^+$ .

### ***N*-(3-(Dibenzhydrylamino)propyl)**

### **2-((3,4-dichlorophenyl)amino)thiazole-4-carboxamide (13b)**



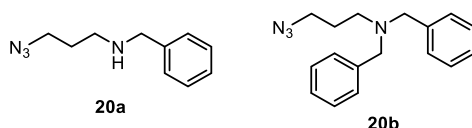
Carboxylic acid **5** (51 mg, 0.18 mmol) was first dissolved in anhydrous DMF (0.5 mL) in a two-necked flask, and NMM (141 mg, 1.39 mmol) was added under nitrogen. A solution of EDCI (110 mg, 0.71 mmol) and HOBt (108 mg, 0.71 mmol) in anhydrous DMF (2 mL) was added, followed by addition of a solution of amine **18b** (65 mg, 0.16 mmol) in anhydrous DMF (1 mL). The mixture was stirred at room temperature for 24 h. Upon completion of the reaction, DMF was removed under reduced pressure. The residue was acidified with 1 M  $\text{HCl}_{(\text{aq})}$ , and then extracted with water and  $\text{CH}_2\text{Cl}_2$ . The organic layer was basified by 1 M  $\text{NaOH}_{(\text{aq})}$ , and extracted with  $\text{CH}_2\text{Cl}_2$ . The organic



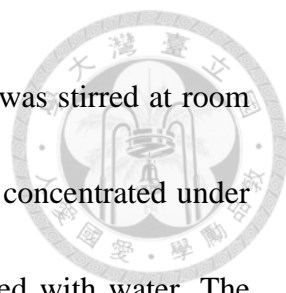
layers were combined, dried over MgSO<sub>4</sub>, filtered, and concentrated under reduced pressure. The residue was purified by flash column chromatography (silica gel, EtOAc/CH<sub>2</sub>Cl<sub>2</sub> = 1:39) to afford amide **13b** (70 mg, 65% yield).

C<sub>39</sub>H<sub>34</sub>Cl<sub>2</sub>N<sub>4</sub>OS; yellow oil; TLC (EtOAc/CH<sub>2</sub>Cl<sub>2</sub> = 1:39) *R<sub>f</sub>* = 0.25; IR  $\nu_{\text{max}}$  (KBr) 3408, 3269, 3175, 3060, 3025, 2926, 2854, 1649, 1594, 1537, 1493, 1474, 1451, 1392, 1306, 1233, 1218, 1178, 1132, 1078, 1027, 866, 812, 757, 701 cm<sup>-1</sup>; <sup>1</sup>H NMR (400 MHz, CDCl<sub>3</sub>)  $\delta$  8.41 (1 H, br, s), 7.70 (1 H, d, *J* = 2.3 Hz), 7.37 (8 H, d, *J* = 7.5 Hz), 7.33 (1 H, d, *J* = 2.3 Hz), 7.24 (8 H, t, *J* = 7.5 Hz), 7.15 (4 H, t, *J* = 7.5 Hz), 6.63 (1 H, t, *J* = 5.8 Hz), 5.10 (2 H, s), 2.79 - 2.91 (4 H, m), 1.76 (1 H, br, s), 0.95 (2 H, quin, *J* = 7.4 Hz); <sup>13</sup>C NMR (100 MHz, CDCl<sub>3</sub>)  $\delta$  162.8, 161.1, 145.8, 142.2, 139.8, 132.8, 130.6, 128.8, 128.3, 126.9, 125.4, 119.4, 117.1, 113.4, 69.2, 45.8, 37.5, 29.0; ESI-HRMS calcd for C<sub>39</sub>H<sub>35</sub>Cl<sub>2</sub>N<sub>4</sub>OS: 677.1909, found: *m/z* 677.1949 [M + H]<sup>+</sup>.

**3-azido-*N*-benzylpropan-1-amine (20a) and 3-azido-*N,N*-dibenzylpropan-1-amine (20b)**



To K<sub>2</sub>CO<sub>3</sub> (552 mg, 4 mmol) in a two-necked flask was added a solution of 3-azidopropan-1-amine (**8**) (200 mg, 2 mmol) in anhydrous MeCN (6 mL) under nitrogen. Subsequently, a diluted solution of benzyl bromide (**19**) (308 mg, 1.8 mmol)



in anhydrous MeCN (14 mL) was added dropwise. The suspension was stirred at room temperature for 18 h. The mixture was filtered, and the filtrate was concentrated under reduced pressure. The residue was dissolved in CH<sub>2</sub>Cl<sub>2</sub>, and washed with water. The organic layer was dried over MgSO<sub>4</sub>, filtered and concentrated under reduced pressure. The residue was purified by flash column chromatography (silica gel, hexane/CH<sub>2</sub>Cl<sub>2</sub> = 1:1 to MeOH/CH<sub>2</sub>Cl<sub>2</sub> = 1:20 gradients) to give mono- and dialkylation products **20a** (154 mg, 45% yield) and **20b** (133 mg, 53% yield).

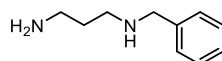
**20a:** C<sub>10</sub>H<sub>14</sub>N<sub>4</sub>; yellow oil; TLC (MeOH/CH<sub>2</sub>Cl<sub>2</sub> = 1:20)  $R_f$  = 0.38; IR  $\nu_{\max}$  (KBr) 3323, 3084, 3063, 3027, 2941, 2819, 2096, 1495, 1453, 1352, 1260, 1122, 1028, 806, 736, 698 cm<sup>-1</sup>; <sup>1</sup>H NMR (400 MHz, CDCl<sub>3</sub>)  $\delta$  7.29–7.36 (4 H, m), 7.22–7.27 (1 H, m), 3.77 (2 H, s), 3.36 (2 H, t,  $J$  = 6.8 Hz), 2.71 (2 H, t,  $J$  = 6.9 Hz), 1.76 (2 H, quin,  $J$  = 6.8 Hz), 1.43 (1 H, br, s); <sup>13</sup>C NMR (100 MHz, CDCl<sub>3</sub>)  $\delta$  140.1, 128.3, 127.9, 126.8, 53.8, 49.4, 46.2, 29.2; ESI-HRMS calcd for C<sub>10</sub>H<sub>15</sub>N<sub>4</sub>: 191.1297, found:  $m/z$  191.1303 [M + H]<sup>+</sup>.

**20b:** C<sub>17</sub>H<sub>20</sub>N<sub>4</sub>; yellow oil; TLC (hexane/CH<sub>2</sub>Cl<sub>2</sub> = 1:1)  $R_f$  = 0.57; IR  $\nu_{\max}$  (KBr) 3085, 3062, 3027, 2947, 2799, 2095, 1601, 1494, 1452, 1365, 1254, 1128, 1074, 1028, 976, 907, 745, 698 cm<sup>-1</sup>; <sup>1</sup>H NMR (400 MHz, CDCl<sub>3</sub>)  $\delta$  7.28–7.35 (8 H, m), 7.20–7.26 (2 H, m), 3.55 (4 H, s), 3.27 (2 H, t,  $J$  = 6.9 Hz), 2.49 (2 H, t,  $J$  = 6.8 Hz), 1.73 (2 H, quin,  $J$  = 6.9 Hz); <sup>13</sup>C NMR (100 MHz, CDCl<sub>3</sub>)  $\delta$  139.4, 128.7, 128.2, 127.0, 58.5, 50.5,

49.5, 26.6; ESI-HRMS calcd for C<sub>17</sub>H<sub>21</sub>N<sub>4</sub>: 281.1766, found: *m/z* 281.1779 [M + H]<sup>+</sup>.



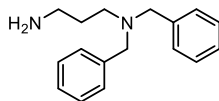
### ***N*-Benzylpropane-1,3-diamine (21a)**



To a solution of azido compound **20a** (68 mg, 0.36 mmol) in MeOH (3.6 mL) was added 5% Lindlar's catalyst (Pd/CaCO<sub>3</sub>) (72 mg, 0.04 mmol). The suspension was stirred under an atmosphere of hydrogen at room temperature for 3 h, and the completion of reaction was confirmed by TLC using ninhydrin as visualizing agent. The mixture was filtered through a pad of Celite. The filtrate was concentrated under reduced pressure to provide diamine compound **21a** (64 mg, 100% yield) without further purification.

C<sub>10</sub>H<sub>16</sub>N<sub>2</sub>; yellow oil; IR  $\nu_{\text{max}}$  (KBr) 3367, 3026, 2931, 2852, 1654, 1561, 1494, 1468, 1308, 1110, 1074, 1027, 975, 910, 816, 738, 699 cm<sup>-1</sup>; <sup>1</sup>H NMR (400 MHz, CDCl<sub>3</sub>)  $\delta$  7.22–7.27 (4 H, m), 7.14–7.20 (1 H, m), 3.71 (2 H, s), 2.73 (2 H, t, *J* = 6.8 Hz), 2.64 (2 H, t, *J* = 6.8 Hz), 2.39 (3 H, br s), 1.61 (2 H, quin, *J* = 6.8 Hz); <sup>13</sup>C NMR (100 MHz, CDCl<sub>3</sub>)  $\delta$  140.0, 128.2, 128.0, 126.8, 53.8, 47.2, 40.3, 32.5; ESI-HRMS calcd for C<sub>10</sub>H<sub>17</sub>N<sub>2</sub>: 165.1392, found: *m/z* 165.1391 [M + H]<sup>+</sup>.

### ***N,N*-Dibenzylpropane-1,3-diamine (21b)**

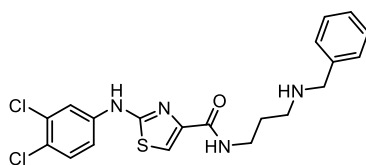


To a solution of azido compound **20b** (100 mg, 0.36 mmol) in MeOH (2.7 mL) and EtOAc (0.9 mL) was added 5% Lindlar's catalyst (76 mg, 0.04 mmol). The suspension was stirred under an atmosphere of hydrogen at room temperature for 3 h, and the completion of reaction was confirmed by TLC using ninhydrin as visualizing agent. The mixture was filtered through a pad of Celite. The filtrate was concentrated under reduced pressure. The residue was purified by column chromatography (silica gel, MeOH/CH<sub>2</sub>Cl<sub>2</sub> = 1:20) to provide diamine compound **21b** (86 mg, 95% yield).

C<sub>17</sub>H<sub>22</sub>N<sub>2</sub>; yellow oil; TLC (MeOH/CH<sub>2</sub>Cl<sub>2</sub> = 1:20) *R<sub>f</sub>* = 0.25; IR *v*<sub>max</sub> (KBr) 3061, 3026, 2936, 2796, 1584, 1494, 1452, 1368, 1310, 1245, 1126, 1074, 1028, 975, 909, 819, 745, 698 cm<sup>-1</sup>; <sup>1</sup>H NMR (400 MHz, CDCl<sub>3</sub>) δ 7.34 (4 H, d, *J* = 7.6 Hz), 7.29 (4 H, t, *J* = 7.4 Hz), 7.21 (2 H, t, *J* = 7.6 Hz), 3.53 (4 H, s), 2.69 (2 H, t, *J* = 6.8 Hz), 2.45 (2 H, t, *J* = 6.8 Hz), 1.62 (2 H, quin, *J* = 6.7 Hz), 1.38 (2 H, br s); <sup>13</sup>C NMR (100 MHz, CDCl<sub>3</sub>) δ 139.8, 128.8, 128.2, 126.8, 58.4, 50.6, 40.1, 30.9; ESI-HRMS calcd for C<sub>17</sub>H<sub>23</sub>N<sub>2</sub>: 255.1861, found: *m/z* 255.1860 [M + H]<sup>+</sup>.

### ***N*-(3-(Benzylamino)propyl)**

### **2-((3,4-dichlorophenyl)amino)thiazole-4-carboxamide (22a)**



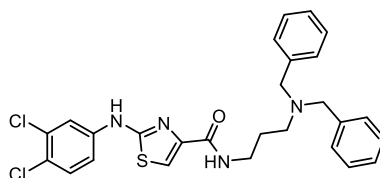
Carboxylic acid **5** (90 mg, 0.31 mmol) was first dissolved in anhydrous DMF (0.6 mL) in a two-necked flask, and NMM (250 mg, 2.47 mmol) was added under nitrogen. A solution of EDCI (193 mg, 1.24 mmol) and HOBT (191 mg, 1.24 mmol) in anhydrous DMF (2 mL) was added, followed by addition of a solution of diamine compound **21a** (43 mg, 0.26 mmol) in anhydrous DMF (2.6 mL). The mixture was stirred at room temperature for 20 h. Upon completion of the reaction, DMF was removed under reduced pressure. The residue was acidified with 1 M HCl<sub>(aq)</sub>, and then extracted with water and CH<sub>2</sub>Cl<sub>2</sub>. The organic layer was basified by 1 M NaOH<sub>(aq)</sub>, and extracted with CH<sub>2</sub>Cl<sub>2</sub>. The organic layers were combined, dried over MgSO<sub>4</sub>, filtered, and concentrated under reduced pressure. The residue was purified by flash column chromatography (silica gel, MeOH/CH<sub>2</sub>Cl<sub>2</sub> = 1:20) to afford amide **22a** (56 mg, 50% yield).

C<sub>20</sub>H<sub>20</sub>Cl<sub>2</sub>N<sub>4</sub>OS; yellow oil; TLC (MeOH/CH<sub>2</sub>Cl<sub>2</sub> = 1:20) *R<sub>f</sub>* = 0.22; IR  $\nu_{\max}$  (KBr) 3406, 3269, 3173, 3095, 3061, 3027, 2927, 2852, 1648, 1593, 1537, 1495, 1474, 1451, 1392, 1306, 1233, 1179, 1130, 1027, 901, 864, 811, 751, 698 cm<sup>-1</sup>; <sup>1</sup>H NMR (400 MHz, CDCl<sub>3</sub>)  $\delta$  9.70 (1 H, br, s), 8.24 (1 H, br, s), 7.82 (1 H, d, *J* = 1.5 Hz), 7.39 (1 H, s), 7.31 (1 H, dd, *J* = 1.5 Hz), 7.25 (2 H, d, *J* = 4.4 Hz), 7.21 (2 H, t, *J* = 7.6 Hz), 7.15 (1 H, t, *J*

= 7.6 Hz), 3.76 (2 H, s), 3.55 (2 H, q,  $J = 5.8$  Hz), 2.78 (2 H, t,  $J = 6.2$  Hz), 1.80 (2 H, quin,  $J = 6.2$  Hz);  $^{13}\text{C}$  NMR (100 MHz,  $\text{CDCl}_3$ )  $\delta$  163.0, 161.8, 145.7, 140.0, 139.3, 132.4, 130.3, 128.2, 128.1, 126.9, 124.7, 119.0, 116.9, 113.3, 53.6, 47.1, 38.5, 28.6; ESI-HRMS calcd for  $\text{C}_{20}\text{H}_{21}\text{Cl}_2\text{N}_4\text{OS}$ : 435.0813, found:  $m/z$  435.0834  $[\text{M} + \text{H}]^+$ .

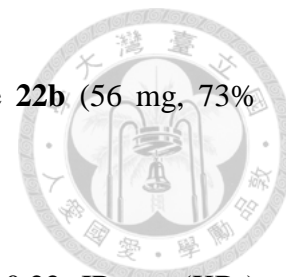
***N*-(3-(Dibenzylamino)propyl)**

**2-((3,4-dichlorophenyl)amino)thiazole-4-carboxamide (22b)**



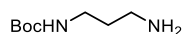
Carboxylic acid **5** (50 mg, 0.17 mmol) was first dissolved in anhydrous DMF (0.4 mL) in a two-necked flask, and NMM (140 mg, 1.38 mmol) was added under nitrogen. A solution of EDCI (108 mg, 0.7 mmol) and HOBT (107 mg, 0.7 mmol) in anhydrous DMF (1.1 mL) was added, followed by addition of a solution of diamine compound **21b** (37 mg, 0.15 mmol) in anhydrous DMF (1.5 mL). The mixture was stirred at room temperature for 20 h. Upon completion of the reaction, DMF was removed under reduced pressure. The residue was acidified with 1 M  $\text{HCl}_{(\text{aq})}$ , and then extracted with water and  $\text{CH}_2\text{Cl}_2$ . The organic layer was basified by 1 M  $\text{NaOH}_{(\text{aq})}$ , and extracted with  $\text{CH}_2\text{Cl}_2$ . The organic layers were combined, dried over  $\text{MgSO}_4$ , filtered, and concentrated under reduced pressure. The residue was purified by flash column

chromatography (silica gel, EtOAc/hexane = 1:2) to afford amide **22b** (56 mg, 73% yield).



$C_{27}H_{26}Cl_2N_4OS$ ; yellow oil; TLC (EtOAc/hexane = 1:2)  $R_f$  = 0.22; IR  $\nu_{max}$  (KBr) 3406, 3270, 3175, 3095, 3061, 3028, 2931, 2799, 1649, 1594, 1537, 1494, 1474, 1451, 1392, 1306, 1234, 1179, 1131, 1028, 974, 902, 865, 811, 749, 698  $cm^{-1}$ ;  $^1H$  NMR (400 MHz,  $CDCl_3$ )  $\delta$  7.87 (1 H, br, s), 7.58 (1 H, d,  $J$  = 2.5 Hz), 7.43 (1 H, s), 7.41 (1 H, t,  $J$  = 5.7 Hz), 7.34 (4 H, d,  $J$  = 7.6 Hz), 7.31 (1 H, s), 7.24 (4 H, t,  $J$  = 7.6 Hz), 7.16 (2 H, t,  $J$  = 7.0 Hz), 3.56 (4 H, s), 3.44 (2 H, q,  $J$  = 6.3 Hz), 2.53 (2 H, t,  $J$  = 6.5 Hz), 1.80 (2 H, quin,  $J$  = 6.6 Hz);  $^{13}C$  NMR (100 MHz,  $CDCl_3$ )  $\delta$  162.8, 161.3, 146.2, 139.6, 139.2, 133.1, 130.8, 129.0, 128.2, 126.9, 125.9, 119.6, 117.2, 113.4, 58.5, 51.2, 38.1, 26.7; ESI-HRMS calcd for  $C_{27}H_{27}Cl_2N_4OS$ : 525.1283, found:  $m/z$  525.1293 [ $M + H$ ] $^+$ .

***Tert*-Butyl (3-aminopropyl)carbamate (**24**)<sup>90, 91</sup>**

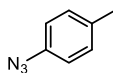


To a solution of 1,3-diaminopropane (**23**) (6.8 g, 91.7 mmol) in  $CHCl_3$  (92 mL) at 0 °C was added a solution of di-*tert*-butyl dicarbonate ( $Boc_2O$ ) (2 g, 9.16 mmol) in  $CHCl_3$  (46 mL) dropwise via a syringe pump over a period of 3 h. The cloudy white solution was allowed to warm to room temperature, and stirred for additional 19 h. The mixture was rinsed with water ( $8 \times 50$  mL). The organic layer was dried over  $Na_2SO_4$ ,

filtered, and concentrated under reduced pressure to give mono-Boc protecting diamine **24** (1.23 g, 77% yield) without further purification.

$C_8H_{18}N_2O_2$ ; pale yellow oil; IR  $\nu_{max}$  (KBr) 3366, 2976, 2931, 2853, 1701, 1529, 1392, 1366, 1282, 1173, 869, 809, 778, 722  $cm^{-1}$ ;  $^1H$  NMR (400 MHz,  $CDCl_3$ )  $\delta$  4.87 (1 H, br s), 3.18 (2 H, q,  $J = 6.0$  Hz), 2.73 (2 H, t,  $J = 6.7$  Hz), 1.58 (2 H, quin,  $J = 6.6$  Hz), 1.41 (9 H, s), 1.28 (2 H, br s);  $^{13}C$  NMR (100 MHz,  $CDCl_3$ )  $\delta$  156.0, 78.6, 39.3, 38.0, 33.2, 28.1; ESI-HRMS calcd for  $C_8H_{19}N_2O_2$ : 175.1447, found:  $m/z$  175.1443 [ $M + H$ ] $^+$ .

#### 1-Azido-4-methylbenzene (**26**)<sup>92</sup>



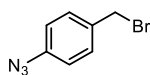
To a solution of *p*-toluidine (**25**) (1 g, 9.33 mmol) in 2 M HCl (14 mL) at  $-5$  °C was added dropwise a solution of sodium nitrite (773 mg, 11.2 mmol) in water (2.5 mL) over 5 min. The clear orange solution was stirred at  $-5$  °C for additional 5 min to form diazonium salt. Urea (67 mg, 1.12 mmol) was added to neutralize the mixture solution. Subsequently, the diazonium salt solution was added slowly to a solution of sodium azide (1.23 g, 18.9 mmol) and sodium acetate (2.33 g, 28.4 mmol) in water (15 mL) at 0 °C over 5 min. The reddish brown solution was stirred at 0 °C for 2 h. The mixture was extracted with  $Et_2O$  ( $3 \times 30$  mL), and the combined organic layers were dried over



MgSO<sub>4</sub>, filtered, and concentrated under reduced pressure to provide 1-azido-4-methylbenzene (**26**) (1.24 g, 100% yield) without further purification.

C<sub>7</sub>H<sub>7</sub>N<sub>3</sub>; reddish brown oil; TLC (CH<sub>2</sub>Cl<sub>2</sub>) *R<sub>f</sub>* = 0.95; <sup>1</sup>H NMR (400 MHz, CDCl<sub>3</sub>) δ 7.13 (2 H, d, *J* = 8.3 Hz), 6.90 (2 H, d, *J* = 8.3 Hz), 2.31 (3 H, s); <sup>13</sup>C NMR (100 MHz, CDCl<sub>3</sub>) δ 137.0, 134.4, 130.2, 118.7, 20.6.

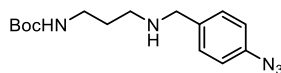
### 1-Azido-4-(bromomethyl)benzene (**27**)<sup>92</sup>



A solution of 1-azido-4-methylbenzene (**26**) (1 g, 7.51 mmol), *N*-bromosuccinimide (NBS) (1.74 g, 9.76 mmol) and azobis(isobutyronitrile) (AIBN) (370 mg, 2.25 mmol) in benzene (23.5 mL) was stirred under reflux for 8 h. Water (20 mL) was added, and the mixture was extracted with Et<sub>2</sub>O (3 × 50 mL). The organic layers were combined, dried over MgSO<sub>4</sub>, filtered, and concentrated under reduced pressure. The residue was purified by flash column chromatography (silica gel, hexane) to give 1-azido-4-(bromomethyl)benzene (**27**) (858 mg, 54% yield).

C<sub>7</sub>H<sub>6</sub>BrN<sub>3</sub>; yellow oil; TLC (hexane) *R<sub>f</sub>* = 0.47; <sup>1</sup>H NMR (400 MHz, CDCl<sub>3</sub>) δ 7.36 (2 H, d, *J* = 8.3 Hz), 6.97 (2 H, d, *J* = 8.5 Hz), 4.46 (2 H, s); <sup>13</sup>C NMR (100 MHz, CDCl<sub>3</sub>) δ 140.0, 134.3, 130.4, 119.2, 32.8.

***Tert*-Butyl (3-((4-azidobenzyl)amino)propyl)carbamate (**28**)**

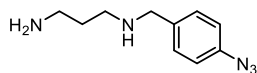


To  $\text{K}_2\text{CO}_3$  (146 mg, 1.06 mmol) in a two-necked flask was added a solution of diamine **24** (92 mg, 0.53 mmol) in anhydrous MeCN (1.3 mL) under nitrogen. Subsequently, a diluted solution of 1-azido-4-(bromomethyl)benzene (**27**) (100 mg, 0.48 mmol) in anhydrous MeCN (4 mL) was added dropwise. The suspension was stirred at room temperature for 19 h. The mixture was filtered, and the filtrate was concentrated under reduced pressure. The residue was dissolved in  $\text{CH}_2\text{Cl}_2$ , and washed with water. The organic layer was dried over  $\text{MgSO}_4$ , filtered, and concentrated under reduced pressure. The residue was purified by flash column chromatography (silica gel,  $\text{MeOH}/\text{CH}_2\text{Cl}_2 = 1:20$ ) to afford monoalkylation product **28** (78 mg, 54% yield).

$\text{C}_{15}\text{H}_{23}\text{N}_5\text{O}_2$ ; yellow oil; TLC ( $\text{MeOH}/\text{CH}_2\text{Cl}_2 = 1:20$ )  $R_f = 0.27$ ; IR  $\nu_{\text{max}}$  (KBr) 3340, 2977, 2931, 2110, 1701, 1606, 1506, 1391, 1365, 1285, 1251, 1172, 1105, 811, 777, 721  $\text{cm}^{-1}$ ;  $^1\text{H}$  NMR (400 MHz,  $\text{CDCl}_3$ )  $\delta$  7.27 (2 H, d,  $J = 8.5$  Hz), 6.93 (2 H, d,  $J = 8.5$  Hz), 5.40 (1 H, br s), 3.70 (2 H, s), 3.16 (2 H, q,  $J = 6.5$  Hz), 2.64 (2 H, t,  $J = 6.5$  Hz), 1.94 (1 H, br s), 1.63 (2 H, quin,  $J = 6.5$  Hz), 1.40 (9 H, s);  $^{13}\text{C}$  NMR (100 MHz,  $\text{CDCl}_3$ )  $\delta$  156.0, 138.4, 136.7, 129.4, 118.7, 78.6, 53.0, 46.8, 38.9, 29.4, 28.2; ESI-HRMS calcd for  $\text{C}_{15}\text{H}_{24}\text{N}_5\text{O}_2$ : 306.1930, found:  $m/z$  306.1949  $[\text{M} + \text{H}]^+$ .



### ***N*-(4-Azidobenzyl)propane-1,3-diamine (29)**

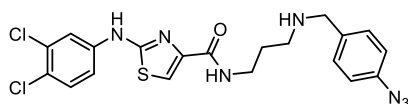


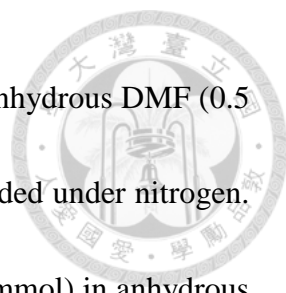
To a solution of mono-Boc protecting diamine **28** (78 mg, 0.25 mmol) in CH<sub>2</sub>Cl<sub>2</sub> (2.54 mL) was slowly added trifluoroacetic acid (TFA) (0.64 mL) at 0 °C. The clear yellow solution was allowed to warm to room temperature, and stirred for 2 h. The mixture was concentrated under reduced pressure. The residue was basified with 1 M NaOH<sub>(aq)</sub>, and then extracted with CH<sub>2</sub>Cl<sub>2</sub>. The organic layers were combined, dried over MgSO<sub>4</sub>, filtered, and concentrated under reduced pressure to provide diamine **29** (46 mg, 88% yield) without further purification.

C<sub>10</sub>H<sub>15</sub>N<sub>5</sub>; yellow oil; IR  $\nu_{\text{max}}$  (KBr) 3371, 2931, 2852, 2407, 2111, 1676, 1606, 1581, 1506, 1468, 1428, 1408, 1288, 1129, 814 cm<sup>-1</sup>; <sup>1</sup>H NMR (400 MHz, CDCl<sub>3</sub>)  $\delta$  7.29 (2 H, d, *J* = 8.0 Hz), 6.96 (2 H, d, *J* = 8.3 Hz), 3.74 (2 H, s), 2.77 (2 H, t, *J* = 5.8 Hz), 2.67 (2 H, t, *J* = 6.3 Hz), 1.89 (2 H, br, s), 1.64 (2 H, quin, *J* = 6.7 Hz); <sup>13</sup>C NMR (100 MHz, CDCl<sub>3</sub>)  $\delta$  138.5, 137.1, 129.4, 118.8, 53.3, 47.2, 40.4, 33.2; ESI-HRMS calcd for C<sub>10</sub>H<sub>16</sub>N<sub>5</sub>: 206.1406, found: *m/z* 206.1417 [M + H]<sup>+</sup>.

### ***N*-(3-((4-Azidobenzyl)amino)propyl)**

### **2-((3,4-dichlorophenyl)amino)thiazole-4-carboxamide (30)**





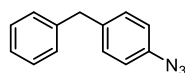
Carboxylic acid **5** (77 mg, 0.27 mmol) was first dissolved in anhydrous DMF (0.5 mL) in a two-necked flask, and NMM (214 mg, 2.12 mmol) was added under nitrogen. A solution of EDCI (166 mg, 1.07 mmol) and HOBt (164 mg, 1.07 mmol) in anhydrous DMF (2 mL) was added, followed by addition of a solution of diamine **29** (46 mg, 0.22 mmol) in anhydrous DMF (2 mL). The mixture was stirred at room temperature for 24 h. Upon completion of the reaction, DMF was removed under reduced pressure. The residue was acidified with 1 M HCl<sub>(aq)</sub>, and then extracted with water and CH<sub>2</sub>Cl<sub>2</sub>. The organic layer was basified by 1 M NaOH<sub>(aq)</sub>, and extracted with CH<sub>2</sub>Cl<sub>2</sub>. The organic layers were combined, dried over MgSO<sub>4</sub>, filtered, and concentrated under reduced pressure. The residue was purified by flash column chromatography (silica gel, MeOH/CH<sub>2</sub>Cl<sub>2</sub> = 1:20) to afford amide **30** (69 mg, 65% yield).

C<sub>20</sub>H<sub>19</sub>Cl<sub>2</sub>N<sub>7</sub>OS; yellow oil; TLC (MeOH/CH<sub>2</sub>Cl<sub>2</sub> = 1:20) *R<sub>f</sub>* = 0.25; IR  $\nu_{\max}$  (KBr) 3404, 3266, 3172, 3098, 3044, 2926, 2851, 2412, 2110, 1644, 1593, 1536, 1504, 1474, 1438, 1390, 1305, 1232, 1179, 1129, 1026, 899, 863, 811, 757, 721 cm<sup>-1</sup>; <sup>1</sup>H NMR (400 MHz, CDCl<sub>3</sub>)  $\delta$  8.89 (1 H, br, s), 8.22 (1 H, br, s), 7.78 (1 H, br, s), 7.41 (1 H, s), 7.27 (1 H, d, *J* = 8.8 Hz), 7.21 (3 H, d, *J* = 8.0 Hz), 6.80 (2 H, d, *J* = 8.0 Hz), 3.72 (2 H, s), 3.55 (2 H, br, s), 2.80 (2 H, br, s), 1.99 (1 H, br, s), 1.80 (2 H, br, s); <sup>13</sup>C NMR (100 MHz, CDCl<sub>3</sub>)  $\delta$  162.9, 161.7, 146.0, 139.8, 138.6, 132.7, 130.5, 129.7, 125.3, 125.1, 119.1, 118.8, 116.9, 113.4, 53.2, 47.6, 38.8, 28.6; ESI-HRMS calcd for C<sub>20</sub>H<sub>20</sub>Cl<sub>2</sub>N<sub>7</sub>OS:

476.0827, found:  $m/z$  476.0847  $[M + H]^+$ .



### 1-Azido-4-benzylbenzene (**32**)

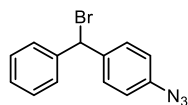


A solution of  $\text{NaNO}_2$  (1.13 g, 16.4 mmol) in water (2.82 mL) was added dropwise to a solution of 4-benzylaniline (**31**) (3 g, 16.4 mmol) in 2 M HCl (34 mL) at 0 °C. The mixture was stirred at 0 °C for 30 min to form diazonium salt, and then neutralized with  $\text{CaCO}_3$ . Next, to the diazonium salt solution was added a solution of  $\text{NaN}_3$  (1.28 g, 19.7 mmol) in water (2.82 mL) dropwise at 0 °C. The mixture was stirred at 0 °C for 2 h, and subsequently extracted with  $\text{CH}_2\text{Cl}_2$ . The organic layers were combined, dried over  $\text{MgSO}_4$ , filtered, and concentrated under reduced pressure. The residue was purified by flash column chromatography (silica gel, hexane/ $\text{CH}_2\text{Cl}_2$  = 1:1) to give 1-azido-4-benzylbenzene (**32**) (3.43 g, 100% yield).

$\text{C}_{13}\text{H}_{11}\text{N}_3$ ; yellow oil; TLC (hexane/ $\text{CH}_2\text{Cl}_2$  = 1:1)  $R_f$  = 0.89; IR  $\nu_{\text{max}}$  (KBr) 3027, 2917, 2412, 2255, 2113, 1606, 1505, 1453, 1431, 1288, 1181, 1128, 1109, 838, 809, 781, 734, 697  $\text{cm}^{-1}$ ;  $^1\text{H}$  NMR (400 MHz,  $\text{CDCl}_3$ )  $\delta$  7.56 (2 H, t,  $J$  = 7.4 Hz), 7.48 (1 H, d,  $J$  = 7.2 Hz), 7.44 (2 H, d,  $J$  = 7.0 Hz), 7.38 (2 H, d,  $J$  = 8.5 Hz), 7.17 (2 H, d,  $J$  = 8.3 Hz), 4.17 (2 H, s);  $^{13}\text{C}$  NMR (100 MHz,  $\text{CDCl}_3$ )  $\delta$  140.6, 137.7, 137.6, 130.0, 128.6, 128.3, 126.0, 118.8, 41.0.



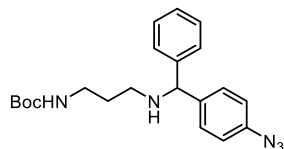
### 1-Azido-4-[bromo(phenyl)methyl]benzene (**33**)



To a solution of 1-azido-4-benzylbenzene (**32**) (200 mg, 0.96 mmol) in  $\text{CCl}_4$  (1.6 mL) were added benzoyl peroxide (12 mg, 0.05 mmol) and 0.5 equiv of NBS (85 mg, 0.48 mmol). The mixture was stirred at 80 °C for 30 min. Another 0.5 equiv of NBS (85 mg, 0.48 mmol) was added. The mixture was stirred at 80 °C for additional 5 h. The suspension was filtered, and the filtrate was washed with saturated  $\text{NaHCO}_3(\text{aq})$ . The organic layer was dried over  $\text{MgSO}_4$ , filtered, and concentrated under reduced pressure to give crude product **33** (212 mg), which was used for next step without further purification.

$\text{C}_{13}\text{H}_{10}\text{BrN}_3$ ; yellow oil;

### *Tert*-Butyl 3-([(4-azidophenyl)(phenyl)methyl]amino)propylcarbamate (**34**)

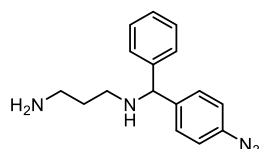


To  $\text{K}_2\text{CO}_3$  (227 mg, 1.64 mmol) in a two-necked flask was added a solution of diamine **24** (143 mg, 0.82 mmol) in anhydrous MeCN (1.2 mL) under nitrogen. Subsequently, a diluted solution of crude bromide **33** (212 mg, 0.74 mmol) in anhydrous MeCN (7 mL) was added dropwise. The suspension was stirred at room

temperature for 19 h. The mixture was filtered, and the filtrate was concentrated under reduced pressure. The residue was dissolved in CH<sub>2</sub>Cl<sub>2</sub>, and washed with water. The organic layer was dried over MgSO<sub>4</sub>, filtered, and concentrated under reduced pressure. The residue was purified by flash column chromatography (silica gel, EtOAc/CH<sub>2</sub>Cl<sub>2</sub> = 1:2) to afford monoalkylation product **34** (136 mg, 38% yield, 2 steps).

C<sub>21</sub>H<sub>27</sub>N<sub>5</sub>O<sub>2</sub>; yellow oil; TLC (EtOAc/CH<sub>2</sub>Cl<sub>2</sub> = 1:2) *R<sub>f</sub>* = 0.56; IR  $\nu_{\text{max}}$  (KBr) 3340, 2976, 2930, 2120, 1701, 1605, 1504, 1452, 1391, 1365, 1288, 1251, 1172, 1129, 1104, 811, 747, 700 cm<sup>-1</sup>; <sup>1</sup>H NMR (400 MHz, CDCl<sub>3</sub>)  $\delta$  7.35 (4 H, t, *J* = 8.2 Hz), 7.28 (2 H, t, *J* = 7.5 Hz), 7.19 (1 H, t, *J* = 7.0 Hz), 6.93 (2 H, d, *J* = 8.5 Hz), 5.23 (1 H, br, s), 4.75 (1 H, s), 3.21 (2 H, q, *J* = 5.9 Hz), 2.60 (2 H, td, *J* = 6.5, 3.5 Hz), 1.65 (2 H, quin, *J* = 6.5 Hz), 1.43 (9 H, s); <sup>13</sup>C NMR (100 MHz, CDCl<sub>3</sub>)  $\delta$  156.0, 143.6, 140.8, 138.5, 128.5 (2 ×), 127.1, 127.0, 119.0, 78.8, 67.0, 45.8, 39.1, 29.9, 28.3; ESI-HRMS calcd for C<sub>21</sub>H<sub>28</sub>N<sub>5</sub>O<sub>2</sub>: 382.2243, found: *m/z* 382.2266 [M + H]<sup>+</sup>.

### ***N*-[(4-azidophenyl)(phenyl)methyl]propane-1,3-diamine (35)**



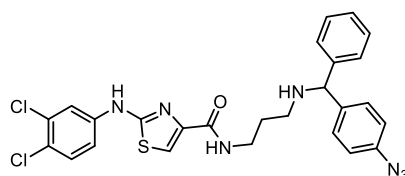
To a solution of mono-Boc protecting diamine **34** (136 mg, 0.36 mmol) in CH<sub>2</sub>Cl<sub>2</sub> (3.57 mL) was slowly added TFA (0.89 mL) at 0 °C. The clear yellow solution was

allowed to warm to room temperature, and stirred for 1 h. The mixture was concentrated under reduced pressure. The residue was basified with 1 M NaOH<sub>(aq)</sub>, and then extracted with CH<sub>2</sub>Cl<sub>2</sub>. The organic layers were combined, dried over MgSO<sub>4</sub>, filtered, and concentrated under reduced pressure to provide diamine **35** (100 mg, 100% yield) without further purification.

C<sub>16</sub>H<sub>19</sub>N<sub>5</sub>; yellow oil; TLC (MeOH/CH<sub>2</sub>Cl<sub>2</sub> = 1:9) *R<sub>f</sub>* = 0.24; IR  $\nu_{\text{max}}$  (KBr) 3026, 2931, 2848, 2120, 1605, 1580, 1503, 1452, 1289, 1179, 1129, 1104, 812, 747, 700 cm<sup>-1</sup>; <sup>1</sup>H NMR (400 MHz, CDCl<sub>3</sub>)  $\delta$  7.35 (4 H, t, *J* = 8.0 Hz), 7.27 (2 H, t, *J* = 7.5 Hz), 7.18 (1 H, t, *J* = 7.2 Hz), 6.93 (2 H, d, *J* = 8.5 Hz), 4.76 (1 H, s), 2.75 (2 H, t, *J* = 6.8 Hz), 2.60 (2 H, td, *J* = 6.8, 1.8 Hz), 1.63 (2 H, quin, *J* = 6.8 Hz), 1.56 (3 H, br, s); <sup>13</sup>C NMR (100 MHz, CDCl<sub>3</sub>)  $\delta$  143.8, 141.0, 138.4, 128.5, 128.4, 127.0, 126.9, 118.9, 67.0, 46.0, 40.3, 33.6; ESI-HRMS calcd for C<sub>16</sub>H<sub>20</sub>N<sub>5</sub>: 282.1719, found: *m/z* 282.1745 [M + H]<sup>+</sup>.

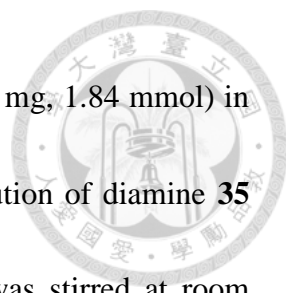
***N*-((3-(((4-azidophenyl)(phenyl)methyl)amino)propyl)**

**2-((3,4-dichlorophenyl)amino)thiazole-4-carboxamide (36)**



Carboxylic acid **5** (133 mg, 0.46 mmol) was first dissolved in anhydrous DMF (1.7 mL) in a two-necked flask, and NMM (369 mg, 3.65 mmol) was added under





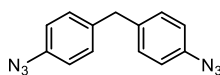
nitrogen. A solution of EDCI (286 mg, 1.84 mmol) and HOBt (282 mg, 1.84 mmol) in anhydrous DMF (3 mL) was added, followed by addition of a solution of diamine **35** (108 mg, 0.38 mmol) in anhydrous DMF (3 mL). The mixture was stirred at room temperature for 22 h. Upon completion of the reaction, DMF was removed under reduced pressure. The residue was acidified with 1 M HCl<sub>(aq)</sub>, and then extracted with water and CH<sub>2</sub>Cl<sub>2</sub>. The organic layer was basified by 1 M NaOH<sub>(aq)</sub>, and extracted with CH<sub>2</sub>Cl<sub>2</sub>. The organic layers were combined, dried over MgSO<sub>4</sub>, filtered, and concentrated under reduced pressure. The residue was purified by flash column chromatography (silica gel, EtOAc/CH<sub>2</sub>Cl<sub>2</sub> = 1:2) to afford amide **36** (144 mg, 68% yield).

C<sub>26</sub>H<sub>23</sub>Cl<sub>2</sub>N<sub>7</sub>OS; yellow oil; TLC (EtOAc/CH<sub>2</sub>Cl<sub>2</sub> = 1:2) *R<sub>f</sub>* = 0.29; IR  $\nu_{\text{max}}$  (KBr) 3406, 3269, 3175, 3104, 3060, 3025, 2927, 2852, 2411, 2120, 1649, 1594, 1537, 1502, 1474, 1451, 1393, 1304, 1233, 1179, 1130, 1027, 865, 813, 756, 700 cm<sup>-1</sup>; <sup>1</sup>H NMR (400 MHz, CDCl<sub>3</sub>)  $\delta$  8.15 (1 H, br, s), 7.78 (1 H, t, *J* = 5.3 Hz), 7.65 (1 H, d, *J* = 2.3 Hz), 7.45 (1 H, s), 7.34 (4 H, d, *J* = 8.3 Hz), 7.31 (1 H, d, *J* = 8.8 Hz), 7.20 - 7.25 (4 H, m), 7.15 (1 H, t, *J* = 8.3 Hz), 6.83 (2 H, d, *J* = 8.3 Hz), 4.77 (1 H, s), 3.55 (2 H, q, *J* = 6.0 Hz), 2.69 (2 H, td, *J* = 6.3, 2.8 Hz), 1.87 (1 H, br, s), 1.80 (2 H, quin, *J* = 6.3 Hz); <sup>13</sup>C NMR (100 MHz, CDCl<sub>3</sub>)  $\delta$  163.1, 161.7, 145.7, 143.5, 140.6, 139.8, 138.4, 132.6, 130.5, 128.5 (2  $\times$ ), 127.1, 127.0, 125.1, 119.2, 118.9, 116.9, 113.5, 67.0, 45.9, 38.3, 29.4;

ESI-HRMS calcd for C<sub>26</sub>H<sub>24</sub>Cl<sub>2</sub>N<sub>7</sub>OS: 552.1140, found: *m/z* 552.1194 [M + H]<sup>+</sup>.



**Bis(4-azidophenyl)methane (38)**<sup>93</sup>

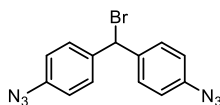


A solution of NaNO<sub>2</sub> (2.64 g, 38.26 mmol) in water (5 mL) was added dropwise to a solution of 4,4'-methylenedianiline (**37**) (3.45 g, 17.4 mmol) in 2 M HCl (36 mL) at 0 °C. The mixture was stirred at 0 °C for 30 min to form diazonium salt, and then neutralized with CaCO<sub>3</sub>. Next, to the diazonium salt solution was added a solution of NaN<sub>3</sub> (3.4 g, 52.3 mmol) in water (5 mL) dropwise at 0 °C. The mixture was stirred at 0 °C for 2 h, and subsequently extracted with CH<sub>2</sub>Cl<sub>2</sub>. The organic layers were combined, dried over MgSO<sub>4</sub>, filtered, and concentrated under reduced pressure. The residue was purified by flash column chromatography (silica gel, hexane/CH<sub>2</sub>Cl<sub>2</sub> = 4:1) to give bis(4-azidophenyl)methane (**38**) (4.28 g, 98% yield).

C<sub>13</sub>H<sub>10</sub>N<sub>6</sub>; yellow oil; TLC (hexane/CH<sub>2</sub>Cl<sub>2</sub> = 4:1) *R<sub>f</sub>* = 0.53; IR *v*<sub>max</sub> (KBr) 2414, 2108, 1606, 1504, 1427, 1407, 1287, 1128, 1114, 809, 770 cm<sup>-1</sup>; <sup>1</sup>H NMR (400 MHz, CDCl<sub>3</sub>) δ 7.17 (4 H, d, *J* = 8.3 Hz), 6.97 (4 H, d, *J* = 8.3 Hz), 3.94 (2 H, s); <sup>13</sup>C NMR (100 MHz, CDCl<sub>3</sub>) δ 137.9, 137.5, 130.0, 119.0, 40.5.



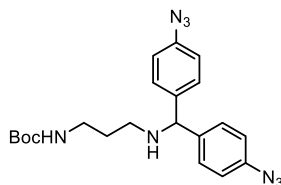
#### 4,4'-Bis(azidophenyl)bromomethane (**39**)



To a solution of bis(4-azidophenyl)methane (**38**) (400 mg, 1.6 mmol) in  $\text{CCl}_4$  (2.7 mL) were added benzoyl peroxide (19 mg, 0.08 mmol) and 0.5 equiv of NBS (142 mg, 0.8 mmol). The mixture was stirred at 80 °C for 30 min. Another 0.5 equiv of NBS (142 mg, 0.8 mmol) was added. The mixture was stirred at 80 °C for additional 5 h. The suspension was filtered, and the filtrate was washed with saturated  $\text{NaHCO}_3(\text{aq})$ . The organic layer was dried over  $\text{MgSO}_4$ , filtered, and concentrated under reduced pressure to give crude product **39** (481 mg), which was used for next step without further purification.

$\text{C}_{13}\text{H}_9\text{BrN}_6$ ; yellow oil;

#### *Tert*-Butyl (3-((bis(4-azidophenyl)methyl)amino)propyl)carbamate (**40**)

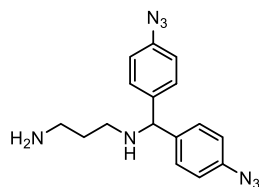


To  $\text{K}_2\text{CO}_3$  (449 mg, 3.25 mmol) in a two-necked flask was added a solution of diamine **24** (283 mg, 1.62 mmol) in anhydrous MeCN (2.2 mL) under nitrogen. Subsequently, a diluted solution of crude bromide **39** (481 mg, 1.46 mmol) in anhydrous MeCN (14 mL) was added dropwise. The suspension was stirred at room

temperature for 21 h. The mixture was filtered, and the filtrate was concentrated under reduced pressure. The residue was dissolved in CH<sub>2</sub>Cl<sub>2</sub>, and washed with water. The organic layer was dried over MgSO<sub>4</sub>, filtered, and concentrated under reduced pressure. The residue was purified by flash column chromatography (silica gel, EtOAc/hexane = 1:4) to afford monoalkylation product **40** (363 mg, 54% yield, 2 steps).

C<sub>21</sub>H<sub>26</sub>N<sub>8</sub>O<sub>2</sub>; yellow oil; TLC (EtOAc/hexane = 1:4) *R<sub>f</sub>* = 0.18; IR *v*<sub>max</sub> (KBr) 3344, 2977, 2930, 2412, 2255, 2122, 1705, 1605, 1581, 1505, 1453, 1391, 1366, 1289, 1251, 1171, 1129, 1015, 832, 770 cm<sup>-1</sup>; <sup>1</sup>H NMR (400 MHz, CDCl<sub>3</sub>) δ 7.32 (4 H, d, *J* = 8.5 Hz), 6.93 (4 H, d, *J* = 8.5 Hz), 5.10 (1 H, br, s), 4.72 (1 H, s), 3.20 (2 H, q, *J* = 5.5 Hz), 2.57 (2 H, t, *J* = 6.5 Hz), 1.64 (2 H, quin, *J* = 6.5 Hz), 1.42 (9 H, s); <sup>13</sup>C NMR (100 MHz, CDCl<sub>3</sub>) δ 156.0, 140.5, 138.7, 128.4, 119.1, 78.9, 66.4, 45.7, 39.0, 30.0, 28.4; ESI-HRMS calcd for C<sub>21</sub>H<sub>27</sub>N<sub>8</sub>O<sub>2</sub>: 423.2257, found: *m/z* 423.2294 [M + H]<sup>+</sup>.

#### ***N*-(Bis(4-azidophenyl)methyl)propane-1,3-diamine (41)**



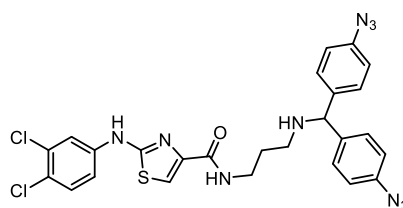
To a solution of mono-Boc protecting diamine **40** (130 mg, 0.31 mmol) in CH<sub>2</sub>Cl<sub>2</sub> (3.1 mL) was slowly added TFA (0.78 mL) at 0 °C. The clear brown solution was allowed to warm to room temperature, and stirred for 1 h. The mixture was concentrated

under reduced pressure. The residue was basified with 1 M NaOH<sub>(aq)</sub>, and then extracted with CH<sub>2</sub>Cl<sub>2</sub>. The organic layers were combined, dried over MgSO<sub>4</sub>, filtered, and concentrated under reduced pressure to provide diamine **41** (89 mg, 89% yield) without further purification.

C<sub>16</sub>H<sub>18</sub>N<sub>8</sub>; yellow oil; TLC (MeOH/CH<sub>2</sub>Cl<sub>2</sub> = 1:9) *R<sub>f</sub>* = 0.25; IR *v*<sub>max</sub> (KBr) 2927, 2855, 2411, 2255, 2121, 1604, 1580, 1503, 1289, 1179, 1129, 1015, 831 cm<sup>-1</sup>; <sup>1</sup>H NMR (400 MHz, CDCl<sub>3</sub>) δ 7.32 (4 H, d, *J* = 8.5 Hz), 6.93 (4 H, d, *J* = 8.5 Hz), 4.73 (1 H, s), 2.75 (2 H, t, *J* = 6.8 Hz), 2.58 (2 H, t, *J* = 6.8 Hz), 1.63 (2 H, quin, *J* = 6.8 Hz), 1.54 (3 H, br, s); <sup>13</sup>C NMR (100 MHz, CDCl<sub>3</sub>) δ 140.8, 138.7, 128.4, 119.1, 66.5, 46.0, 40.4, 33.7; ESI-HRMS calcd for C<sub>16</sub>H<sub>19</sub>N<sub>8</sub>: 323.1733, found: *m/z* 323.1763 [M + H]<sup>+</sup>.

***N*-((bis(4-azidophenyl)methyl)amino)propyl**

**2-((3,4-dichlorophenyl)amino) thiazole-4-carboxamide (42)**



Carboxylic acid **5** (95 mg, 0.33 mmol) was first dissolved in anhydrous DMF (1 mL) in a two-necked flask, and NMM (264 mg, 2.61 mmol) was added under nitrogen. A solution of EDCI (205 mg, 1.32 mmol) and HOBt (202 mg, 1.32 mmol) in anhydrous DMF (2 mL) was added, followed by addition of a solution of diamine **41** (89 mg, 0.27

mmol) in anhydrous DMF (2.5 mL). The mixture was stirred at room temperature for 22

h. Upon completion of the reaction, DMF was removed under reduced pressure. The residue was acidified with 1 M HCl<sub>(aq)</sub>, and then extracted with water and CH<sub>2</sub>Cl<sub>2</sub>. The organic layer was basified by 1 M NaOH<sub>(aq)</sub>, and extracted with CH<sub>2</sub>Cl<sub>2</sub>. The organic layers were combined, dried over MgSO<sub>4</sub>, filtered, and concentrated under reduced pressure. The residue was purified by flash column chromatography (silica gel, EtOAc/CH<sub>2</sub>Cl<sub>2</sub> = 1:5) to afford amide **42** (108 mg, 67% yield).

C<sub>26</sub>H<sub>22</sub>Cl<sub>2</sub>N<sub>10</sub>OS; yellow oil; TLC (EtOAc/CH<sub>2</sub>Cl<sub>2</sub> = 1:5) *R<sub>f</sub>* = 0.19; IR *v*<sub>max</sub> (KBr) 3402, 3270, 3175, 3099, 3053, 2925, 2853, 2412, 2120, 1647, 1594, 1537, 1503, 1474, 1441, 1394, 1290, 1232, 1179, 1130, 1028, 1015, 866, 816, 756, 700 cm<sup>-1</sup>; <sup>1</sup>H NMR (400 MHz, CDCl<sub>3</sub>) δ 8.78 (1 H, s), 7.77 (1 H, t, *J* = 6.0 Hz), 7.75 (1 H, d, *J* = 2.5 Hz), 7.44 (1 H, s), 7.28 (4 H, d, *J* = 8.5 Hz), 7.25 (1 H, d, *J* = 8.6 Hz), 7.23 (1 H, dd, *J* = 8.6, 2.5 Hz), 6.82 (4 H, d, *J* = 8.5 Hz), 4.72 (1 H, s), 3.57 (2 H, q, *J* = 6.2 Hz), 2.67 (2 H, t, *J* = 6.2 Hz), 1.80 (2 H, quin, *J* = 6.2 Hz); <sup>13</sup>C NMR (100 MHz, CDCl<sub>3</sub>) δ 163.0, 161.6, 145.8, 140.3, 139.7, 138.7, 132.8, 130.5, 128.4, 125.3, 119.2, 119.0, 116.9, 113.6, 66.4, 45.9, 38.2, 29.4; ESI-HRMS calcd for C<sub>26</sub>H<sub>23</sub>Cl<sub>2</sub>N<sub>10</sub>OS: 593.1154, found: *m/z* 593.1158 [M + H]<sup>+</sup>.

## References



1. Taubenberger, J. K.; Morens, D. M. The pathology of influenza virus infections. *Annu. Rev. Pathol.* **2008**, *3*, 499–522.
2. Ng, A. K.-L.; Zhang, H.; Tan, K.; Li, Z.; Liu, J.-h.; Chan, P. K.-S.; Li, S.-M.; Chan, W.-Y.; Au, S. W.-N.; Joachimiak, A.; Walz, T.; Wang, J.-H.; Shaw, P.-C. Structure of the influenza virus A H5N1 nucleoprotein: implications for RNA binding, oligomerization, and vaccine design. *FASEB J.* **2008**, *22*, 3638–3647.
3. Morens, D. M.; Fauci, A. S. The 1918 influenza pandemic: insights for the 21st century. *J. Infect. Dis.* **2007**, *195*, 1018–1028.
4. Simonsen, L. The global impact of influenza on morbidity and mortality. *Vaccine* **1999** *17*, S3–10.
5. Johnson, N. P.; Mueller, J. Updating the accounts: global mortality of the 1918–1920 “Spanish” influenza pandemic. *Bull. Hist. Med.* **2002**, *76*, 105–115.
6. Clancy, S. Genetics of the influenza virus. *Nature Education* **2008**, *1*, 83.
7. Tong, S.; Li, Y.; Rivaller, P.; Conrardy, C.; Castillo, D. A. A.; Chen, L.-M.; Recuenco, S.; Ellison, J. A.; Davis, C. T.; York, I. A.; Turmelle, A. S.; Moran, D.; Rogers, S.; Shi, M.; Tao, Y.; Weil, M. R.; Tang, K.; Rowe, L. A.; Sammons, S.; Xu, X.; Frace, M.; Lindblade, K. A.; Cox, N. J.; Anderson, L. J.; Rupprecht, C. E.; Donis, R. O. A distinct lineage of influenza A virus from bats. *Proc. Natl. Acad. Sci.*





- U. S. A.* **2012**, *109*, 4269–4274.
8. Tong, S.; Zhu, X.; Li, Y.; Shi, M.; Zhang, J.; Bourgeois, M.; Yang, H.; Chen, X.; Recuenco, S.; Gomez, J.; Chen, L.-M.; Johnson, A.; Tao, Y.; Dreyfus, C.; Yu, W.; McBride, R.; Carney, P. J.; Gilbert, A. T.; Chang, J.; Guo, Z.; Davis, C. T.; Paulson, J. C.; Stevens, J.; Rupprecht, C. E.; Holmes, E. C.; Wilson, I. A.; Donis, R. O. New world bats harbor diverse influenza A viruses. *PLoS Pathog.* **2013**, *9*, e1003657.
  9. Wagner, R.; Matrosovich, M.; Klenk, H. D. *Rev. Med. Virol.* **2002**, *12*, 66–159.
  10. Steinhauer, D. A. Role of hemagglutinin cleavage for the pathogenicity of influenza virus. *Virology* **1999**, *258*, 1–20.
  11. von Itzstein, M. The war against influenza: discovery and development of sialidase inhibitors. *Nat. Rev. Drug. Discov.* **2007**, *6*, 967–974.
  12. Hutchinson, E. C.; Fodor, E. Transport of the influenza virus genome from nucleus to nucleus. *Viruses* **2013**, *5*, 2424–2446.
  13. Pons, M. W.; Schulze, I. T.; Hirst, G. K. Isolation and characterization of the ribonucleoprotein of influenza virus. *Virology* **1969**, *39*, 250–259.
  14. Zheng, W.; Tao, Y. J. Structure and assembly of the influenza A virus ribonucleoprotein complex. *FEBS Lett.* **2013**, *587*, 1206–1214.
  15. Arranz, R.; Coloma, R.; Chichón, F. J.; Conesa, J. J.; Carrascosa, J. L.; Valpuesta, J. M.; Ortín, J.; Martín-Benito, J. The Structure of native influenza virion






- ribonucleoproteins. *Science* **2012**, 338, 1634–1637.
16. Coloma, R.; Valpuesta, J. M.; Arranz, R.; Carrascosa, J. L.; Ortín, J.; Martín-Benito, J. The structure of a biologically active influenza virus ribonucleoprotein complex. *PLoS Pathog.* **2009**, 5, e1000491.
17. Ortega, J.; Martín-Benito, J.; Zürcher, T.; Valpuesta, J. M.; Carrascosa, J. L.; Ortín, J. Ultrastructural and functional analyses of recombinant influenza virus ribonucleoproteins suggest dimerization of nucleoprotein during virus amplification. *J. Virol.* **2000**, 74, 156–163.
18. Martín-Benito, J.; Area, E.; Ortega, J.; Llorca, O.; Valpuesta, J. M.; Carrascosa, J. L.; Ortín, J. Three-dimensional reconstruction of a recombinant influenza virus ribonucleoprotein particle. *EMBO Rep.* **2001**, 2, 313–317.
19. Resa-Infante, P.; Jorba, N.; Coloma, R.; Ortín, J. The influenza RNA synthesis machine: Advances in its structure and function. *RNA Biol.* **2011**, 8, 207–215.
20. Biswas, S. K.; Boutz, P. L.; Nayak, D. P. Influenza virus nucleoprotein interacts with influenza virus polymerase proteins. *J. Virol.* **1998**, 72, 5493–5501.
21. Ye, Q.; Krug, R. M.; Tao, Y. J. The mechanism by which influenza A virus nucleoprotein forms oligomers and binds RNA. *Nature* **2006**, 444, 1078–1082.
22. Chenavas, S.; Estrozi, L. F.; Slama-Schwok, A.; Delmas, B.; Di Primo, C.; Baudin, F.; Li, X.; Crépin, T.; Ruigrok, R. W. H. Monomeric nucleoprotein of influenza A

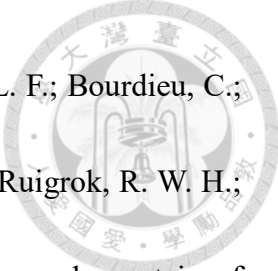
- 
- virus. *PLoS Pathog.* **2013**, *9*, e1003275.
23. Marklund, J. K.; Ye, Q.; Dong, J.; Tao, Y. J.; Krug, R. M. Sequence in the influenza A virus nucleoprotein required for viral polymerase binding and RNA synthesis. *J. Virol.* **2012**, *86*, 7292–7297.
24. Kobayashi, M.; Toyoda, T.; Adyshev, D. M.; Azuma, Y.; Ishihama, A. Molecular dissection of influenza virus nucleoprotein: deletion mapping of the RNA binding domain. *J. Virol.* **1994**, *68*, 8433–8436.
25. Shen, Y.-F.; Chen, Y.-H.; Chu, S.-Y.; Lin, M.-I.; Hsu, H.-T.; Wu, P.-Y.; Wu, C.-J.; Liu, H.-W.; Lin, F.-Y.; Lin, G.; Hsu, P.-H.; Yang, A.-S.; Cheng, Y.-S. E.; Wu, Y.-T.; Wong, C.-H.; Tsai, M.-D. E339...R416 salt bridge of nucleoprotein as a feasible target for influenza virus inhibitors. *Proc. Natl. Acad. Sci. U. S. A.* **2011**, *108*, 16515–16520.
26. Ye, Q.; Guu, T. S. Y.; Mata, D. A.; Kuo, R.-L.; Smith, B.; Krug, R. M.; Tao, Y. J. Biochemical and structural evidence in support of a coherent model for the formation of the double-helical influenza A virus ribonucleoprotein. *mBio* **2013**, *4*.
27. Turrell, L.; Lyall, J. W.; Tiley, L. S.; Fodor, E.; Vreede, F. T. The role and assembly mechanism of nucleoprotein in influenza A virus ribonucleoprotein complexes. *Nature Commun.* **2013**, *4*, 1591.
28. Honda, A.; Ueda, K.; Nagata, K.; Ishihama, A. RNA polymerase of influenza virus:

- 
- role of NP in RNA chain elongation. *J. Biochem.* **1988**, *104*, 1021–1026.
29. Resa-Infante, P.; Recuero-Checa, M. Á.; Zamarreño, N.; Llorca, Ó.; Ortín, J. Structural and functional characterization of an influenza virus RNA polymerase-genomic RNA complex. *J. Virol.* **2010**, *84*, 10477–10487.
30. Lee, M. T. M.; Bishop, K.; Medcalf, L.; Elton, D.; Digard, P.; Tiley, L. Definition of the minimal viral components required for the initiation of unprimed RNA synthesis by influenza virus RNA polymerase. *Nucleic Acids Res.* **2002**, *30*, 429–438.
31. Newcomb, L. L.; Kuo, R.-L.; Ye, Q.; Jiang, Y.; Tao, Y. J.; Krug, R. M. Interaction of the influenza A virus nucleocapsid protein with the viral RNA polymerase potentiates unprimed viral RNA replication. *J. Virol.* **2009**, *83*, 29–36.
32. Zhang, S.; Weng, L.; Geng, L.; Wang, J.; Zhou, J.; Deubel, V.; Buchy, P.; Toyoda, T. Biochemical and kinetic analysis of the influenza virus RNA polymerase purified from insect cells. *Biochemical and Biophysical Research Communications* **2010**, *391*, 570–574.
33. Fodor, E.; Pritlove, D. C.; Brownlee, G. G. The influenza virus panhandle is involved in the initiation of transcription. *J. Virol.* **1994**, *68*, 4092–4096.
34. Luo, G. X.; Luytjes, W.; Enami, M.; Palese, P. The polyadenylation signal of influenza virus RNA involves a stretch of uridines followed by the RNA duplex of



- the panhandle structure. *J. Virol.* **1991**, *65*, 2861–2867.
35. Hagen, M.; Chung, T. D.; Butcher, J. A.; Krystal, M. Recombinant influenza virus polymerase: requirement of both 5' and 3' viral ends for endonuclease activity. *J. Virol.* **1994**, *68*, 1509–1515.
36. Baudin, F.; Bach, C.; Cusack, S.; Ruigrok, R. W. Structure of influenza virus RNP. I. Influenza virus nucleoprotein melts secondary structure in panhandle RNA and exposes the bases to the solvent. *EMBO J.* **1994**, *13*, 3158–3165.
37. Shaw, M.; Palese, P. *Orthomyxoviridae*. In *Fields Virology*, 6th ed.; Knipe, D.M., Howley, P., Eds.; Lippincott Williams & Wilkins: Philadelphia, PA, USA, 2013; Chapter 40, Volume 1, pp. 1151–1185.
38. York, A.; Hengrung, N.; Vreede, F. T.; Huiskonen, J. T.; Fodor, E. Isolation and characterization of the positive-sense replicative intermediate of a negative-strand RNA virus. *Proc. Natl. Acad. Sci. U. S. A.* **2013**, *110*, E4238–E4245.
39. Vreede, F. T.; Jung, T. E.; Brownlee, G. G. Model suggesting that replication of influenza virus is regulated by stabilization of replicative intermediates. *J. Virol.* **2004**, *78*, 9568–9572.
40. Vreede, F. T.; Ng, A. K.-L.; Shaw, P.-C.; Fodor, E. Stabilization of influenza virus replication intermediates is dependent on the RNA-binding but not the homo-oligomerization activity of the viral nucleoprotein. *J. Virol.* **2011**, *85*,

- 12073–12078.
- 
41. Jorba, N.; Coloma, R.; Ortín, J. Genetic trans-complementation establishes a new model for influenza virus RNA transcription and replication. *PLoS Pathog.* **2009**, *5*, e1000462.
42. Robertson, J. S.; Schubert, M.; Lazzarini, R. A. Polyadenylation sites for influenza virus mRNA. *J. Virol.* **1981**, *38*, 157–163.
43. Poon, L. L. M.; Pritlove, D. C.; Fodor, E.; Brownlee, G. G. Direct evidence that the poly(A) tail of influenza A virus mRNA is synthesized by reiterative copying of a U track in the virion RNA template. *J. Virol.* **1999**, *73*, 3473–3476.
44. Vreede, F. T.; Brownlee, G. G. Influenza virion-derived viral ribonucleoproteins synthesize both mRNA and cRNA in vitro. *J. Virol.* **2007**, *81*, 2196–2204.
45. Beaton, A. R.; Krug, R. M. Transcription antitermination during influenza viral template RNA synthesis requires the nucleocapsid protein and the absence of a 5' capped end. *Proc. Natl. Acad. Sci. U. S. A.* **1986**, *83*, 6282–6286.
46. Shapiro, G. I.; Krug, R. M. Influenza virus RNA replication in vitro: synthesis of viral template RNAs and virion RNAs in the absence of an added primer. *J. Virol.* **1988**, *62*, 2285–2290.
47. Tao, Y. J.; Ye, Q. RNA virus replication complexes. *PLoS Pathog.* **2010**, *6*, e1000943.

- 
48. Tarus, B.; Bakowicz, O.; Chenavas, S.; Duchemin, L.; Estrozi, L. F.; Bourdieu, C.; Lejal, N.; Bernard, J.; Moudjou, M.; Chevalier, C.; Delmas, B.; Ruigrok, R. W. H.; Di Primo, C.; Slama-Schwok, A. Oligomerization paths of the nucleoprotein of influenza A virus. *Biochimie* **2012**, *94*, 776–785.
49. Davey, J.; Dimmock, N. J.; Colman, A. Identification of the sequence responsible for the nuclear accumulation of the influenza virus nucleoprotein in *Xenopus* oocytes. *Cell* **1985**, *40*, 667–675.
50. Yamanaka, K.; Ishihama, A.; Nagata, K. Reconstitution of influenza virus RNA-nucleoprotein complexes structurally resembling native viral ribonucleoprotein cores. *J. Biol. Chem.* **1990**, *265*, 11151–11155.
51. Mena, I.; Jambrina, E.; Albo, C.; Perales, B.; Ortín, J.; Arrese, M.; Vallejo, D.; Portela, A. Mutational analysis of influenza A virus nucleoprotein: identification of mutations that affect RNA replication. *J. Virol.* **1999**, *73*, 1186–1194.
52. Tao, Y. J.; Ye, Q. Influenza A virus nucleoprotein in influenza: molecular virology. *Caister Academic, Norfolk, UK* **2010**, 53–68.
53. Arrese, M.; Portela, A. Serine 3 is critical for phosphorylation at the N-terminal end of the nucleoprotein of influenza virus A/Victoria/3/75. *J. Virol.* **1996**, *70*, 3385–3391.
54. Momose, F.; Naito, T.; Yano, K.; Sugimoto, S.; Morikawa, Y.; Nagata, K.





- Identification of Hsp90 as a stimulatory host factor involved in influenza virus RNA synthesis. *J. Biol. Chem.* **2002**, *277*, 45306–45314.
55. Naito, T.; Kiyasu, Y.; Sugiyama, K.; Kimura, A.; Nakano, R.; Matsukage, A.; Nagata, K. An influenza virus replicon system in yeast identified Tat-SF1 as a stimulatory host factor for viral RNA synthesis. *Proc. Natl. Acad. Sci.* **2007**, *104*, 18235–18240.
56. Momose, F.; Handa, H.; Nagata, K. Identification of host factors that regulate the influenza virus RNA polymerase activity. *Biochimie* **1996**, *78*, 1103–1108.
57. Kawaguchi, A.; Momose, F.; Nagata, K. Replication-coupled and host factor-mediated encapsidation of the influenza virus genome by viral nucleoprotein. *J. Virol.* **2011**, *85*, 6197–6204.
58. Momose, F.; Basler, C. F.; O'Neill, R. E.; Iwamatsu, A.; Palese, P.; Nagata, K. Cellular splicing factor RAF-2p48/NPI-5/BAT1/UAP56 interacts with the influenza virus nucleoprotein and enhances viral RNA synthesis. *J. Virol.* **2001**, *75*, 1899–1908.
59. Yoshimura, A.; Ohnishi, S. Uncoating of influenza virus in endosomes. *J. Virol.* **1984**, *51*, 497–504.
60. Babcock, H. P.; Chen, C.; Zhuang, X. Using single-particle tracking to study nuclear trafficking of viral genes. *Biophys. J.* **2004**, *87*, 2749–2758.

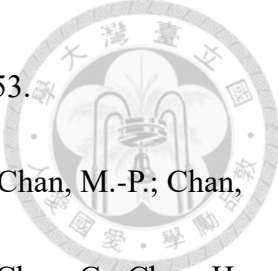



61. Martin, K.; Helenius, A. Transport of incoming influenza virus nucleocapsids into the nucleus. *J. Virol.* **1991**, *65*, 232–244.
62. O'Neill, R. E.; Jaskunas, R.; Blobel, G.; Palese, P.; Moroianu, J. Nuclear import of influenza virus RNA can be mediated by viral nucleoprotein and transport factors required for protein import. *J. Biol. Chem.* **1995**, *270*, 22701–22704.
63. Neumann, G.; Hughes, M. T.; Kawaoka, Y. Influenza A virus NS2 protein mediates vRNP nuclear export through NES-independent interaction with hCRM1. *EMBO J.* **2000**, *19*, 6751–6758.
64. O'Neill, R. E.; Talon, J.; Palese, P. The influenza virus NEP (NS2 protein) mediates the nuclear export of viral ribonucleoproteins. *EMBO J.* **1998**, *17*, 288–296.
65. Huang, S.; Chen, J.; Chen, Q.; Wang, H.; Yao, Y.; Chen, J.; Chen, Z. A second CRM1-dependent nuclear export signal in the influenza A virus NS2 protein contributes to the nuclear export of viral ribonucleoproteins. *J. Virol.* **2013**, *87*, 767–778.
66. Paterson, D.; Fodor, E. Emerging roles for the influenza A virus nuclear export protein (NEP). *PLoS Pathog.* **2012**, *8*, e1003019.
67. Eisfeld, A. J.; Neumann, G.; Kawaoka, Y. Human immunodeficiency virus rev-binding protein is essential for influenza A virus replication and promotes genome trafficking in late-stage infection. *J. Virol.* **2011**, *85*, 9588–9598.

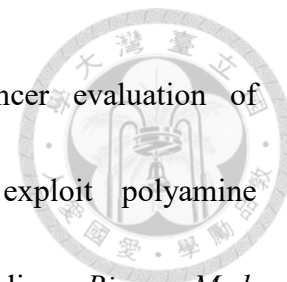


- 
68. Eisfeld, A. J.; Kawakami, E.; Watanabe, T.; Neumann, G.; Kawaoka, Y. RAB11A is essential for transport of the influenza virus genome to the plasma membrane. *J. Virol.* **2011**, *85*, 6117–6126.
69. Amorim, M. J.; Bruce, E. A.; Read, E. K. C.; Foeglein, Á.; Mahen, R.; Stuart, A. D.; Digard, P. A Rab11- and microtubule-dependent mechanism for cytoplasmic transport of influenza A virus viral RNA. *J. Virol.* **2011**, *85*, 4143–4156.
70. Momose, F.; Sekimoto, T.; Ohkura, T.; Jo, S.; Kawaguchi, A.; Nagata, K.; Morikawa, Y. Apical transport of influenza A virus ribonucleoprotein requires Rab11-positive recycling endosome. *PLoS ONE* **2011**, *6*, e21123.
71. Avilov, S. V.; Moisy, D.; Naffakh, N.; Cusack, S. Influenza A virus progeny vRNP trafficking in live infected cells studied with the virus-encoded fluorescently tagged PB2 protein. *Vaccine* **2012**, *30*, 7411–7417.
72. Bruce, Emily A.; Stuart, A.; McCaffrey, Mary W.; Digard, P. Role of the Rab11 pathway in negative-strand virus assembly. *Biochem. Soc. T.* **2012**, *40*, 1409–1415.
73. Rossman, J. S.; Jing, X.; Leser, G. P.; Lamb, R. A. Influenza virus M2 protein mediates ESCRT-independent membrane scission. *Cell* **2010**, *142*, 902–913.
74. Fodor, E.; Seong, B. L.; Brownlee, G. G. Photochemical cross-linking of influenza A polymerase to its virion RNA promoter defines a polymerase binding site at residues 9 to 12 of the promoter. *J. Gen. Virol.* **1993**, *74*, 1327–1333.

- 
75. Elton, D.; Medcalf, L.; Bishop, K.; Harrison, D.; Digard, P. Identification of amino acid residues of influenza virus nucleoprotein essential for RNA binding. *J. Virol.* **1999**, *73*, 7357–7367.
76. Chan, W.-H.; Ng, A. K.-L.; Robb, N. C.; Lam, M. K.-H.; Chan, P. K.-S.; Au, S. W.-N.; Wang, J.-H.; Fodor, E.; Shaw, P.-C. Functional analysis of the influenza virus H5N1 nucleoprotein tail loop reveals amino acids that are crucial for oligomerization and ribonucleoprotein activities. *J. Virol.* **2010**, *84*, 7337–7345.
77. Sumranjit, J.; Chung, S. Recent advances in target characterization and identification by photoaffinity probes. *Molecules* **2013**, *18*, 10425–10451.
78. Vodovozova, E. L. Photoaffinity labeling and its applicaiotn in structural biology. *Biochem. Moscow.* **2007**, *72*, 1–20.
79. Dubinsky, L.; Krom, B. P.; Meijler, M. M. Diazirine based photoaffinity labeling. *Bioorg. Med. Chem.* **2012**, *20*, 554–570.
80. Cianci, C.; Gerritz, S. W.; Deminie, C.; Krystal, M. Influenza nucleoprotein: promising target for antiviral chemotherapy. *Antivir. Chem. Chemoth.* **2013**, *23*, 77–91.
81. Cheng, H.; Wan, J.; Lin, M.-I.; Liu, Y.; Lu, X.; Liu, J.; Xu, Y.; Chen, J.; Tu, Z.; Cheng, Y.-S. E.; Ding, K. Design, synthesis, and in vitro biological evaluation of 1*H*-1,2,3-triazole-4-carboxamide derivatives as new anti-influenza A agents

- 
- targeting virus nucleoprotein. *J. Med. Chem.* **2012**, *55*, 2144–2153.
82. Kao, R. Y.; Yang, D.; Lau, L.-S.; Tsui, W. H. W.; Hu, L.; Dai, J.; Chan, M.-P.; Chan, C.-M.; Wang, P.; Zheng, B.-J.; Sun, J.; Huang, J.-D.; Madar, J.; Chen, G.; Chen, H.; Guan, Y.; Yuen, K.-Y. Identification of influenza A nucleoprotein as an antiviral target. *Nat. Biotech.* **2010**, *28*, 600–605.
83. Su, C.-Y.; Cheng, T.-J. R.; Lin, M.-I.; Wang, S.-Y.; Huang, W.-I.; Lin-Chu, S.-Y.; Chen, Y.-H.; Wu, C.-Y.; Lai, M. M. C.; Cheng, W.-C.; Wu, Y.-T.; Tsai, M.-D.; Cheng, Y.-S. E.; Wong, C.-H. High-throughput identification of compounds targeting influenza RNA-dependent RNA polymerase activity. *Proc. Natl. Acad. Sci. U. S. A.* **2010**, *107*, 19151–19156.
84. Gerritz, S. W.; Cianci, C.; Kim, S.; Pearce, B. C.; Deminie, C.; Discotto, L.; McAuliffe, B.; Minassian, B. F.; Shi, S.; Zhu, S.; Zhai, W.; Pendri, A.; Li, G.; Poss, M. A.; Edavettal, S.; McDonnell, P. A.; Lewis, H. A.; Maskos, K.; Mörtl, M.; Kiefersauer, R.; Steinbacher, S.; Baldwin, E. T.; Metzler, W.; Bryson, J.; Healy, M. D.; Philip, T.; Zoeckler, M.; Schartman, R.; Sinz, M.; Leyva-Grado, V. H.; Hoffmann, H.-H.; Langley, D. R.; Meanwell, N. A.; Krystal, M. Inhibition of influenza virus replication via small molecules that induce the formation of higher-order nucleoprotein oligomers. *Proc. Natl. Acad. Sci. U. S. A.* **2011**, *108*, 15366–15371.

- 
85. Wu, X.; Wu, X.; Sun, Q.; Zhang, C.; Yang, S.; Li, L.; Jia, Z. Progress of small molecular inhibitors in the development of anti-influenza virus agents. *Theranostics* **2017**, *7*, 826–845.
86. Kakisaka, M.; Sasaki, Y.; Yamada, K.; Kondoh, Y.; Hikono, H.; Osada, H.; Tomii, K.; Saito, T.; Aida, Y. A novel antiviral target structure involved in the RNA binding, dimerization, and nuclear export functions of the influenza A virus nucleoprotein. *PLoS Pathog.* **2015**, *11*, e1005062.
87. LoCoco, M. D.; Zhang, X.; Jordan, R. F. Chelate-controlled synthesis of racemic ansa-zirconocenes. *J. Am. Chem. Soc.* **2004**, *126*, 15231–15244.
88. Lee, J. W.; Jun, S. I.; Kim, K. An efficient and practical method for the synthesis of mono-N-protected  $\alpha,\omega$ -diaminoalkanes. *Tetrahedron Lett.* **2001**, *42*, 2709–2711.
89. Shi, Y.; Pierce, J. G. Synthesis of the 5,6-dihydroxymorpholin-3-one fragment of monanchocidin A. *Org. Lett.* **2015**, *17*, 968–971.
90. Montero, A.; Goya, P.; Jagerovic, N.; Callado, L. F.; Meana, J. J.; Girón, R. O.; Goicoechea, C.; Martín, M. I. Guanidinium and aminoimidazolium derivatives of N-(4-piperidyl)propanamides as potential ligands for  $\mu$  opioid and I2-imidazoline receptors: synthesis and pharmacological screening. *Bioorgan. Med. Chem.* **2002**, *10*, 1009–1018.
91. Chadwick, J.; Jones, M.; Mercer, A. E.; Stocks, P. A.; Ward, S. A.; Park, B. K.;

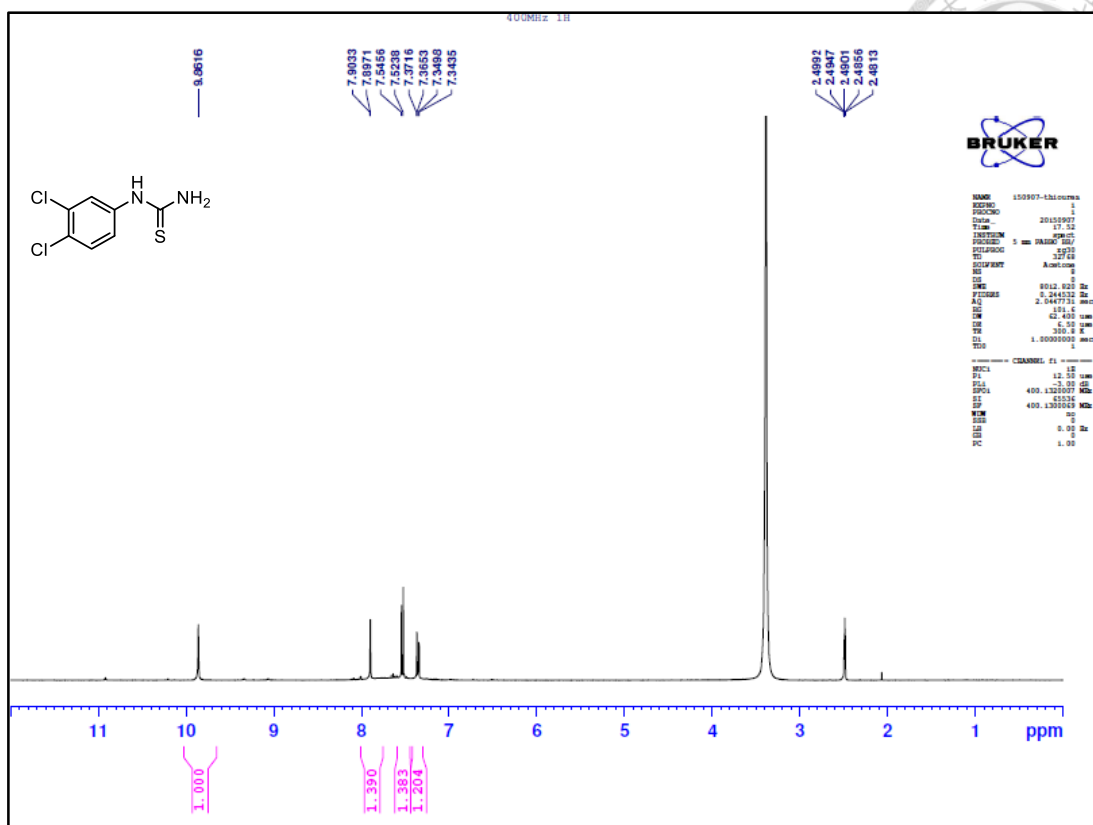


- O'Neill, P. M. Design, synthesis and antimalarial/anticancer evaluation of spermidine linked artemisinin conjugates designed to exploit polyamine transporters in *Plasmodium falciparum* and HL-60 cancer cell lines. *Bioorg. Med. Chem.* **2010**, *18*, 2586–2597.
92. Maruani, A.; Alom, S.; Canavelli, P.; Lee, M. T. W.; Morgan, R. E.; Chudasama, V.; Caddick, S. A mild TCEP-based para-azidobenzyl cleavage strategy to transform reversible cysteine thiol labelling reagents into irreversible conjugates. *Chem. Commun.* **2015**, *51*, 5279–5282.
93. Thomas, J. R.; Liu, X.; Hergenrother, P. J. Size-specific ligands for RNA hairpin loops. *J. Am. Chem. Soc.* **2005**, *127*, 12434–12435.
94. Yu, Z.; Wang, W.; Chen, L. Synthesis of [<sup>2</sup>H<sub>5</sub>]-ebastine fumarate and [<sup>2</sup>H<sub>5</sub>]-hydroxyebastine. *J. Labelled. Compd. Rad.* **2011**, *54*, 352–356.
95. Shi, H.-B.; Zhang, S.-J.; Ge, Q.-F.; Guo, D.-W.; Cai, C.-M.; Hu, W.-X. Synthesis and anticancer evaluation of thiazolyl–chalcones. *Bioorg. Med. Chem. Lett.* **2010**, *20*, 6555–6559.

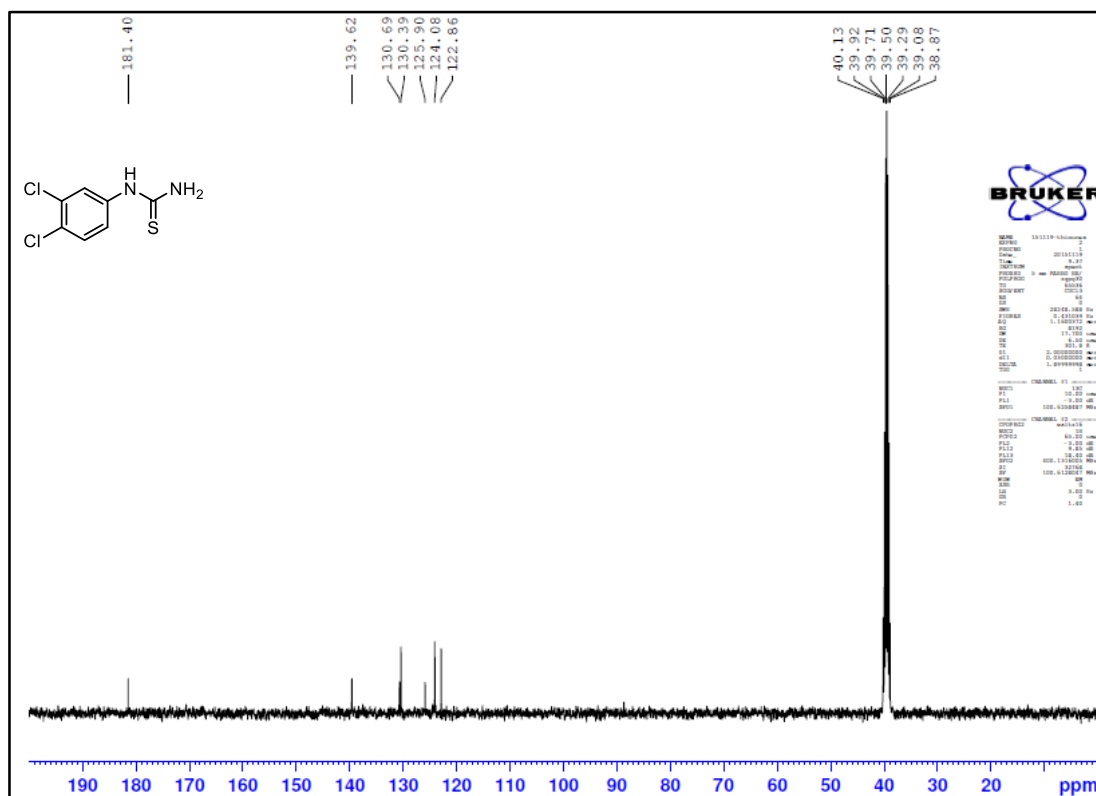


## **Appendix**

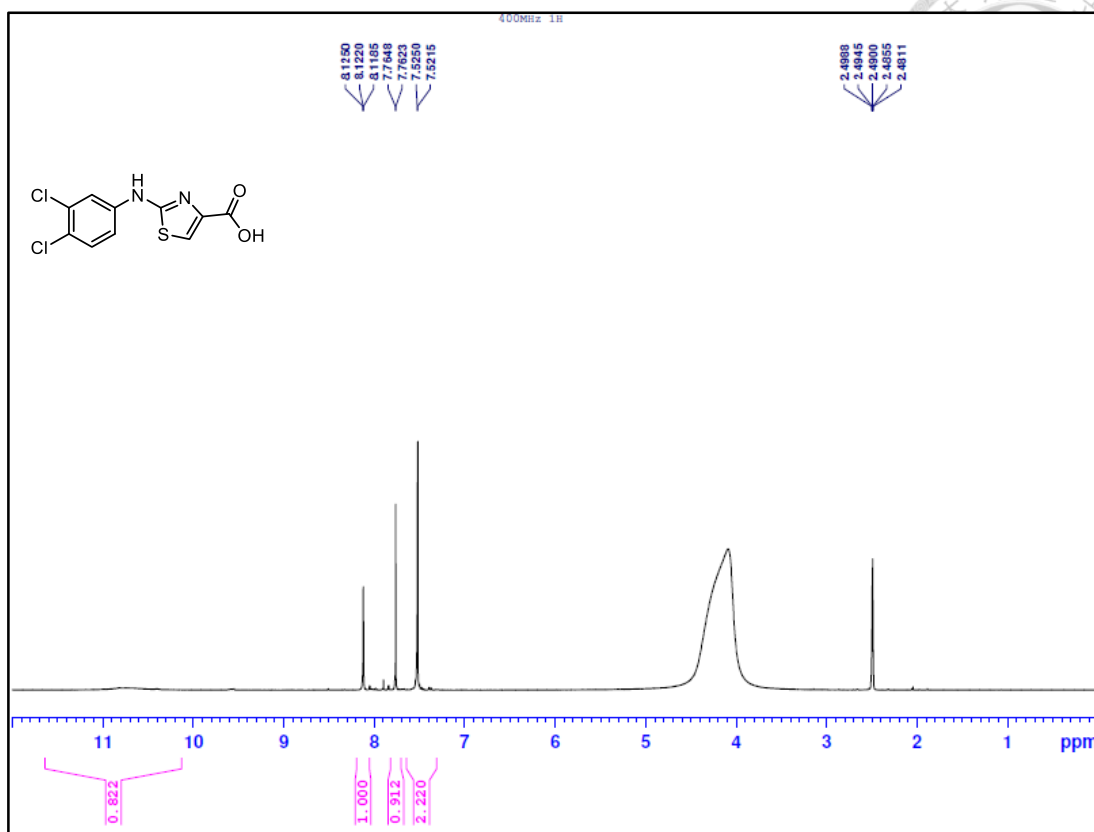
### **$^1\text{H}$ and $^{13}\text{C}$ NMR Spectra and HPLC Diagrams of Synthesized Compounds**



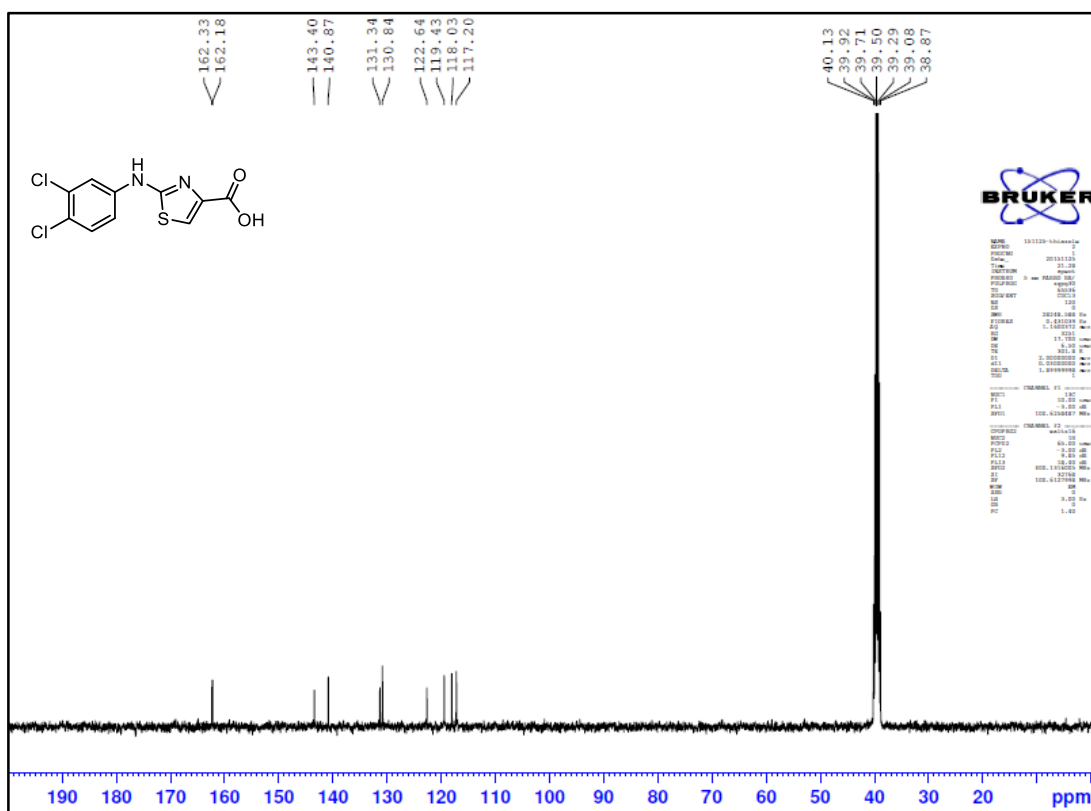
<sup>1</sup>H NMR spectrum of compound 3 (400 MHz, DMSO-*d*<sub>6</sub>)



<sup>13</sup>C NMR spectrum of compound 3 (100 MHz, DMSO-*d*<sub>6</sub>)

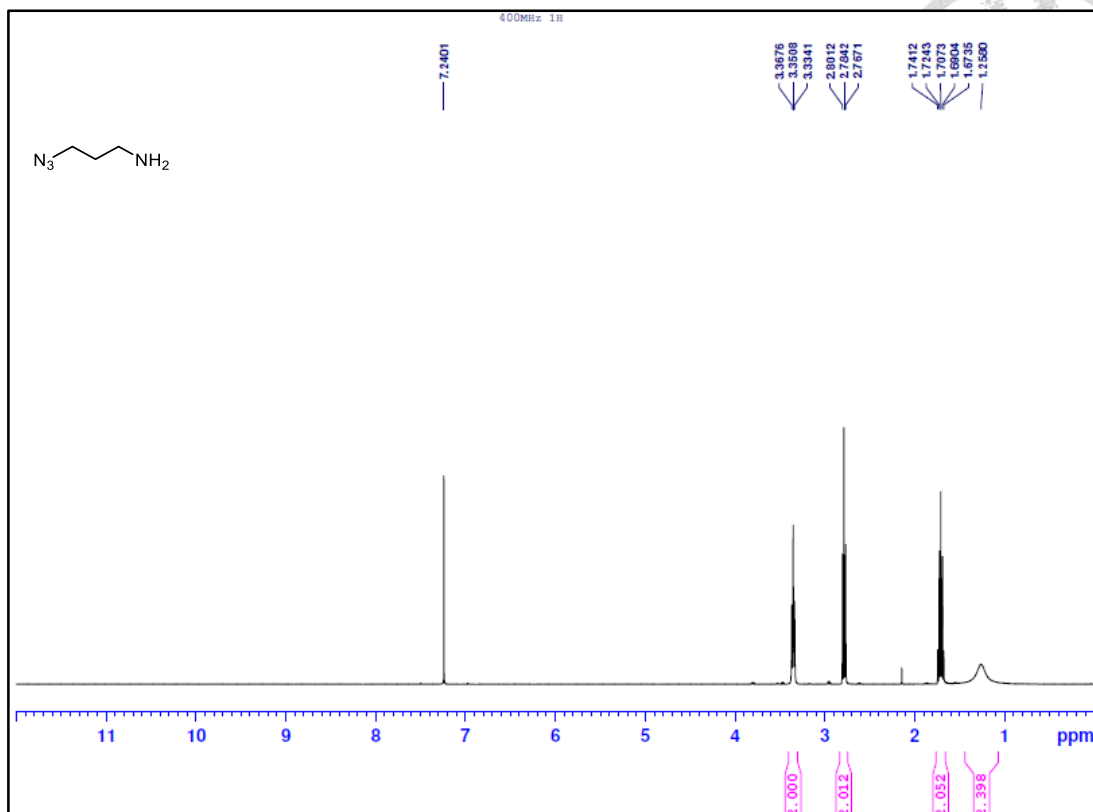


<sup>1</sup>H NMR spectrum of compound 5 (400 MHz, DMSO-*d*<sub>6</sub>)

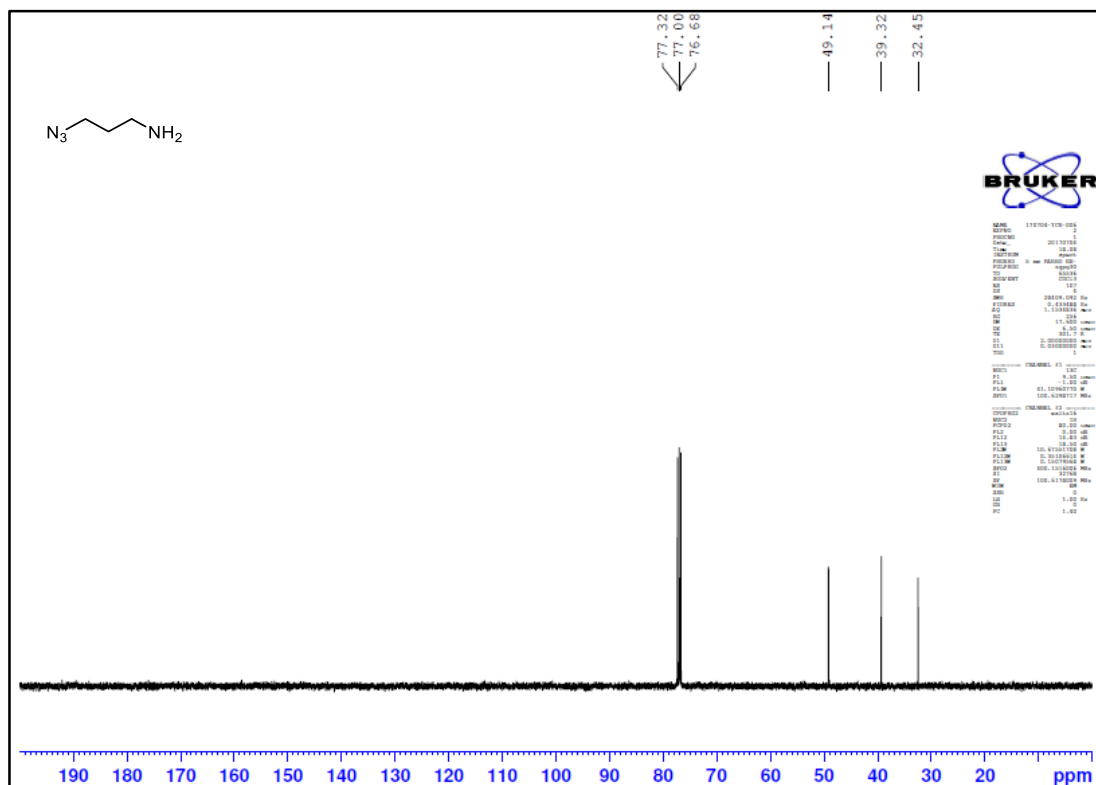


<sup>13</sup>C NMR spectrum of compound 5 (100 MHz, DMSO-*d*<sub>6</sub>)

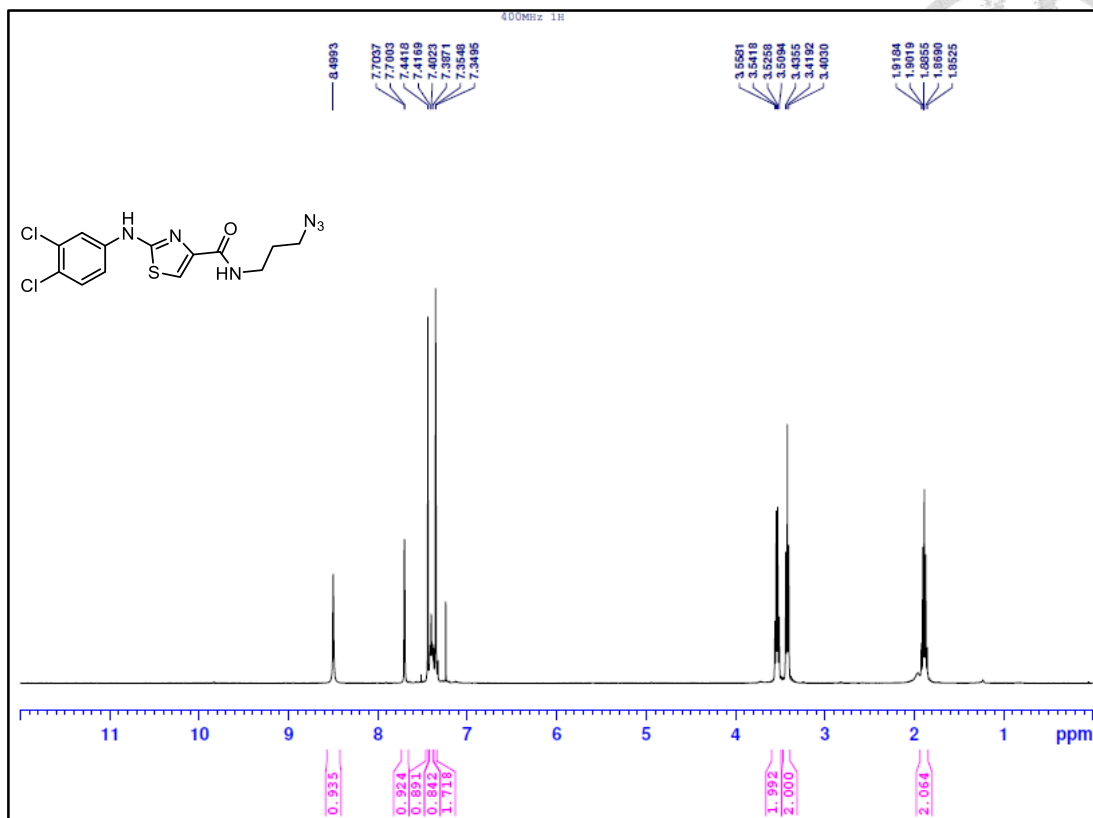




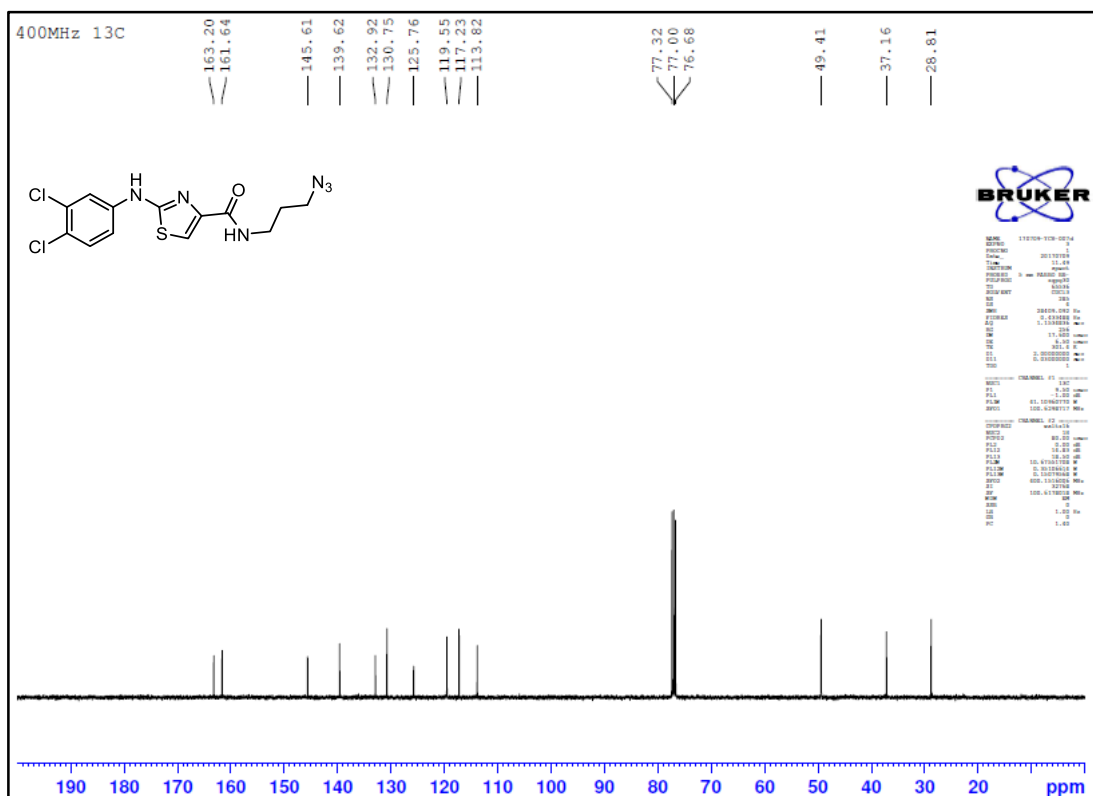
$^1\text{H}$  NMR spectrum of compound **8** (400 MHz,  $\text{CDCl}_3$ )



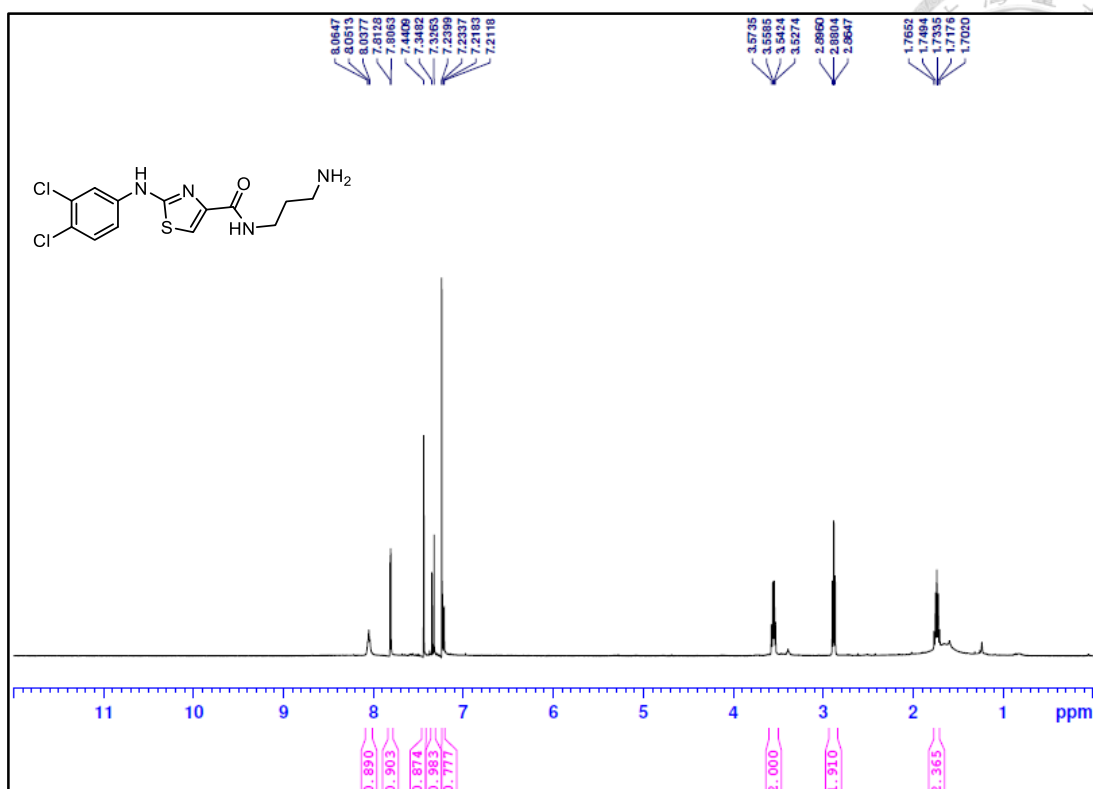
$^{13}\text{C}$  NMR spectrum of compound **8** (100 MHz,  $\text{CDCl}_3$ )



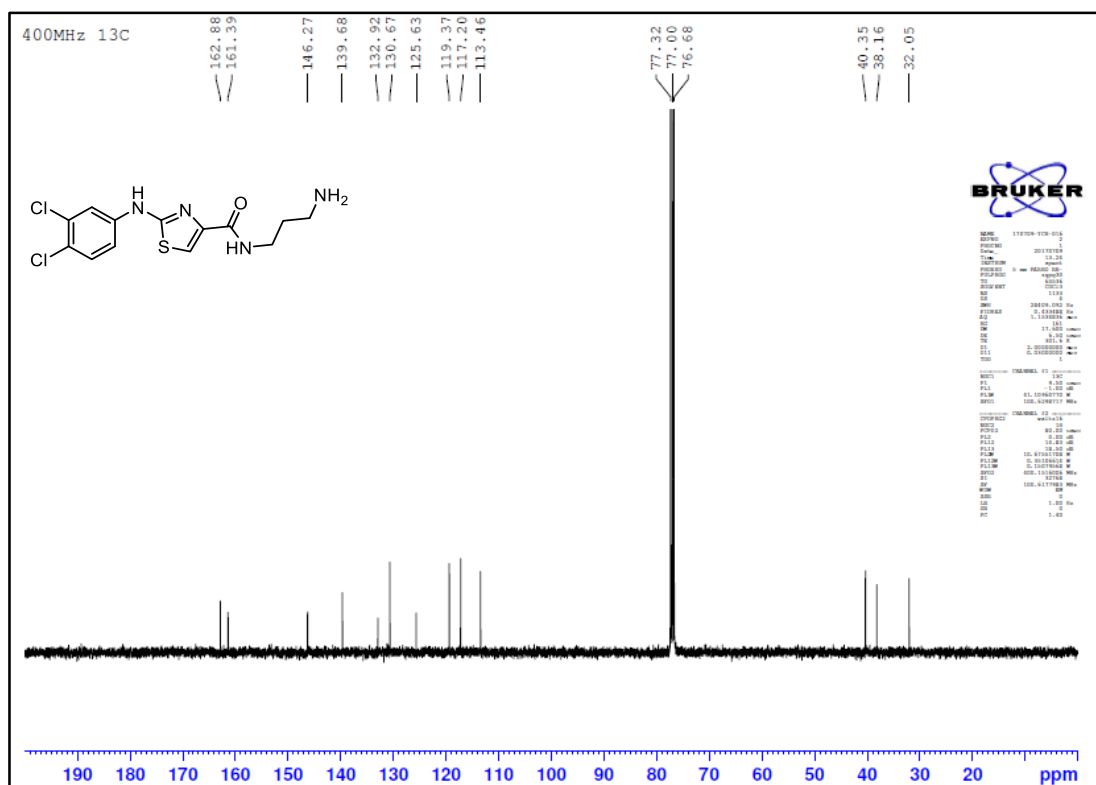
<sup>1</sup>H NMR spectrum of compound **10** (400 MHz, CDCl<sub>3</sub>)



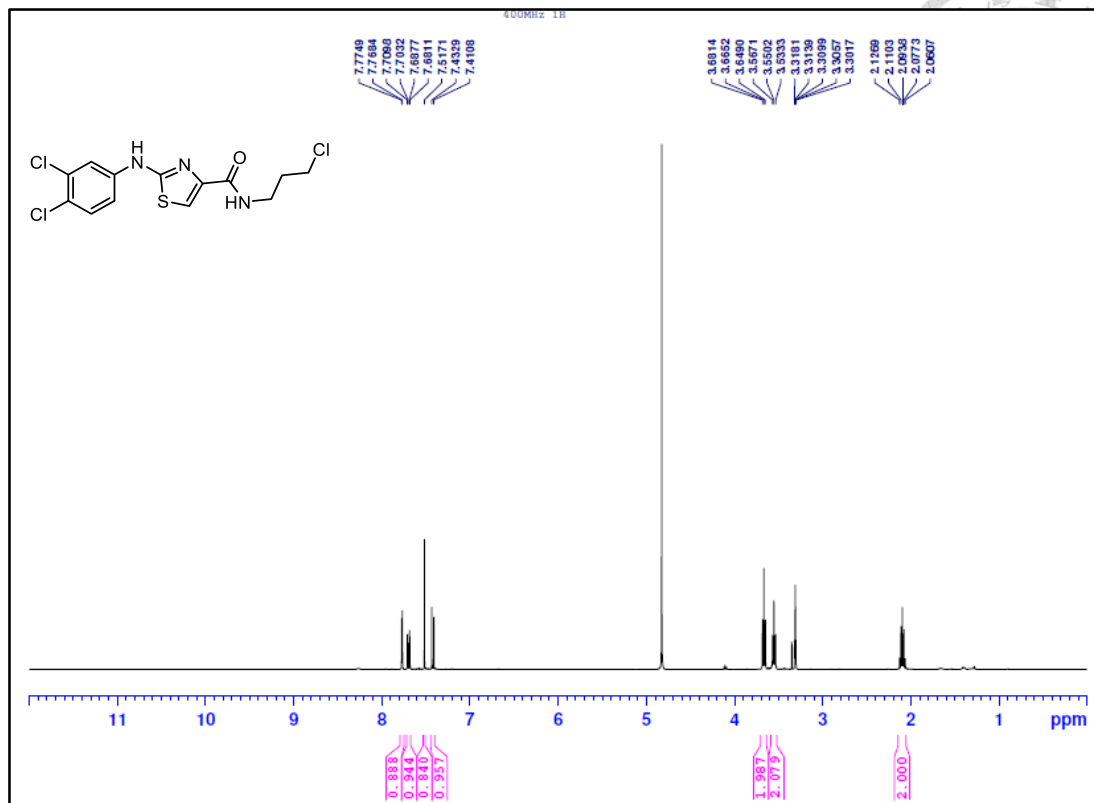
<sup>13</sup>C NMR spectrum of compound **10** (100 MHz, CDCl<sub>3</sub>)



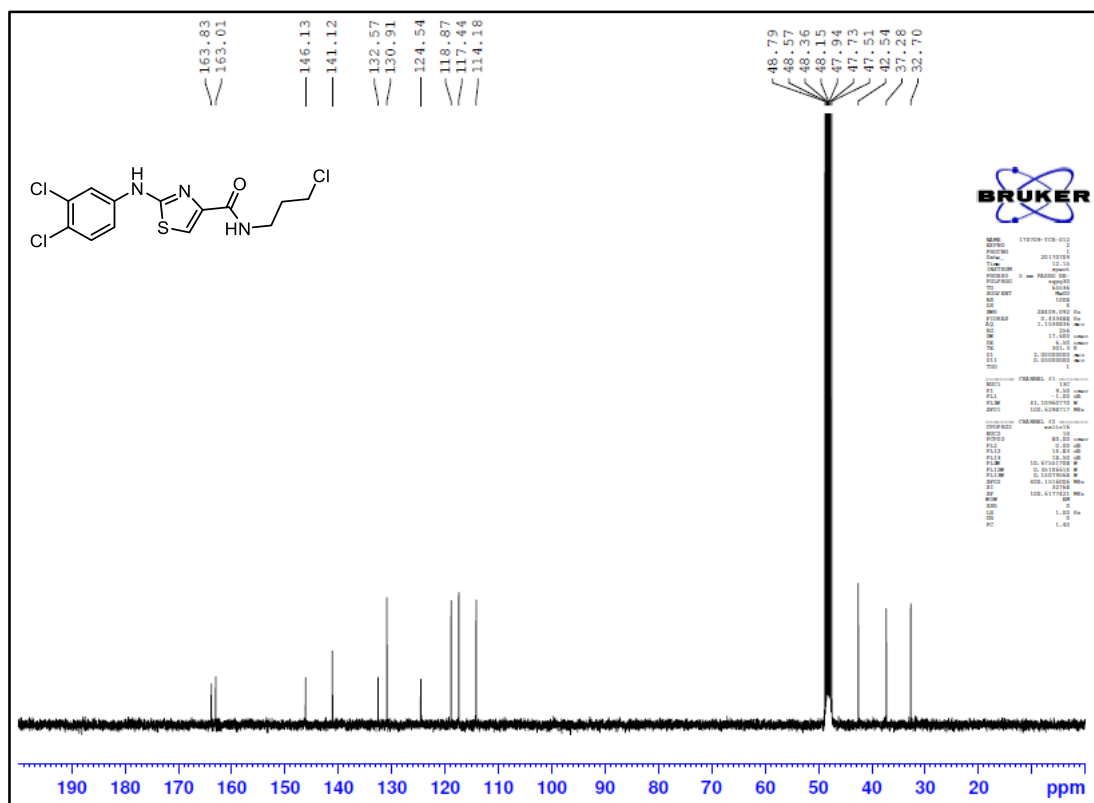
<sup>1</sup>H NMR spectrum of compound 11 (400 MHz, CDCl<sub>3</sub>)



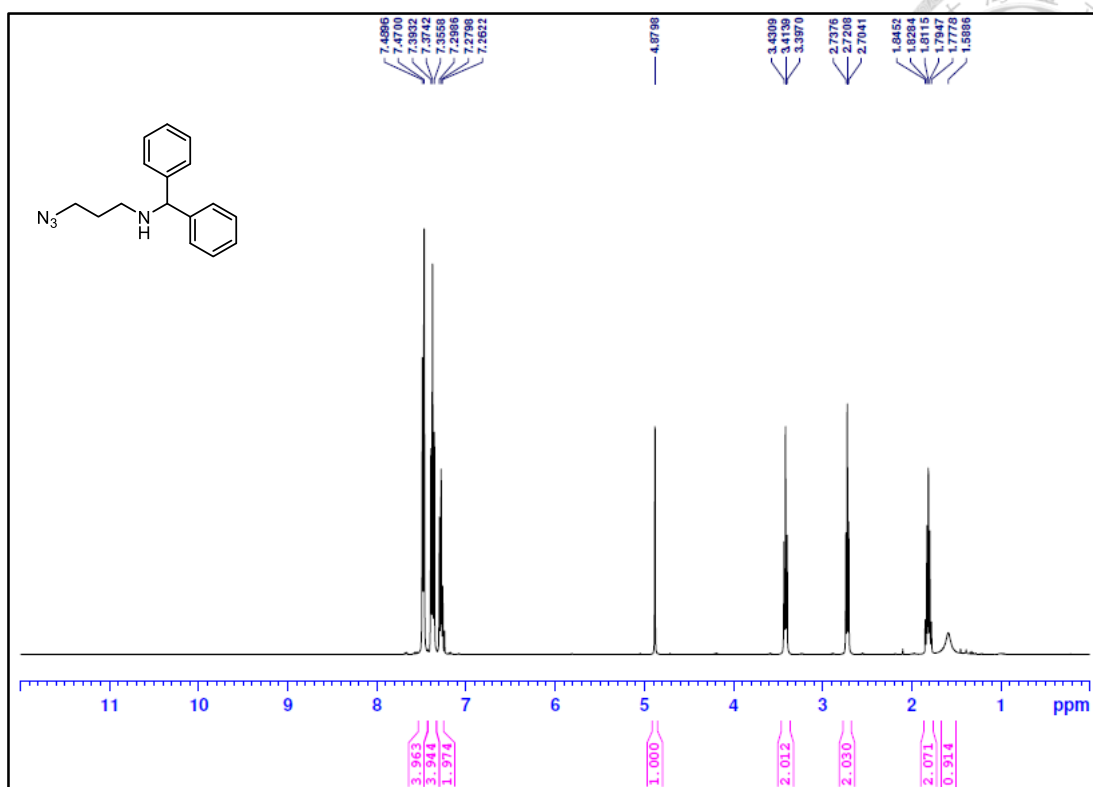
<sup>13</sup>C NMR spectrum of compound 11 (100 MHz, CDCl<sub>3</sub>)



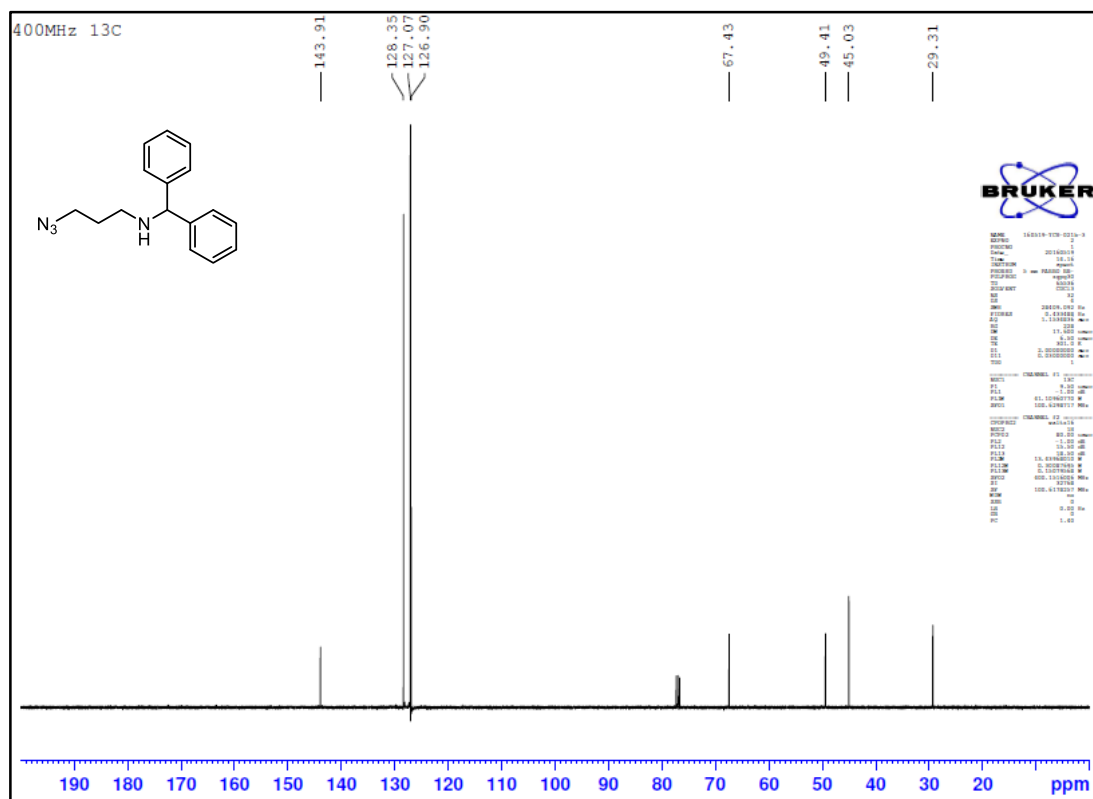
<sup>1</sup>H NMR spectrum of compound 15 (400 MHz, CD<sub>3</sub>OD)



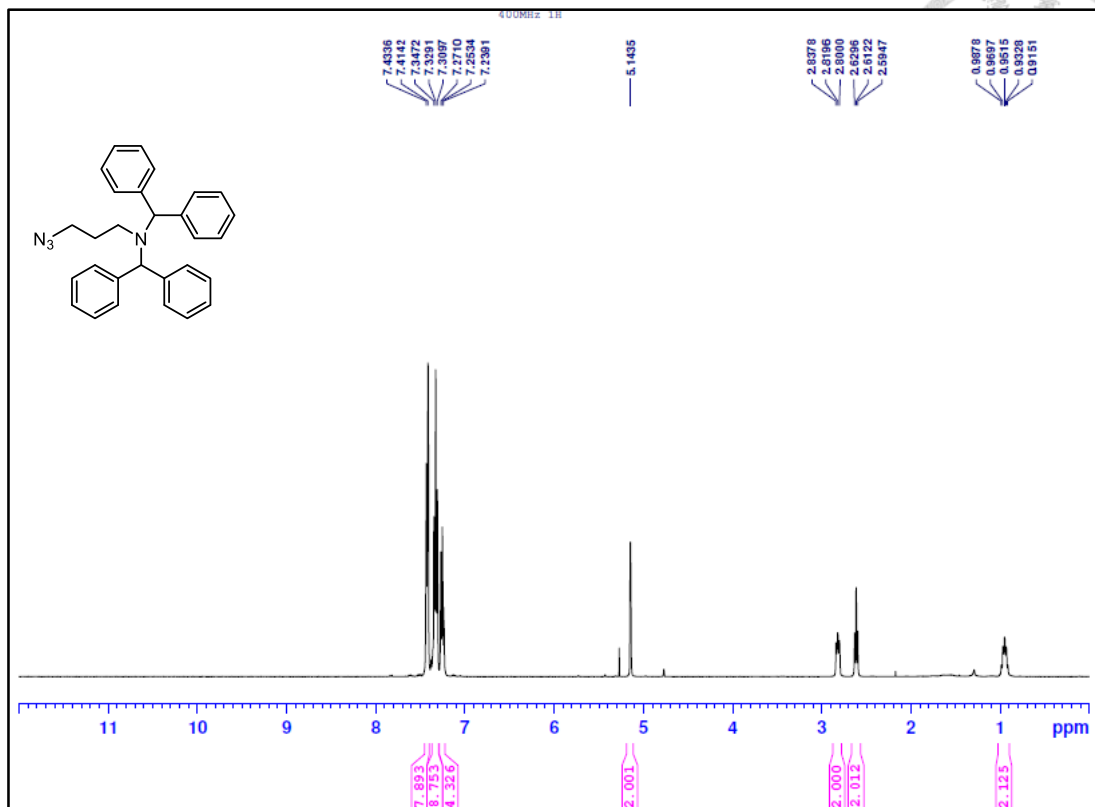
<sup>13</sup>C NMR spectrum of compound 15 (100 MHz, CD<sub>3</sub>OD)



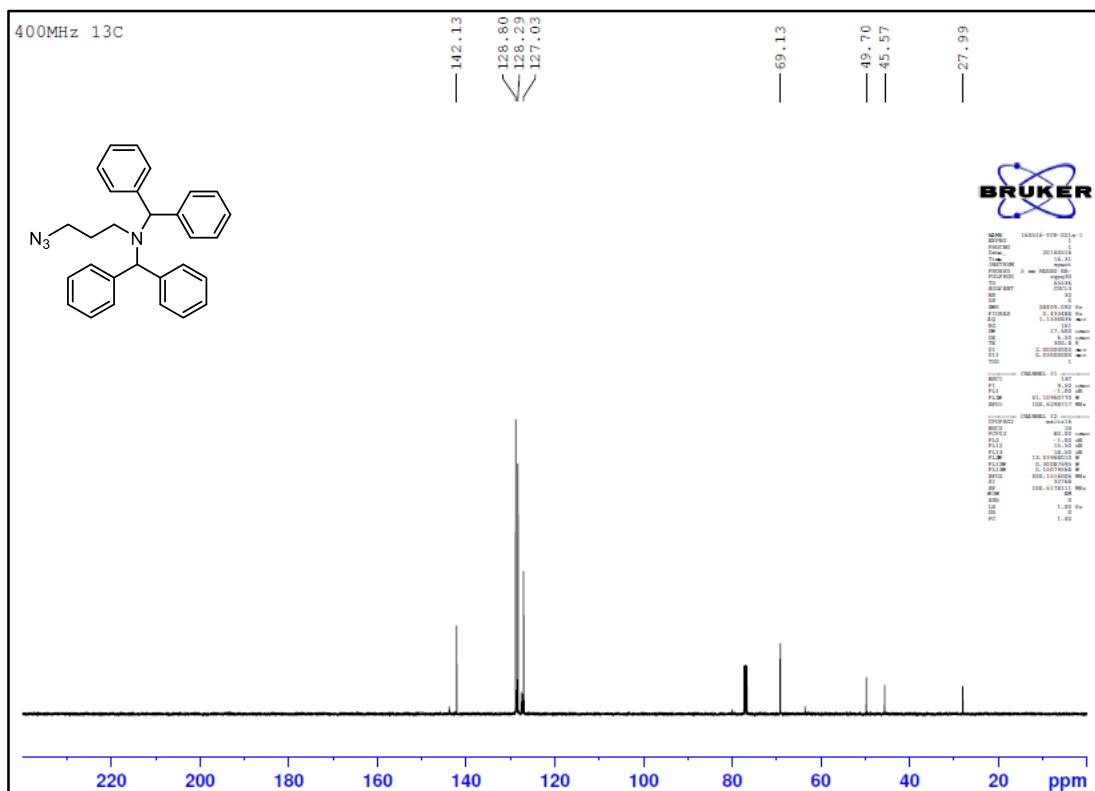
<sup>1</sup>H NMR spectrum of compound 17a (400 MHz, CDCl<sub>3</sub>)



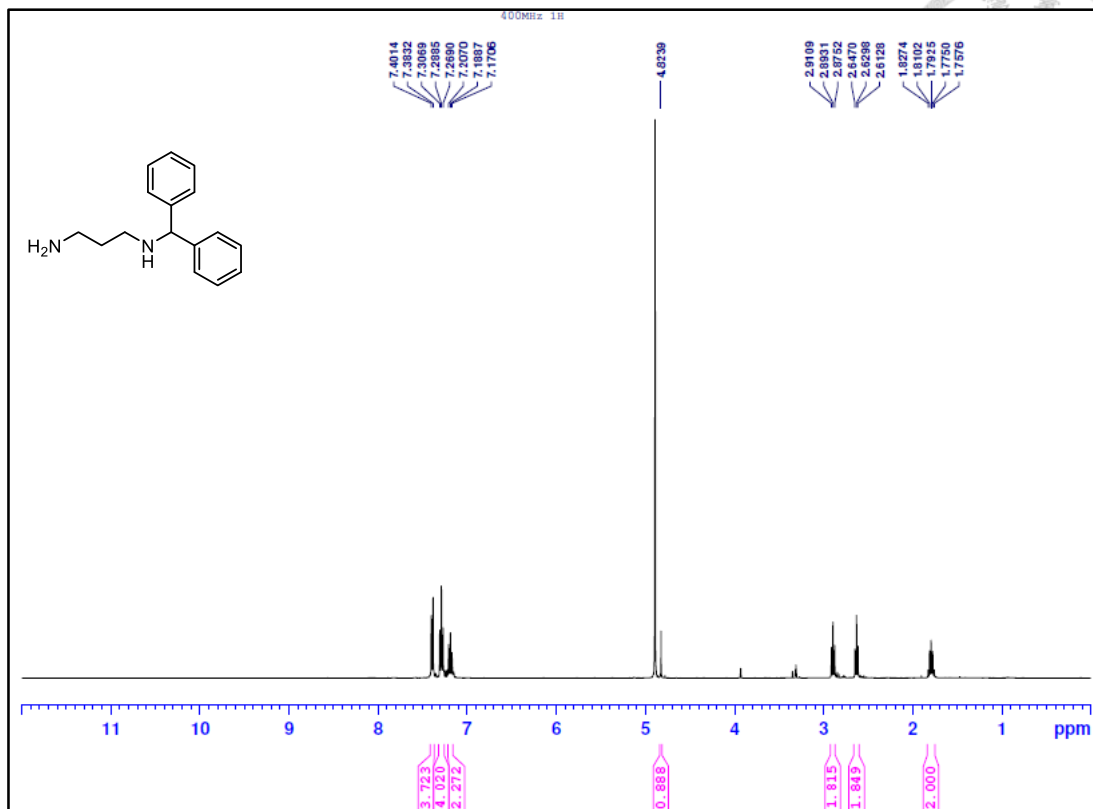
<sup>13</sup>C NMR spectrum of compound 17a (100 MHz, CDCl<sub>3</sub>)



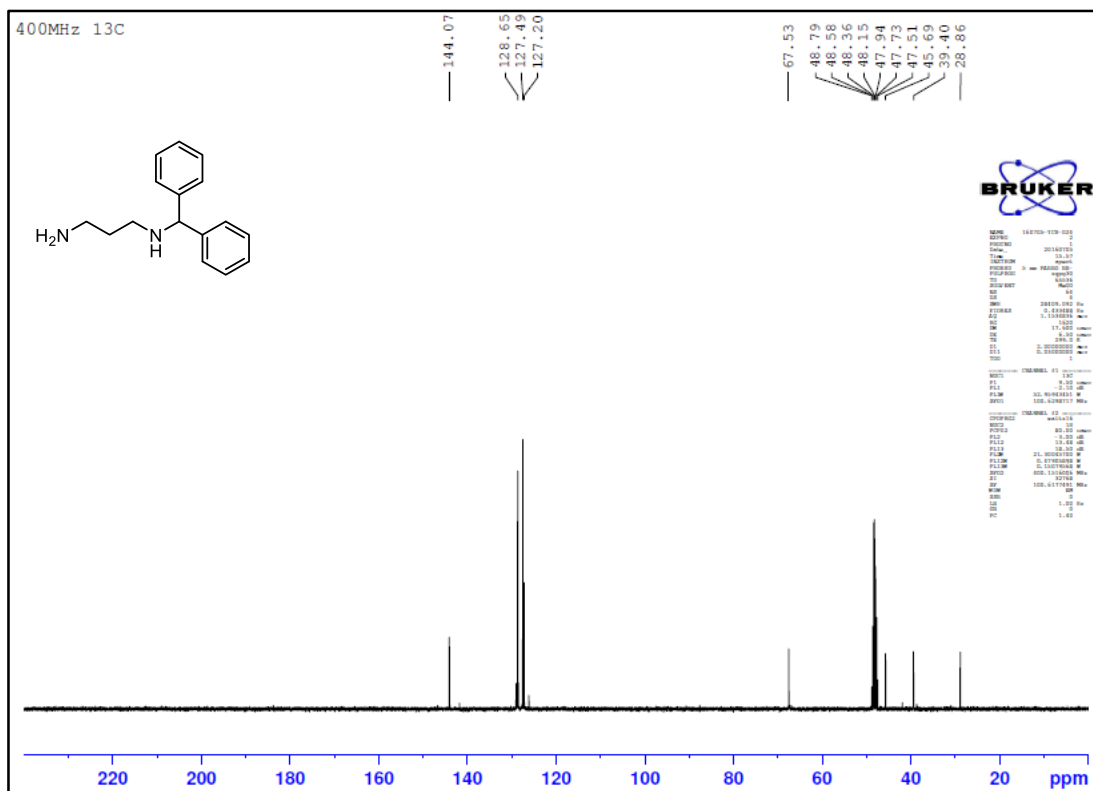
<sup>1</sup>H NMR spectrum of compound **17b** (400 MHz, CDCl<sub>3</sub>)



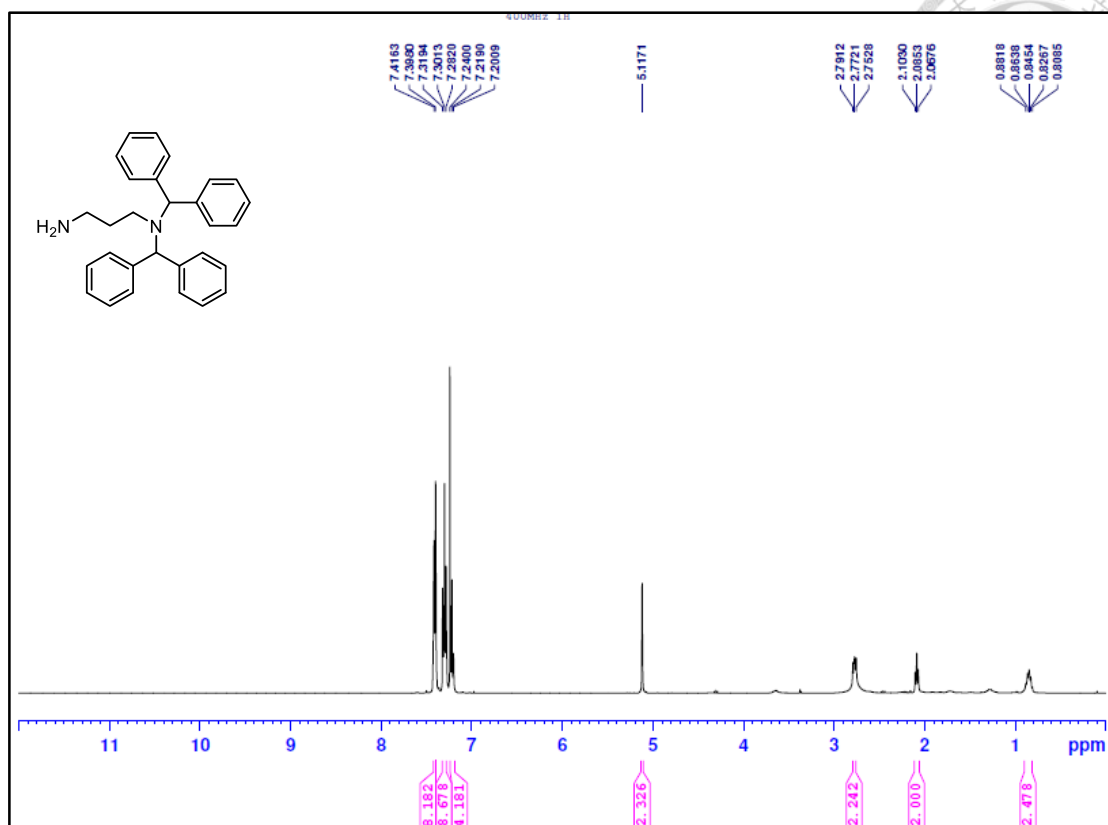
<sup>13</sup>C NMR spectrum of compound **17b** (100 MHz, CDCl<sub>3</sub>)



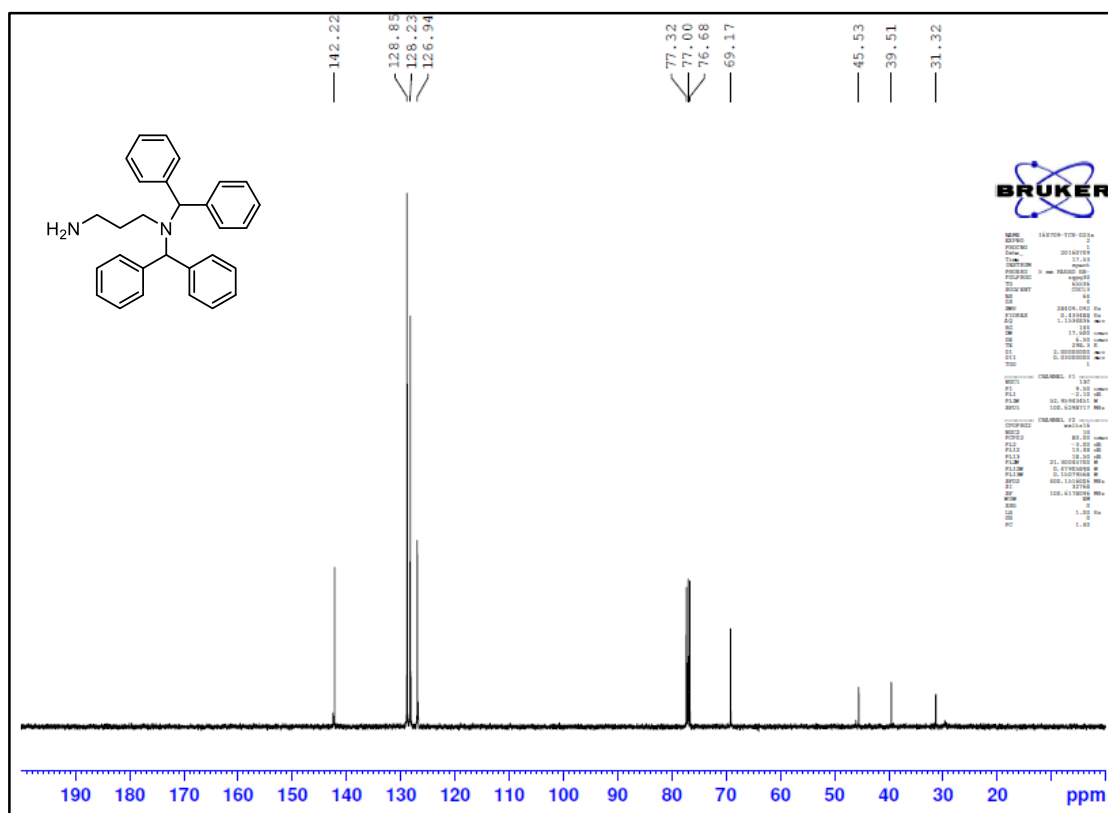
<sup>1</sup>H NMR spectrum of compound **18a** (400 MHz, CD<sub>3</sub>OD)



<sup>13</sup>C NMR spectrum of compound **18a** (100 MHz, CD<sub>3</sub>OD)

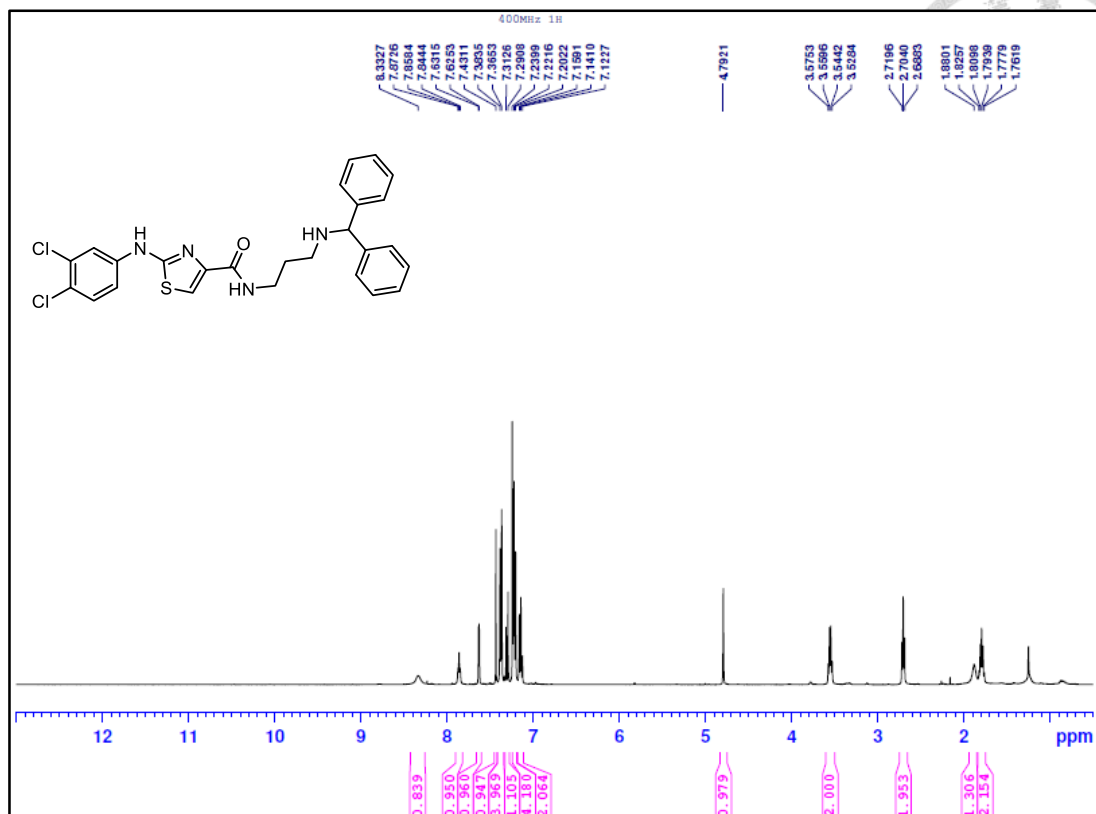


<sup>1</sup>H NMR spectrum of compound **18b** (400 MHz, CDCl<sub>3</sub>)

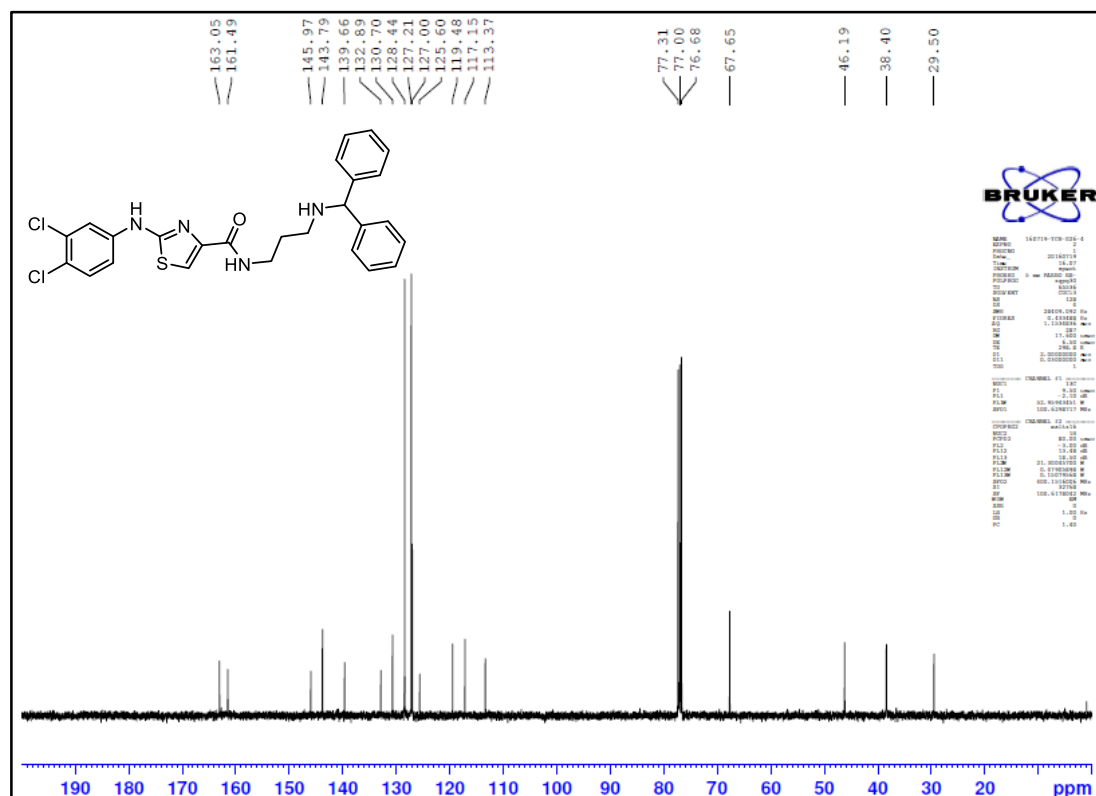


<sup>13</sup>C NMR spectrum of compound **18b** (100 MHz, CDCl<sub>3</sub>)

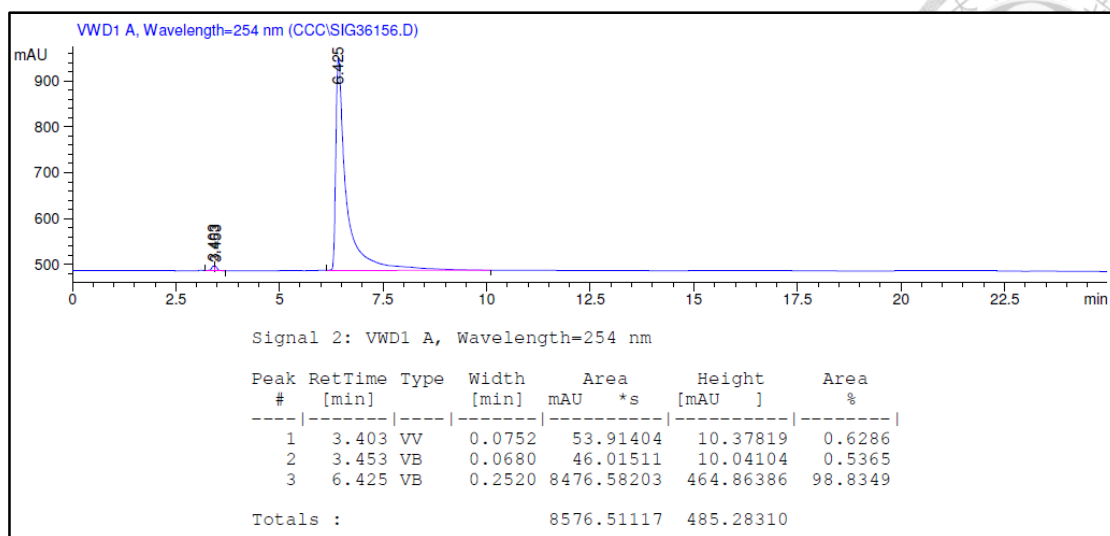




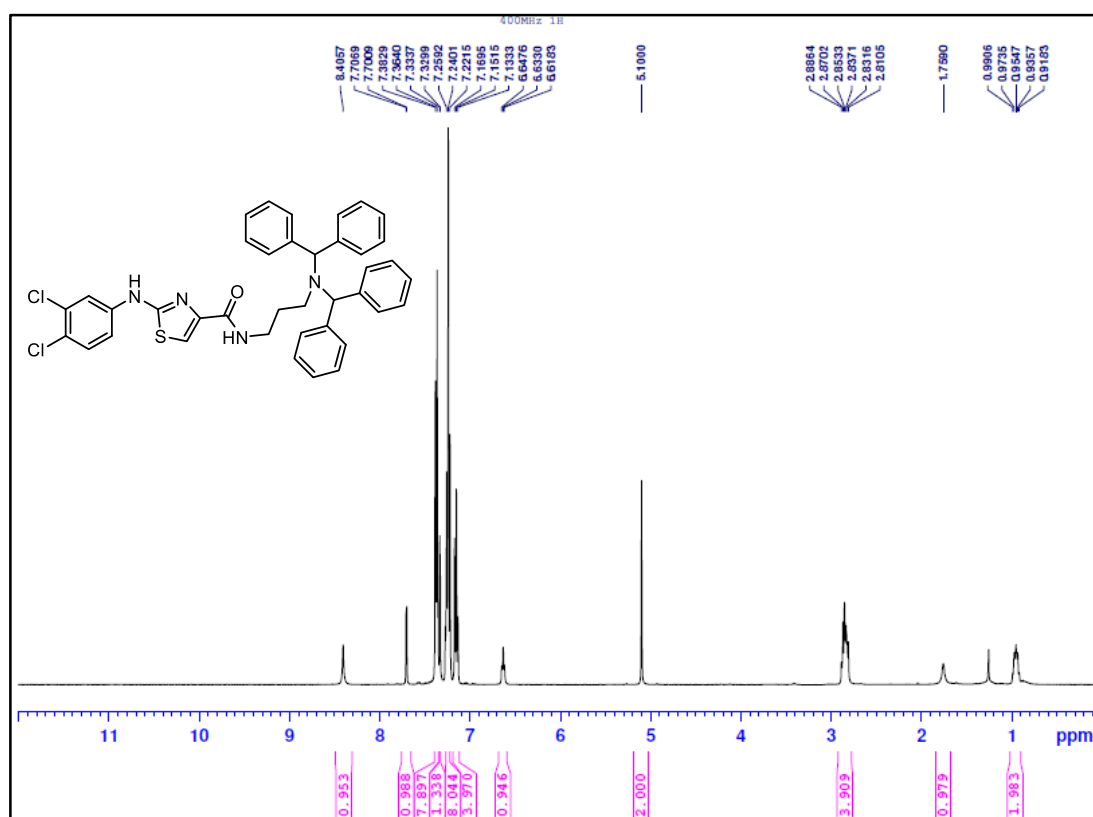
<sup>1</sup>H NMR spectrum of compound **13a** (400 MHz, CDCl<sub>3</sub>)



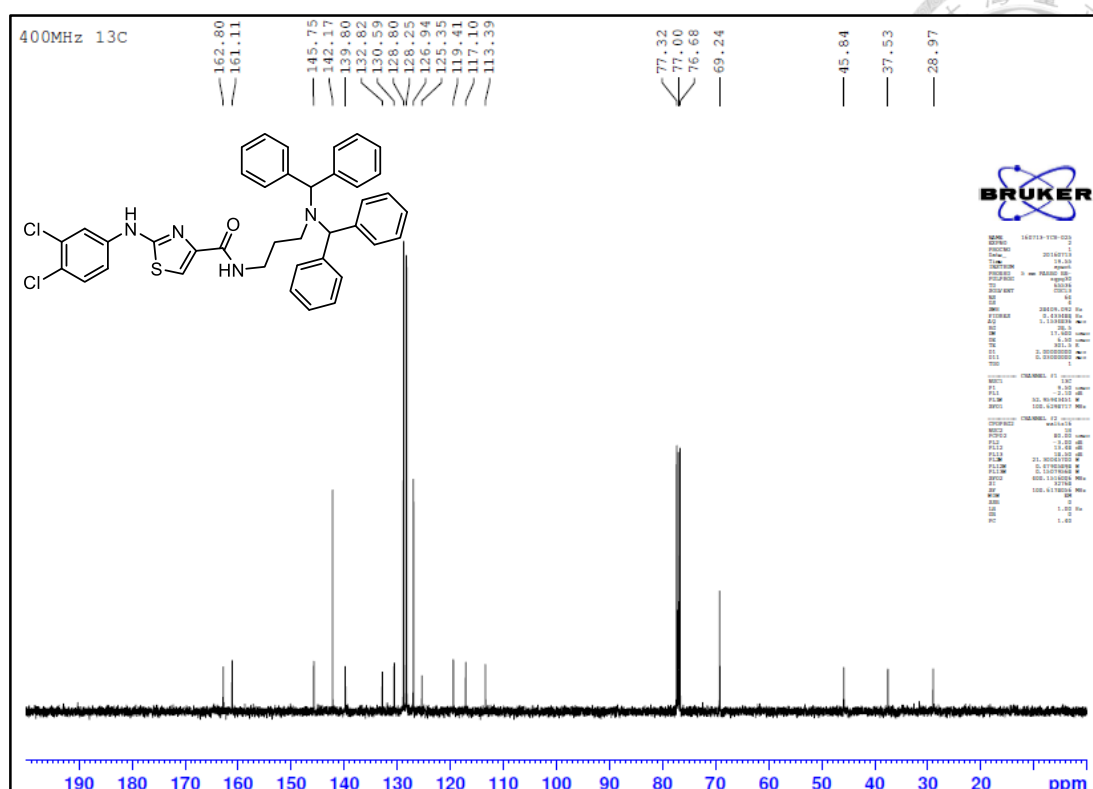
<sup>13</sup>C NMR spectrum of compound **13a** (100 MHz, CDCl<sub>3</sub>)



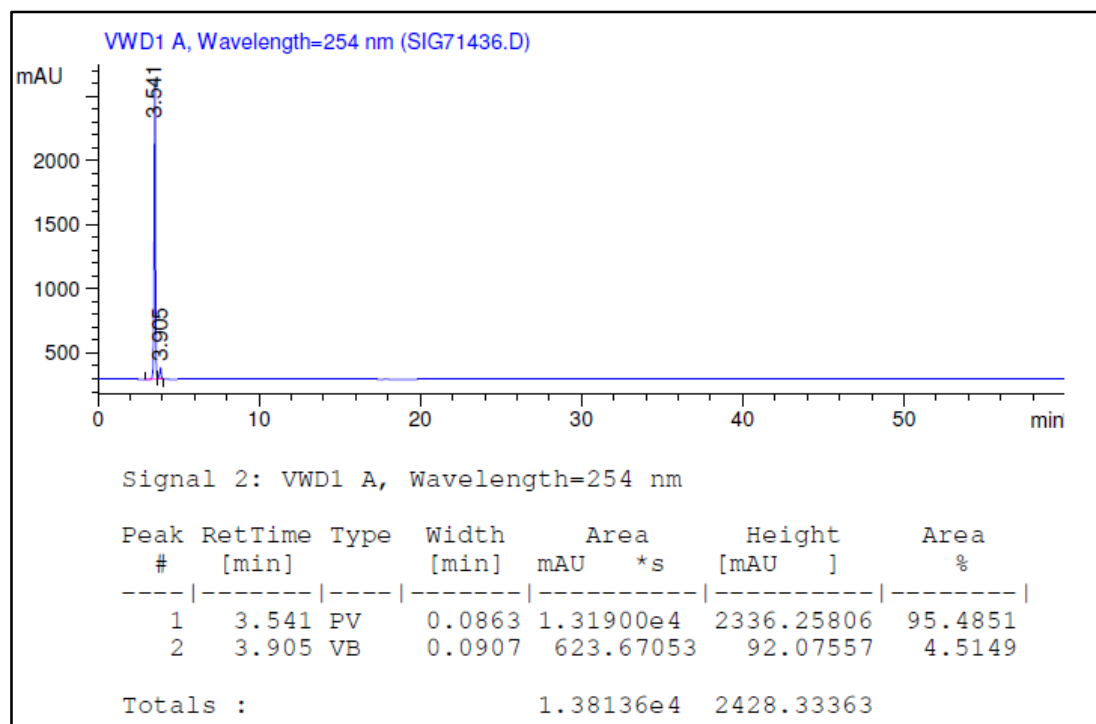
HPLC diagram of compound **13a**. Platisil Silica column (Dikma, 250 × 4.6 mm, 5 μm particle size),  $t_R = 6.4$  min [MeOH:EtOAc = 1:24] at flow rate of 1.0 mL/min.



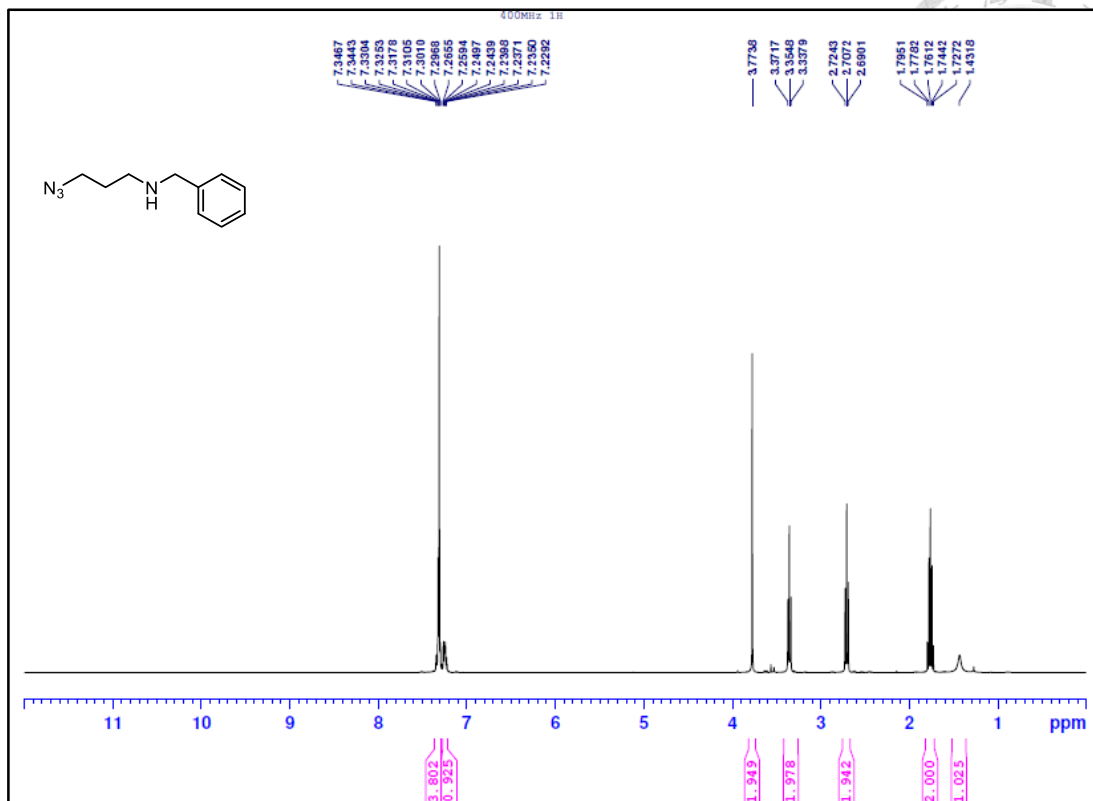
<sup>1</sup>H NMR spectrum of compound **13b** (400 MHz, CDCl<sub>3</sub>)



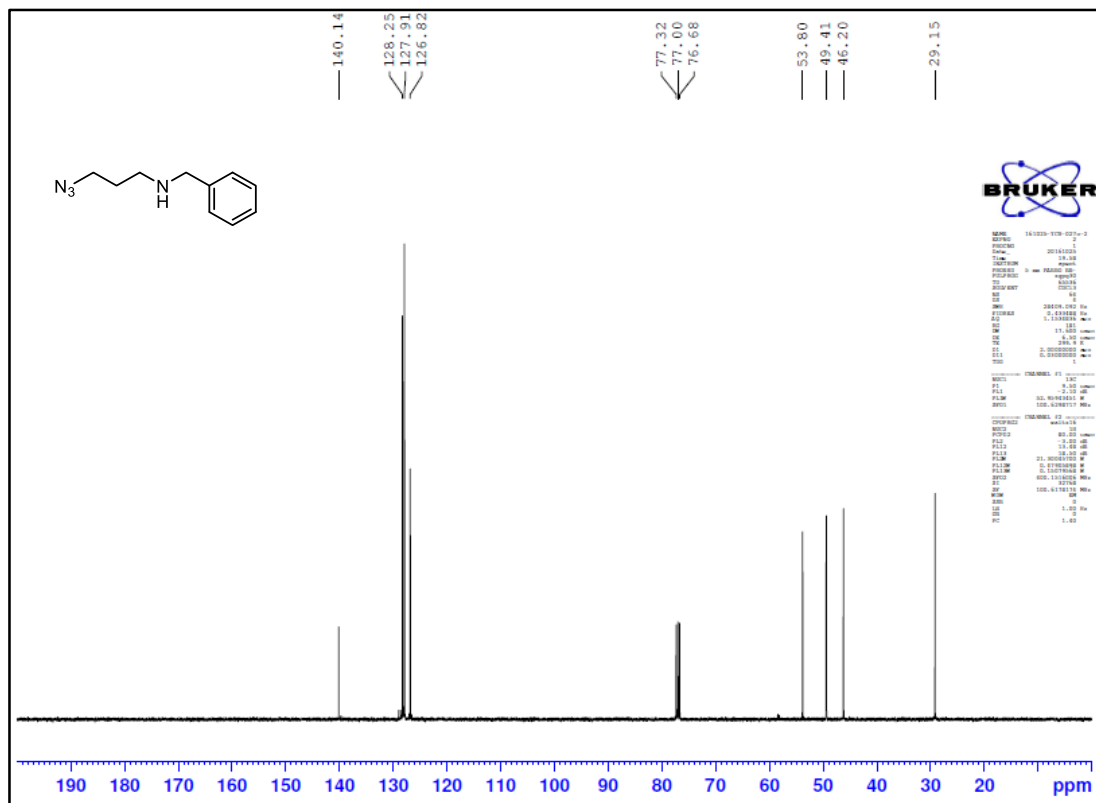
$^{13}\text{C}$  NMR spectrum of compound **13b** (100 MHz,  $\text{CDCl}_3$ )



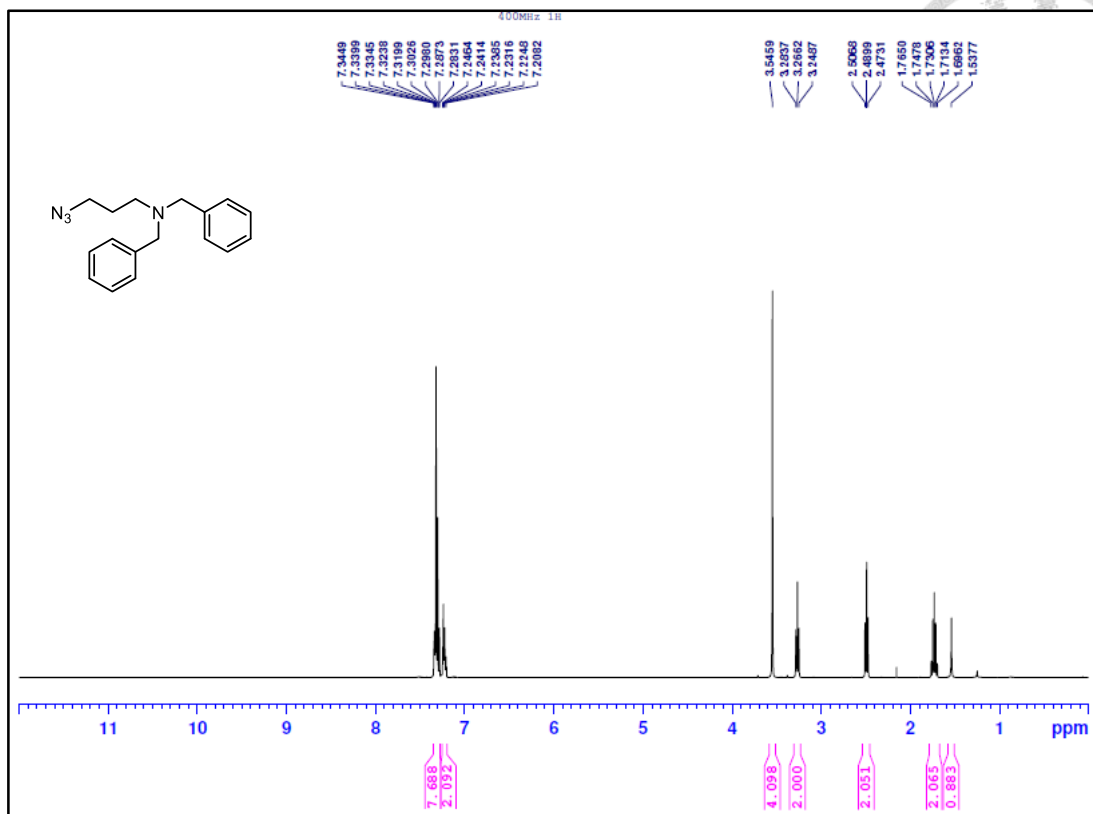
HPLC diagram of compound **13b**. Platisil Silica column (Dikma,  $250 \times 4.6$  mm, 5  $\mu\text{m}$  particle size),  $t_{\text{R}} = 3.9$  min [EtOAc:hexane = 1:1] at flow rate of 1.0 mL/min.



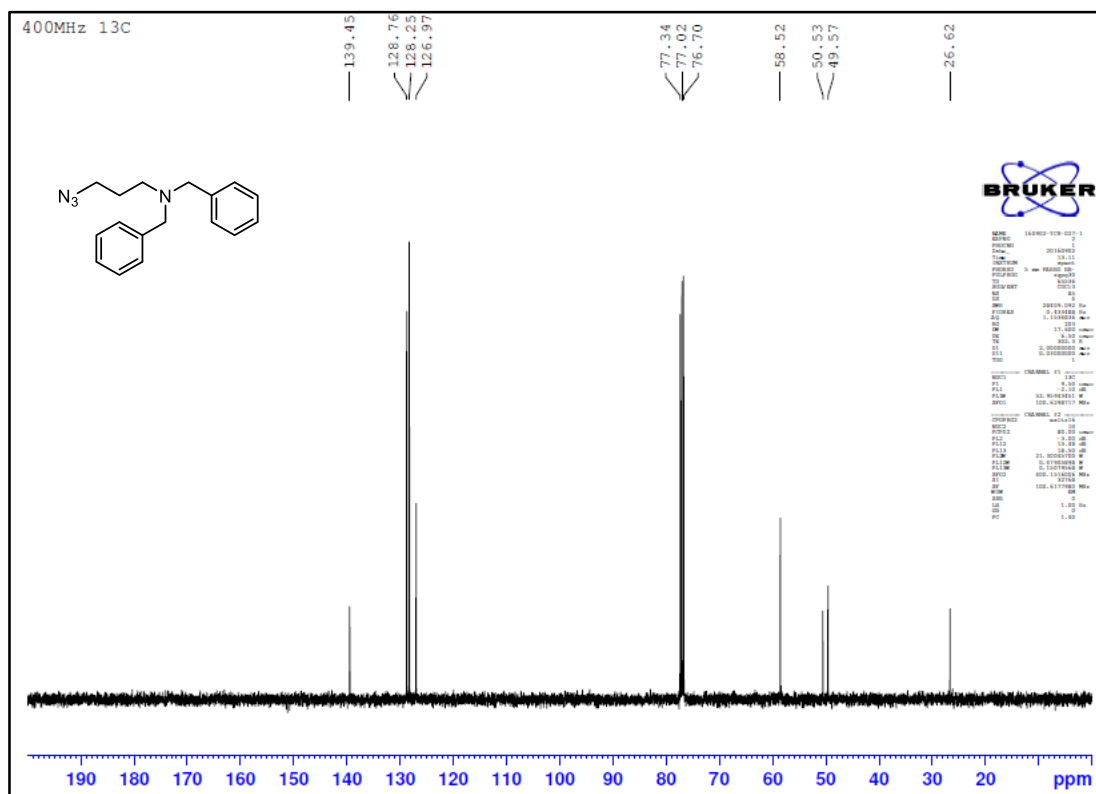
$^1\text{H}$  NMR spectrum of compound **20a** (400 MHz,  $\text{CDCl}_3$ )



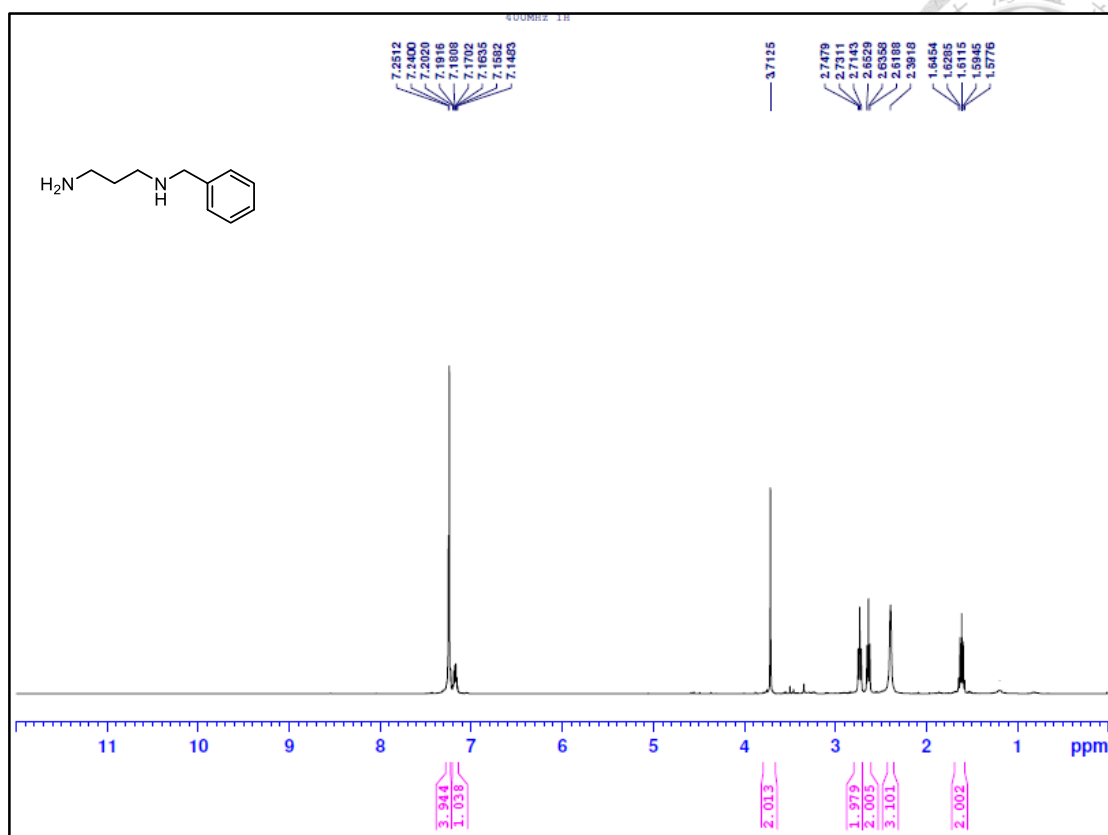
$^{13}\text{C}$  NMR spectrum of compound **20a** (100 MHz,  $\text{CDCl}_3$ )



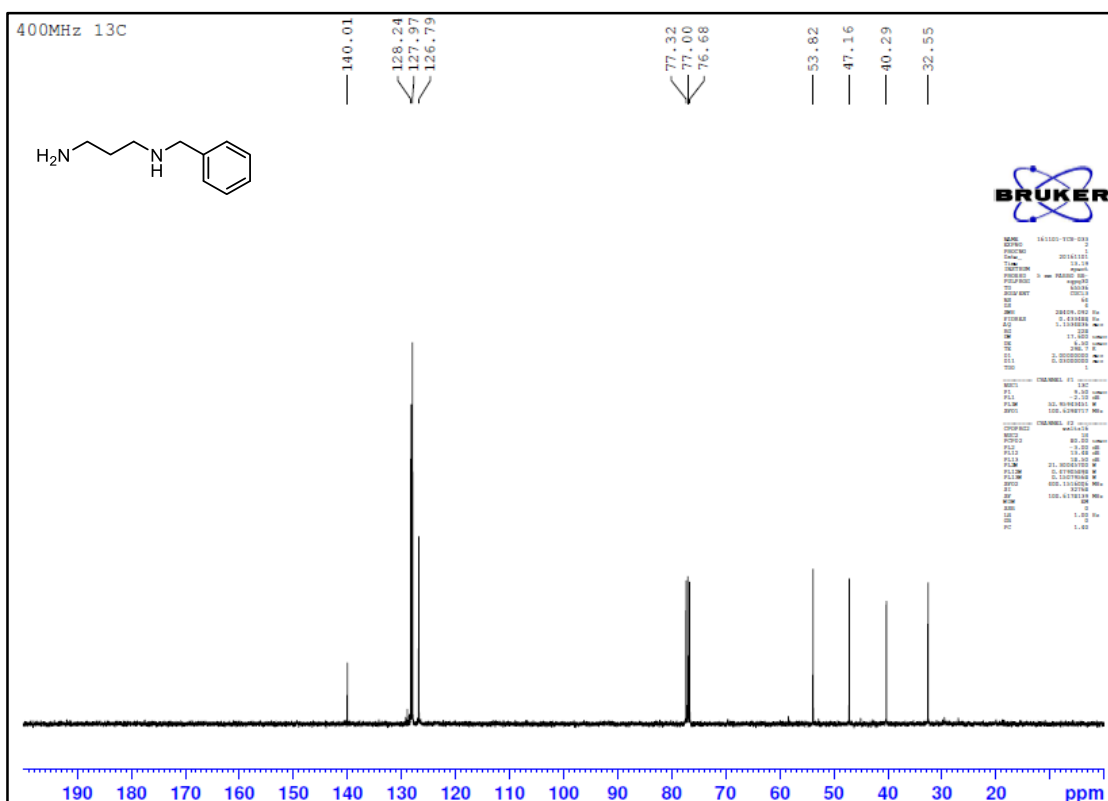
<sup>1</sup>H NMR spectrum of compound **20b** (400 MHz, CDCl<sub>3</sub>)



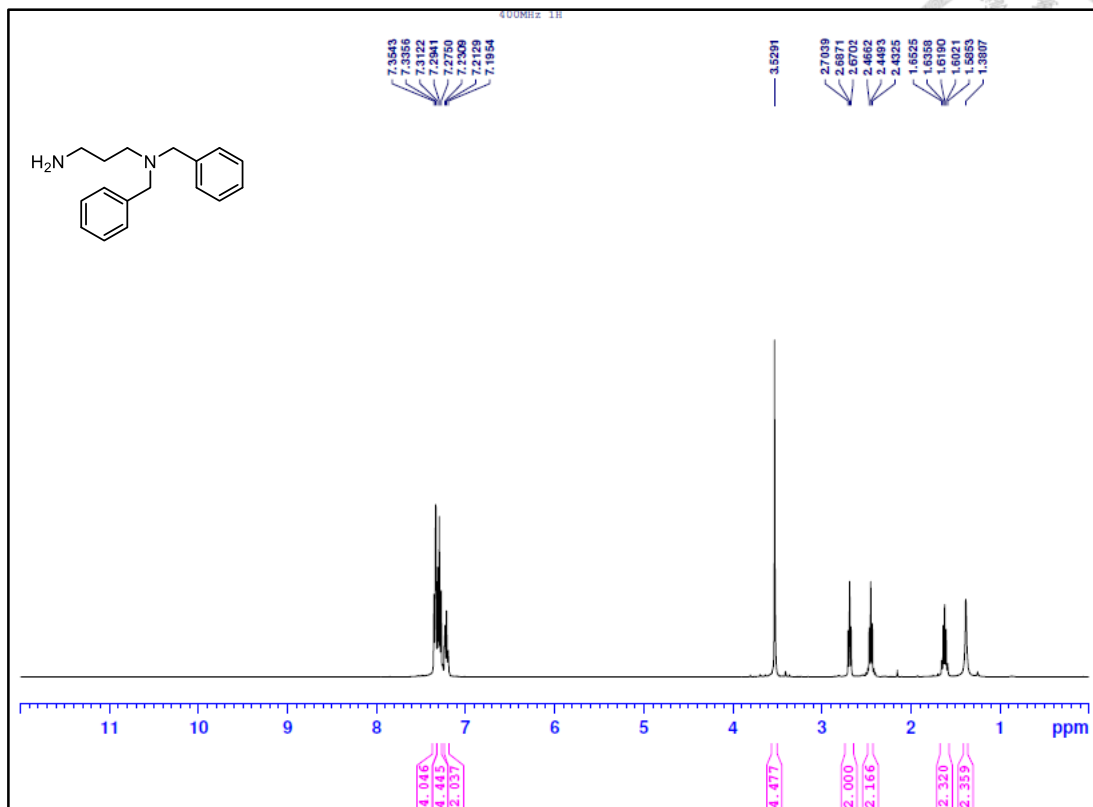
<sup>13</sup>C NMR spectrum of compound **20b** (100 MHz, CDCl<sub>3</sub>)



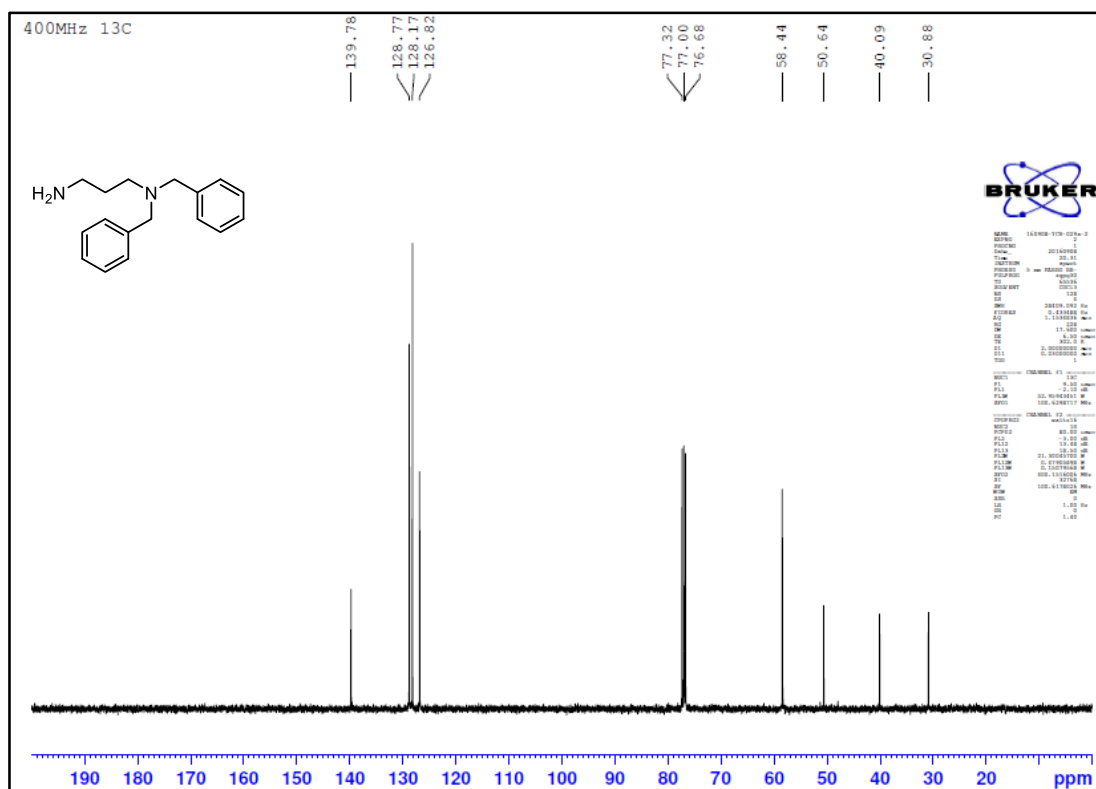
<sup>1</sup>H NMR spectrum of compound **21a** (400 MHz, CDCl<sub>3</sub>)



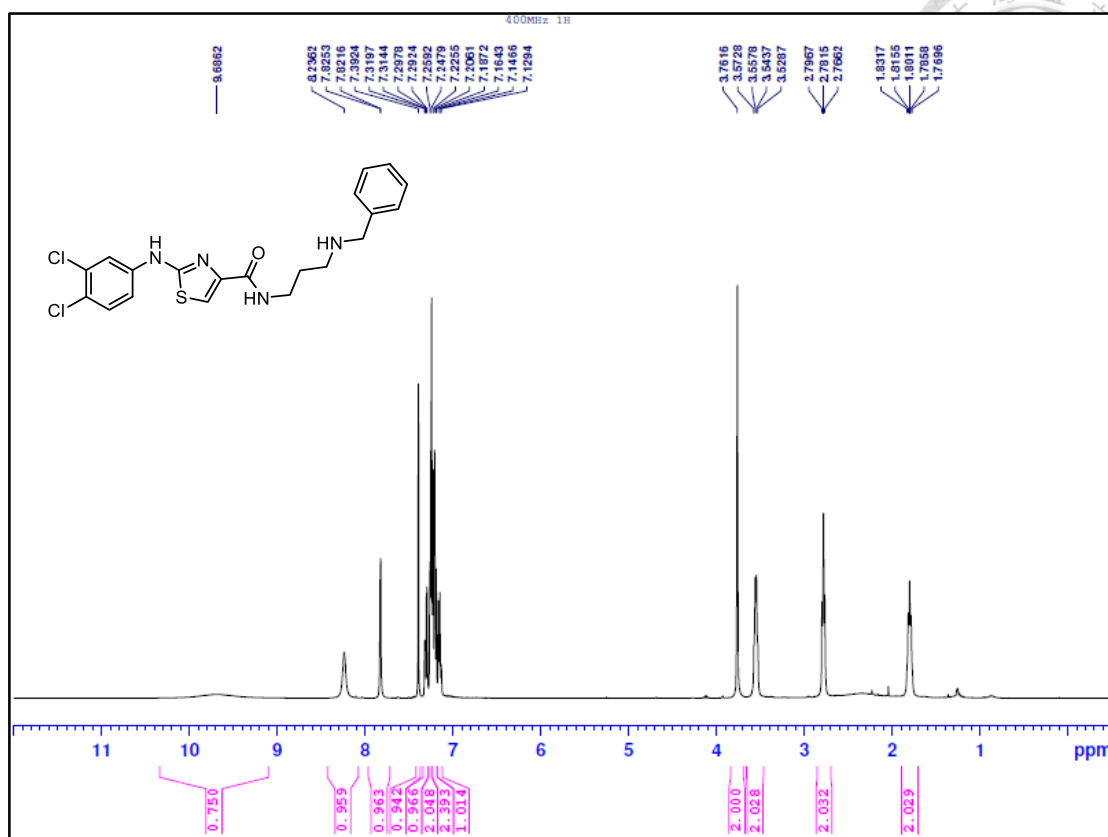
<sup>13</sup>C NMR spectrum of compound **21a** (100 MHz, CDCl<sub>3</sub>)



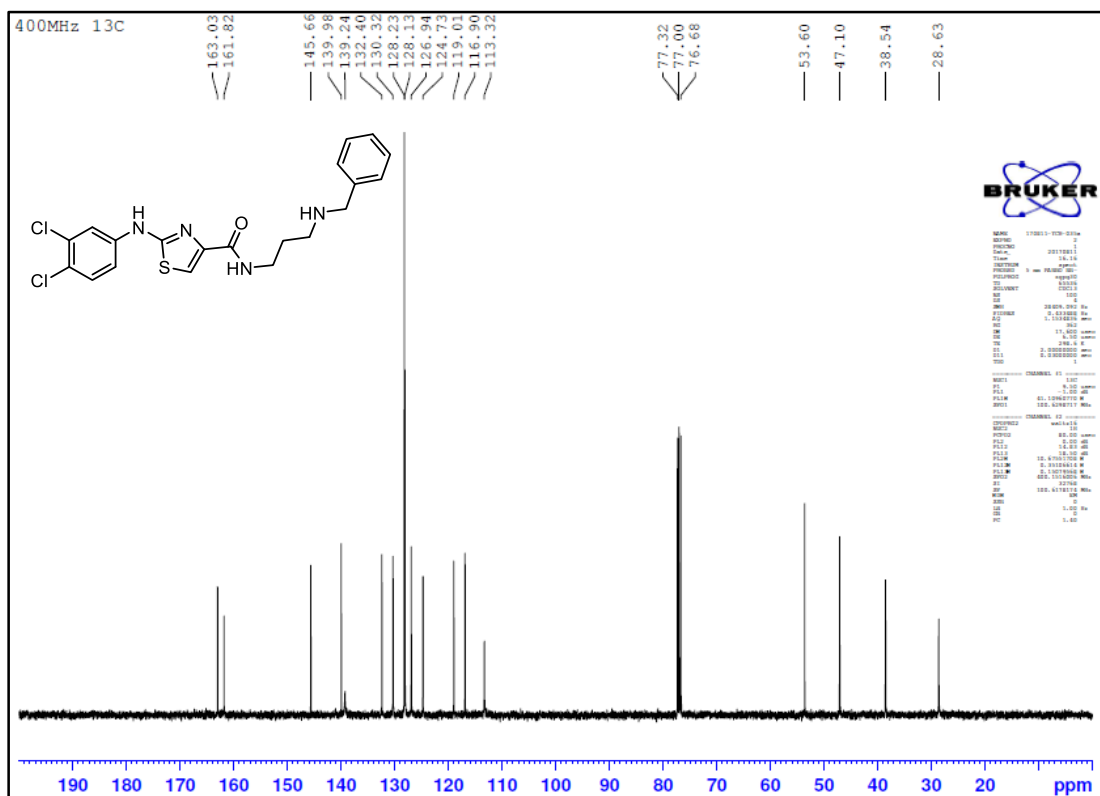
<sup>1</sup>H NMR spectrum of compound **21b** (400 MHz, CDCl<sub>3</sub>)



<sup>13</sup>C NMR spectrum of compound **21b** (100 MHz, CDCl<sub>3</sub>)

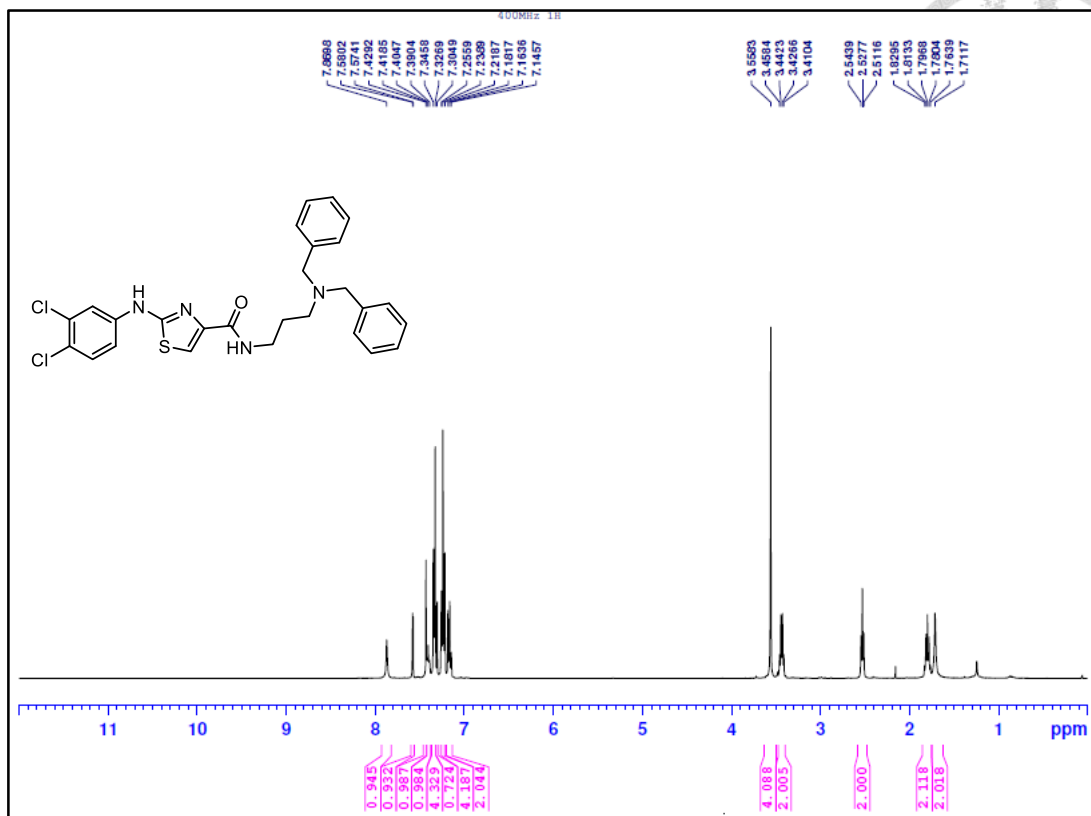


<sup>1</sup>H NMR spectrum of compound **22a** (400 MHz, CDCl<sub>3</sub>)

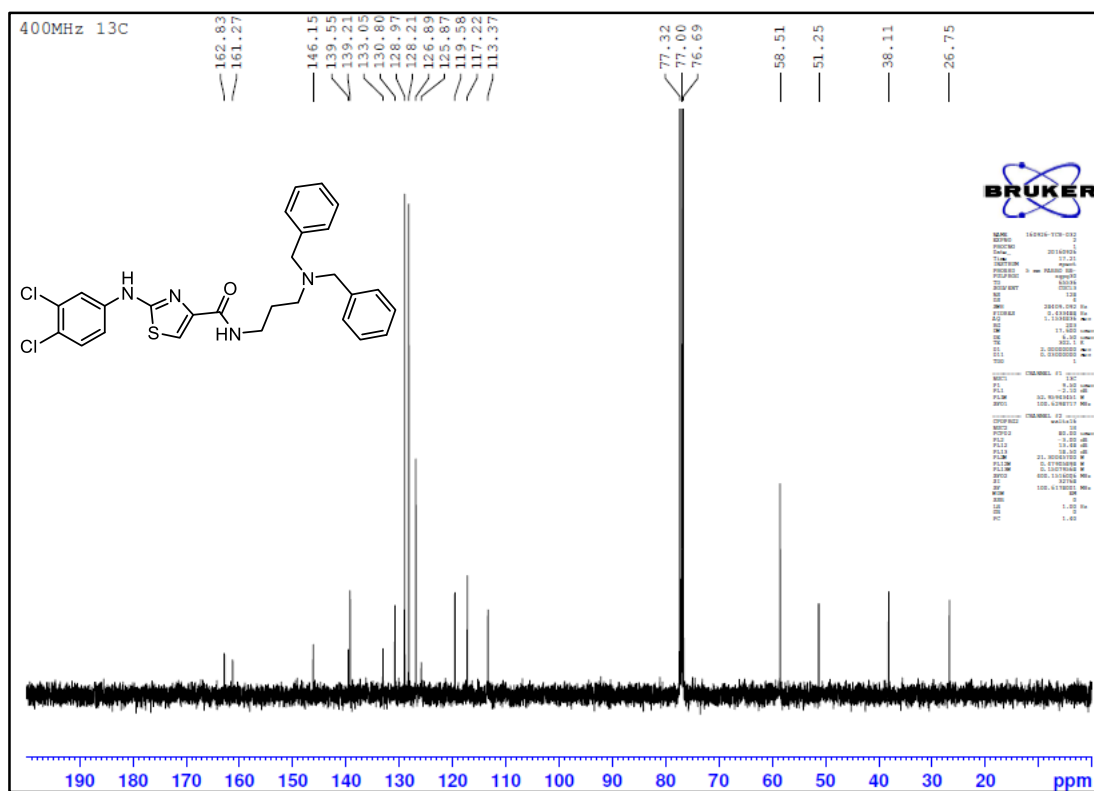


<sup>13</sup>C NMR spectrum of compound **22a** (100 MHz, CDCl<sub>3</sub>)

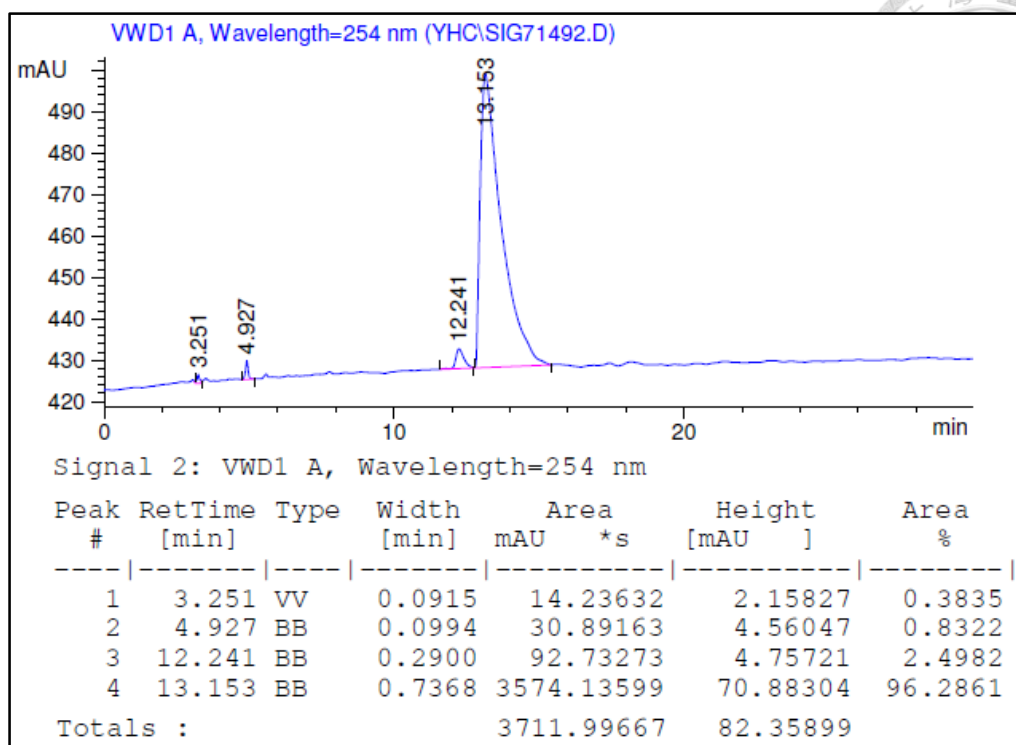




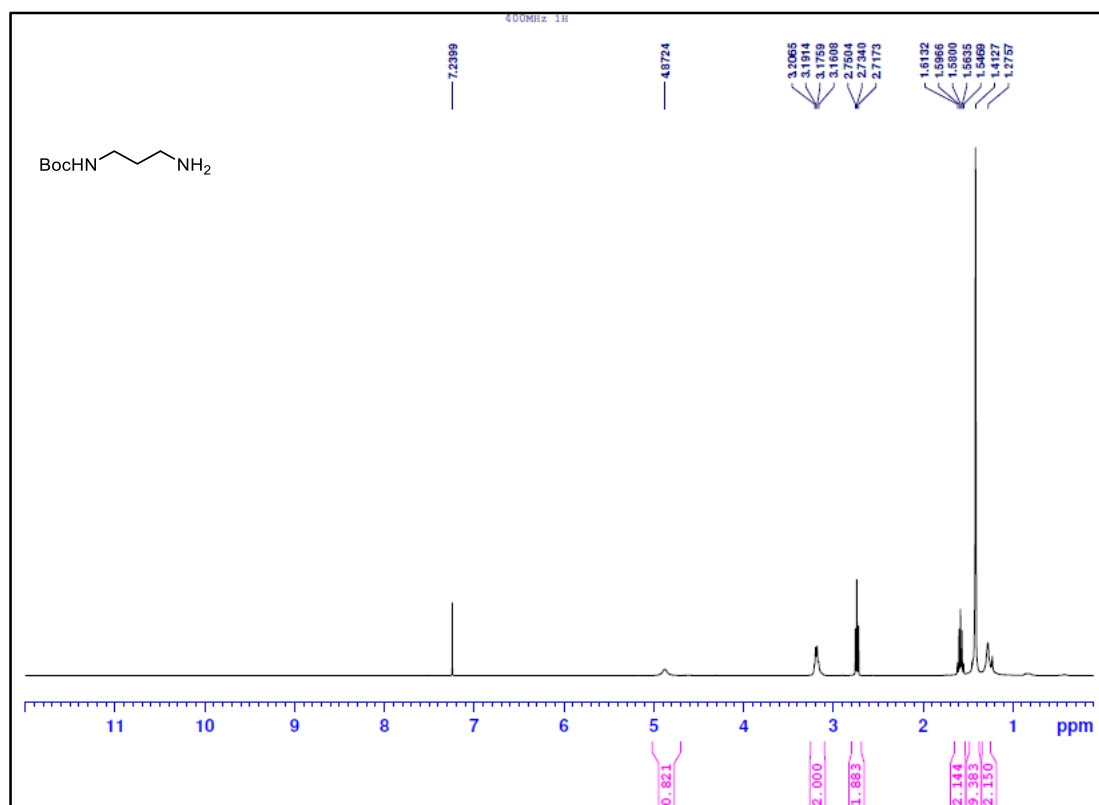
<sup>1</sup>H NMR spectrum of compound **22b** (400 MHz, CDCl<sub>3</sub>)



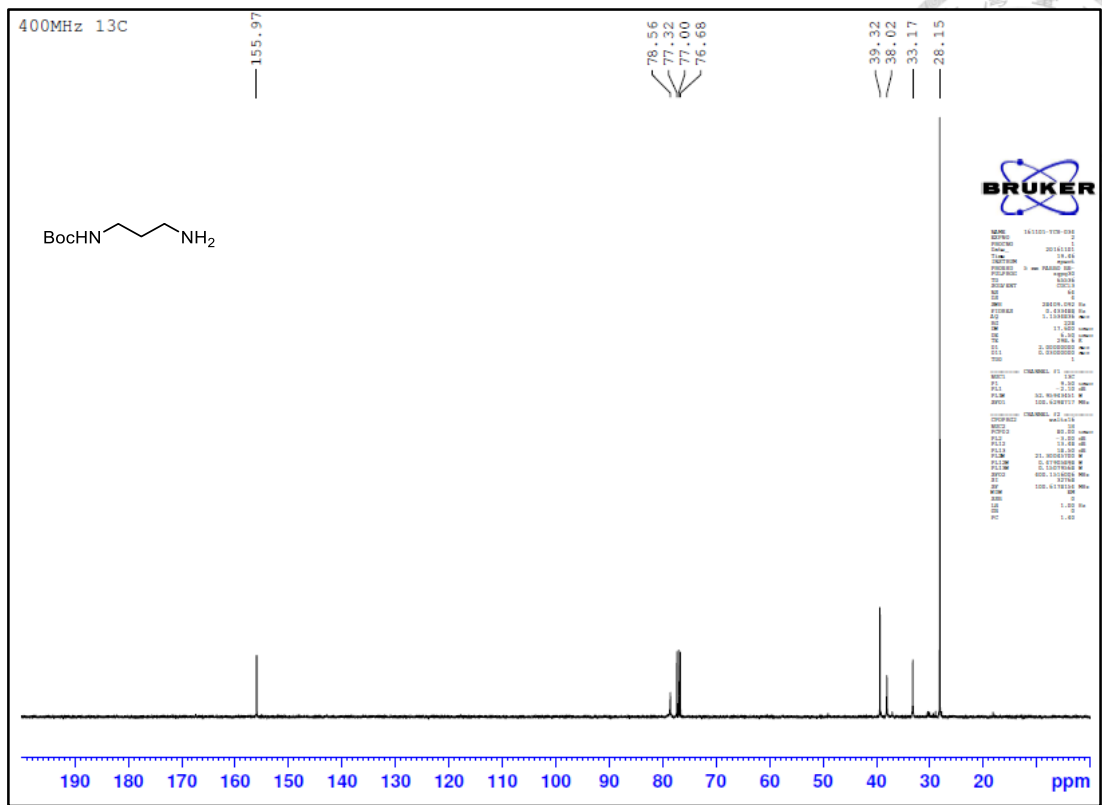
<sup>13</sup>C NMR spectrum of compound **22b** (100 MHz, CDCl<sub>3</sub>)



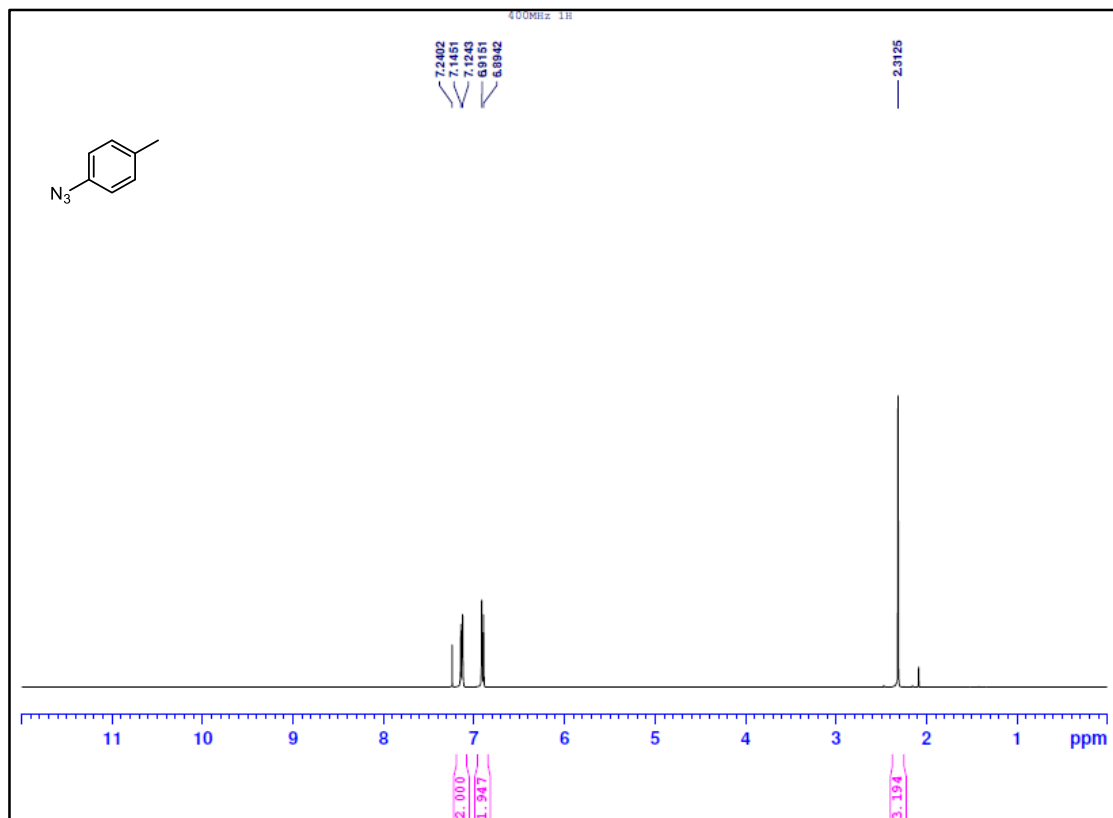
HPLC diagram of compound **22b**. Platisil Silica column (Dikma, 250 × 4.6 mm, 5 μm particle size),  $t_R = 13$  min [EtOAc:hexane = 1:2] at flow rate of 1.0 mL/min.



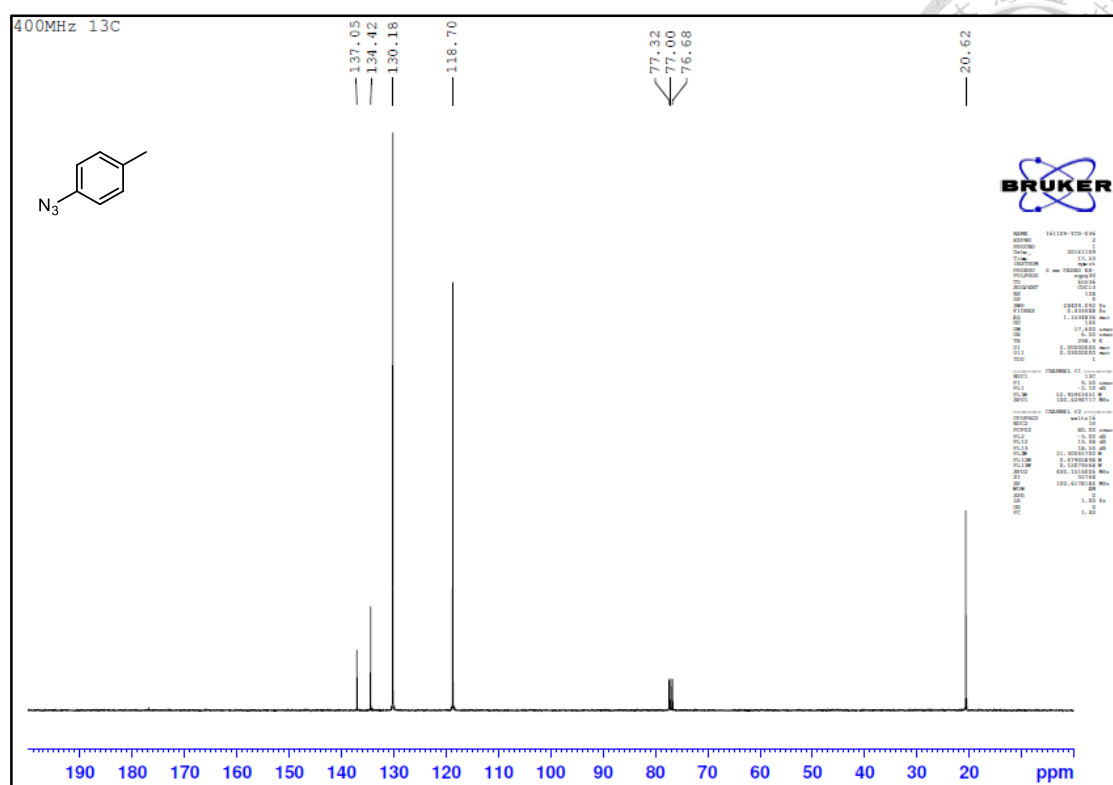
<sup>1</sup>H NMR spectrum of compound **24** (400 MHz, CDCl<sub>3</sub>)



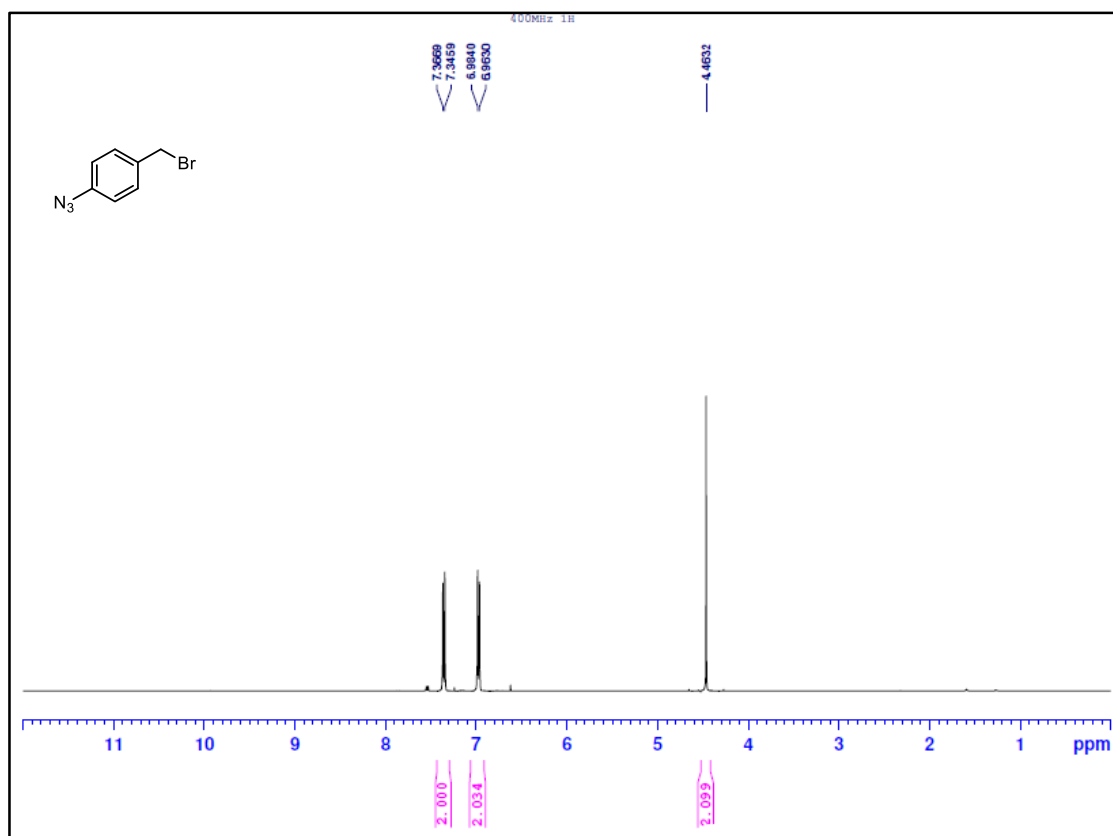
<sup>13</sup>C NMR spectrum of compound **24** (100 MHz, CDCl<sub>3</sub>)



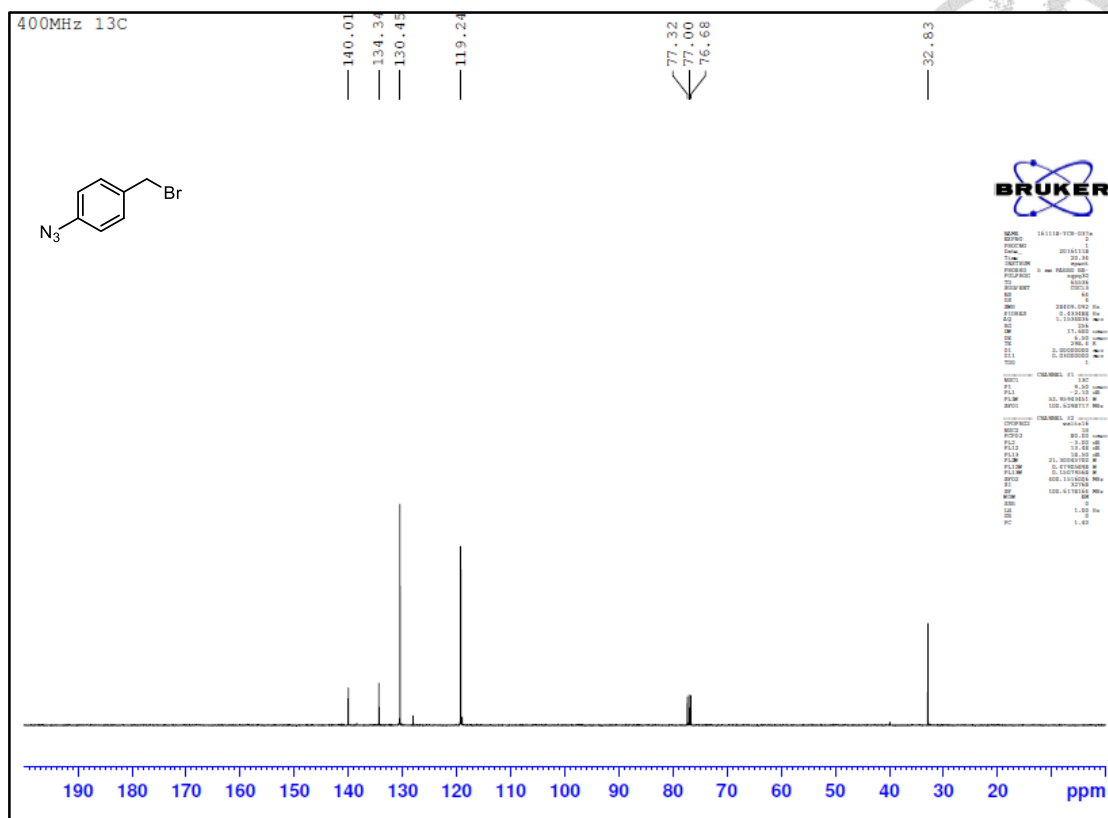
<sup>1</sup>H NMR spectrum of compound **26** (400 MHz, CDCl<sub>3</sub>)



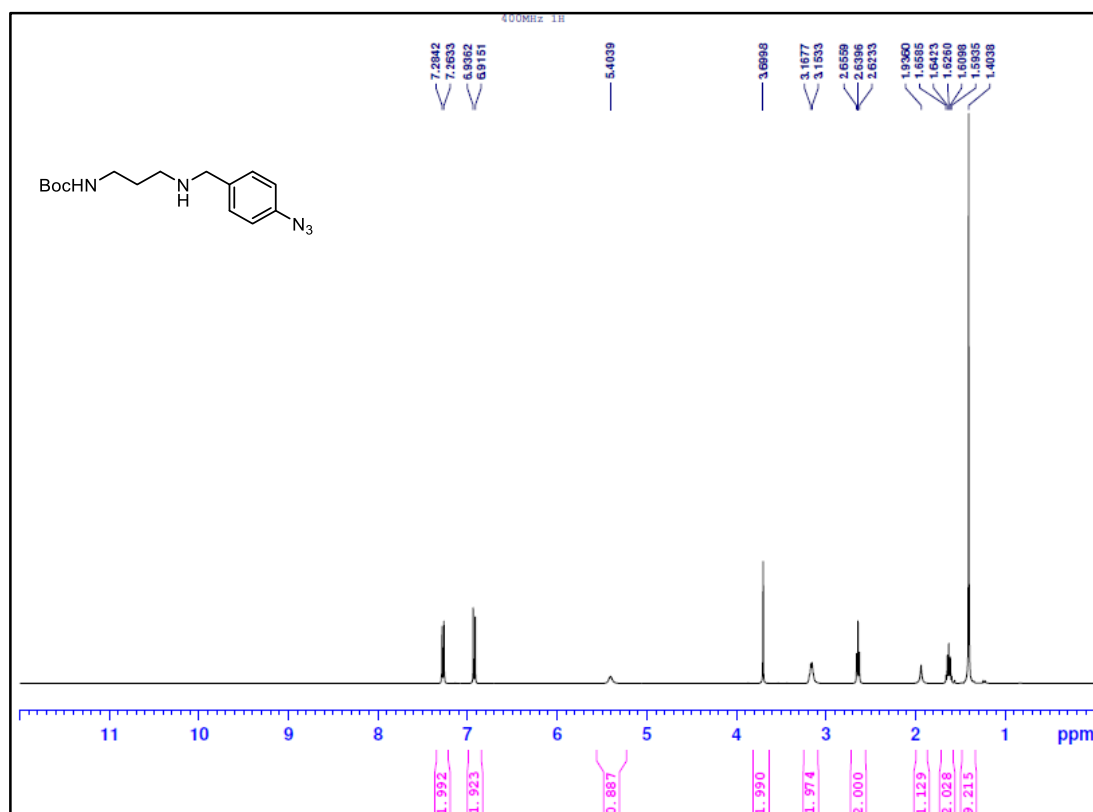
<sup>13</sup>C NMR spectrum of compound **26** (100 MHz, CDCl<sub>3</sub>)



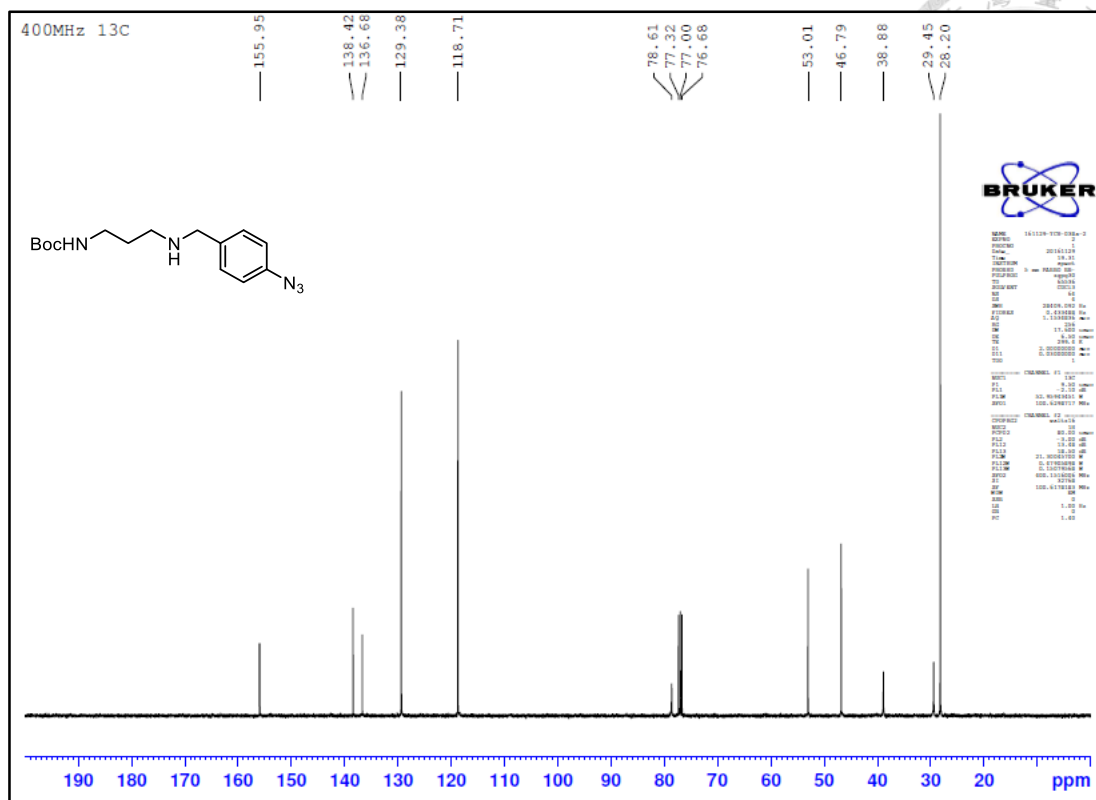
<sup>1</sup>H NMR spectrum of compound **27** (400 MHz, CDCl<sub>3</sub>)



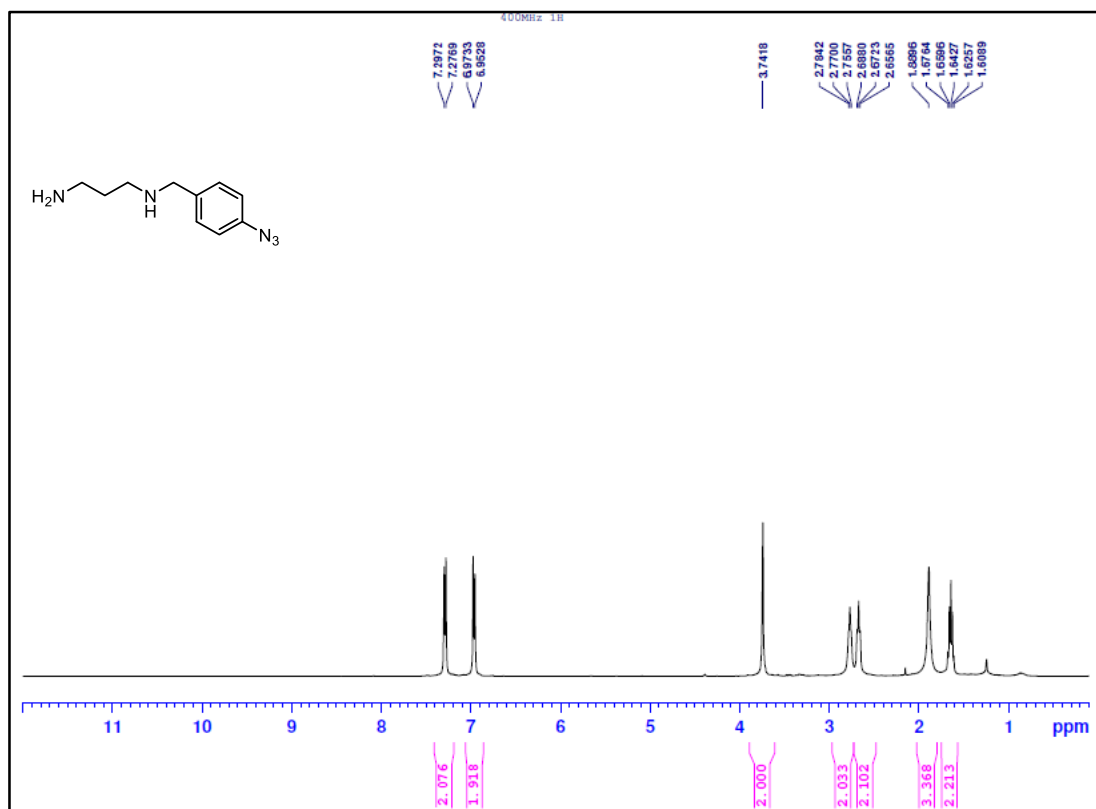
$^{13}\text{C}$  NMR spectrum of compound **27** (100 MHz,  $\text{CDCl}_3$ )



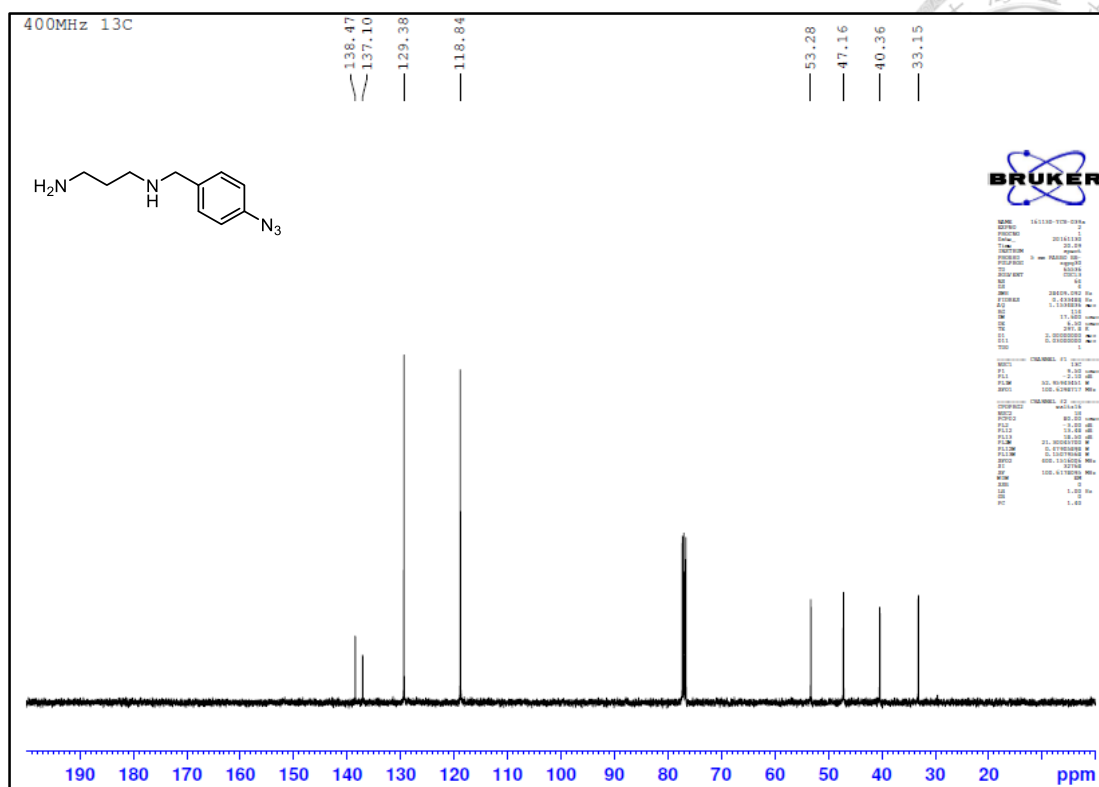
$^1\text{H}$  NMR spectrum of compound **28** (400 MHz,  $\text{CDCl}_3$ )



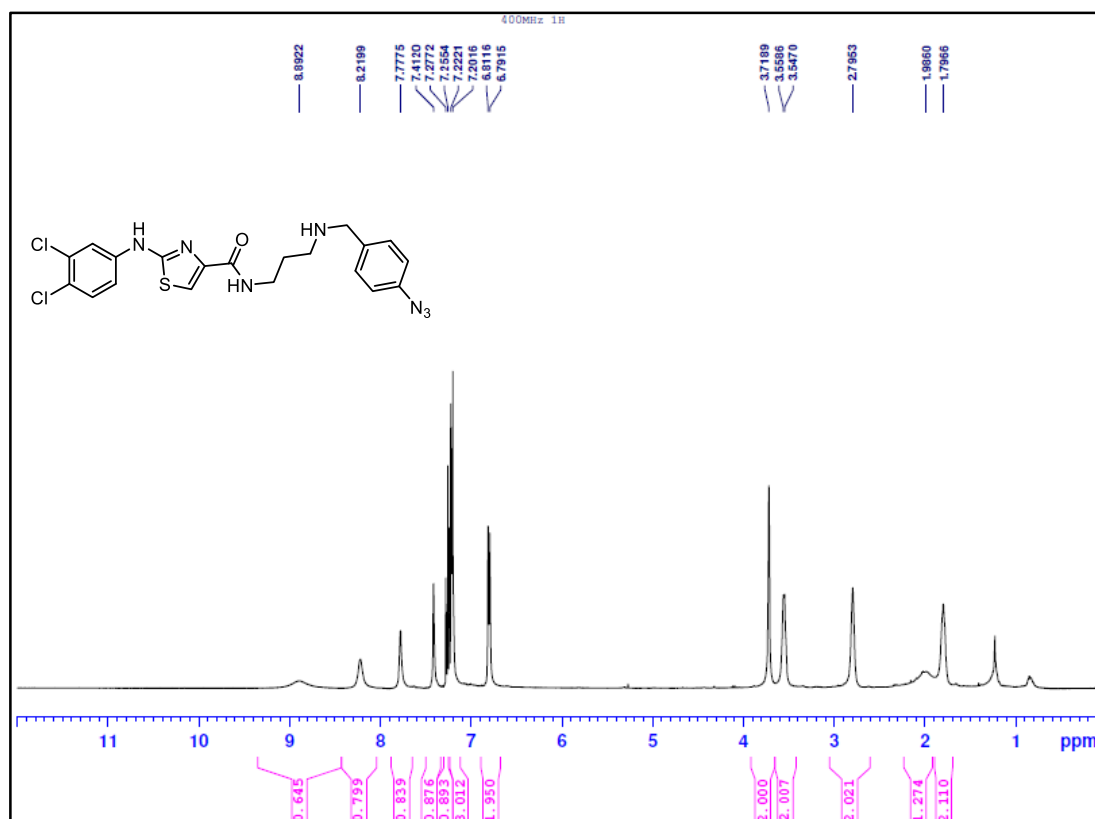
$^{13}\text{C}$  NMR spectrum of compound **28** (100 MHz,  $\text{CDCl}_3$ )



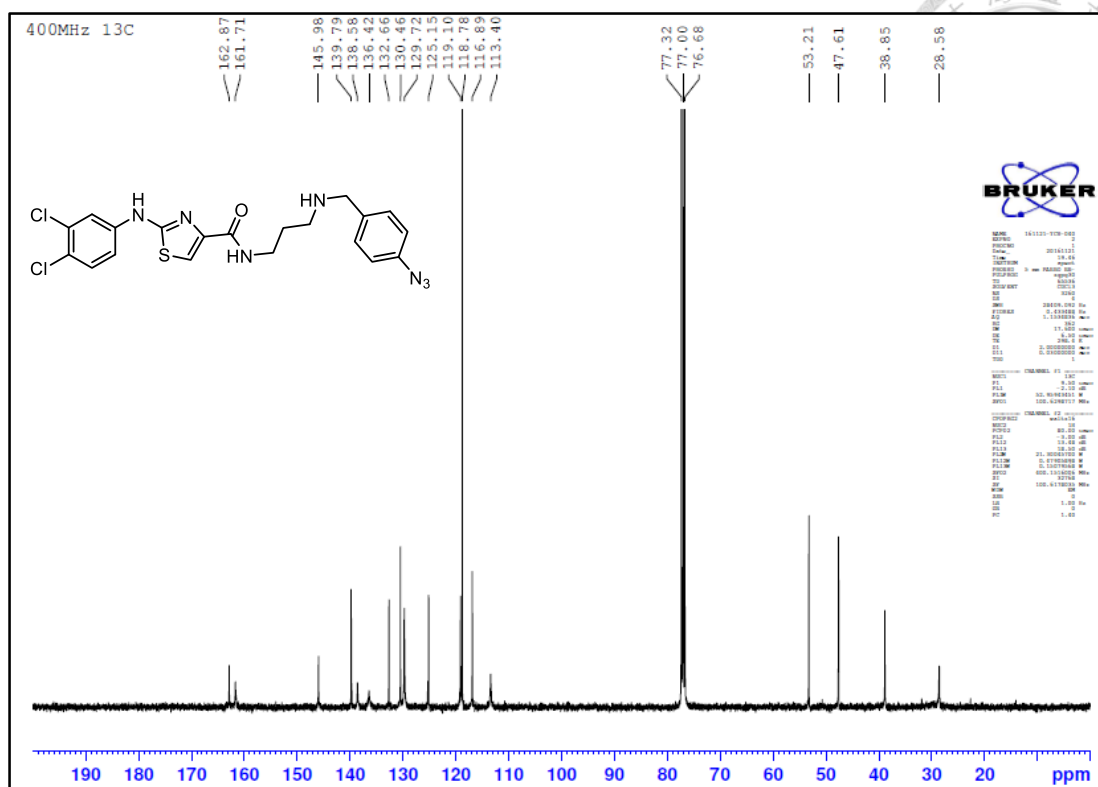
$^1\text{H}$  NMR spectrum of compound **29** (400 MHz,  $\text{CDCl}_3$ )



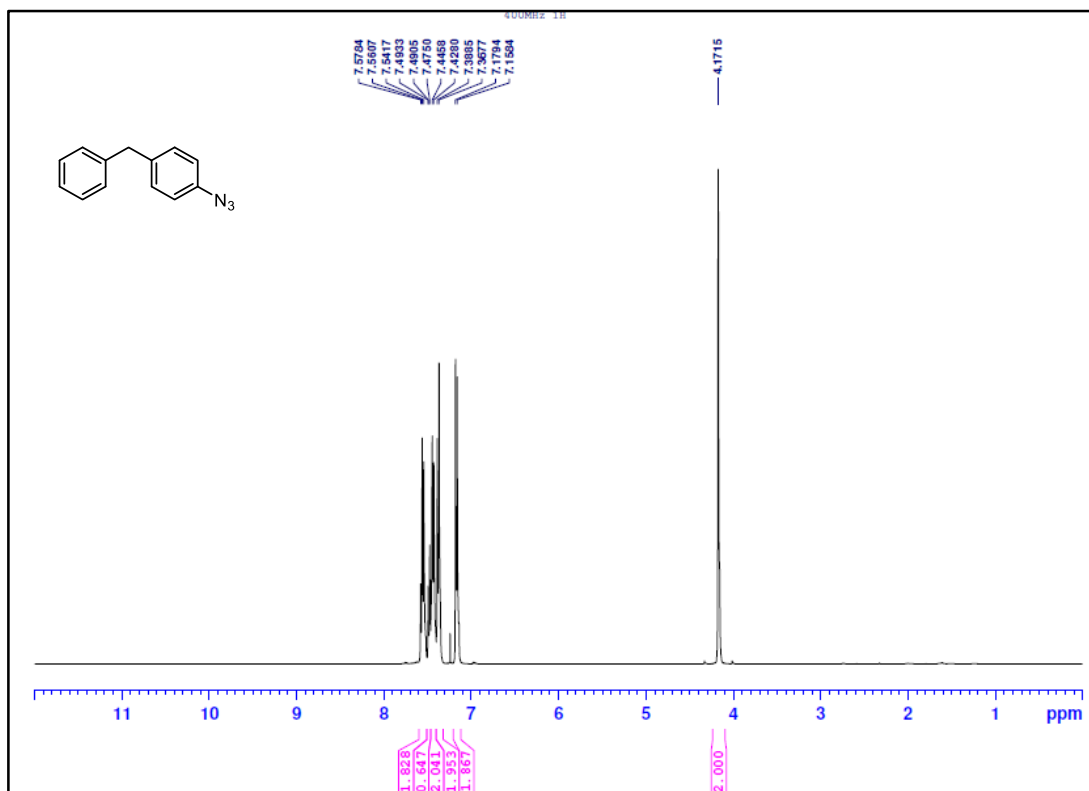
$^{13}\text{C}$  NMR spectrum of compound **29** (100 MHz,  $\text{CDCl}_3$ )



$^1\text{H}$  NMR spectrum of compound **30** (400 MHz,  $\text{CDCl}_3$ )

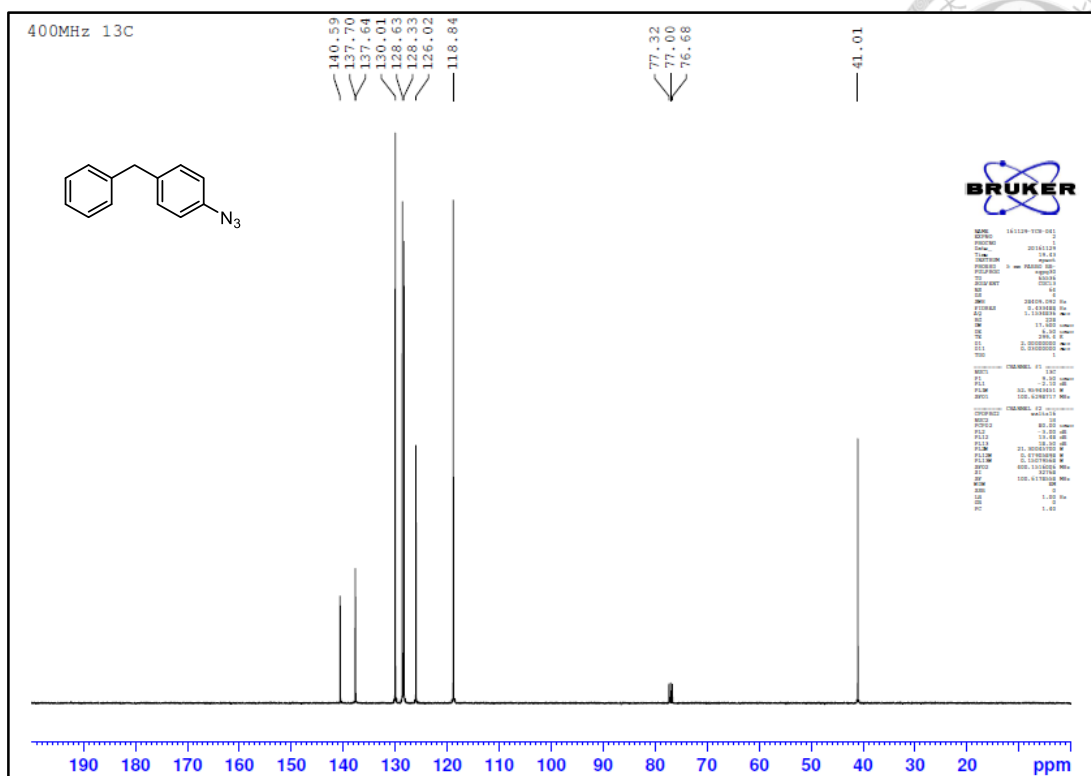


$^{13}\text{C}$  NMR spectrum of compound **30** (100 MHz,  $\text{CDCl}_3$ )

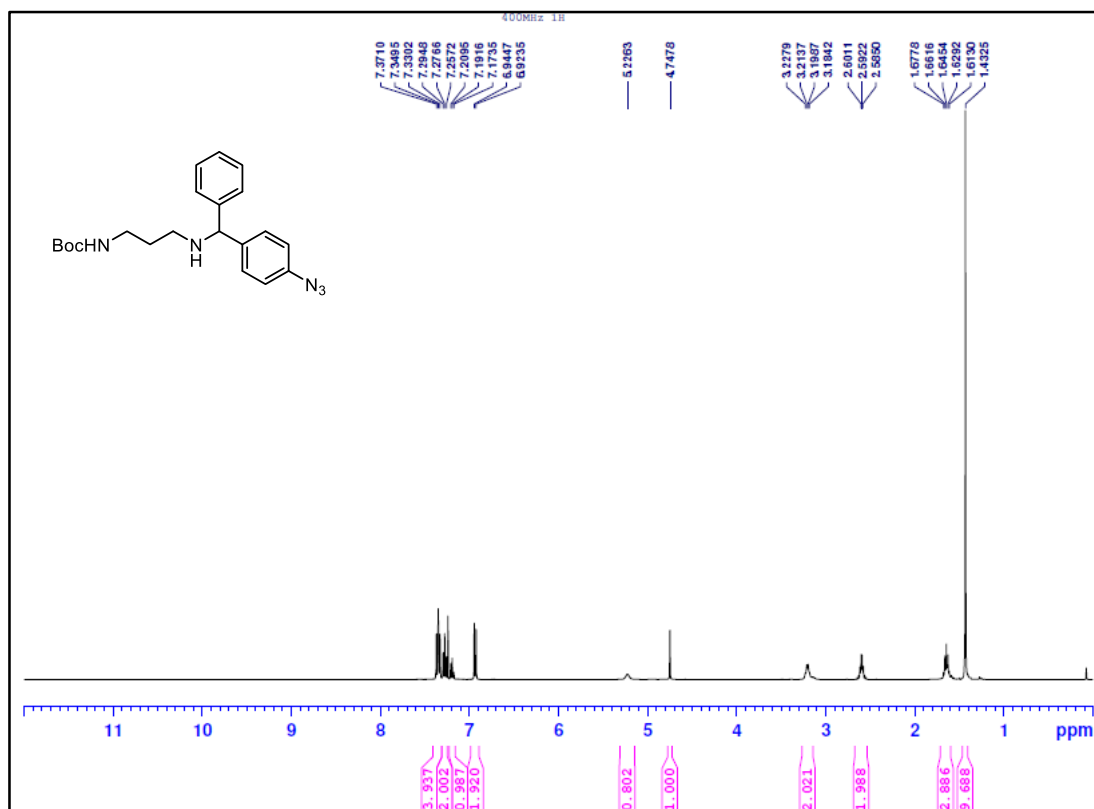


$^1\text{H}$  NMR spectrum of compound **32** (400 MHz,  $\text{CDCl}_3$ )



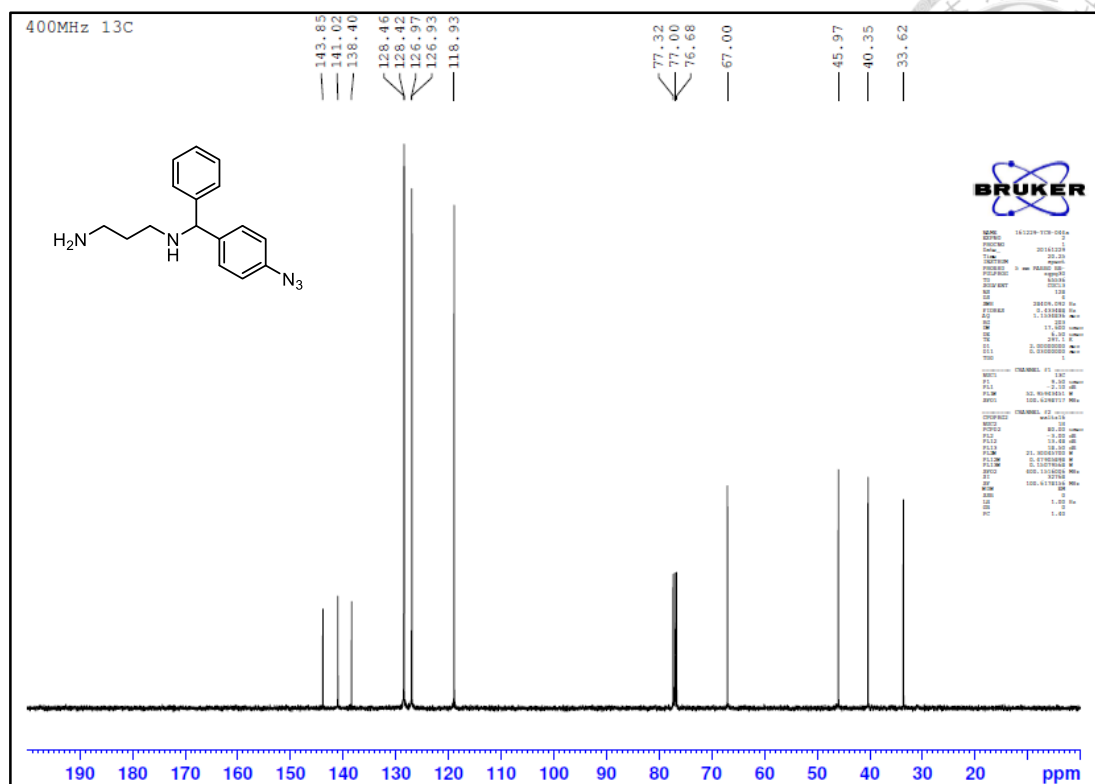


$^{13}\text{C}$  NMR spectrum of compound **32** (100 MHz,  $\text{CDCl}_3$ )

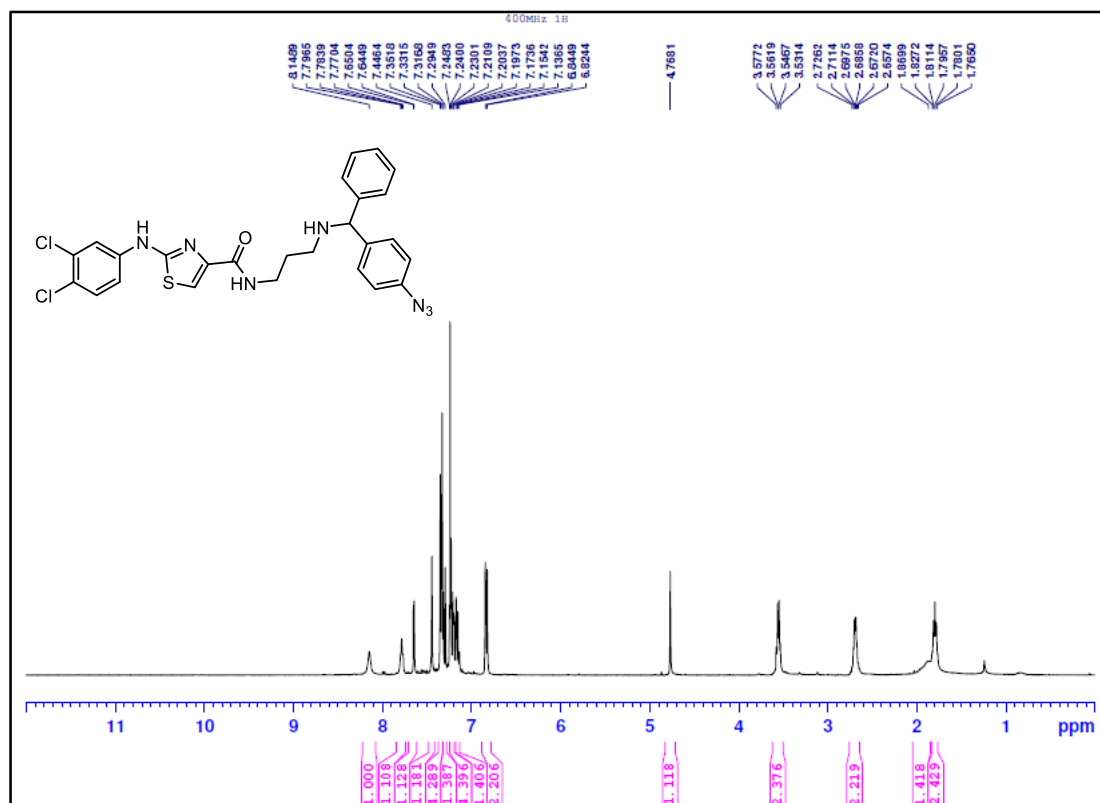


$^1\text{H}$  NMR spectrum of compound **34** (400 MHz,  $\text{CDCl}_3$ )

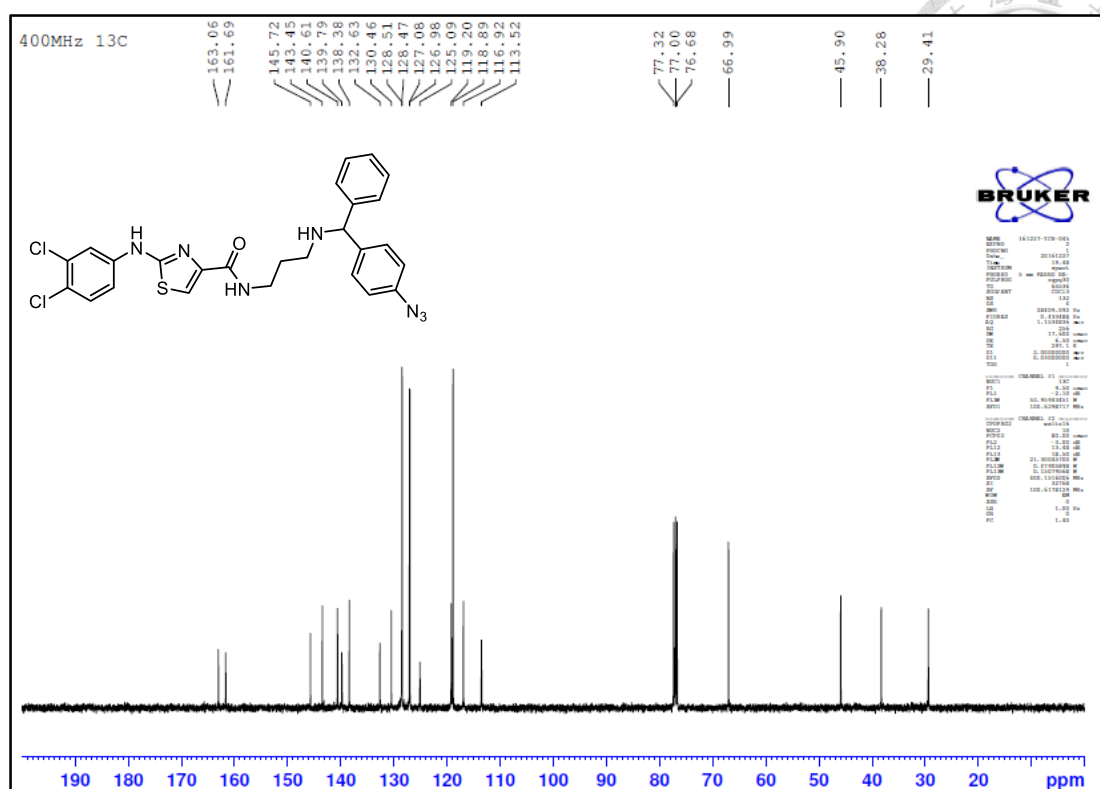




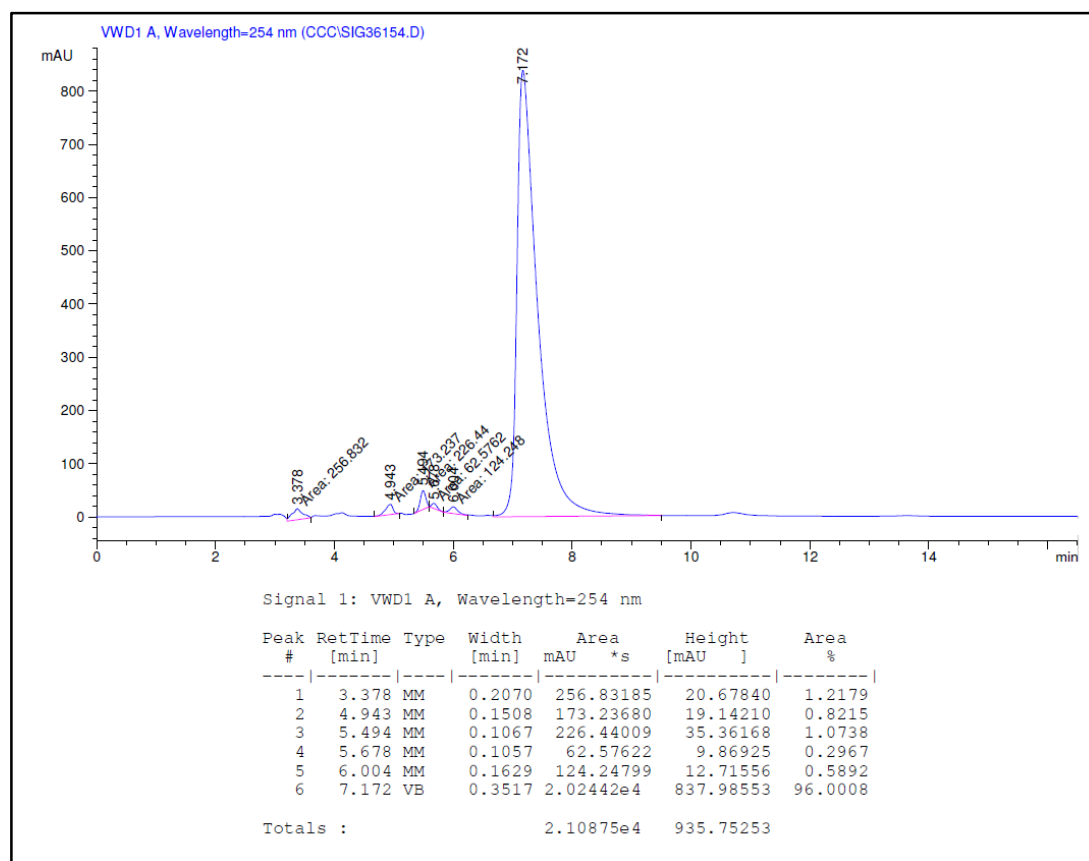
$^{13}\text{C}$  NMR spectrum of compound **35** (100 MHz,  $\text{CDCl}_3$ )



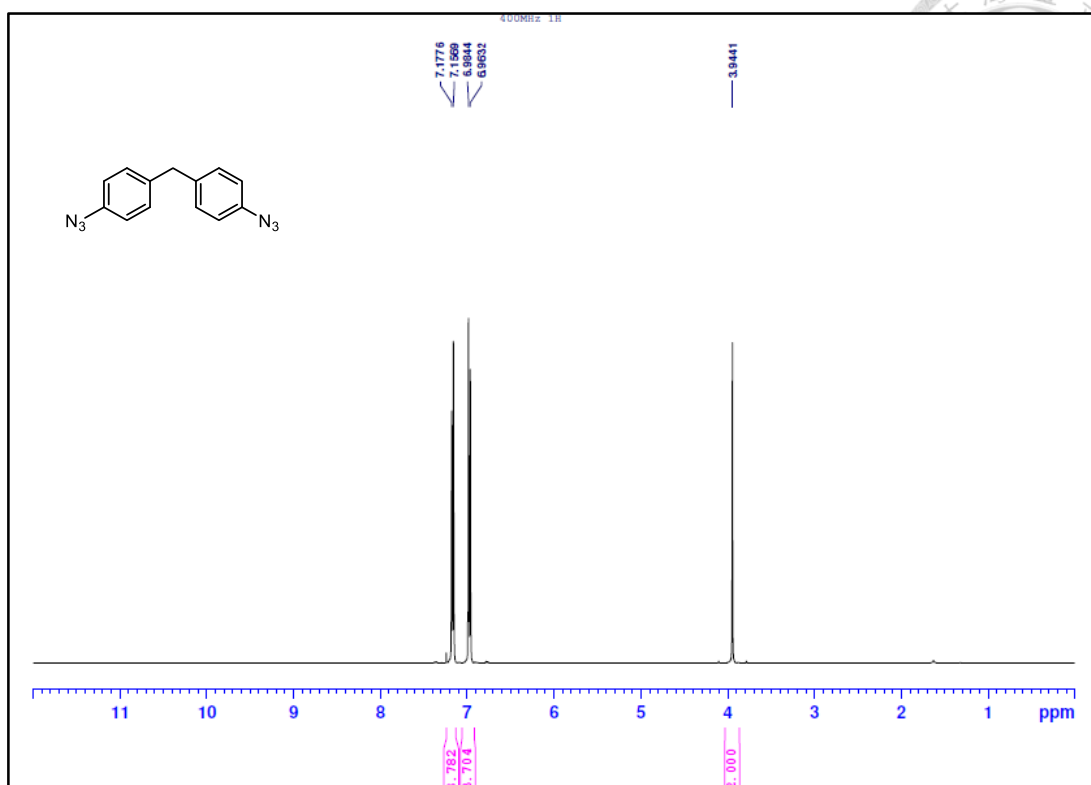
$^1\text{H}$  NMR spectrum of compound **36** (400 MHz,  $\text{CDCl}_3$ )



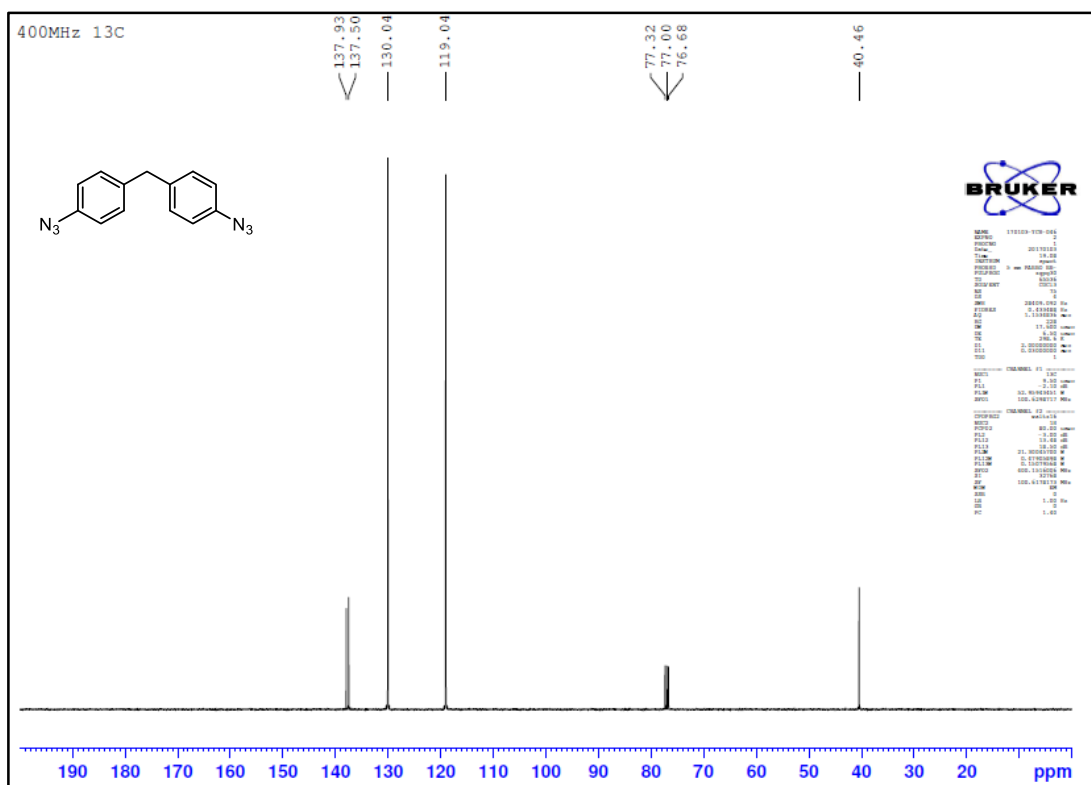
$^{13}\text{C}$  NMR spectrum of compound **36** (100 MHz,  $\text{CDCl}_3$ )



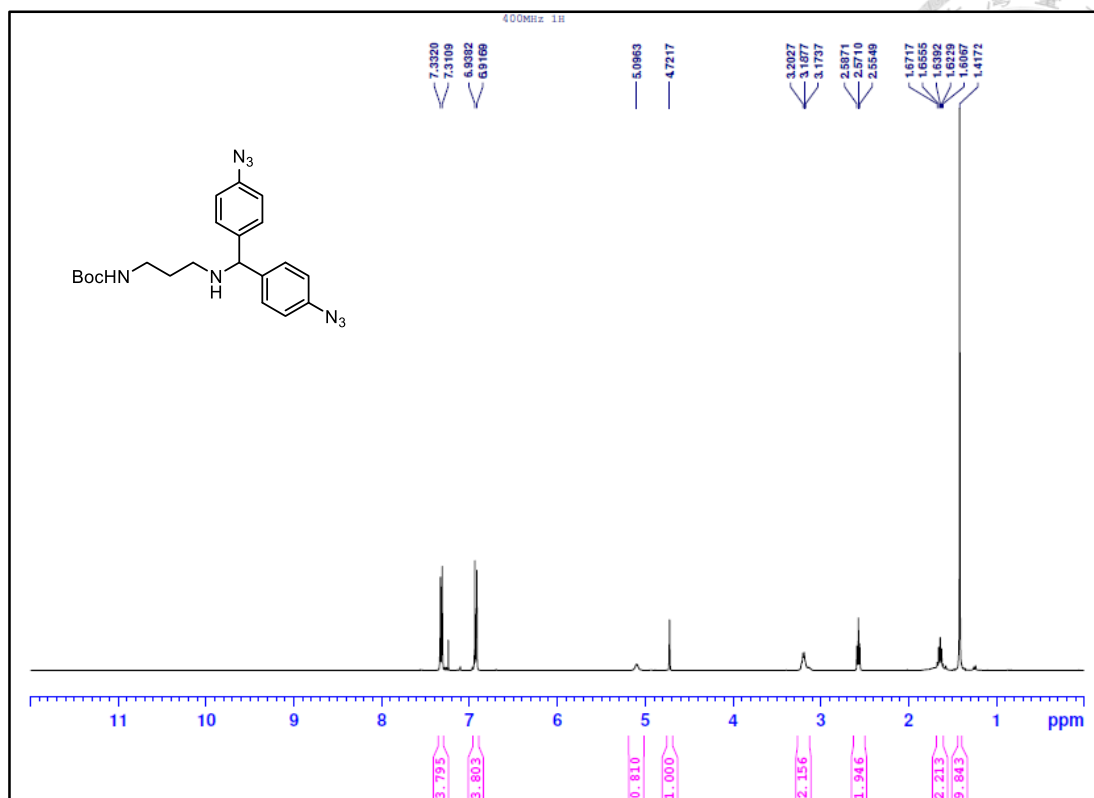
HPLC diagram of compound **36**. Platisil Silica column (Dikma,  $250 \times 4.6$  mm,  $5 \mu\text{m}$  particle size),  $t_R = 7.2$  min [ $\text{MeOH}:\text{CH}_2\text{Cl}_2 = 1:24$ ] at flow rate of 1.0 mL/min.



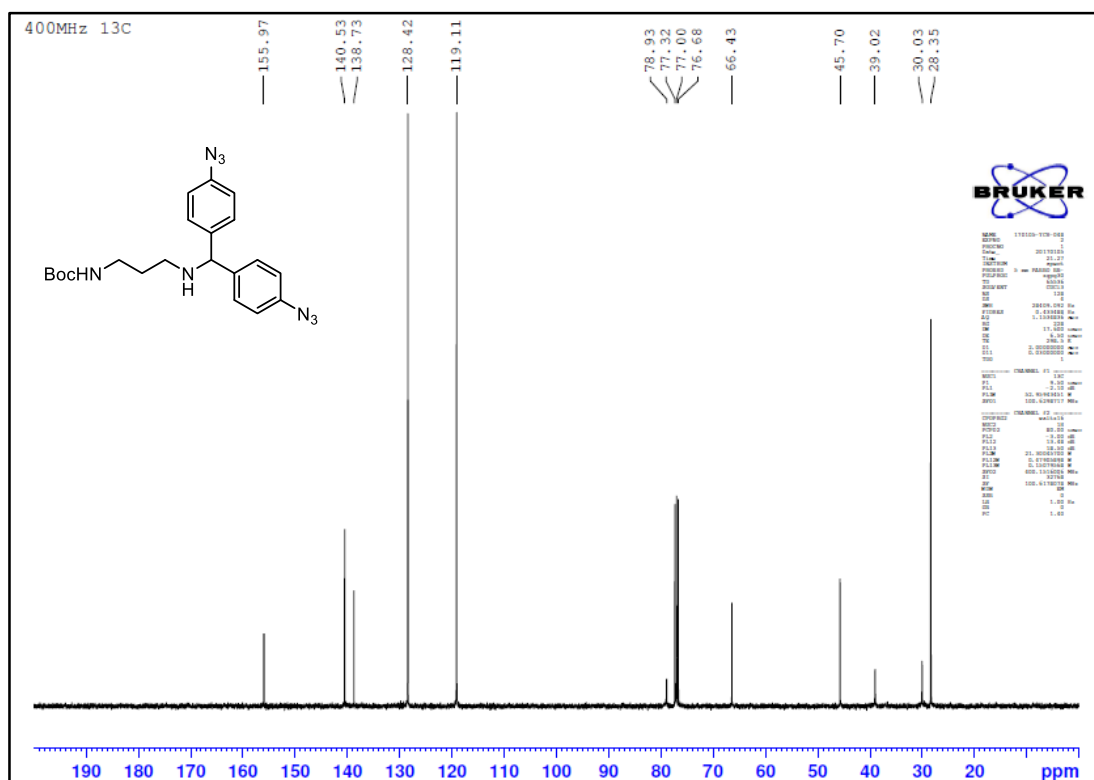
$^1\text{H}$  NMR spectrum of compound **38** (400 MHz,  $\text{CDCl}_3$ )



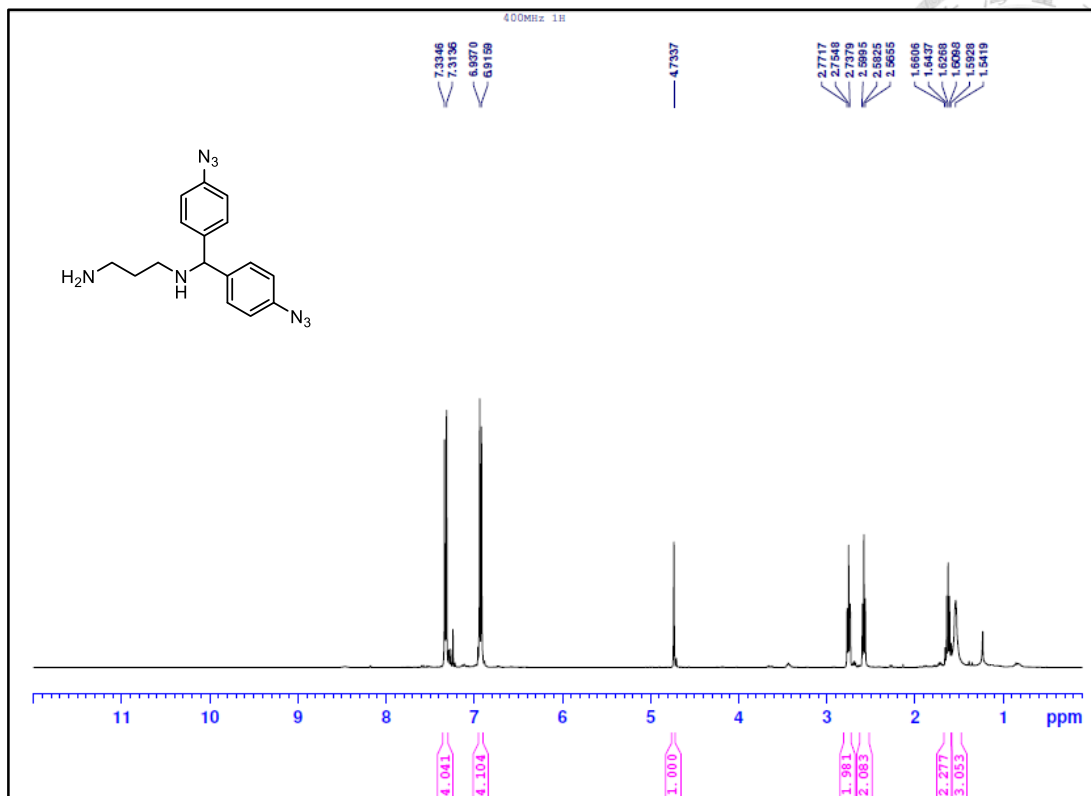
$^{13}\text{C}$  NMR spectrum of compound **38** (100 MHz,  $\text{CDCl}_3$ )



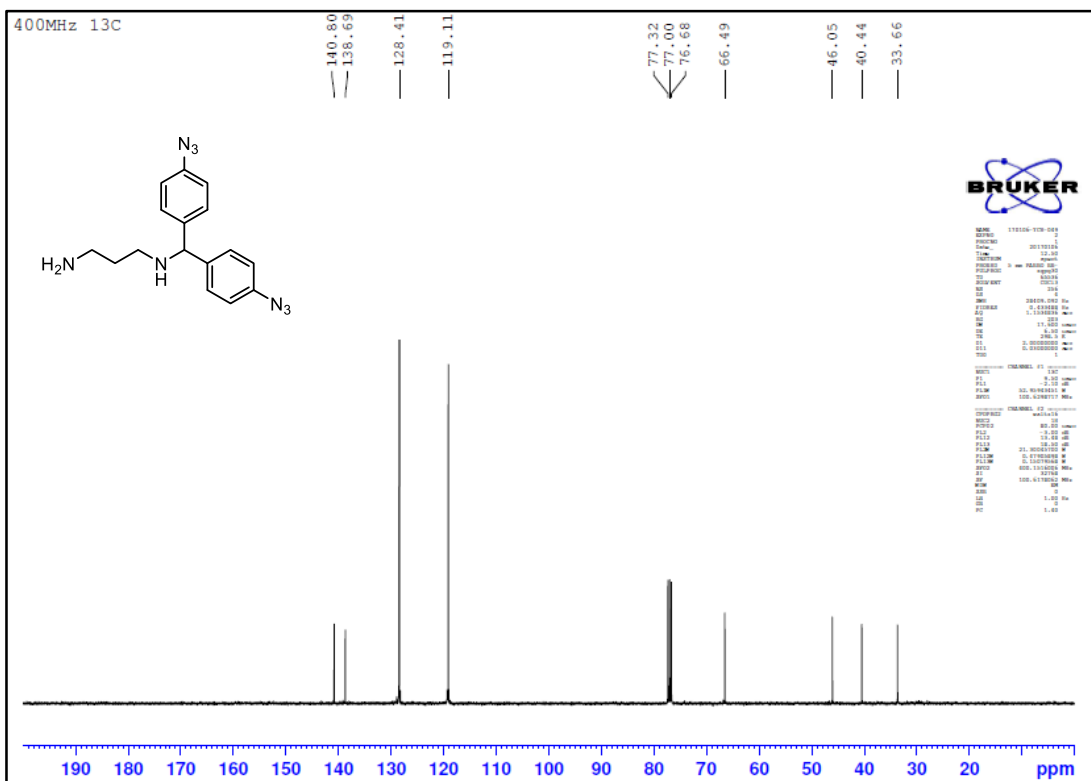
<sup>1</sup>H NMR spectrum of compound **40** (400 MHz, CDCl<sub>3</sub>)



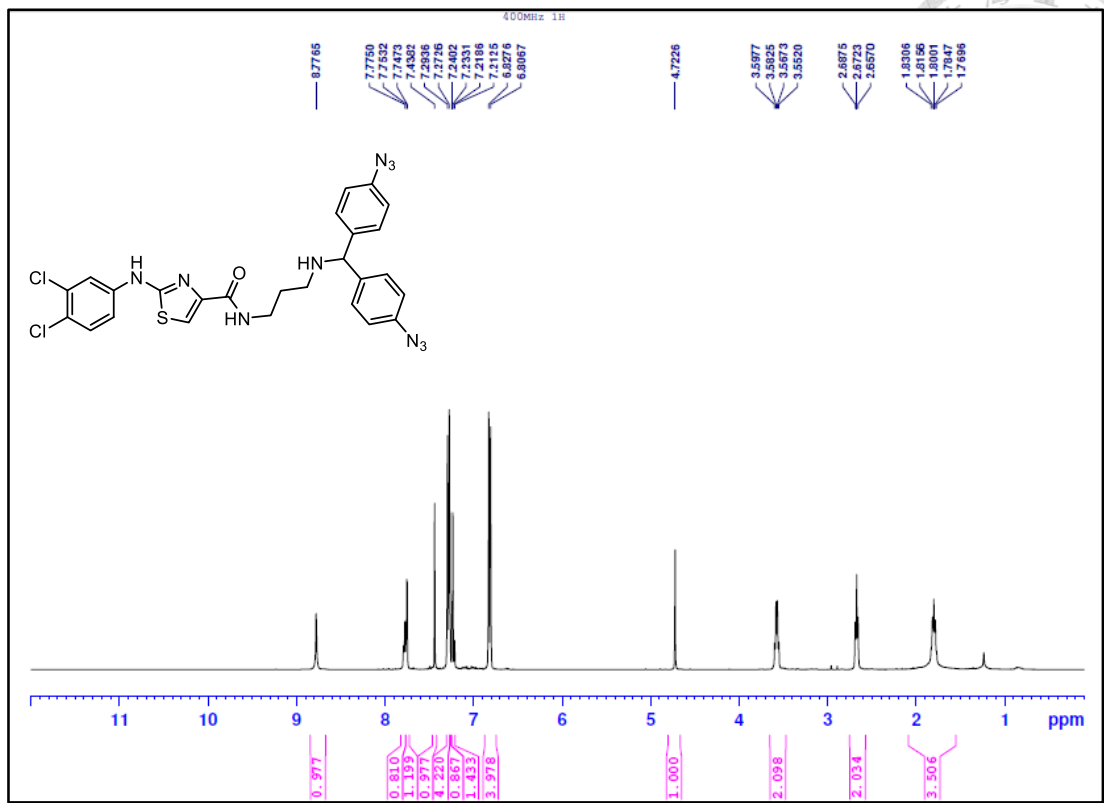
<sup>13</sup>C NMR spectrum of compound **40** (100 MHz, CDCl<sub>3</sub>)



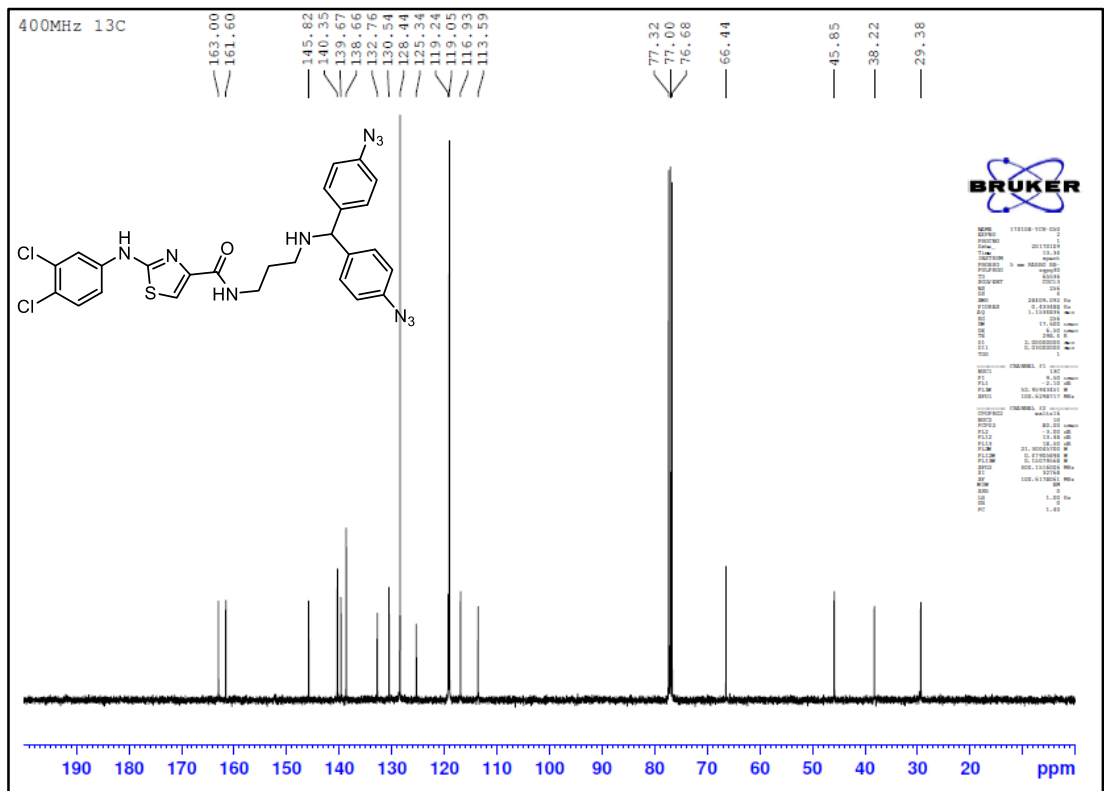
$^1\text{H}$  NMR spectrum of compound **41** (400 MHz,  $\text{CDCl}_3$ )



$^{13}\text{C}$  NMR spectrum of compound **41** (100 MHz,  $\text{CDCl}_3$ )

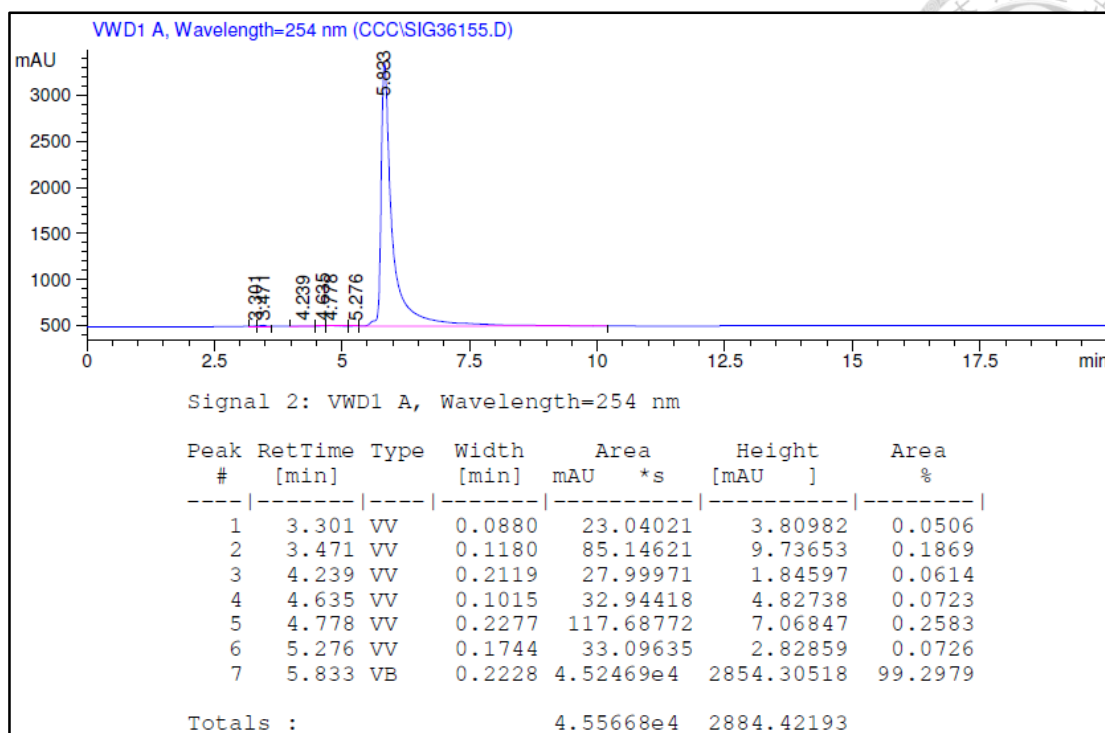


<sup>1</sup>H NMR spectrum of compound 42 (400 MHz, CDCl<sub>3</sub>)



<sup>13</sup>C NMR spectrum of compound 42 (100 MHz, CDCl<sub>3</sub>)





HPLC diagram of compound **42**. Platisil Silica column (Dikma, 250 × 4.6 mm, 5 μm particle size),  $t_R = 5.8$  min [MeOH:EtOAc = 1:24] at flow rate of 1.0 mL/min.